Salinity Gradient Power-Reverse Electrodialysis is among the emerging membrane-based technologies for renewable energy generation. In Reverse Electrodialysis, cation exchange membranes and anion exchange membranes are alternatively aligned to create a high concentration compartment and low concentration compartment. When the compartments are fed by a low concentration and high concentration solution, salinity gradient is created which initiates the diffusive flux of ions towards electrodes. Electricity is generated by the redox process occurring at the electrodes. The total voltage generated (open circuit voltage) is proportional to the number of membrane pairs (cells). One of the challenges pertaining to the Ohmic losses when using very low concentration salt solutions like river water can be reduced by working with highly concentrated brines. Salinity gradient energy generated in this way can also be used for continuous fueling of water electrolyzers and sustainable hydrogen production.

Renewable Energy Generation and Hydrogen Production from Concentrated Brine by Reverse Electrodialysis Ramato Ashu Tufa 2015

Renewable Energy Generation and Hydrogen Production from Concentrated Brine by Reverse Electrodialysis

Ramato Ashu Tufa

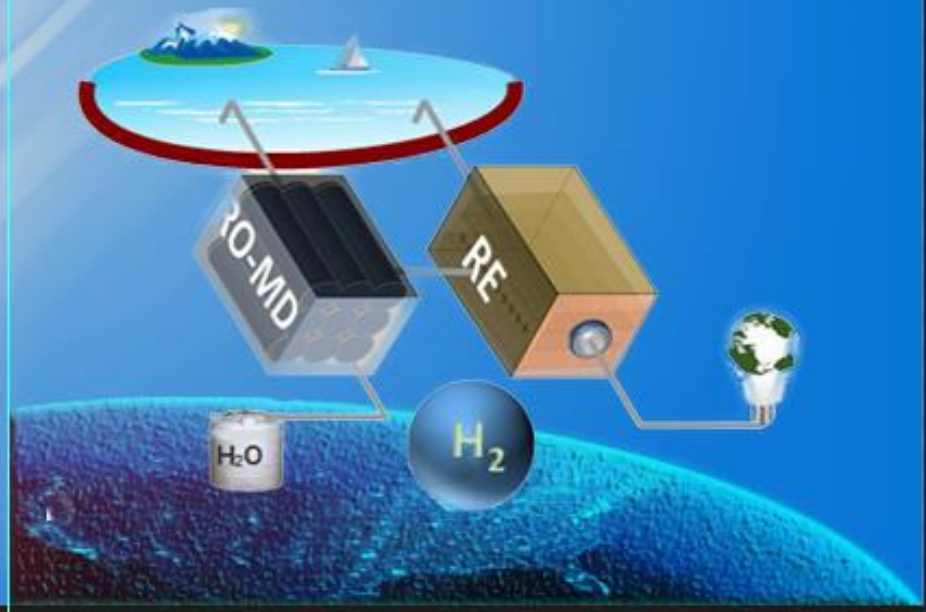

Università della Calabria

Dottorato di Ricerca in Ingegneria Chimica e dei Materiali
SCUOLA DI DOTTORATO " PITAGORA " IN SCIENZE INGEGNERISTICHE

Tesi

Renewable Energy Generation and Hydrogen Production from Concentrated Brine by Reverse Electrodialysis

Settore Scientifico Disciplinare CHIM07 – Fondamenti chimici delle tecnologie

Ciclo XXVIII

Candidato
Ramato Ashu TUFA

Supervisori
Ch.mo Prof. E. DRIOLI

Prof. Efrem CURCIO

Il Coordinatore del Corso Di Dottorato
Ch.mo Prof. R. MOLINARI

A.A. 2014-2015

Dedicated to my parents ***Teyibe Aman Wosho***
and ***Ashu Tufa Washo***

Relazione del Collegio dei Docenti del Dottorato di Ricerca in
Ingegneria Chimica e dei Materiali
Dipartimento di Ingegneria per l'Ambiente e il Territorio e Ingegneria Chimica
Università della Calabria
XXVIII Ciclo

Il dottorando **Ramato Ashu TUFA**, laureato in Chimica Analitica (Addis Ababa University – Ethiopia) e Eramsus Mundus Master Quality in Analytical Laboratories (Gdansk University of Technology – Poland) ha affrontato il Dottorato di Ricerca in Ingegneria Chimica e dei Materiali allo scopo di completare le conoscenze nella scienza dell'Ingegneria Chimica e dei Materiali, con particolare riferimento all'applicazione di elettrodialisi inversa per la produzione di energia elettrica e idrogeno da gradienti salini. Gli sforzi profusi dal dottorando, unitamente all'entusiasmo col quale è stata affrontata l'attività di ricerca, hanno fatto sì che egli fosse in grado integrare le problematiche emerse nel corso del lavoro sperimentale in un ambito più ampio di interesse anche industriale, avendo acquisito, nel contempo, notevoli conoscenze dei fondamenti delle tematiche oggetto degli studi.

Il dottorando **Ramato Ashu TUFA** ha condotto nel suo triennio di Dottorato uno studio sulla possibilità di impiegare membrane a scambio ionico per la generazione di potenziale elettrico, recuperando l'energia libera di miscelazione di correnti saline a differente concentrazione. Questo lavoro è stato sottoposto a pubblicazione su riviste internazionali (3 articoli pubblicati su riviste scientifiche, 1 sottoposto, 5 in preparazione), ed è stato oggetto di 7 presentazioni orali e di 5 presentazioni in forma di poster in differenti congressi internazionali.

Nel lavoro di tesi sono stati approfonditi argomenti quali: i) l'analisi dell'influenza di diverse variabili operative (concentrazione soluzioni saline, portata, temperatura) sull'efficienza dell'elettrodialisi inversa; ii) integrazione in processi di dissalazione a membrana, con particolare riguardo alla Distillazione a Membrana; iii) potenzialità nell'ibridizzazione con elettrolisi alcalina per la produzione di idrogeno.

Lo studio preliminare al lavoro ha avuto lo scopo di valutare lo stato dell'arte sull'applicazione delle membrane a scambio cationico ed anionico per la generazione di potenziale elettrochimico. Dalla constatazione che larga parte dei lavori in letteratura si riferissero all'impiego di soluzioni di acquose di NaCl, si è inteso studiare l'effetto di soluzioni reali multi-ioni sulla densità di potenza generata. Rispetto allo stato dell'arte sono stati altresì effettuati studi di stabilità delle membrane rispetto a fenomeni di fouling sia organico che inorganico.

Nel corso di tutto il suo lavoro il Dott. **Ramato Ashu TUFA** ha dimostrato doti di entusiasmo per la ricerca, dedizione allo studio e capacità di approfondimento, privilegiando gli aspetti di interesse ingegneristico della problematica affrontata.

Il Collegio dei Docenti, visto l'impegno profuso e la qualità della sua attività, esprime un giudizio pienamente favorevole ai fini dell'ammissione del Dott. **Ramato Ashu TUFA** all'esame finale per il conseguimento del titolo di Dottore di Ricerca in Ingegneria Chimica e dei Materiali.

Rende, 11.11.2015

Il Coordinatore del Collegio
Prof. Raffaele Molinari

Contents

Summary

Renewable Energy Generation and Hydrogen Production from Concentrated Brine by Reverse Electrodialysis

Salinity Gradient Power-Reverse Electrodialysis (SGP-RE) is among the emerging membrane-based technologies for renewable energy generation. In RE, cation exchange membranes (CEM) and anion exchange membranes (AEMs) are alternatively aligned to create a high concentration compartment (HCC) and low concentration compartment (LCC). When the compartments are feed by a low concentration and high concentration solution, salinity gradient is created which initiates the diffusive flux of ions towards electrodes. Electricity is generated by the redox process occurring at the electrodes. The total voltage generated (open circuit voltage, OCV) is proportional to the number of membrane pairs (cells). One of the challenges pertaining to the Ohmic losses when using very low concentration salt solutions like river water can be reduced by working with highly concentrated brines **(Chapter 1)**.

Investigation of the performance of RE under realistic high-salinity conditions is crucial for implementation of RE under natural condition. The most abundant ions in natural waters involve sodium, magnesium, calcium, chloride, sulfate, and bicarbonate. Under this condition, the presence of multivalent ions, in particular Mg^{2+}, have a lowering effect on OCV and hence a reduction of power density. This could be attributed to the enhancement of cell resistance in the presence Mg^{2+} ion resulting in an increase of membrane resistance. The SGP potential and comparable decrease in **power density of RE operated with solutions mimicking real brackish water and exhaust brine from a solar pond** depicts the pretreatment requirement in RE for better performance **(Chapter 2)**.

Seawater reverse osmosis (SWRO) is the most widespread technology for fresh water production in many parts of the world. Extensive research have been carried out to tackle the technological challenges coming along with the expansion of SWRO practice with time, specifically the reduction of energy consumption. The integrated application RE in desalination technologies in the logic of process intensification is an interesting approach towards low energy desalination. Simultaneous production of energy and desalted water is possible by hybrid application of Direct Contact Membrane Distillation (DCMD) and RE units operated on the

retentate stream from a SWRO desalination plant. The use of concentrated brine for energy recovery also leads to Near-Zero Liquid Discharge from desalination systems. This avoids the adverse ecological effect of discharging hypersaline solution into natural water bodies. Thus, integrated application of RE with RO and DCMD for simultaneous water and energy production represent an innovative approach **towards low energy desalination and Near-Zero Liquid Discharge** paradigm **(Chapter 3)**.

The possibilitity to exploit the chemical potential of sulfate wastes by SGP-RE can be a promising alternative renewable energy source. The key challenge remains the property of membrane in sulphate solution. Although the trends in the variation of desirable membrane properties (high permselectivity and low resistance) in Na_2SO_4 test solutions with varying operating conditions remain similar with that of NaCl test solution, their performance is comparatively low. This has a negative impact on the performance of the RE mainly on the obtained OCV and power density. Hence, design of well optimized and high performance membranes is required for practical applicability of SGP-RE for renewable energy generation from sulfate bearing waste resources **(Chapter 4)**.

Ion exchanging membranes (IEMs) are key components in RE. Low resistance and highly permeable ion exchange membranes are required for optimal performance of RE system. For practical applications of RE under real condition, IEMs which are less susceptible to fouling are required. There is a potential risk of fouling (for example, scaling of sparingly soluble salts) of IEM operated in concentrated brine. Operations under real conditions also require feed quality control, as the presence of multivalent ions negatively impact RE performance. The variation in Total Organic Carbon (TOC) and Total Hardness (TH) of feed samples may alter the membranes physico-chemical and electrochemical properties. In addition, long term stability of IEMs in concentrated brine govern their life time. Investigation on **fouling and stability of IEMS**, specifically in concentrated brines, would be essential to set a clear pretreatment requirement for the performance of RE under natural conditions **(Chapter 5)**.

For techno-economic optimization and feasibility study of RE, performance of large scale (industrial scale) systems need to be investigated under varying experimental conditions. Comparative assessment of operating conditions like feed concentration, flow velocity and temperature in a small scale RE and large scale RE systems is essential. In general, the trends in OCV and power density for industrial scale operations remain more or less similar to that of

small scales operations. However, the internal losses seem to be manifested for large scale operations. When the cell size increases (scale-up), Ohmic losses are enhanced. Unlike power density, the efficiency of the industrial scale RE reduces with an increasing temperature, but at lower rate compared to small scale operations. In general, **experimental tests on industrial scale RE** for identification of optimal operating conditions is useful for techno-economic evaluations and generate economic figures **(Chapter 6)**.

The integrated application of RE can also be extended into the hydrogen technologies. Currently, above 90 % hydrogen is produced from fossil-based raw materials. Clean energy obtained from mixing seawater or brackish water with concentrated brine can be used to fuel a separate water electrolysis system for sustainable hydrogen production. SGP is a non-periodic and predictable power source in comparison to wind and sun, thus improving process efficiency and capacity factor. In particular, **integrated application of RE with alkaline polymer electrolyte (APE) water electrolysis** is also a favorable route in terms of economics since no precious catalysts are involved. However, this is accompanied by low current efficiency which needs further optimization **(Chapter 7)**.

The energy consumption of desalination technologies is mainly met by the use of fossil fuel which is accompanied by the emission of greenhouse gases. However, there is a possibility to use brine from RO and MD plants for energy recovery by RE which can provide an extra energy for desalination technologies. In addition, the use of pressure exchangers (PX) to recover the pressure over the brine at the outlet of desalination plants can also facilitate a step towards low energy desalination. Thus, **energetic and exegetic analysis of the integrated application of RE with RO and MD** following different scenarios of energy recovery from concentrated brine is useful for assessment of practical applicability on large scale **(Chapter 8)**.

The view on **environmental ethics of practicing membrane-based technologies for water and energy production** can be used in sustainability assessment of such processes. Identification of key impacts of desalination practice on environment and ecosystem is an important strategy in decision making during process design and material development. A pre-set value criteria for sustainability can be used to assess the process in terms of socio-economic and environmental benefits. From environmental ethical point of view, it’s important to keep an upstream balance of social benefits and burdens for the present and future generations. Thus, determination of the level of ethical significance of the main environmental effects from

membrane based water and energy technologies (based on the difficulties to meet sustainability criteria) helps in identification of technological gaps and strategic solution **(Chapter 9)**.

Future research on RE will be focusing on optimal design and development of high performance membrane in hyper-saline solution. This will extend from design of highly permeable and low resistance ion exchange membranes to the development of fouling resistant and stable membrane, particularly in concentrated brine. The relationship between physico-chemical membrane properties and fouling tendency under hyper-saline environment need to be assessed. The effect of other multivalent ions in seawater like SO_4^{2-} and Ca^{2+} on the performance of RE under extreme operating conditions should be clearly outlined. For integrated applications in desalination technologies, for example with DCMD, the risk of scaling and fouling for practical applications should be investigated deeply. Better membranes and module designs are required for membrane desalination systems in general. For efficient application of RE in hydrogen technologies, specifically with APE water electrolysis, development of highly conductive and durable anion selective membranes as well as highly active and stable catalysts in corrosive alkaline environment is of future research interest. Above all, well established techno-economic evaluations of a standalone and integrated applications of RE is essential in order to evaluate the feasibility of scale-up and commercialization of the technology as a renewable energy source **(Chapter 10).**

Samenvatting

Hernieuwbare energie- en waterstofproductie uit geconcentreerde pekel door omgekeerde elektrodialyse

Saliniteit gradiënt vermogen-omgekeerde elektrodialyse (SGV-OE) behoort tot de opkomende membraan-gebaseerde technologieën voor hernieuwbare energieproductie. In OE, kation uitwissel membranen (KUM) en anion uitwissel membranen (AUM) zijn om en om uitgelijnd om hoge concentratie compartimenten (HCC) en lage concentratie compartimenten (LCC) te maken. Wanneer de compartimenten door een laag en hoog geconcentreerde oplossing worden gevoed, ontstaat er een saliniteit gradiënt welke de diffusieve stroming van ionen naar de elektrodes initieert. Elektriciteit wordt gegenereerd door een redox proces bij de elektroden. Het totale voltage dat gegenereerd wordt (het zogenoemde open circuit voltage, OCV) is proportioneel met het aantal membraanparen (ookwel cellen genoemd). Een van de uitdagingen met werken met heel laag geconcentreerd zout water, zoals rivier water, zijn de ohmische verliezen. Deze kunnen worden gereduceerd door te werken met hoog geconcentreerde pekel **(Hoofdstuk 1)**.

Onderzoek naar de prestatie van OE onder realistische hoge saliniteit condities is cruciaal voor het implementeren van OE in natuurlijke condities. De meest voorkomende ionen in natuurlijk water zijn natrium, magnesium, calcium, chloride, sulfaat en bicarbonaat. Onder deze conditie zorgt de aanwezigheid van multivalente ionen, vooral Mg^{2+}, voor een verlaging van de OCV en daardoor vermogensdichtheid. Dit kan toegeschreven worden aan de toename in membraan weerstand en cel weerstand als gevolg van de aanwezigheid van Mg^{2+}. De potentie en **vergelijk in vermogensverlies in OE met oplossingen die lijken op natuurlijk brakwater en pekel uit een zonnevijver** geven de voorbehandelingseisen voor OE aan **(Hoofdstuk 2)**.

Zeewater omgekeerde osmose (ZWOO) is de meest gebruikte techniek om zoet water te maken in grote delen van de wereld. Uitgebreid onderzoek is uitgevoerd om technologische uitdaging op te lossen, met name de vermindering van energie consumptie. De geïntegreerde applicatie van OE in ontzoutingstechnologieën voor intensiveren van processen is een interessante benadering voor ontzouting met minder energie. Simultane productie van energie en ontzout water is mogelijk door gebruik te maken van hybride Direct Contact Membraan

Destillatie (DCMD) en OE eenheden te gebruiken op de retentaat stroom van een ZWOO fabriek. Het gebruik van geconcentreerde pekel voor energie terugwinning leidt ook tot Near-Zero Liquid Discharge van ontzoutingsinstallaties. Dit ontwijkt de negatieve ecologische effecten van het lozen van hyperzoute oplossingen in natuurlijke waterlichamen. Dus de geïntegreerde applicatie van OE met ZWOO en DCMD voor het **simultaan produceren van water en energie is een innovatieve benadering naar lage energie ontzouting en Near-Zero Liquid Discharge (Hoofdstuk 3)**.

De mogelijkheid om de chemische potential van sulfaat afvalstromen door OE te gebruiken is een potentieel interessante bron van alternatieve hernieuwbare energie. De voornaamste uitdaging is de uitdaging van het membraan in de sulfaat oplossing. Alhoewel de trend in de variatie van goede membraaneigenschappen (hoge permselectiviteit en lage weerstand) in Na_2SO_4 oplossing vergelijkbaar zijn met NaCl oplossingen, is de prestatie in vergelijking lager. Dit heeft een negatieve impact op de prestatie van OE voornamelijk op de OCV en vermogensdichtheid. Dus het ontwerpen van geoptimaliseerde en hoge prestatie membranen is nodig voor praktische applicatie van OE voor sulfaat-dragende afvalstromen **(Hoofdstuk 4)**.

Ion uitwissel membranen (IUM) zijn sleutelcomponenten voor OE. Lage weerstand en hoog permeabele ion uitwissel membranen zijn nodig voor optimale prestatie van OE systemen. Voor praktische applicatie van OE onder natuurlijke condities, zijn er IUMs nodig die minder gevoelig zijn voor vervuiling. Het gevaar van vervuiling (bijvoorbeeld door neerslaan van slecht oplosbare zouten) is aanwezig voor IUMs in geconcentreerde pekel. Opereren onder natuurlijke condities vergen ook kwaliteitscontrole van de voedingsstromen, gezien de aanwezigheid van multivalente ionen een negatieve invloed heeft op de OE prestatie. De variatie in totale organische koolstof (TOK) en totale hardheid (TH) van voedingsstromen kan de membraan eigenschappen veranderen. Bovendien, lange termijn stabiliteit van IUMs in geconcentreerde pekel bepaalt hoe lang ze gebruikt kunnen worden. **Onderzoek naar vervuiling en stabiliteit van IUMs**, specifiek in geconcentreerde pekel, is essentieel om duidelijke voorbehandelingseisen te definiëren voor optimale OE prestatie **(Hoofdstuk 5)**.

Voor technisch-economische optimalizatie en haalbaarheidsstudie van OE, is het nodig om prestatie of grote (industriële) schaal te onderzoeken onder variabele experimentele condities. Vergelijkbare analyse van uitvoerende condities zoals voedingsconcentraties,

doorstroomsnelheid en temperatuur zowel in een kleine en grote schaal OE systeem is essentieel. In het algemeen zijn de trends van de OCV en vermogensdichtheid vergelijkbaar tussen de kleine en industriële schaal. Maar, de interne verliezen zijn vooral zichtbaar bij de industriële schaal. Wanneer de cel-grootte toeneemt (opschalen), nemen de ohmische verliezen toe. Tegenovergesteld aan de vermogensdichtheid, neemt de efficiëntie af van een industriële OE met toenemende temperatuur, maar met lagere snelheid dan kleinere schaal. In het algemeen zijn **experimentele testen op industriële schaal voor OE bruikbaar** om optimale gebruikscondities en techno-economische analyses te kunnen maken (**(Hoofdstuk 6)**.

De geïntegreerde applicatie van OE kan ook verlengd worden naar waterstof technologieën. Momenteel is 90% van de waterstof gemaakt uit fossiele grondstoffen. Schone energie verkregen uit het mengen van zeewater of brak water met geconcentreerde pekel kan gebruikt worden om een los water elektrolyse systeem voor hernieuwbare waterstofproductie aan te drijven. SGV is een continue en voorspelbare vermogensbron in vergelijking met wind en zon, waardoor de proces efficiëntie en capaciteit toeneemt. Specifiek, **integreren van OE met alkalische polymeren elektroliet (APE) water elektrolyse** is een goede route qua economie gezien er geen edelmetalen gebruikt worden. Maar dit gaat gepaard met een lage efficiëntie voor stroomverbruik welke verdere verbetering nodig heeft **(Hoofdstuk 7).**

De energie consumptie van ontzoutingstechnieken wordt voornamelijk geleverd door fossiele brandstof wat gepaard gaat met emissie van broeikasgassen. Maar er is een mogelijkheid om pekel van OO en MD fabrieken voor energie terugwinst met OE te gebruiken, welke extra energie kan leveren voor ontzoutingstechnieken. Bovendien geeft het gebruik van druk uitwisselaars (DU) op de uitstroompekel een mogelijkheid om lage energie ontzouting te ontwikkelen. Dus, **energetisch en exegetische analyse van de geïntegreerde applicatie van OE met OO en MD** met verschillende scenario's is toepasbaar om de praktische haalbaarheid op grote schaal in te schatten **(Hoofdstuk 8).**

De visie op **milieu ethiek van het uitvoeren van membraanprocessen voor water en energie productie** kan gebruikt worden voor de duurzaamheidsanalyse van zulke processen. Het identificeren van sleutel factoren van ontzoutingstechnieken op milieu en ecosystemen is een belangrijke strategie in het keuze proces en materiaal ontwikkeling. Een voorafgezette waarde-criteria voor hernieuwbaarheid kan gebruikt worden om het proces voor socio-economisch en milieu aspecten te evalueren. Vanuit een milieu ethisch oogpunt is het belangrijk om een balans

te vinden tussen sociale winst en lasten voor huidige en toekomstige generaties. Dus het bepalen van het niveau van de ethische significantie van de voornaamste milieu effecten door membraan-gebaseerde water en energie technologieën helpt om te identificeren waar technologische gaten en strategische oplossingen zitten **(Hoofdstuk 9).**

Toekomstig onderzoek op OE richt zijn aandacht op het optimaal ontwerpen en ontwikkelen van hoge prestatie membranen in hypersaliniteit condities. Deze reiken van het ontwikkelen van hoog permeabele en lage weerstand ionen uitwissel membranen naar de ontwikkeling van niet vervuilende en stabiele membranen, vooral in geconcentreerde pekel. De relatie tussen fysisch-chemische membraan eigenschappen en waarschijnlijkheid tot vervuiling onder hypersaliniteitsomgeving moet worden onderzocht. Het effect van andere multivalente ionen in zeewater zoals SO_4^{2-} en Ca^{2+} op de prestatie van OE onder extreme condities moet verduidelijkt worden. Voor geïntegreerde applicaties in ontzoutingstechnologieën, bijvoorbeeld met DCMD, het risico van neerslag en vervuiling in praktische applicaties moet worden onderzocht. Betere membranen en modules zijn nodig voor membraan ontzoutingssystemen in het algemeen. Voor efficiënte applicatie van OE voor waterstoftechnologieën, voornamelijk met APE water elektrolyse, ontwikkeling van hoog geleidende en duurzame anion selectieve membranen net als hoog actieve en stabiele katalyse in corrosief en alkalisch milieu is van academische interesse. Bovendien zijn duidelijke techno-economische evaluaties van losse en geïntegreerde applicaties van OE essentieel om opschaalmogelijkheden en commercialisering van de hernieuwbare technologie te kunnen evalueren **(Hoofdstuk 10)**.

Souhrn

Obnovitelná výroba elektrické energie a vodíku z koncentrované solanky za pomoci reverzní elektrodialýzy

Reverzní elektrodialýza využívající gradientu solnosti vodných roztoků (Salinity Gradient Power - Reverse Electrodialysis, SGP-RE) patří k intenzivně rozvíjeným technologiím obnovitelné výroby energie založeným na využití iontově selektivních membrán. Jednotka reverzní elektrodialýzy (Reverse Electrodialysis, RE) sestává z alternativně umístněných kationselektivních membrán (CEM) a anionselektivních membrán (AEM) tvořících střídavě koncentrátové (HCC) a diluátové (LCC) komory**. Jsou-li tyto komory naplněny odpovídajícími roztoky vhodných solí o vysoké a nízké koncentraci**, vzniká na membránách odpovídající koncentrační gradient rozpuštěných solí. Ten je hnací silou difúze iontů mezi uvedenými oddíly spojené s přenosem elektrického náboje přes membránový pár a zároveň příčinou rozdílu elektrických potenciálů mezi oddíly**.** Elektrická energie pro vnější elektrický okruh je pak generována redukčně-oxidačními ději probíhajícími na elektrodách umístněných na koncích svazku. Celkové generované elektrické napětí (napětí otevřeného obvodu, OCV) je přímo úměrné počtu membránových párů ve svazku. Jeden z významných problémů představuje omezení vlivu ohmických ztrát napětí spojených s použitím vody s nízkým obsahem solí, jako je například voda říční. Tento negativní efekt lze omezit použitím vysoce koncentrovaných roztoků solanky **(Kapitola 1)**.

Výzkum chování RE za podmínek použití roztoků s realisticky vysokou solností o složení blízkém roztokům vyskytujícím se běžně v přírodě představuje klíčový aspekt vzhledem k využití RE. V takových vodách jsou nejvíce zastoupeny ionty sodíku, hořčíku a vápníku a dále pak chloridy, sírany a hydrogenuhličitany. Avšak vícevalentní ionty, jako například Mg^{2+}, vykazují negativní vliv na OCV a v důsledku toho na výkon svazku. To může být přičteno zejména nárůstu ohmického odporu membrán v přítomnosti Mg^{2+} vedoucího k nárůstu odporu celého RE svazku. Snížení SGP potenciálu a odpovídající pokles **výkonové hustoty RE provozované při použití roztoků simulujících reálnou brakickou vodu a zbytkovou solanku ze solární saliny** poskytuje podklady pro návrh odpovídajícího čištění zajišťujícího lepší výkon RE **(Kapitola 2)**.

Reverzní osmóza představuje celosvětově nejrozšířenější technologii přípravy sladké vody z mořské (SWRO). V minulosti proběhl velmi rozsáhlý výzkum zaměřený na odstranění problémů spojených s využíváním této techniky. Jedná se zejména o snížení jejích energetických nároků. Zapojení RE do integrovaných odsolovacích procesů představuje zajímavý způsob, jak dosáhnout dalšího snížení jejích stávajících energetických nároků. Současné produkce energie a odsolené vody lze dosáhnout pomocí integrované hybridní technologie zahrnující membránovou destilaci (DCMD) a RE, využívající proud retentátu z SWRO. Využití koncentrované solanky ke zpětné generaci energie umožňuje rovněž dosáhnout koncentrace soli v odpadním proudu z odsolovací technologie blízké původním roztokům. To umožní eliminovat nežádoucí efekty spojené s přímým vracením vysoce zasolených roztoků do životního prostředí. Lze tedy konstatovat, že využití technologie integrující RE, RO a DCMD pro současné odsolení vody a produkci energie představuje inovativní přístup **odsolení vody s nízkými energetickými nároky a koncentrací solí ve vodě vypuštěné do životního prostředí blízkou vstupním roztokům (Kapitola 3)**.

Chemický potenciál uložený v odpadních roztocích síranů představuje ve spojení s SGP-RE slibný alternativní zdroj energie. Klíčovou otázku představují vlastnosti membrán v prostředí roztoku síranových iontů. Ačkoliv změny sledovaných vlastností (selektivita a odpor k přenosu náboje) membrán v závislosti na provozních podmínkách vykazují v roztocích Na_2SO_4 podobné trendy jako v roztocích NaCl, jejich výkonnost zůstává nižší. To má negativní dopady na výkonnost RE, zejména na dosahované OCV a proudovou hustotu. Je tedy zřejmé, že je zapotřebí navrhnout optimalizované vysoce výkonné membrány, aby byla SGP-RE prakticky uplatnitelná v oblasti generace obnovitelné energie ze solných roztoků obsahujících vysoká množství síranů **(Kapitola 4)**.

Iontově selektivní membrány (Ion Exchange Membranes, IEMs) představují klíčové komponenty RE. Jejich nízký ohmický odpor a zejména vysoká permeabilita je předpokladem optimální funkce RE. Pro praktické aplikace RE jsou navíc vyžadovány membrány méně citlivé k blokaci povrchu. Příčinou je vyšší nebezpečí takovéto blokace (např. sraženinami málo rozpustných solí), je-li IEM provozována v koncentrovaném roztoku solí. Proces vyžaduje za reálných podmínek rovněž spolehlivou kontrolu složení vstupního proudu, mimo jiné indikaci vícevaletních iontů majících negativní vliv na výkonnost zařízení. Rovněž proměnlivý obsah organických látek (Total Organic Carbon, TOC) a tvrdosti vody (Total Hardness, TH) může

ovlivňovat fyzikálně-chemické a elektrochemické vlastnosti IEM. Zároveň je zřejmé, že dlouhodobá stabilita IEM v roztoku soli je tím parametrem, který řídí její životnost. **Výzkum blokace povrchu a stability IEMs** v prostředí koncentrovaných solí tedy představuje jeden ze základních požadavků umožňujících nastavení jasných požadavků na úpravu vstupního proudu za reálných podmínek **(Kapitola 5)**.

Aby bylo možno získat dostatečně přesnou technicko-ekonomickou analýzu a studii proveditelnosti využití RE v praxi, je nezbytné získat odpovídající údaje o provozu technologie v průmyslovém měřítku nebo v měřítku průmyslovému alespoň blízkém, a to za různých provozních podmínek. Porovnání vlivu koncentrace vstupních proudů, rychlosti průtoku či provozní teploty jak v malém, tak velkém měřítku tedy představuje nezbytnou součást tohoto výzkumu. Na základě provedených studií lze říci, že odezva systému (OCV a proudová hustota) na tyto parametry je v laboratorním a průmyslovém měřítku v souladu s očekáváním podobná. V průmyslovém měřítku však byla pozorována větší ohmická ztráta napětí na jednotce RE. Zároveň, na rozdíl od proudové hustoty, účinnost procesu RE klesala s rostoucí teplotou. V laboratorním měřítku pak je tento pokles pomalejší, než v průmyslovém. Obecně lze říci, **že experimentální ověření funkce RE** v průmyslovém měřítku poskytlo významné vstupy k optimalizaci procesu, technicko-ekonomickému vyhodnocení a odhadu ekonomických ukazatelů technologie RE **(Kapitola 6)**.

Využití RE jako součásti integrované technologie může být rozšířeno rovněž do oblasti vodíkových technologií. V současnosti je více než 90 % vodíku produkováno z fosilních surovin. Čistá energie získaná z technologie založené na smíchání mořské nebo brakické vody s koncentrovaným roztokem solanky může být využita v nezávislé technologii elektrolytického rozkladu vody. SGP představuje kontinuální a predikovatelný zdroj energie. To umožňuje, zejména v porovnání s větrnou a solární energií, dosáhnout vyšší energetické účinnosti a kapacity produkce. **Integrace RE a alkalické elektrolýzy vody (APE)** představuje preferenční způsob rovněž z ekonomické stránky. To je způsobeno zejména tím, že APE nevyžaduje použití katalyzátorů na bázi drahých kovů. Na druhou stranu, ovšem, je tato technologie dosud zatížena relativně malou účinností a intenzitou děje. Vyžaduje tedy další optimalizaci **(Kpitola 7).**

Energetické nároky odsolovacích technologií jsou typicky spojovány s využitím fosilních paliv. Tento přístup je nezbytně spojen s uvolňováním skleníkových plynů a dalších polutantů do atmosféry. Existuje však možnost využít koncentrátové proudy z RO a MD a s pomocí RE získat

elektrickou energii využitelnou k alespoň částečnému pokrytí nároků odsolovacích technologií. Dále lze použít přenašeče tlaku (Pressure Exchangers, PX) ke zpětnému získání tlaku na výstupu z odsolovací technologie. Tímto způsobem lze dále snížit energetické nároky procesu. **Energetická a exergická analýza integrovaného využití RE ve spojení s RO a MD** dovolující porovnat různé scénáře zpětného získání energie z koncentrovaného roztoku solí je pak velmi přínosná z hlediska odhadu praktického využití uvažovaných variant ve velkém měřítku **(Kapitola 8)**.

Pro vyhodnocení navržené technologie z hlediska trvale udržitelného rozvoje lze použít přístup založený na **posouzení etiky využití technologií založených na membránových procesech pro úpravy vody a výrobu energie**. Vyhodnocení klíčových dopadů desalinačních technologií na životní prostředí a ekosystémy představuje efektivní strategii v rozhodovacím procesu v průběhu návrhu a vývoje průmyslového procesu. Pro posouzení udržitelnosti technologie a jejích socio-ekonomických a environmentálních dopadů mohou být využity přednastavené hodnoty jednotlivých kritérií. Z hlediska environmentální etiky je důležité vždy zachovat rostoucí bilanci společenského prospěchu a snížení zátěže pro stávající populaci i generace budoucí. Stanovení těchto kritérií pro technologie čištění vody a produkce energie napomůže (vzhledem k obtížnosti dosažení požadované úrovně kritérií) identifikaci nedostatků navržených technologií a vhodných řešení **(Kapitola 9)**.

Další výzkum v oblasti RE se soustředí na optimalizaci procesu a vývoj membrán splňujících požadavky procesu v prostředí vysoce zasolených roztoků. Vycházet bude z vývoje vysoce propustných membrán s nízkým ohmickým odporem a směřovat k membránám odolným proti blokaci povrchu a stabilním v koncentrované solance. Za tímto účelem bude rovněž nezbytné nalézt vztah mezi fyzikálně-chemickými vlastnostmi IEMs a jejich tendenci k blokaci v uvedeném prostředí. Jasně vymezen bude muset být rovněž vliv vícevalentních iontů přítomných v mořské vodě, jako SO_4^{2-} a Ca^{2+}, na výkonnost RE za extrémních provozních podmínek. Zvláštní pozornost je zapotřebí věnovat nebezpečí blokace povrchu membrán za reálných provozních podmínek pro případ kombinovaných odsolovacích technik, jako např. DCMD. Obecně je nutné rovněž říci, že desalinační procesy vyžadují další výzkum v oblasti optimalizace designu membránových modulů. Rovněž na poli účinného využití RE v oblasti vodíkových technologií je zapotřebí, zvláště v procesu APE elektrolýzy vody, vyvinout vysoce vodivé a dlouhodobě stabilní iontově selektivní membrány. Obdobné tvrzení lze použít rovněž v

případě vysoce stabilních a aktivních katalyzátorů. Přes všechny tyto aspekty pak přesahuje technicko-ekonomické vyhodnocení samostatného využití RE vs. její kombinace s dalšími procesy. To umožní vyhodnotit schůdnost a smysluplnost nárůstu rozměrů technologie do průmyslového měřítka a její komercionalizace jako obnovitelného zdroje energie **(Kapitola 10).**

Chapter 1

Introduction: Reverse Electrodialysis in Standalone and Integrated Applications

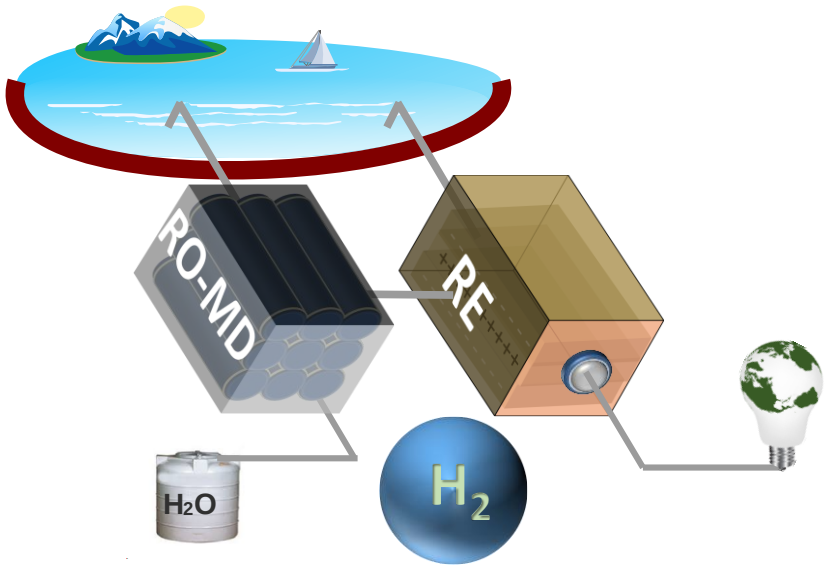

"We must and we can start the world development process that leads to an environmentally sustainable world habitat for humanity there is no alternative… there is none."

Dr. John P. Craven
Common Heritage Corporation
Doherty Lecture, 2001

1.1 Energy and climate issues

Energy is a key resource determining the overall growth and socio-economic development. It is omnipresent in modern economy and plays a vital role in almost all fields of activity including industry, residential (households) and tertiary sectors or transport. A robust energy supply must be secured for a sustainable growth and improved living standard.

Energy representing the basis of industrial revolution had an exponential growth since the birth of industrial electricity at the end of the 19th century. Since then, the global energy consumption is increasing at astonishing rate. It is estimated that global consumption will grow by 56 % between 2010 and 2040 [1]. Global energy consumption profile indicates that the residential, transport and industrial sectors consume 75% of total global energy whereas the manufacturing industry alone accounts for 31% of the global energy use. On the other hand, with the projected increase of population with time, it is estimated that 2 billion new energy consumers are added in emerging economies by 2050. In the same time range, the global energy-related carbon dioxide emissions are expected to increase by 46%, corresponding to 45 billion metric tons [2]. In addition, energy represents the largest source of emissions of greenhouse gases (GHGs); about 69% (See Figure 1). If energy demand continues in the current rate, there will definitely be a significant prospect of energy crisis and associated climate change. Thus, energy security and climate change issues can be addressed by improving energy saving and energy efficiency through sustainable and cost effective ways to ensure a continuous economic growth. Based on the current projections, it is estimated that worldwide implementation of energy efficiency measures could save over 8 Gt-CO_2/yr by 2030 considering a share of common interests among global corporations [3].

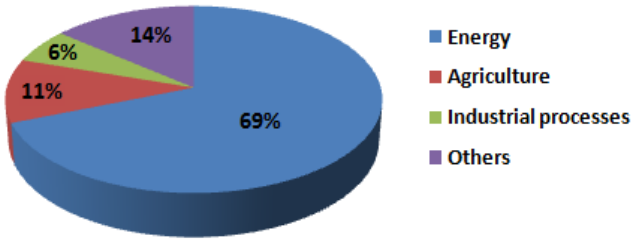

Figure 1.1. Contributions of different sectors to the global GHGs emissions [4].

From social point of view, international agreements targeting at control of potential threats to the environment and the whole ecosystem are very crucial. Important milestones involve the

'Kyoto Protocol' proposed in 1997 agreed between 145 nations targeting the reduction of the emission of greenhouse gases and ozone depleting gases. In the meantime (March 2007), EU has set ambitious targets stated in the EU "20–20–20" Climate Action and Renewable Energy Package aiming at 20% reduction of GHG emission compared to 1991 levels, 20% increment in share of renewable energy consumption and 20% improvements in energy efficiency by 2020. Later on (December 2009), the United Nations Climate Change Conference commonly known as the Copenhagen Summit proposed negotiations aimed at establishing a comprehensive, legally binding international treaty to reduce GHG emissions as well as its major deriving forces to replace the 'Kyoto Protocol' which expired in 2012. Thus, the Conference of Parties (COP15) and all major emitting countries had submitted their reduction pledges and action plans for 2020 to the United Nation Framework Convention on Climate Change (UNFCCC) documented as the 'Copenhagen accord' [5]. This also included long-term goal of limiting the maximum global average temperature below 2 ^{o}C, however, with no agreement on the way to achieve this practically. A recent action of the US on climate change i.e. the 'US Clean Power Plan' sets standards to reduce CO_2 emissions by 32% from 2005 levels by 2030, which is 9% more than the proposed rules. This is also expected to boost the 'Copenhagen accord' and encourage other countries to take further actions.

In general, the global socio-economic profile which is mainly determined by the available energy is susceptible in a varying extent to a naturally and/or anthropogenically induced climate changes. This is directly connected with the current energy and environmental issues which are considered as the serious global challenges for sustainable development if appropriate measures are not taken in advance[6]. Alternative clean energy resources are urgently required to alleviate the skyrocketing demand for clean energy and related environmental issues [7]. For this reason, redesigning of the available production and distribution technologies and establishment of new ones is very crucial. Salinity gradient energy plays a crucial role in this aspect.

Our main focus in this thesis is to investigate alternative clean energy resources in order to secure energy and environmental sustainability.

1.2 Salinity Gradient Power (blue energy)

Salinity gradient power (SGP), also called blue energy, is generated by conversation of osmotic energy of salt solutions into mechanical or electrical energy in a sustainable way. It is an

energy captured by mixing two solutions of different salinity. The concept was first proposed long ago by Pattle in 1954, however, gaining much attention nowadays due to increasing demand of sustainable energy resources in order to avoid the environmental threats and projecting costs of the limited and non-renewable fossil fuel. Growing availability of membranes also account for the current research interest on SGP.

SGP can be produced in an environmentally safe way without any thermal pollution, emission of harmful gases and radioactive substances. It's clean, green, sustainable and completely renewable with no consumption of salt solutions. Although other renewable energy resources like wind and sun have larger theoretical potential than SGP, they are intermittent with the available energy varying depending on season. However, SGP is a predictable source of renewable energy without any periodicity. This energy is potentially available;

- Wherever fresh water mixes with salt water
- Wherever brine solutions are available either from anthropogenic sources (desalinations technologies, salt mines, solar ponds) or natural sources (Dead Sea)
- Wherever aqueous waste water with sufficient salinity is discharged continuously
- Wherever themolytic solutions (e.g. Ammonium bicarbonate) can be can be regenerated by waste heat

SGP is a renewable energy resource that can supply clean energy continuously. This can be demonstrated with the natural water. Solar energy evaporates water from the ocean, lakes and rivers. The evaporated water cools and turns back into tiny water droplets by forming clouds in a process called condensation. These droplets fall back to earth as fresh water by precipitation. The fresh water in the form of streams, river water or brackish water flow into lakes or the sea and maintains a closed water cycle. On the other hand, huge amount of brine is generated from anthropogenic activities like seawater desalination, solar ponds and mining sites. SGP originates when the river water, brackish water or brine discharge mixes with seawater. Alternatively, brackish water or river water can also be mixed to capture SGP. Figure 1.2 demonstrates the possibility of continuous capture of SGP as a renewable energy source in relation to the natural water cycle.

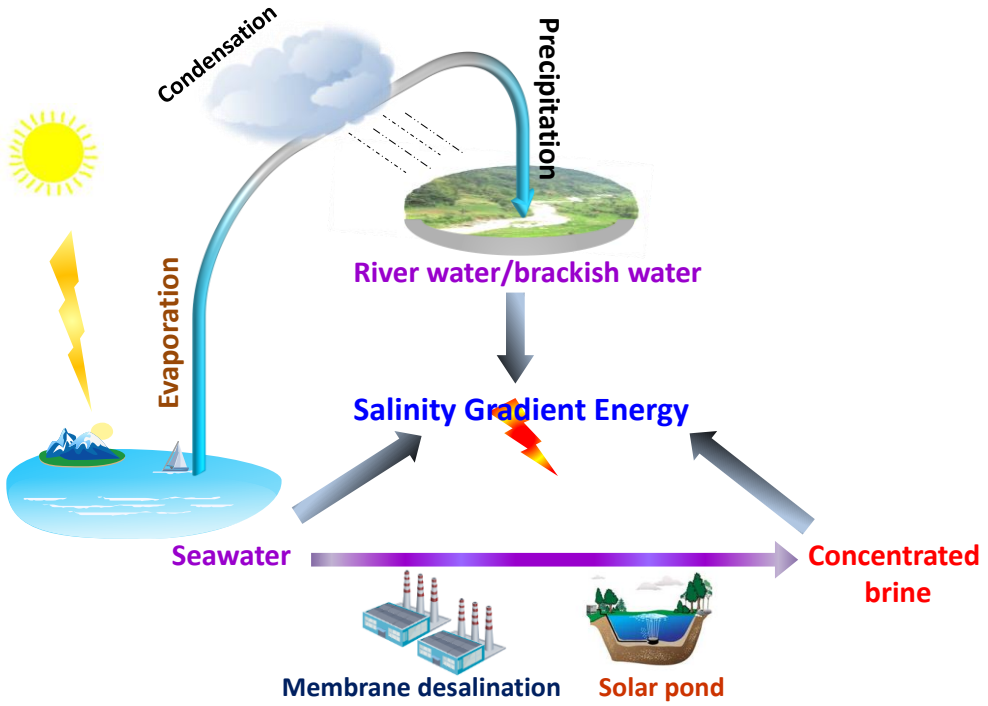

Figure 1.2. Illustration of the possibility of continuous exploitation of SGP in relation to natural water cycle; concentrated brine can be obtained mainly from anthropogenic sources like desalination plants and solar ponds.

The free energy of mixing of two salt solutions could be obtained as the difference between the total chemical potential of the unmixed solutions and chemical potentials of the final mixture. For brine and seawater mixing; considering constant pressure and temperature operating conditions and no charge transport, the resulting free energy ($\Delta G_{b,s}$) can be calculated as [8, 9];

$$\Delta G_{b,s} = 2RT\left[V_s C_s \ln\frac{C_s}{C_M} + V_b C_b \ln\frac{C_b}{C_M}\right] \tag{1.1}$$

where R is the universal gas constant (8.31432 $Jmol^{-1}$ K^{-1}), T the absolute temperature (K), C_s and C_b are the concentrations of seawater and brine, respectively, and with V the volume of the respective solutions with the subscripts *s* and *b* standing for seawater and brine, respectively. The equilibrium concentration of solutions after mixing (C_m) is given as;

$$C_m = \frac{V_s C_s + V_b C_b}{V_s + V_b} \tag{1.2}$$

For example, the theoretically available amount of free energy from mixing 1 m^3 seawater (~0.5 M NaCl) and 1 m^3 RO brine (~1 M NaCl) both at a temperature of 293 K is ~0.3 MJ.

However, using MD brine (~5 M NaCl) instead of seawater, the extracted energy reaches ~4.7 MJ, which is ~0.5 kWh of energy corresponding to the hydroelectric equivalent of 1 m3 of water flowing down 175 m hill. This energy from mixing brine and seawater is about 3-fold of the energy obtained from mixing 1 m3 river water (0.017 mol/L) and 1 m3 seawater (i.e. 1.4 MJ). Moreover, the energy from mixing 1 m3 of brackish water (0.1 mol/L) and 1 m3 brine reaches up to 6.6 MJ. Huge amount of energy (16.9 MJ) can be extracted theoretically when mixing similar volume of brine and river water, but the experimental yield at this condition is highly limited by the high Ohmic resistance due to river water [10]. Our main focus is to avoid this challenges associated with this problem by the use of concentrated brines for SGP generation.

Salinity gradient energy (from total river flowing into the sea) with a total global potential of 1.4-2.6 TW is placed to be the second largest marine-based renewable energy source next ocean waves [8]. The extractable part of this reaches about 960 GW quite higher than the electrical power obtained from the hydroelectric power which is 800 GW [11]. Moreover, considering all the global water bodies, the gross global potential of SGP is estimated to be 27,667 TWh/year [12], and the extractable part of this reaches about 2000 TWh/year which is approximately 5 % of the total global potential of renewable energy resources [13]. This estimation may vary depending on technical and operational factors like flow rates, temperatures, recovery rate, and source properties like salinity level and its temporal variations. Figure 1.3. presents the gross values of the theoretical and technical potential of salinity gradient power for different parts of the world [12]. Asia with 8,890 TWh/year has the largest potential followed by South America with 8,492 TWh/year.

The total global potential will be even much higher if the potential of SGP from waste streams and hybrid applications are considered. For example, the potential only from waste water discharged into an ocean is estimated to be 18 GW [10]. In addition, large amounts of SGP can be harnessed from the brine solutions coming from various sources. However, development and use of appropriate conversion technologies at an affordable are pre-requisites to achieve this target.

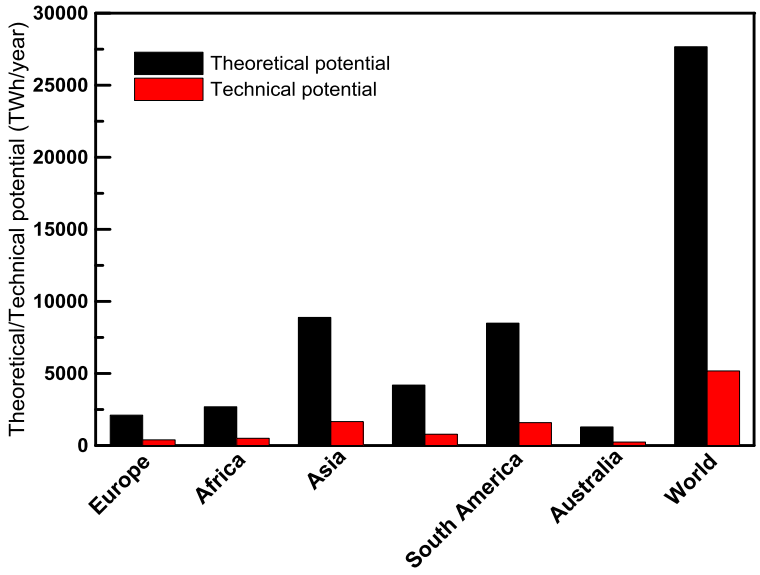

Figure 1.3. Theoretical and technical potential of SGP than can be harnessed annually from different parts of the world [10].

1.2.1 Reverse Electrodialysis

Salinity gradient energy can be harnessed by different technologies like pressure-retarded osmosis (PRO) [11, 12], Reverse Electrodialysis (RE) [9, 13-18], Vapour Pressure Difference utilization (VPD) [19], Capacitive Mixing (CAPMIX) [20, 21], Hydrocratic Generators (HG)[22], Mixing Entropy Battery (MEB)[23]. Membrane based technologies like RE and PRO are currently drawing attention with a satisfactory research progress although these techniques are still limited by some factors like cost of membranes, poor membrane performance in terms of resistance and permselectivity, fouling of membranes and reducing the useful lifetimes of the membrane-packed module. This theses is mainly devoted to RE technology.

Reverse electrodialysis (RE) is among the emerging membrane-based technologies for energy production that have a potential contribution to the share renewable energy sources in the future. It is a young technology generating energy from salinity difference created by mixing of salt and fresh water. Figure 1.4 presents typical RE set up for energy generation from concentrated brine and seawater. Two types of compartments are created in RE by alternatively aligning cation exchange membranes (CEM) and anion exchange membranes (AEM): high concentration compartment (HCC) and low concentration compartment (LCC). The ion exchange materials are mostly separated by a woven fabric (non-conductive) material called spacer to keep a space in the channel and allow the feed flow there by promoting the hydrodynamic mixing. The driving force

here is the concentration gradient and the ion exchanger membranes allow ions to move selectively to anode (the anions) and to cathode (the cations). The resulting ionic flux is converted into an electricity through a redox reaction occurring at the electrodes connected to an external circuit. Low over-potential of the electrode is maintained by proper selection of electrode materials and use of appropriate electrode rinse solutions [24, 25]. The method is inherently sustainable and clean [26] and is close to commercialization, whereas its application is mainly limited by cost and insufficient performance of membranes.

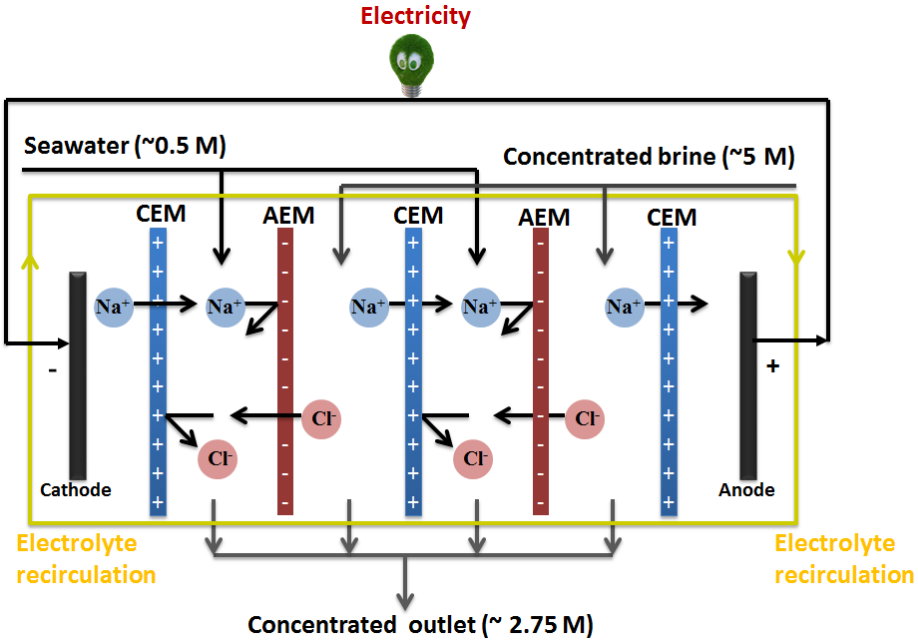

Figure 1.4. Scheme of a RE with 2 cells operating with concentrated brine and sea water; outlets from this RE system is also a concentrated brine which can be recycled in a tandem RE mode or further concentrated in desalination systems for water production and re-use in energy generation.

The total electromotive force over the membranes in RE termed as the Open Circuit Voltage (OCV) is given as follows;

$$OCV = \frac{2NRT}{F}\left[\frac{\alpha_{CEM}}{z_c}\ln\frac{\gamma_b^c C_b}{\gamma_s^c C_s} + \frac{\alpha_{AEM}}{z_a}\ln\frac{\gamma_b^a C_b}{\gamma_s^a C_s}\right] \quad (1.2)$$

where N is the number of membrane pairs, R is the gas constant (8.314 $J{\cdot}mol^{-1}K^{-1}$), T is the temperature (K), F is the Faraday number (96485 $Cmol^{-1}$), α is the permselectivity of the membrane, z is the valence, C is concentrations (in mol/m^3), γ is the activity coefficient, subscripts '*a*', '*c*', '*s*' and '*r*' stand for 'anion', 'cation', 'sea' and 'brine', respectively. OCV is mainly

dependent on the membrane permselectivity and concentration gradient, and valence of the ions involved in the process. Theoretically, a potential of about 0.16 V, 0.12 V and 0.2 V can be generated from a pair of IEMs (considering a 100 % selective membranes) by mixing sea water/river water, brine/seawater and brine/brackish water, respectively.

1.3 Research milestones

The application of RE in harnessing clean energy can be viewed in two aspects;

- **Standalone applications**: this follows energy generation from mixing two salt solutions of different salinity for example from river water/seawater, seawater/brine, aqueous waste streams of different salinity and other potentially extractable solutions line ammonium bicarbonate
- **Integrated applications**: this follows hybrid application of RE with other technologies like desalination technologies (e.g. reverse osmosis and/or membrane distillation) or hydrogen technologies (e.g. alkaline water electrolysis) in the logic of process intensification.

Important advances have been noticed recently in the field of RE investigations. Various areas have been covered: process analysis and optimization [9, 27-34], improvements in stack design [35-39], membrane design and development [40-44], fouling investigations [45, 46] and process modelling and simulations [47-49]. Besides, its worthy to mention applications of RE for other feed resources like sulphate bearing industrial effluents and thermolytic solutions for closed loop applications [50, 51]. Promising progress have also been noticed regarding the hybrid applications of RE in desalination technologies [13, 52-55], bioelectrochemical systems [56-58] and hydrogen technologies [57, 59] in the logic of process intensification.

1.3.1 Stack design

Component wise, the design of RE stack is more or less similar to electrodialysis stack, however with the main difference lying in the operational principle. In the course of RE research, improvements have been made with respect to stack design for better performance. Development of stacks with ion conductive spacers [37], profiled membranes [35, 42], capacitive electrodes [36] and segmented electrodes [60] are worthy to mention. Various flow modes like cross flow and co-flow [28, 60], and performances of pilot scale plants have been tested so far [14, 60, 61].

The main advantage of using ion conductive spacers is the reduction of Ohmic losses due to the spacer shadow effect. Długołecki *et al.* (2010) prepared ion conductive spacers by cutting commercial membrane materials of CMX and AMX (Tokuyana, Japan) using a press and a mould with the desired geometry as shown in Figure 1.5 [37]. Two different configurations were tested: placing the cation/anion conductive part of the spacer over the CEM/AEM (normal configuration) or cation/anion conductive part of the spacer over the AEM/CEM (reverse configuration). Overall, a significant reduction (about 2-fold compared to the use of non-conductive spacers) in internal resistance is observed by the use of ion conductive spacers, however, with the effect being much lower for the case of reverse configuration. This directly led to an increase in power density for the stacks with ion conductive spacers by a factor of 3-4 compared to the use of non-conductive spacers with similar geometry [37].

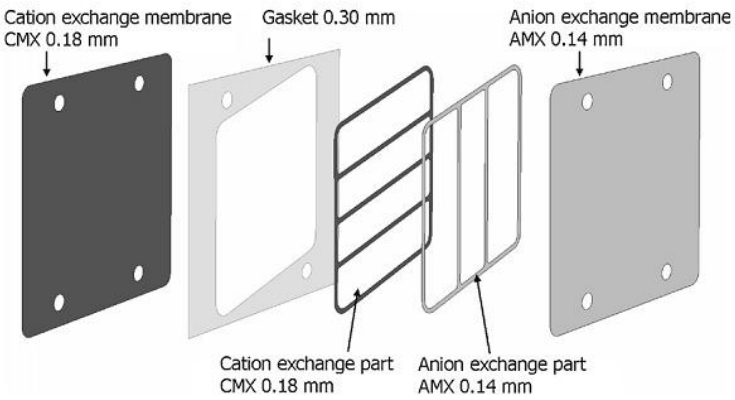

Figure 1.5. Preparation of ion conductive spacers from IEMs and placement in the stack for performance tests [37].

Another strategic design to reduce the spacer shadow effect in RE is the use of profiled membranes. Vermaas *et al*. (2014) prepared profiles on one side of membranes in the form of ridges (about 200 μm in height and width) by hot pressing [35]. Membrane profiles can also be made in other designs like pillars and wave structures [42]. The SEM image of this kind of membranes is presented in Figure 1.6. Such stack designs with profiled membranes showed a significant reduction in stack resistance, however, accompanied with a slight decrease of membrane permselectivty and increase in boundary layer resistance [35].

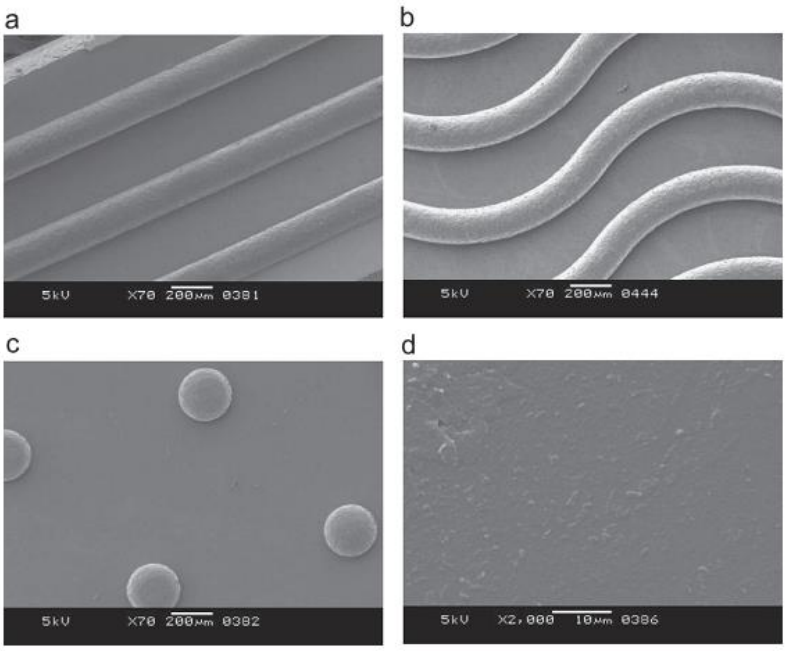

Figure 1.6. SEM images of surface morphology of tailor made membranes designed in a) ridges b) waves c) Pillars and d) flat membranes [42].

The use of capacitive electrodes to create a novel system named as "capacitive RE (CRED)", has been demonstrated to have a much higher power densities than that obtained previously for capacitive electrode systems i.e in capacitive mixing (CAPMIX) [36]. In CPMIX, seawater and river water flow subsequently through a compartment with capacitive electrodes (activated carbon supported by Ti/Pt mesh) on either side of the compartment: positively or negatively charged ions can be stored in the large pore area available in the electrodes when seawater flows (charging) and when seawater is replaced by river water, ions move out from the electrodes (discharging). A net charge transport is created using ion exchange membranes or an electric field. Thus, an electrical current is generated by the charge accumulation on the capacitive electrodes when ion exchange membranes are placed between the electrodes or even without membranes [21, 62]. In CRED system, AEMs and CEMs are alternatively aligned to create two compartments like a RE system. Since capacitive electrodes systems do not require redox reactions, NaCl solution can be used as an electrode rinse solution. Thus, the selective transport of ions driven by the concentration gradient induces a potential difference over each membranes and hence an electrical current in the external circuit. CRED can be operated in cyclic stages where electricity is generated during mixing of the salt water and fresh water, and ions are stored in the large pore surface area of the activated carbon when switching the feed solutions. Here, longer

switching intervals leads to reduced time of the periods without power production which intern has an advantage in terms of average power density [36]. The main advantage of CRED is a synergetic combination of the CAPMIX and RE thus expected to generate more power, benefit in terms of safety (no redox reaction) and economical attractiveness. In general, sufficient power density is obtained by CRED although a bit lower compared to the conventional RE systems working with $Fe(CN)_6^{3-/4-}$ as periodic switching of feed water is not required. Environmental benefit obtained from the exemption of using potentially hazardous $Fe(CN)_6^{3-/4-}$ electrode rinse solutions is another advantage.

Incorporations of segmentation of electrodes in a RE system could also be beneficial in terms of performance. Up to 11% more power output was obtained by triple segmentation of electrodes compared to using a single electrode [60] whereas energy efficiencies of more than 80% have been recorded for segmented electrodes, quite higher than a case of single electrode (~53%) [28].

RE designs with different flow modes could also have a direct contribution to its performance in terms of power density and energy efficiency. Various flow modes are possible in RE: counter-flow, co-flow and cross-flow as shown in Figure 1.7 In many processes, counter-flow operation is more efficient due to its higher driving force. However, the case is a bit different for RE as demonstrated by Vermaan *et al*. (2010) who tested large scale RE stacks (25×75 cm^2 active area) for the efficiency in terms of co-flow and counter-flow operational modes [60]. Higher electrical output was obtained when operating in co-flow mode. In co-flow mode, the Nernst potential is maximum near the inlet while minimum near the outlet, however, with the conductivity of the law concentration solution following the reverse trend near the inlet and outlet. This results in almost a constant power density along the flow channel. In the case of counter flow, stack deformation is expected due to the pressure differences of the fresh water and salt water compartments which results in an increase of hydrodynamic losses and hence performance losses. Thus, RE designs with in co-flow mode will have a huge advantage in terms of economics as well as efficiency since optimal hydrodynamics avoids leakage in the manifolds and allow an opportunity to use very thin low resistance membranes [60]. On the other hand, Vermaas *et al.* (2013) compared the energy extraction efficiencies the three flow modes in RE stack both with single and multiple electrodes pairs (segmentation) [28]. They observed that the energy efficiency in the case of counter-flow is higher than that of cross-flow at about 0.15 fraction of salt water,

whereas the co-flow mode is observed to be less efficient (2-fold lower). The counter-flow mode allows non-zero local electromotive force along the flow channels as the outflow positions are aligned oppositely enabling efficient utilization of salinity difference. Ohmic losses are also higher in the case of co-flow mode compared to other operational modes. Moreover, electrode segmentation is observed to increase the energy efficiency further compared to the use of single electrodes in all flow modes.

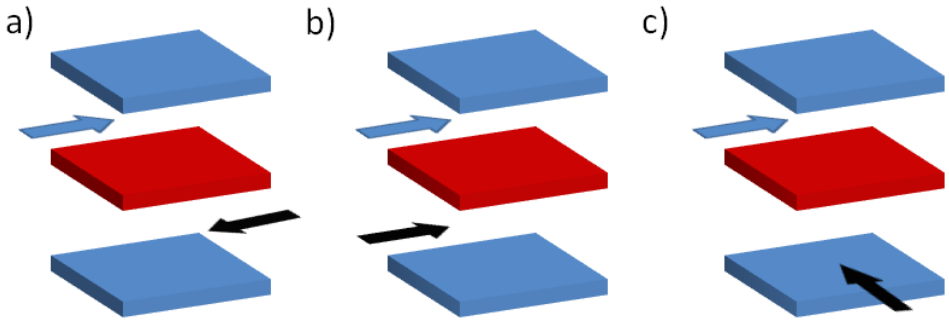

Figure 1.7. RED designs with different flow modes across ion exchange membranes: a) counter- flow b) co-flow and c) cross-flow.

1.3.2 Membrane development

Recently, membrane design and development projects for RE have been carried out on a lab-scale and pilot-scale operations. The first tailor made membranes for lab-scale RE were tested by Guler *et al*. (2012) [63]. They reported a power density of 1.27 W/m^2 for RE using homogenous AEM based on polyepichlorohydrin active polymer backbone and ion exchange functional groups based on tertiary diamine (1,4-diazabicyclo [2.2.2]octane, DABCO). In addition, they showed that the performance of tailor made membranes was better than that of commercially available membranes in most cases [64]. Membranes based on other materials for example porous nanocomposite cation exchange membranes with inorganic functional groups have also been prepared and tested for RE applications [43, 44]. In the phase inversion preparation protocol, the membrane with a blend ratio of 0.7%wt Fe_2O_3-SO_4^{2-} having a thickness of 300 μm resulted in the highest power density of 1.4 W/m^2 [44].

In an attempt to solve problems related to the spacer shadow effects, profiled membranes have been designed for RE applications. Compared to classical stacks using non-conductive ion spacers, RE stacked equipped with profiled membranes showed up to 30 % reduction in internal resistance and 25 % reduction in hydrodynamic losses [35]. Furthermore, tailor-made micro-

structured anion exchange membranes have been prepared in three different forms (ridges, waves and pillars) by casting and solvent evaporation methods [42]. After electrochemical characterization, performance testes in RE stacks indicated the highest power density (up to 0.6 W/m^2) for membranes with pillar profiles.

A company working close to the development of RE specific IEMs is Fujifilm Europe B.V. (The Netherlands). IEMs are prepared for tests done using RE stacks designed by the REDstack B.V. (The Netherlands), a company participating in the blue energy project of the European Centre of Excellence for Sustainable Water Technology (Wetsus). This companies were both involved in an EU-FP-7 funded REAPower project (www.reapower.eu) which aims in optimization of RE for power generation using concentrated brines in order to overcome problems related to Ohmic losses when using low concentration salt solutions like river water [65]. Interesting outcomes from this project involve optimization of a RE stack equipped with Fuji membrane for better hydrodynamics [47, 66] as well as experiments and modelling for feasibility of scaled-up applications [14, 48]. Recently, Tufa *et al*. (2014) reported a power density of 1.5 W/m^2 for a RE stack equipped with Fuji membranes specifically designed for RE applications and operated using concentrated brine and brackish water. The performance can further be enhanced by working at higher temperatures: a power density up to 4 W/m^2 was obtained when working at 40 ^oC using similar membranes operated with concentrated brine and brackish water [14].

1.3.3 Fouling in RE

Although RE is less susceptible to fouling phenomenon, there is still concern in relation to performance of RE under natural conditions. Generally, fouling may occur due to accumulation of biofilms formation in the stack, clogging of particles in the spacer and membrane surface, accumulation of organic components on membrane surface, alteration of performance due to the presence of multivalent ions or charged organic species and scaling of sparingly soluble salts may occur in RE, particularly when operated with concentrated brine. The consequences of fouling is mainly an increase in pressure drop in RE and loss in performances attributed to damage on membrane during operations over a long period of time. On the other hand, this will limit the feasibility of the process due to an increased costs for maintenance and chemical usage, as well as the energy demand attributed to the pretreatment procedures. This will be highly useful for clarity of the required economic Figures in RE process.

Literatures investigating the fouling phenomenon in RE are quite limited. Systematic study

of the effect of biofouling and its mitigation strategies have been demonstrated by Post *et al*. (2009) [46]. The feed stream was dosed by concentrated solution of biodegradable compounds to promote microbial growth using appropriate acetic carbon, together with phosphate and nitrate in appropriate amounts. Here, the total organic carbon (TOC) determination was used to estimate the amount of biomass. The biofilm is accumulated over the spacers more of near the inlet than the outlet. Results indicate an increase in pressure drop over the river compartment after 8 days. The effect is seen a bit later (5 more days) on the seawater compartment. Later on, the pressure drop was increasing exponentially with time. This rapid increase of pressure drop and membrane degradation by the microorganism composing biofilms is also accompanied by the decline in OCV. Furthermore, membrane degradation and insulating effect of fouled spacers directly result in an increase of Ohmic losses. Post *et al.* (2009) propose periodical reversal of feed streams thereby changing the polarity of the stack as control strategy in prevention of the fouling, a strategy mostly used in electrodialysis. This was demonstrated by an increase in the delay period (14 days) before the rise of pressure-drop for the stack with periodic reversal of every 24 hours [46]. In addition, the delay period can further be increased (up to 17 days) by using shorter reversal time (every hour). Periodic reversal also accounts for the stability of the OCV and decrease in Ohmic losses. Periodic reversal with flow direction can further increase the performance due to the difference in distribution of biofilms near the inlet and outlet of the stack compared to the reversal without change in flow directions.

In addition to biofouling, other kind of fouling due to colloids and organics as well as scaling may also be expected in RE process. Although the study of these type of fouling in RE is quite limited, previous investigations on electrodialysis [67, 68] indicate the requirement of control strategies for better process performance. These are all relevant to operations of RE under natural conditions. Vermaas *et al.* (2013) was the first to operate a RE stack under natural conditions to see the effect of various fouling expected to occur during operations over a longer period to time. They compared three different stack designs: a stack with flat ion exchange and spacers, a stack equipped with profiled membranes without spacers and a stack with profiled non-conductive plastic sheets without spacers. The stacks were fed with natural sea water and fresh water continuously after only microfiltration (20 μm). As shown in Figure 1.7a, the pressure drop in the stacks with spacers increased rapidly (5 days) to the maximum value (~1.5 bar) whereas the stacks with profiled membranes shows a slow (20 days) rise in pressure to the maximum value. This is

attributed to the fact that the smooth and parallel channels due to profiled membrane reduces the adhesion of colloids and particulates compared to the stack with woven spacers having crosswise filaments and knits that leaves only small openings for the feed water flow and easy trap of colloids and particulates [45]. This effect was even much slower (23 days) for the stack with profiled plastic sheets due to reduced effect of charged colloids and other species in this case. With respect to the power density, the stack with profiled membranes performs better than the stack with spacers (see Figure 1.8b). The decrease in power density is much faster than the pressure drops since other effects also come into account in this case for example effect organic fouling, preferential channelling or deposits of particulates that could enhance the Ohmic losses (see Figure 1.8c) as a result of the partial coverage of the ion conductive part of IEMs. The reduced effective surface charge of the membranes and hence limitation of the ion transport is the cause for the decrease of both perm-selectivity and Ohmic resistance. Vermaas *et al.* (2013) have pointed out that periodical switching of the electrical current direction, application of short electrical pulses in opposite direction and chemical modification of membrane surface by high molecular weight surfactants as control strategy to reduce the effect of fouling on RE performance [45].

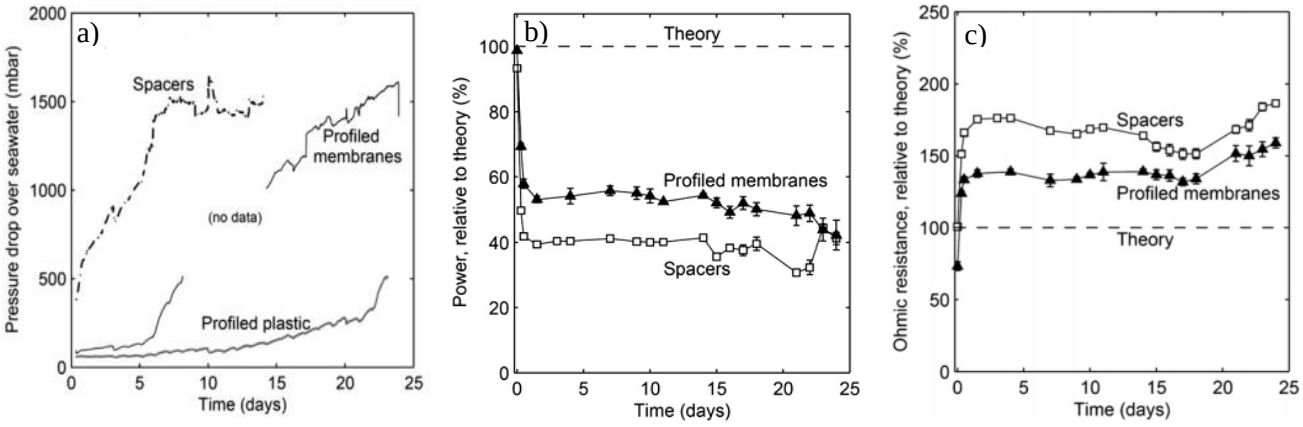

Figure 1.8. Variation of a) pressure drops over the seawater compartments b) power densities and c) Ohmic resistances with time for different stack designs operated under natural conditions [45].

Membrane modification was also investigated as one strategy to reduce the fouling in RE. Guler *et al.* (2012) made an attempt to coat RE specific membranes and some commercial membranes using UV irradiation method [41]. Coating layer used was formed by copolymerization of 2-acryloylamido-2-methylpropanesulfonic acid (AMPS) as the active polymer and N, N-methylenebis (acrylamide) (MBA) as the cross linker. The SEM image and surface roughness

determinations of some of these membranes are presented in Figure 1.9. Such membranes with a negatively charged coating retained increased hydrophilicity and sufficient antifouling potential against organic foulants [41].

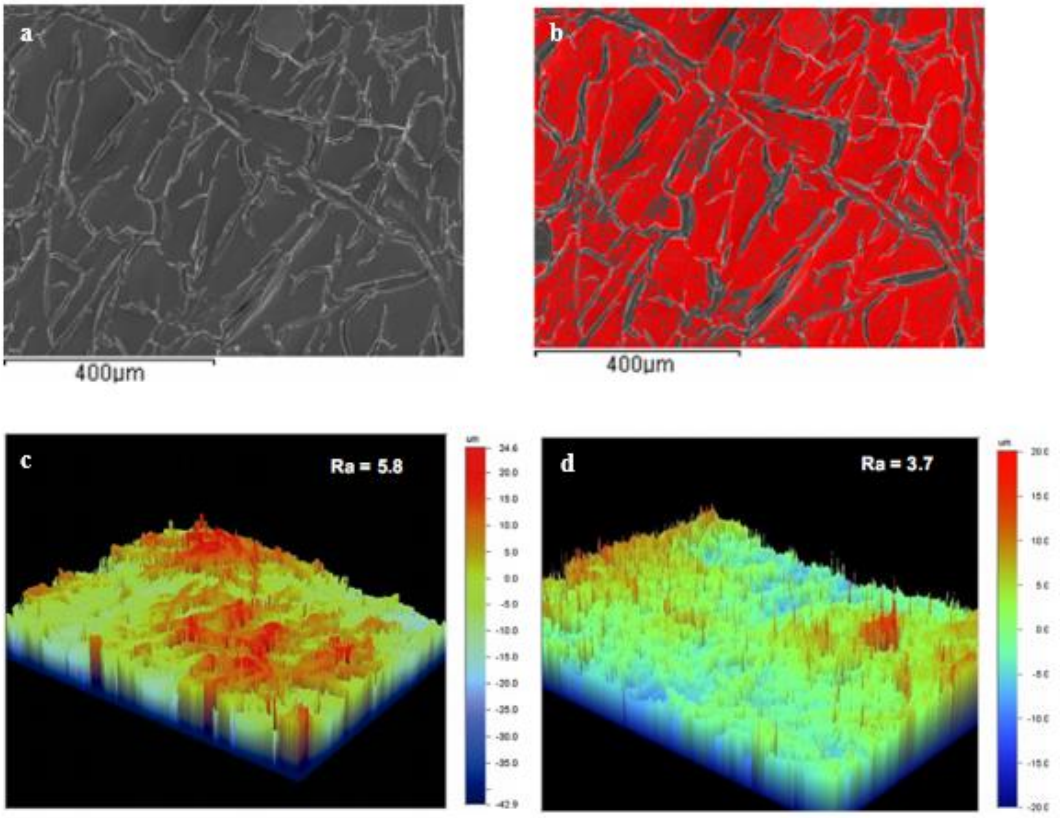

Figure 1.9. i) EDX element mapping SEM images of a) membrane surface and (b) overlay of sulfur map on SEM image (red dots representing sulfur-containing areas) for modified Fuji membranes; ii) optical interferometry images for surface roughness of membranes: (c) original Fuji membrane and (d) modified Fuji membranes (dimensions of the membranes: 1257x942 mm)[41].

1.3.4 Power densities

Results from early stage RE optimization were not satisfactory mainly related to the inadequacy in membrane and stack design. For example, tests performed by Turek and Bandura (2007) on a RE stack operating with concentrated brine and river water resulted in a low power density (up to 0.4 W/m^2) which could be attributed to the extremely low working area enhancing ionic shortcut currents [33]. From 2009 onwards, power densities were significantly improved.

Vermaas *et al.* (2011) reported a power density of 1.2 W/m^2 for a RE operated with seawater/river water. At ambient experimental conditions, the maximum power density was reported by Vermaas *et al.* (2011) using a RE stack equipped with special membranes designed

for low resistance (based on modification of Fumatech membranes, Germany) [30]. Their test on seawater/river water resulted in maximum power density of 2.2 W/m^2 which is the maximum value reported so far.

However, the technological challenge when using river water and seawater for RE is the Ohmic losses over the LCC. In order to overcome this, the use of highly concentrated solutions like brine is a promising way. The EU-FP7 REAPower (Reverse Electrodialysis Alternative Power Production) was particularly devoted for material and stack design and development in order to minimize such losses and enhance the output power as pointed earlier. It has been shown that there is a possibility of reducing the Ohmic losses by up to 50%, when using concentrated brine and brackish water instead of seawater and river water [29]. In addition, power densities were also increased by increasing the temperature under high salinity gradient conditions (use of concentrated brine). In a recent investigation, Tedesco *et al*. (2015) reported a power density of 6 W/m^2 at 40 ^oC from mixing brine (0.5 M NaCl) and brackish water (0.1 M NaCl)[14]. Moreover, Daniilidis *et al.* (2014) reported a power density up to 6.7 W/m^2 at 60 ^oC from mixing brine (5 M NaCl) and river water (0.01 M NaCl)[69]. Although these values are higher compared to previous determinations, exergy-energy and economic analysis is required for scale-up and commercialization of the process. Table 1.1 summarizes the power densities reported so far for applications of RE in different scenarios: from mixing river water and seawater (part I) and from mixing brine and brackish, river, or seawater (part II).

Table 1.1. Summary of literatures on RE for potential application in harnessing SGP.

Part I- mixing of seawater and river water

Topics covered	**Focus point**	**Membranes**			**N**	**Spacers (thickness, µm)**	**Redox couple**		$P_{d,max}$, **(W/m^2)**	**Ref.**
		Type	**single active area (cm^2)**	**thickness (µm)**			**Electrolyte**	**Electrode**		
Fouling	Effect fouling on power production using different RE designs and potential mitigation strategies	Ralex CMH/AMH(MEGA AS, Czech Republic)	10x10	700-714	5	Woven (245)	0.05 M $K_3Fe(CN)_6$, 0.05 M $K_4Fe(CN)_6$ and 0.25 M NaCl	Ti/Pt mesh	0.05-0.08	[45]
		Profiled Ralex CMH/AMH(MEGA AS, Czech Republic)	10x10	477±15	5	Spacerless	0.05 M $K_3Fe(CN)_6$, 0.05 M $K_4Fe(CN)_6$ and 0.25 M NaCl	Ti/Pt mesh	0.11-0.14	[45]
	Effect of preferential channelling on output power	Profiled Ralex CMH/AMH, (MEGA AS, Czech Republic)	10x10	477±15	5	Spacerless	0.05 M $K_3Fe(CN)_6$, 0.05 M $K_4Fe(CN)_6$ and 0.25 M NaCl	Ti/Pt mesh	0.62 ~0.32***	[70]
Flow hydrodynamics	Effect of cell number on pressure drop	Ralex CMH-PES/AMH-PES, (MEGA AS, Czech Republic)	64	700-714	5	Non-conductive (485)	-	Ti coated with Pt	0.5	[71]
	Reduction of pressure drops by varying the flow rate of HCC and LCC solutions	PC-SK and PC-SA (PCCell, Germany)	8x8	90-130	10	Non-conductive (500)	~0.6 M NaCl	Ti coated with Pt	0.28	[34]
Feed quality/ion transport	Effect of multivalent ions (Mg^{2+}, SO_4^{2-}) on RE performance	Ralex CMH/AMH, (MEGA AS, Czech Republic)	10x10	<725	5	Woven (200)	0.05 M $K_3Fe(CN)_6$, 0.05 M $K_4Fe(CN)_6$ and 0.25 M NaCl	Ti-Ru/Ir mesh	~0.26 (10 % $MgSO_4$ in feed)	[27]
		Neosepta AMX/CMX (Tokuyama Inc., Japan)	10x10	155	5	Woven (200)	0.05 M $K_3Fe(CN)_6$, 0.05 M $K_4Fe(CN)_6$ and 0.25 M NaCl	Ti-Ru/Ir mesh	~0.42 (10 % $MgSO_4$ in feed)	[27]

Table 1.1. (Continued)

Feed quality/ion transport	Effect of multivalent ions (Mg^{2+}, SO_4^{2-}) on RE performance	Fuji AEM/CEM, (Fujifilm Europe B.V., The Netherlands)	10x10	125	5	Woven (200)	0.05 M $K_3Fe(CN)_6$, 0.05 M $K_4Fe(CN)_6$ and 0.25 M NaCl	Ti-Ru/Ir mesh	~0.5 (10 % $MgSO_4$ in feed)	[27]
Stack design, testing, analysis and optimization	Effect of feed concentration on performance	Neosepta ACS/CMS (Tokuyama Inc., Japan)	10x10	120-200	5	Woven (100)	0.1 M $K_3Fe(CN)_6$, 0.1M $K_4Fe(CN)_6$ and 0.5 M NaCl	Ti-RuO_2/IrO_2	3.8	[69]
	Comparison of small scale and large scale stacks in different flow mode (co-current counter-current)	FumasTech FAD/FKD (GmbH, Germany)	10x10	82	50	Woven spacers (200)	0.05 M $K_4Fe(CN)_6$, 0.05 M $K_3Fe(CN)_6$ and 0.25 M NaCl	Ti-RuO_2/IrO_2	6.7 (60 ºC), 0.71**	[60]
		Qianqiu AEM/ CEM, (Hangzhou Qianqiu Industry Co, China)	25x75	205-294	25	Woven spacers (200)	0.05 M $K_4Fe(CN)_6$, 0.05 M $K_3Fe(CN)_6$ and 0.25 M NaCl	Ti-RuO_2/IrO_2	0.4**	[60]
	Evaluation of thermodynamic efficiency in RE as a function losses due to co-ion transport, osmosis and Ohmic resistances for different commercial membranes	Fumasep FKD and FAD (Fumatech, Germany)	10x10	40-80	25	Woven spacers (200)	~0.25 M NaCl	Ti-RuO_2/IrO_2	1.17	[32]
			10x10	82	50	Woven spacers (200)	0.05 M $K_4Fe(CN)_6$, 0.05 M $K_3Fe(CN)_6$ and 1 M NaCl	Ti-RuO_2/IrO_2	0.93	[9]
		Qianqiu Heterogeneous AEM/CEM (Hangzhou QianQiu Industry Co., China)	10x10	40-80	5	Woven spacers (200)	~0.25 M NaCl	Ti-RuO_2/IrO_2	0.49	[32]
		Qianqiu Homogeneous AEM/CEM (Hangzhou QianQiu Industry Co., China)	10x10	40-80	5	Woven spacers (200)	~0.25 M NaCl	Ti-RuO_2/IrO_2	1.05	[32]
		Selemion AMV/CMV (Asahi Glass, Japan)	10x10	110-150	5	Woven spacers (200)	~0.25 M NaCl	Ti-RuO_2/IrO_2	1.18	[32]
		Neosepta ACS/CMS (Tokuyama Co., Japan)	10x10	120-200	5	Woven spacers (200)	~0.25 M NaCl	Ti-RuO_2/IrO_2	0.60	[32]
		Neosepta AMX/CMX (Tokuyama Co., Japan)	10x10	134-164	5	Woven spacers (200)	~0.25 M NaCl	Ti-RuO_2/IrO_2	0.65	[32]

Table 1.1. (Continued)

Stack design, testing, analysis and optimization	Power optimization	AEM-103QZL and CEM-61CZL (Ionics, Inc.)	232	560-700	30	Turbulence promoter (1000)	-	-	0.17	[72]
	Reduction of the spacer shadow effect by ion conductive spacers	Neosepta AMX/CMX (Tokuyama Co., Japan)	10x10	134-164	4	Ion conductive AMX/CMX (320)	0.5 M NaCl	$Ti\text{-}RuO_2/IrO_2$	~0.8	[37]
	Characterization of concentration polarization, spacer shadow effects and stack resistance	Neosepta AMX/CMX (Tokuyama Co., Japan)	100	138 ± 2 for AMX and 181± 2 for CMX	3	Woven (200)	0.5 M NaCl	$Ti\text{-}RuO_2/IrO_2$	0.87	[31]
		Neosepta CMX/AMX (Tokuyama Co., Japan)	100	138 ± 2 for AMX and 181± 2 for CMX	3	Woven (485)	0.5 M NaCl	$Ti\text{-}RuO_2/IrO_2$	0.56	[31]
	Optimization of intermembrane distance and flow velocity	FumaTech FKS/FAS (Germany)	10x10	30-40	5	Woven (60)	0.025 M $K_3Fe(CN)_6$, 0.025 M $K_4Fe(CN)_6$ and 0.25 M NaCl	$Ti\text{-}RuO_2/IrO_2$	1.8	[30]
		FumaTech FKS/FAS (Germany)	10x10	30-40	5	Woven (100)	0.025 M $K_3Fe(CN)_6$, 0.025 M $K_4Fe(CN)_6$ and 0.25 M NaCl	$Ti\text{-}RuO_2/IrO_2$	2.2	[30]
		FumaTech FKS/FAS (Germany)	10x10	30-40	5	Woven (200)	0.025 M $K_3Fe(CN)_6$, 0.025 M $K_4Fe(CN)_6$ and 0.25 M NaCl	$Ti\text{-}RuO_2/IrO_2$	1.25	[30]
		FumaTech FKS/FAS (Germany)	10x10	30-40	5	Woven (485)	0.025 M $K_3Fe(CN)_6$, 0.025 M $K_4Fe(CN)_6$ and 0.25 M NaCl	$Ti\text{-}RuO_2/IrO_2$	0.5	[30]
Membrane development and characterization	Testing performance and monovalenet selectivity of commercial ion exchange membranes after modification	Neosepta CMX (Tokuyama Co., Japan), modified Fuji AEMs (Fujifilm Europe B.V., The Netherlands)	10x10	120-124	3	Woven (200)	0.05 M $K_3Fe(CN)_6$, 0.05 M $K_4Fe(CN)_6$ and 0.25 M NaCl	Ti-Ru/Ir	0.91-1.01	[41]
		Neosepta CMX (Tokuyama Co., Japan), modified Neosepta ACS (Tokuyama Co., Japan)	10x10	134-164	3	Woven (200)	0.05 M $K_3Fe(CN)_6$, 0.05 M $K_4Fe(CN)_6$ and 0.25 M NaCl	Ti-Ru/Ir	0.79-0.85	[41]

Table 1.1. (Continued)

Membrane development and characterization	Use of profiled/ microstructured membranes for reduction of Ohmic losses by comparison of performances with flat-sheet membranes	Ralex CMH-PES/AMH-PES (MEGA, Czech Republic)	5x5	580±25*	5	Normal spacer (143)	0.05 M $K_3Fe(CN)_6$, 0.05 M $K_4Fe(CN)_6$ and 0.25 M NaCl	Ti/Pt mesh	~6.2	[73]
		Ralex CMH-PES/AMH-PES (MEGA, Czech Republic)	5x5	580±25*	5	2 layer, twisted spacers (64)	0.05 M $K_3Fe(CN)_6$, 0.05 M $K_4Fe(CN)_6$ and 0.25 M NaCl	Ti/Pt mesh	~0.65	[73]
		Profiled - Ralex CMH-PES/AMH-PES (MEGA, Czech Republic)	5x5	477±15* (excluding ridges)	6	No spacer	0.05 M $K_3Fe(CN)_6$, 0.05 M $K_4Fe(CN)_6$ and 0.25 M NaCl	Ti/Pt mesh	~0.95	[73]
		Sub-corrugated Profiles - Ralex CMH-PES/AMH-PES (MEGA, Czech Republic)	5x5	520±20* (excluding profiles and sub-corrugations)	6	No spacer	0.05 M $K_3Fe(CN)_6$, 0.05 M $K_4Fe(CN)_6$ and 0.25 M NaCl	Ti/Pt mesh	~0.82	[73]
		Profiled - Ralex CMH-PES/AMH-PES (MEGA, Czech Republic)	5x5	510±15 for profiled Ralex CMH-PES 475±10 profiled Ralex AMH-PES (excluding ridges)	5	No spacer	0.05 M $K_3Fe(CN)_6$, 0.05 M $K_4Fe(CN)_6$ and 0.25 M NaCl	Ti/Pt mesh	~0.80	[35]
		Neosepta CMX (Tokuyama Co., Japan), microstructured (Pillar) PECH AEM	10x10	200	3	Woven (100)	0.05 M $K_3Fe(CN)_6$, 0.05 M $K_4Fe(CN)_6$ and 0.25 M NaCl	Ti/Ir-Ru	1.3	[42]
		Neosepta CMX (Tokuyama Co., Japan), microstructured (waves) PECH AEM	10x10	200	3	Woven (100)	0.05 M $K_3Fe(CN)_6$, 0.05 M $K_4Fe(CN)_6$ and 0.25 M NaCl	Ti/Ir-Ru	~1.25	[42]

Table 1.1. (Continued)

Membrane development and characterization		Neosepta CMX (Tokuyama Co., Japan), microstructured (ridges) PECH AEM	10x10	200	3	Woven (100)	0.05 M $K_3Fe(CN)_6$, 0.05 M $K_4Fe(CN)_6$ and 0.25 M NaCl	Ti/Ir-Ru	~1.15	[42]
		Neosepta CMX (Tokuyama Co., Japan), Flat PECH AEM	10x10	200	3	Woven (100)	0.05 M $K_3Fe(CN)_6$, 0.05 M $K_4Fe(CN)_6$ and 0.25 M NaCl	Ti/Ir-Ru	~0.85	[42]
	Comparison of performance of tailor made and commercial membranes	Neosepta CMX/AMX (Tokuyama Co., Japan)	10x10	134-164	5	Woven (100)	0.05 M $K_3Fe(CN)_6$, 0.05 M $K_4Fe(CN)_6$ and 0.25 M NaCl	Ti/Ir-Ru	1.07	[64]
		Tailored SPEEK65/PECH B2	10x10	53-77	5	Woven (100)	0.05 M $K_3Fe(CN)_6$, 0.05 M $K_4Fe(CN)_6$ and 0.25 M NaCl	Ti/Ir-Ru	1.18	[64]
	Performance of porous inorganic-organic nano composite ion exchange membranes: Effect of inorganic nanopartile loading	AEM (Selemeim® ASV), tailored nanocomposite CEM (0.7 wt% blend ratio of Fe_2O_3, SO_4^{2-})	4x9	30-120	3	Woven (250)	0.05 M $K_3Fe(CN)_6$, 0.05 M $K_4Fe(CN)_6$ and 0.25 M NaCl	Ti-Ir plasma	~0.85	[44]
Modelling and simulation	Modelling the power generated by RE to study the effect of monovalent and multivalent ions (NaCl + $MgCl_2$)	FumaTech FKB/ FAB (Germany)	4x9	90-115	10	Woven (500)	0.003 M NaCl	Ti-Ir plasma	~0.8	[74]

Table 1.1. (Continued)

Modelling and simulation	Modelling power generated by RE to study the effect of monovalent and multivalent ions (NaCl + Na_2SO_4)	FumaTech FKB/ FAB (Germany)	4x9	90-115	10	Woven (500)	0.003 M NaCl	Ti-Ir plasma	~0.75	[74]
	Modelling power generated by RE to study the effect of monovalent and multivalent ions (NaCl + $MgSO_4$)	FumaTech FKB/ FAB (GmbH, Germany)	4x9	90-115	10	Woven (500)	0.003 M NaCl	Ti-Ir plasma	~0.5	[74]
New design	Use of capacitive electrodes	Neosepta CMX/AMX (Tokuyama Co., Japan)	10x10	134-164	2-30	Woven (200)	0.25 M NaCl	Capacitive electrodes; Ti mesh coated Pt and a layer of activated carbon and PVDF	~0.95	[36]

*Wet membrane thickness; **Net power density; ***Value obtained at 30 % feed channel blockage

II- mixing of brine and seawater, river water or brackish water.

Topics covered	**Focus points**	**Membranes**			**N**	**Spacers (δ, μm)**	**Redox couple**		**P_d (W/m^2)**	**Ref.**
		Type	**A (cm^2)**	**δ, (μm)**			Electrolyte	Electrode		
Performance analysis and testing	Potential of coal-mine brine (2 M NaCl) and river water	Neosepta AMX/CMX (Tokuyama Co., Japan)	4	134-164	4	Non-conductive (190)	~0.035 M Na_2SO_4	Ti coated with Pt	1.18	[75]
	Comparison of performance under pure NaCl feed solutions and artificial brackish water/solar pond brine feed solutions	Fuji AEM/CEM (Fujifilm Europe B.V., The Netherlands)	10x10	109-170	25	Woven (270)	0.3 M $K_3Fe(CN)_6$, 0.3 0.3 M $K_4Fe(CN)_6$ and 2.5 M NaCl	Ti–Ru/Ir mesh	1.5 (LCC: brackish water)	[29]
	Effect of feed concentration on performance	Neosepta ACS/CMS (Tokuyama Inc., Japan)	10x10	120-200	5	Woven (100)	0.1 M $K_3Fe(CN)_6$, 0.1M $K_4Fe(CN)_6$ and 0.5 M NaCl	Ti-RuO_2/IrO_2	~1.5 (LCC: sea water) ~2.25 (LCC: brackish water) ~6.7 (60 ºC; LCC: river water)	[69]
	Effect of main operating conditions on output power of RE stacks constructed in different size	Fuji AEM/CEM (Fujifilm Europe B.V., The Netherlands)	10x10	120	50	Woven (270)	0.1 M $K_3Fe(CN)_6$, 0.1M $K_4Fe(CN)_6$ and 2.5 M NaCl	Ti-RuO_2/IrO_2	4 (40 ºC; LCC: brackish water)	[14]
		FumaTech FAS/ FKS (GmbH, Germany)	10x10	20	50	Woven (270)	0.1 M $K_3Fe(CN)_6$, 0.1M $K_4Fe(CN)_6$ and 2.5 M NaCl	Ti-RuO_2/IrO_2	6 (60 ºC; LCC: brackish water)	[14]
		Fuji AEM/CEM (Fujifilm Europe B.V., The Netherlands)	20x20	120	100	Woven (270)	0.1 M $K_3Fe(CN)_6$, 0.1M $K_4Fe(CN)_6$ and 2.5 M NaCl	Ti-RuO_2/IrO_2	~3.4 (40 ºC; LCC: brackish water)	[14]
Modelling and simulation	Modelling the influence of main operational factors (flow velocity, feed concentration and temperatures) on performance	Fuji AEM/CEM (Fujifilm Europe B.V., The Netherlands)	10x10	120	50	Woven (270)	0.1 M $K_3Fe(CN)_6$, 0.1M $K_4Fe(CN)_6$ and 2.5 M NaCl	Ti-RuO_2/IrO_2	~2 (LCC: seawater)	[48]
	Modelling for optimal stack design	Fuji AEM/CEM (Fujifilm Europe B.V., The Netherlands)	10x10	120	50	Woven (270)	0.1 M $K_3Fe(CN)_6$, 0.1 M $K_4Fe(CN)_6$ and 2.5 M NaCl	Ti-RuO_2/IrO_2	~2.5 (40 ºC; LCC: brackish water)	[76]

1.4 Hybrid approaches: process intensification

The concept of hybrid application in the logic of process intensification will be of a great importance when it comes to simultaneous generation of green energy and potable water. Large part of the earth's surface (75 %) is covered with water. Thus, there is high possibility to access saline seawater and implement desalination as well as power generation by hybrid technologies. The requirement of a concentrated solution as an input system makes RE a potentially suitable technology that can be integrated with sea water desalination technologies (SWDT) like membrane distillation (MD) and reverse osmosis (RO). Moreover, integration with bio-electrochemical systems and hydrogen technologies is a promising way for process intensification with many advantages. Table 1.2 summarizes literatures on hybrid applications of RE involving desalination technologies and hydrogen technologies.

1.4.1 Integrated approach in desalination technologies

Currently, desalination of seawater and brackish water are the most viable ways of producing clean water for drinking and human consumption, representing 58.9% and 21.2% of industrial shares, respectively [77]. The total global desalination capacity is estimated to be 85.9 MCM (millions of cubic meter)/day as of 2013 with expected projection of 100 MCM/day by 2015 [78]. Considering 50% water recovery in seawater and brackish water desalination practices, for example in RO, about 12,118 MCM of brine is discharged annually [77]. Mixing this brine (assuming ~ 1 M in NaCl) with sea water (~0.5 M NaCl) has a salinity gradient energy potential of about 3.6 GJ at standard conditions. Thus, introduction of RE for integrated applications in desalinations technologies will be highly beneficial not only in terms of energy but also mitigation of environmental issues related to concentrated brine.

The integrated approach of SGP process involves direct feeding of brine concentrates from seawater desalination systems to RE system. Seawater or brackish water and concentrated discharges from desalination technologies could be mixed in the RE for SGP generation. RO brine can be directly fed to RE system or can be further concentrated by membrane distillation (MD) or solar energy in solar ponds (SP) [13, 54]. Economical advantage is gained from MD due to the possibility of using low-grade waste heat to heat up the RO brine. The use of more concentrated brine allows more efficient energy extraction since the Ohmic losses are minimized. The generated renewable energy by RE can potentially be used in powering desalination technologies and thus minimizing the energy consumption. The less saline RE effluents could be recycled back to be

used in RO or MD processes thereby avoiding environmental problems related to brine discharge. Integration of either RO or MD to a RE system can be done either separately or in a combined way depending on level of efficiency required and affordability of the system setup. Figure 1.10 shows an integrated process involving the membrane based desalination technologies and RE system.

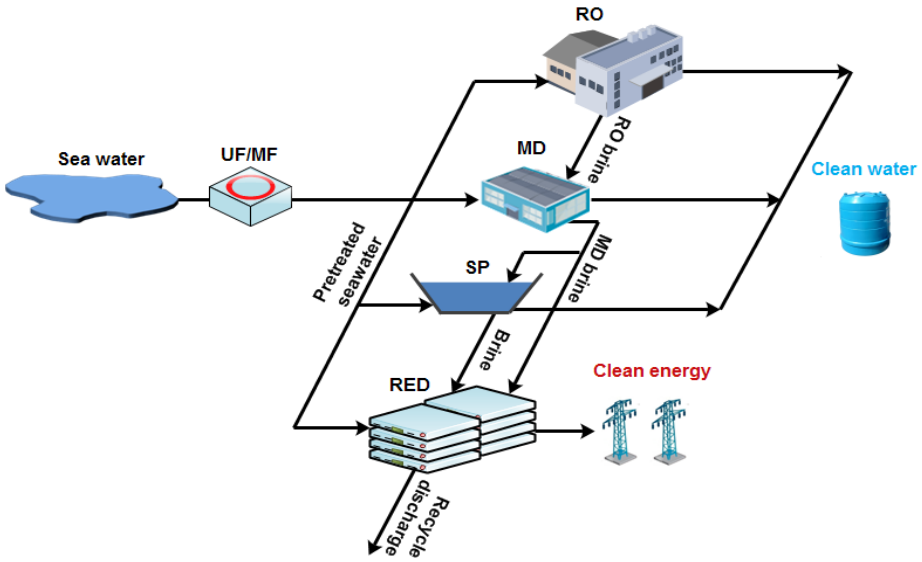

Figure 1.10. Illustration of opportunities for the applicability of RE in integrated membrane desalination technologies.

Literatures on the hybrid applicability of RE in SWDT are scarce. The application of the hybrid SWDT and a RE system for production of SGP and fresh water has been pointed out theoretically by Etienne Brauns [13, 54, 79]. Opportunities are considered from various desalination technologies potentially driven by renewable energy sources like solar energy. The use of solar energy to heat or evaporate process streams is particularly important in the hybrid system as it is abundantly available for example with a potential above 1000 W/m² per day only in the Middle East region [13]. The use of solar power will not only increase the concentration of brine discharge from other desalination units and hence their electrochemical potential, but also heating up of the feeds before consumption in RE increases the SGP output. Literatures demonstrate experimentally that the RE power output can be increased directly by increasing the feed temperatures [14, 69]. Moreover, energy requirements can also be reduced by heating up the RO feeds for high flux at lower pressures. In addition to MD which can be used for further concentration of RO brine, other alternative evaporative technologies like TVC (Thermal Vapour

Compression) and MVC (Mechanical Vapour Compression) can potentially be coupled to the hybrid system [13]. The overall benefit of the hybrid system is that the osmotic potential of brine stored as a SGP is limitless as long as the feed solutions are available for RE and this overtakes the potential over intermittent renewable energy resources like wind energy. In the meantime, the consumption of brine makes the process to approach the concept of Near-Zero Liquid Discharge.

In a specific work by Li *et al*. (2013)[52], different configurations for coupling RE with RO are proposed with the corresponding mathematical models. The investigated RE-RO configurations are presented in Figure 10. The main target was identification of the variation of energy consumption and discharge brine concentration with varying system configuration and the operating conditions. The different configurations are based on the possibility of using RE as a pre-treatment (Figure 1.11a) or a post-treatment technique for RO (Figure 1.11b). Thus, RE effluent (treated seawater) can be fed directly to RO as a low saline solution (low osmotic pressure) which leads to a lower energy consumption as a result of reduced pumping power without affecting recovery. On the other hand, the retentate from RO with higher salinity than seawater can be used as a feed solution for RE thereby enhancing the potential of SGP with simultaneous reduction of environmental threat from discharging concentrated brine. The two configurations can be cascade further for combined advantage from both systems. Considering a RE stacks (50 cells and active membrane area of 600 cm^2) in 20 parallel branches of RE network (5 RE stacks in each branch), model predictions indicate the possibility of 56 % reduction (from 1.8 kWh/m^3 to 0.8 kWh/m^3) in RO energy consumption when using RE treated sea water (RE effluent) as an RO feed [52]. A sharp increase in efficiency of RE is predicted when the RO retentate is post-treated by RE. However, experimental works are required to validate these concepts and hence achieve the realization of the hybrid process.

Recently, the applications of RE in an integrated approach with desalination technologies have also been demonstrated experimentally. Brine solutions generated from RO and FO desalination plants in combination with river water and sea water were tested for power generation by RE [53]. The maximum power density 1.86 W/m^2 was obtained by combining river water and FO brine for RE application at an intermembrane distance of 0.2 mm. In addition, the variation of output power with intermembrane distance and feed flow rate was evaluated. Decreasing the intermembrane distance by 95 % (0.01 mm) resulted in 83 % (3.4 W/m^2) increase of the maximum power density when using FO brine and river water for power generation [53]. An interesting

finding was that the use of brine for energy generations is directly linked with reduction of energy costs, 7.8% for RO at specific energy consumption of the 2.77 kWh/m^3 and 13.5% for FO at specific energy consumption of 0.84 kWh/m^3.

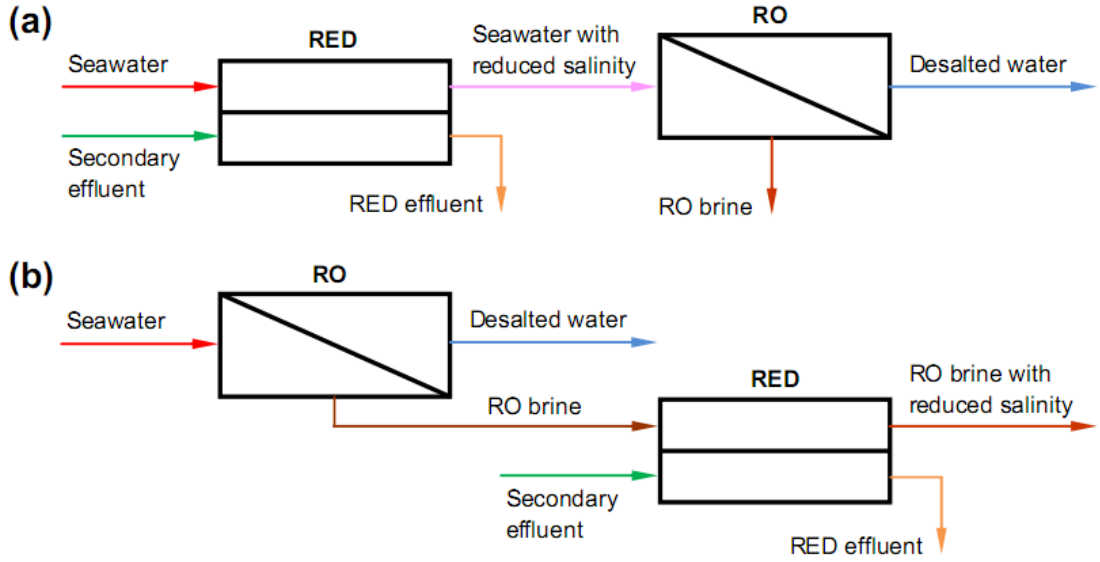

Figure 1.11. Schematic diagrams of the hybrid process involving RE and RO: (a) RE-RO configuration; (b) RO-RE configuration [52].

Among the different MD configurations, Direct Contact Membrane Distillation (DCMD); which is a simple, low cost and low energy intensive emerging desalination technology; is the most widely used technology mainly applied for desalination of seawater and brackish waters [80-84]. High quality distillate, a simple pretreatment step and low temperature requirement makes it an attractive desalination process, especially where low-grade thermal energy or solar heat sources are available. In this process, a water molecule evaporates from the hot feed solution to the cold distillate water stream separated by microporous hydrophobic membranes. Condensation of volatile molecules takes places inside the membrane module resulting in a highly concentrated hot brine as a retentate and pure water as a permeate. The driving force for the mass transfer is the vapour pressure difference across the membrane. Through a temperature controlled experiments, supersaturated brine retentate with concentration up to 6 M can be obtained by DCMD. Recently, Tufa *et al*. (2015) tested an innovative RE-DCMD system for simultaneous production of blue energy and drinking water in the logic of Near-Zero Liquid Discharge (N-ZLD) and low energy consumption in seawater RO desalination [85]. The capability of DCMD to reach a significant Volume Reduction Factor (VRF) up to 83.6% and to increase the concentration of NaCl solution

even up to saturation level (5.4 M NaCl) is demonstrated. A $P_{d,max}$ of 2.4 W/m$^2_{MP}$ was achievable when using the brine from DCMD (~5.4 M) as a HCC solution and seawater (~0.5 M) as a LCC solution. However, a thermo-economic analysis is required to find out the optimal operating conditions for both RE and DCMD for feasibility of the process.

1.4.2 Integrated approach in hydrogen technologies

Hydrogen is the most abundant element, however exclusively present as water, hydrates, in biomass as well as fossilized raw materials with only ~1% present as molecular hydrogen gas (H_2). It is considered as clean, efficient and versatile energy carrier in the near future that can address issues of energy, environment and sustainability. The chemical energy per mass of hydrogen is about 142 MJ kg^{-1}. This is larger (about 3-fold) than that of other chemical fuels like liquid hydrocarbons (47 MJ kg^{-1}) [86]. The applicability of hydrogen ranges from mobility and industries up to household and even for a grid power supply.

The two main industrial routes to produce hydrogen involve petrochemical processes including gasification of coal (above 90%) and water electrolysis (~4%). Currently, steam reforming of the natural gas holds the highest share (50%) of hydrogen production capacities installed world-wide. Hydrogen can also be formed in large quantities as a by-product in petrochemical processes, refineries and in chemical and electrochemical processes like chloralkali-electrolysis.

Water electrolysis is a mature technology for the production of hydrogen by applying a direct electric current to split water. There is a possibility to produce high purity hydrogen (up to 99.9 % v/v) and the cost of production ranges from 3-5 Euros/kg of hydrogen depending on the plant size. For the sustainability of the overall process, the primary energy used for water splitting should come from renewable energy a resource, which is currently gaining a lot of attention with the exhaustion of the available energy resources and rise in the environmental footprint of the existing energy systems.

Wind and sun energy resources have been widely investigated for this purpose, however, with reliability and stability issues caused by power fluctuations. Some electrolysis systems may not work well with fluctuating power input as for example in the case of alkaline electrolyser which have a low partial load range and affected by constant operations and sudden shutdowns. Rapid fluctuations result in degradation of the separator as well as poor performance of the catalyst. Long term intermittent operations could also result in gas crossovers and affect the gas purity [87]. In

this way, the capacity factor and efficiency of the electrolyser is much affected when compared to the system operating with a perpetual power input.

SGP can be harnessed from the available water bodies by a suitable technology and be used as an alternative to wind and sun energy systems in order to promote water splitting. A potential of SGP about 2000 TWh/year is available globally that can be used as a perpetual power source for hydrogen production regardless of the varying weather conditions.

Table 1.2. Systems involving integrated application of RE for renewable energy generations

Application area	Focus points	Membranes			N	Spacers (δ, μm)	Redox couple		$P_{max,d,}$ W/m^2 (OCV, V)	Ref.
		Type	A (cm^2)	δ, (μm)			Electrolyte	Electrode		
Eenergy generation for use in Desalination systems	Use of RO/FO brine for RE	Nocepta AMX/ CMX (Tokuyama, Japan)	7x7	134-164	5	Woven (280)	0.05 M $K_3Fe(CN)_6$, 0.05 M $K_4Fe(CN)_6$, 0.3 M NaCl	Ti-Ir/Ru	1.86	[53]
	Use of DCMD brine for power generation	Fuji AEM/CEM (Fujifilm Europe B.V., The Netherlands)	10x10	109-170	25	Woven (270)	0.3 M $K_3Fe(CN)_6$, 0.3 0.3 M $K_4Fe(CN)_6$ and 2.5 M NaCl	Ti-Ru/Ir mesh	1.2 (seawater LCS)	[29]
Hydrogen production	Use of RED as a power sources for a water electrolyzer	PC-SK and PC-SA (PCCell, Germany)	195	-	20	-	1 M NH_4HCO_3	Ti-Pt/Ir as anode, Pt/C on C cloth as cathode	~0.18	[88]
	Analysis and optimization of an integrated RE-microbial electrolysis cell for a single step hydrogen production	Selemion CMV/AMV (Asashi glass, Japan)	4x2	110-150	5	Polyethylene mesh (1300)	Catholyte: 1 M sodium bicarbonate Anolyte: 1.0 g/L of sodium acetate in sodium bicarbonate buffer with vitamins and minerals	Graphite fiber brushes anodes, Stainless steel mesh cathode	(0.21-348)	[89]
		Selemion CMV/ AMV (AGC Engineering Co.)	4x2	110-150	5	Polyethylene mesh (1300)	Catholyte: synthetic seawater; Anolyte: 1.0 g/L sodium acetate in a phosphate buffer with minerals and vitamins	Stainless steel mesh cathode, graphite fiber brush anode	(0.5-0.6)	[57]
	Impact of RE design (cell number) on the performance of hybrid RE-microbial electrolysis cell for a single step hydrogen production	PC-SK and PC-SA (PCCell, Germany)	195	500	5-10	-	Catholyte: 1 M sodium bicarbonate Anolyte: 1.0 g/L of sodium acetate in sodium bicarbonate buffer with vitamins and minerals	Stainless steel mesh cathode, carbon fiber brush anodes	(0.6-0.75)	[90]
Energy generation and waste water treatment	Integrated application RE with microbial fuel cell for conversion of organic matter and salinity gradient energy into electrical power	Selemion CMV/AMV (Asahi glass, Japan)	4x2	110-150	10	Polyethylene mesh (1300)	Catholyte: synthetic seawater; Anolyte: 1.0 g/L sodium acetate in a phosphate buffer with minerals and vitamins	Stainless steel mesh cathode, graphite fiber brush anode	4.3	[91]

1.5 Alternative approaches

There is a possibility of extending RE applications to other solutions apart from NaCl for a closed loop applications, like for example using heat regenerative solution based on NH_4HCO_3.

The prominent advantage of such solution is the salinity difference created by using waste heat in a distillation column which can be used for power generation by RE stack in a closed loop mode [15, 88]. Waste heat accounts for above 50% of the total heat generated in industry nowadays. However, power densities reported are very low 0.33 W/m^2 [88] which require further optimizations.

An attempt have also been made for power generation using RE with compartments based on silica nanochannels using KCl solutions [92].

Another interesting application is in bioelectrochemical systems for electricity generation, hydrogen production with the possibility of treating waste water as well [56-58, 89, 90, 93, 94]. In microbial fuel cell, simultaneous generation of electricity and waste water treatment is possible [91]. Integration of RE with microbial fuel cell has an advantage in terms of synergetic power enhancement. Similarly, a RE stack can be integrated with microbial electrolysis cells for continuous hydrogen production in a sustainable manner [93]. In all such systems, the current limitations of RE remains and improvements are required for intensification of these processes. Table 1.3 summarizes literatures related to an alternative applications of RE in other electrochemical systems.

Table 1.3. Stack components and performance of RE employed in alternative applications.

Feed	Focus points	Membranes/ion selective material			N	Spacers (δ, μm)	Redox couple		$P_{d,\,max}$ (W/m^2_{MP})	Ref.
		Type	A (cm^2)	δ, (μm)			Electrolyte	Electrode		
LCC: Distilled water, HCC: 1.5 M NH_4HCO_3	Comparison of direct and indirect hydrogen production by RE	PC-SK and PC-SA (PCCell, Germany)	414.2	90-130	20	-	1 M NH_4HCO_3	Ti-Pt/Ir as anode, Pt/C on C cloth as cathode	0.72	[88]
LCC: 0.02 M NH_4HCO_3 HCC: 1.5 M solution of NH_4HCO_3	Conversion of waste heat into electricity by a closed loop system	Selemion CMV/ AMV (Asashi Glass, Japan)	10.5x7.5	110-150	20	Woven (500)	0.1 M $K_3Fe(CN)_6$, 0.1 M $K_4Fe(CN)_6$	Ti-RuO_2/IrO_2	0.33	[15]
0.1 mM KCl as LCS, and 1 M as HCS	Test of a RE stack with inorganic nanochannels	Ion selective silica nanochannels	$4x10^{-7}$ x 0.014	-	10	-	Feed solutions*	Ag/AgCl electrodes	7.7	[92]

*Electrodes were dipped into the feed solutions

1.6 Challenges

In the aspect of applying RE for both the low salinity gradient (river water/seawater) as well as higher salinity gradient (brine/seawater/brackish water), the major limitation is the high electrical resistance of the membranes as well as their insufficient permselectivity when working with concentrated brines. Tremendous work is required to design RE operating with low resistance membranes which are available at an affordable cost. Low resistance and high permselectivity in membranes are the challenge for the RE process or any process involving the use of RE. Optimization of stack design and membrane material has a commutative effect on the reduction of both the Ohmic resistances (due to stack components like spacers, membranes, feed water compartments) and non-Ohmic resistances (due to opposition to interfacial ionic charge transfer). Reduction of the total internal resistance is the major strategy for enhancing the power output in order to approach economical figures for large scale implementation and commercialization [95]. Special membranes are required in order to avoid fouling as well as the influence of multivalent ions on the power output. A previous research indicates the use of profiled membranes has a huge potential in avoiding fouling problems as well as enhancing the power outputs [35, 42]. Investigations are required in order to predict the time period and stability of the membranes with respect to fouling over a long term operations in concentrated brines. Their performance need to be investigated on the time basis for prediction of the membrane life time. Moreover, huge reduction in power density have been demonstrated recently when using a solution containing Mg^{2+} ion [29]. This requires clear understanding of the phenomenon occurring when operating membranes in multi-ion solutions at high concentration in particular the complex ion transport in this case. The occurrence of uphill transport to keep electroneutrality is not clear when working with solutions of multivalent ions at high concentrations. All these need to be inspected for appropriate design of the operational strategies particularly related to pretreatment requirements.

Integrated application of RE in desalination and hydrogen energy systems is an interesting application when it comes to sustainable hydrogen production. Novel approachs based on the use of RE coupled to DCMD enables the brine management due to the possibility of achieving high VRD as well as low energy desalination with extra energy provided by RE operated with the hot brine retentate from DCMD [85]. However, parametric optimization for enhancing the performance of both systems is required. Optimal module design and suitable membranes are among the challenges in DCMD [96]. The use of hot brine in RE is supposed to enhance the power

density but thermo-economic analysis is required if the integrated approach is feasible when working at larger temperature gradients.

Practical applicability of hybrid system involving RE and water electrolysis is possible, however, with the requirement of parametric optimizations and techno-economic evaluations for large scale applications. With respect to water electrolysis, stack design but more importantly development of highly conductive and stable membranes, electrode and highly active catalyst materials that are stable in the harsh electrolytic environments is very crucial.

1.7 Scope

This scope of the thesis lies in demonstrating opportunities obtained from electrochemical potential of concentrated brine solutions for renewable energy generation by reverse electrodialysis and for *ex situ* hydrogen production by water electrolysis in an integrated approach following the logic of process intensification. RE is tested with solutions mimicking real brine and brackish water in order to predict the SGP potential from this solutions. An attempt is made in order to optimize RE for an integrated application with two other membrane technologies: DCMD and Alkaline Polymer Electrolyte (APE) water electrolysis. Investigations on fouling and stability of ion exchange membranes were also carried out in concentrated brine. Analysis and experiments were carried out in predicting parametric variations in an industrial scale RE operations with a separate investigations on energy and exergy analysis of membrane desalination systems involving RE. Ethical assessment were also performed for sustainability evaluations of the envisaged technologies.

1.8 Outline

Figure 1.12. summarizes the main tasks performed in the present work. The overall work performed in this thesis can be divided in to three parts;

- Firstly, the behaviour of ion exchange membranes and their performance in RE operated with concentrated brines from different sources (mainly anthropogenic ones) is evaluated through experimental testes under pure NaCl feed compositions as well as solutions prepared mimicking real feed compositions.
- Once efficient extraction of renewable energy from concentrated brines by RE is demonstrated, novel applications involving integrated approaches with other membrane-based technologies like DCMD and APE water electrolysis were targeted.

- Finally, experimental investigations on large (industrial) scale RE unit, energy-exergy analysis of RE in membrane desalination systems, and general perspectives on environmental ethics of membrane technologies in water-energy nexus is addressed setting an outlook on future research directions.

So far, RE is widely investigated for applications involving river water and seawater. However, this procedure is accompanied by performance limitations due to pronounced Ohmic losses attributed to the low conductivity of solutions particularly the river water. The use of concentrated brine and brackish/sea water for power generation in RE is envisaged to minimize this problem, decreasing internal stack resistance and increasing the driving force. In **chapter 2**, SGP-RE unit was tested for power generation from mixing concentrated brine and brackish water obtained from solar ponds. Investigations were performed employing membrane materials specifically designed for use in concentrated brine and seawater or brackish water under an EU-FP7 REAPower project. The effect of feed composition of SGP-RE performance was also evaluated systematically.

The possibility of power generation by RE from mixing of concentrated brine and seawater or brackish water leads to several opportunities for novel applications in an integrated approach. For example, RE can be integrated with seawater desalinations technologies in order to take an advantage from the huge amount of discharged brine which is considered as threat to an environment. **Chapter 3** indicates an application of a hybrid DCMD-RE system for low energy desalination and near zero liquid discharge. Thus, feasibility of simultaneous production of clean water and renewable energy is assessed for the possibility of reducing the adverse environmental effects of brine discharges and minimizing energy consumption of desalinations plants through recovery of brine energy.

Globally available SGP from water bodies exists mainly with high concentration of NaCl salt. However, there exist industrial effluents with high load of Na_2SO_4 salt. Potential extension of applicability of RE for exploitation of SGP from mixing Na_2SO_4 solutions of different concentrations is presented in **Chapter 4**. In order to understand the behaviour of ion exchange membranes in sulphate stream, electrochemical characterization in terms of membrane resistance and permselectivity is performed for comparison with the membrane properties reported in a standard NaCl solution. Optimization for harnessing SGP from aqueous sulphate wastes and prediction of maximal output power at the current state-of-art-technology is performed.

Ion exchange membranes are the heart of RE. Although good electrochemical properties are highly determinant for the overall performance, other properties like resistance to fouling, mechanical strength and stability, particularly when operated over a long period with concentrated solutions like brine is highly desirable. Research on the impact of membrane fouling on SGP generation by RE and aging (stability) of ion exchange membranes in concentrated brine and seawater is scarce. Thus, **chapter 5** evaluates the fouling propensity of commercial ion exchange membranes for potential application in a RE system operated with real brine and seawater samples (Sicily, Italy) considered under the EU-FP7 REAPower project. Theoretical model is developed and implemented for prediction of potential scaling, colloidal and organic fouling of the membranes. Possible pre-treatment strategies for real feed streams under constrain of low-energy consumption is identified and analysed for in order to evaluate the practical applicability of RE.

When it comes to the large scale application, RE power plants up to 50 kW is foreseen in Afsluitdijk (the Netherlands) generating blue energy from mixing of salt water and fresh water under natural conditions. In addition, an attempt of electricity generation from concentrated brine and brackish water using RE prototype by researchers at University of Palermo (Italy) showed a promising results. However, literature lacks experimental data for a large (industrial) scale RE system (up to 200 cells) to the best of our knowledge. **Chapter 6** demonstrates performance analysis and evaluations on an industrial scale RE unit operated with NaCl as well as Na_2SO_4 ions. Interface resistances, power density and energy efficiency were determined in order to have a clear insight on the behaviour of RE in the process of scale-up for real implementations.

Another interesting application of RE in an integrated approach is presented in **Chapter 7** where the renewable energy generated by RE is used for continues fuelling APE water electrolysis system for inexhaustive hydrogen production in a sustainable manner. This investigation targets on indirect (*ex situ*) conversion of electrochemical potential of concentrated brine into useful hydrogen produced by alkaline water electrolysis. The influence of various operating parameters is analyzed systematically in order to evaluate their significance during the optimization procedure for maximization of hydrogen production. The performance of the hybrid system under optimized conditions in terms of hydrogen production rate is clearly shown here.

Chapter 8 gives a general overview of the energetic and exegetic analysis of RE, particularly employed for energy recovery using brine discharged from membrane desalination plants.

Chapter 9 evaluates sustainability of integrated membrane based processes for water and energy production through identification of main environmental and ecosystem impacts. The ethical significance of the identified impacts was predicted for upstream balance of social benefits and burdens to the present and future generations in order to assure sustainability of the processes.

Chapter 10 provides key discussions regarding RE optimization for power generation using concentrated brine, both for electricity and hydrogen production, outlining future research trends.

Figure 1.12. Schematic illustration of the main tasks performed in this thesis.

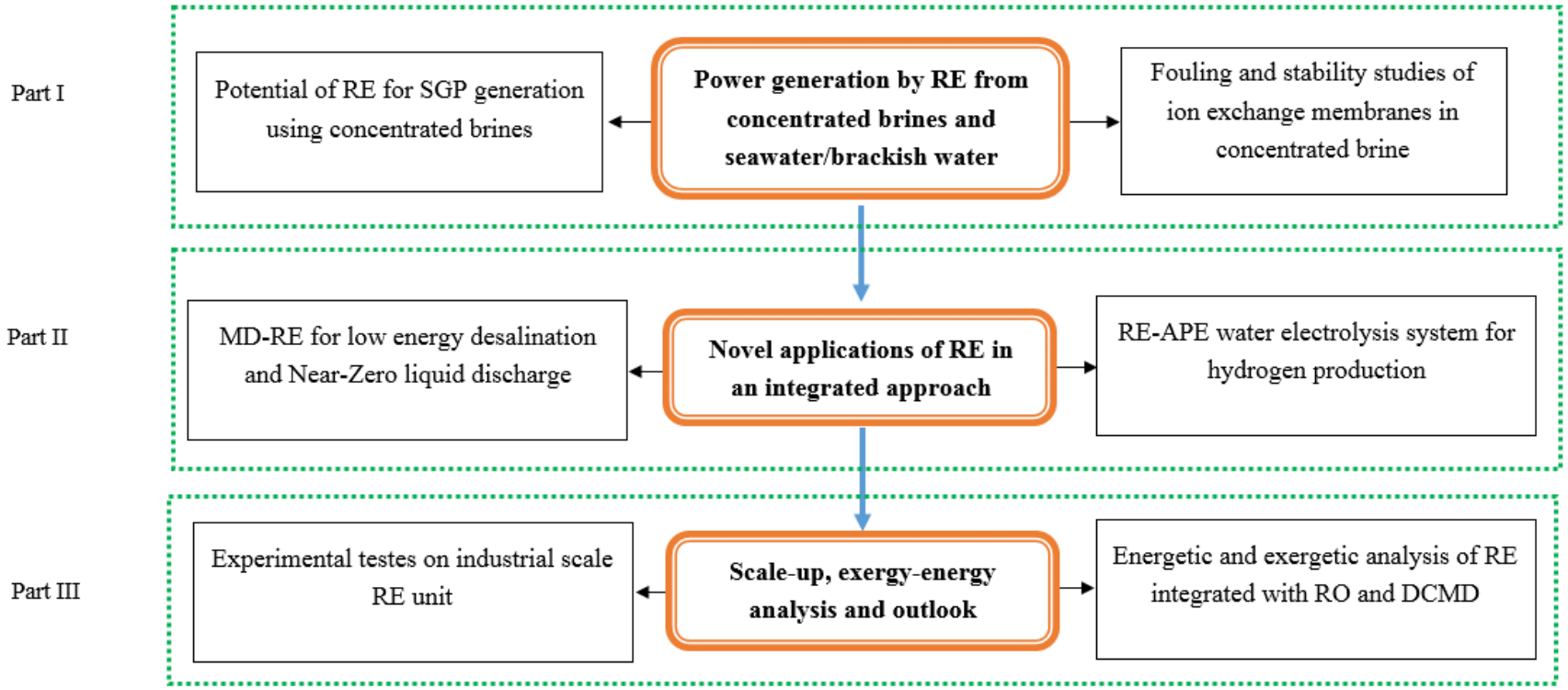

References

[1] A. Sieminski, International Energy Outlook, (2014).
[2] U. EIA, Annual energy outlook 2013, US Energy Information Administration, Washington, DC, (2013).
[3] IPEEC, Knowledge Management Portal: Overview, (2015).
[4] I.E. Agency, CO_2 Emissions From Fuel Combustion Highlights, in, 2014.
[5] C. Accord, Decision 2/CP. 15 Copenhagen Accord, in, FCCC/CP/2009/11/Add. 1, 2009.
[6] R.E. Smalley, Future global energy prosperity: the terawatt challenge, Mrs Bulletin, 30 (2005) 412-417.
[7] M. Elimelech, W.A. Phillip, The Future of Seawater Desalination: Energy, Technology, and the Environment, Science, 333 (2011) 712-717.
[8] G.Z. Ramon, B.J. Feinberg, E.M.V. Hoek, Membrane-based production of salinity-gradient power, Energy & Environmental Science, 4 (2011) 4423-4434.
[9] J. Veerman, M. Saakes, S.J. Metz, G.J. Harmsen, Reverse electrodialysis: Performance of a stack with 50 cells on the mixing of sea and river water, Journal of Membrane Science, 327 (2009) 136-144.
[10] F.N. François Lienard, Salinity Gradient Power in Europe: State of the Art in, 2011.
[11] C. Klaysom, T.Y. Cath, T. Depuydt, I.F.J. Vankelecom, Forward and pressure retarded osmosis: potential solutions for global challenges in energy and water supply, Chemical Society Reviews, 42 (2013) 6959-6989.
[12] A. Achilli, A.E. Childress, Pressure retarded osmosis: From the vision of Sidney Loeb to the first prototype installation — Review, Desalination, 261 (2010) 205-211.
[13] E. Brauns, Towards a worldwide sustainable and simultaneous large-scale production of renewable energy and potable water through salinity gradient power by combining reversed electrodialysis and solar power?, Desalination, 219 (2008) 312-323.
[14] M. Tedesco, E. Brauns, A. Cipollina, G. Micale, P. Modica, G. Russo, J. Helsen, Reverse Electrodialysis with saline waters and concentrated brines: a laboratory investigation towards technology scale-up, Journal of Membrane Science, (2015).
[15] X. Luo, X. Cao, Y. Mo, K. Xiao, X. Zhang, P. Liang, X. Huang, Power generation by coupling reverse electrodialysis and ammonium bicarbonate: Implication for recovery of waste heat, Electrochemistry Communications, 19 (2012) 25-28.
[16] Ramato A. Tufa, E. Curcio, E. Brauns, W. van Baak, E. Fontananova, G. Di Profio, Membrane Distillation and Reverse Electrodialysis for Near-Zero Liquid Discharge and low energy seawater desalination, Journal of Membrane Science, 496 (2015) 325-333.
[17] D.A. Vermaas, J. Veerman, M. Saakes, K. Nijmeijer, Influence of multivalent ions on renewable energy generation in reverse electrodialysis, Energy & Environmental Science, (2014).
[18] J.W. Post, H.V.M. Hamelers, C.J.N. Buisman, Energy recovery from controlled mixing salt and fresh water with a reverse electrodialysis system, Environmental Science and Technology, 42 (2008) 5785-5790.
[19] M. OLSSON, G.L. WICK, J.D. ISAACS, Salinity Gradient Power: Utilizing Vapor Pressure Differences, Science, 206 (1979) 452-454.
[20] F. Liu, O. Schaetzle, B.B. Sales, M. Saakes, C.J.N. Buisman, H.V.M. Hamelers, Effect of additional charging and current density on the performance of Capacitive energy extraction based on Donnan Potential, Energy & Environmental Science, 5 (2012) 8642-8650.
[21] D. Brogioli, R. Zhao, P.M. Biesheuvel, A prototype cell for extracting energy from a water salinity difference by means of double layer expansion in nanoporous carbon electrodes, Energy & Environmental Science, 4 (2011) 772-777.
[22] W. Finley, E. Pscheidt, Hydrocratic generator, in, Google Patents, 2001.
[23] F. La Mantia, M. Pasta, H.D. Deshazer, B.E. Logan, Y. Cui, Batteries for Efficient Energy Extraction from a Water Salinity Difference, Nano Letters, 11 (2011) 1810-1813.
[24] J. Veerman, M. Saakes, S.J. Metz, G.J. Harmsen, Reverse electrodialysis: evaluation of suitable electrode systems, Journal of Applied Electrochemistry, 40 (2010) 1461-1474.
[25] O. Scialdone, C. Guarisco, S. Grispo, A.D. Angelo, A. Galia, Investigation of electrode material - Redox couple systems for reverse electrodialysis processes. Part I: Iron redox couples, Journal of Electroanalytical Chemistry, 681 (2012) 66-75.
[26] J. Veerman, M. Saakes, S. Metz, G. Harmsen, Reverse electrodialysis: evaluation of suitable electrode systems, Journal of Applied Electrochemistry, 40 (2010) 1461-1474.
[27] D.A. Vermaas, J. Veerman, M. Saakes, K. Nijmeijer, Influence of multivalent ions on renewable energy generation in reverse electrodialysis, Energy & Environmental Science, 7 (2014) 1434-1445.

[28] D.A. Vermaas, J. Veerman, N.Y. Yip, M. Elimelech, M. Saakes, K. Nijmeijer, High Efficiency in Energy Generation from Salinity Gradients with Reverse Electrodialysis, ACS Sustainable Chemistry & Engineering, 1 (2013) 1295-1302.
[29] R.A. Tufa, E. Curcio, W. van Baak, J. Veerman, S. Grasman, E. Fontananova, G. Di Profio, Potential of brackish water and brine for energy generation by salinity gradient power-reverse electrodialysis (SGP-RE), RSC Advances, 4 (2014) 42617-42623.
[30] D.A. Vermaas, M. Saakes, K. Nijmeijer, Doubled Power Density from Salinity Gradients at Reduced Intermembrane Distance, Environmental Science & Technology, 45 (2011) 7089-7095.
[31] P. Długołęcki, A. Gambier, K. Nijmeijer, M. Wessling, Practical potential of reverse electrodialysis as process for sustainable energy generation, Environmental Science and Technology, 43 (2009) 6888-6894.
[32] J. Veerman, R.M. de Jong, M. Saakes, S.J. Metz, G.J. Harmsen, Reverse electrodialysis: Comparison of six commercial membrane pairs on the thermodynamic efficiency and power density, Journal of Membrane Science, 343 (2009) 7-15.
[33] M. Turek, B. Bandura, Renewable energy by reverse electrodialysis, Desalination, 205 (2007) 67-74.
[34] X. Zhu, W. He, B.E. Logan, Reducing pumping energy by using different flow rates of high and low concentration solutions in reverse electrodialysis cells, Journal of Membrane Science, 486 (2015) 215-221.
[35] D.A. Vermaas, M. Saakes, K. Nijmeijer, Power generation using profiled membranes in reverse electrodialysis, Journal of Membrane Science, 385-386 (2011) 234-242.
[36] D.A. Vermaas, S. Bajracharya, B.B. Sales, M. Saakes, B. Hamelers, K. Nijmeijer, Clean energy generation using capacitive electrodes in reverse electrodialysis, Energy and Environmental Science, 6 (2013) 643-651.
[37] P. Długołecki, J. Dabrowska, K. Nijmeijer, M. Wessling, Ion conductive spacers for increased power generation in reverse electrodialysis, Journal of Membrane Science, 347 (2010) 101-107.
[38] J. Veerman, J.W. Post, M. Saakes, S.J. Metz, G.J. Harmsen, Reducing power losses caused by ionic shortcut currents in reverse electrodialysis stacks by a validated model, Journal of Membrane Science, 310 (2008) 418-430.
[39] A. Daniilidis, R. Herber, D.A. Vermaas, Upscale potential and financial feasibility of a reverse electrodialysis power plant, Applied Energy, 119 (2014) 257-265.
[40] E. Guler, Y. Zhang, M. Saakes, K. Nijmeijer, Tailor-Made Anion-Exchange Membranes for Salinity Gradient Power Generation Using Reverse Electrodialysis, ChemSusChem, 5 (2012) 2262-2270.
[41] E. Güler, W. van Baak, M. Saakes, K. Nijmeijer, Monovalent-ion-selective membranes for reverse electrodialysis, Journal of Membrane Science, 455 (2014) 254-270.
[42] E. Güler, R. Elizen, M. Saakes, K. Nijmeijer, Micro-structured membranes for electricity generation by reverse electrodialysis, Journal of Membrane Science, 458 (2014) 136-148.
[43] J.G. Hong, Y. Chen, Nanocomposite reverse electrodialysis (RED) ion-exchange membranes for salinity gradient power generation, Journal of Membrane Science, 460 (2014) 139-147.
[44] J. Gi Hong, Y. Chen, Evaluation of electrochemical properties and reverse electrodialysis performance for porous cation exchange membranes with sulfate-functionalized iron oxide, Journal of Membrane Science, 473 (2015) 210-217.
[45] D.A. Vermaas, D. Kunteng, M. Saakes, K. Nijmeijer, Fouling in reverse electrodialysis under natural conditions, Water Research, 47 (2013) 1289-1298.
[46] J.W. Post, Blue Energy: electricity production from salinity gradients by reverse electrodialysis, publisher not identified, 2009.
[47] M. Tedesco, A. Cipollina, A. Tamburini, W. van Baak, G. Micale, Modelling the Reverse ElectroDialysis process with seawater and concentrated brines, Desalination and Water Treatment, 49 (2012) 404-424.
[48] M. Tedesco, P. Mazzola, A. Tamburini, G. Micale, I.D.L. Bogle, M. Papapetrou, A. Cipollina, Analysis and simulation of scale-up potentials in reverse electrodialysis, Desalination and Water Treatment, (2014) 1-13.
[49] J. Veerman, M. Saakes, S.J. Metz, G.J. Harmsen, Reverse electrodialysis: A validated process model for design and optimization, Chemical Engineering Journal, 166 (2011) 256-268.
[50] X. Luo, X. Cao, Y. Mo, K. Xiao, X. Zhang, P. Liang, X. Huang, Power generation by coupling reverse electrodialysis and ammonium bicarbonate: Implication for recovery of waste heat, Electrochemistry Communications, 19 (2012) 25-28.
[51] M.C. Hatzell, I. Ivanov, R.D. Cusick, X. Zhu, B.E. Logan, Comparison of hydrogen production and electrical power generation for energy capture in closed-loop ammonium bicarbonate reverse electrodialysis systems, Physical Chemistry Chemical Physics, 16 (2014) 1632-1638.
[52] W. Li, W.B. Krantz, E.R. Cornelissen, J.W. Post, A.R.D. Verliefde, C.Y. Tang, A novel hybrid process of reverse electrodialysis and reverse osmosis for low energy seawater desalination and brine management, Applied Energy, 104 (2013) 592-602.

[53] K. Kwon, J. Han, B.H. Park, Y. Shin, D. Kim, Brine recovery using reverse electrodialysis in membrane-based desalination processes, Desalination, 362 (2015) 1-10.
[54] E. Brauns, An alternative hybrid concept combining seawater desalination, solar energy and reverse electrodialysis for a sustainable production of sweet water and electrical energy, Desalination and Water Treatment, 13 (2010) 53-62.
[55] E.C. R. A. Tufa, Enrico Drioli, Practical Applicability of Reverse Elecrodialysis in Integrated Membrane Desalination Technologies for Salinity Gradient Power Generation, in: ICOM 2014, Suzhou, China, 2014.
[56] Y. Kim, B.E. Logan, Microbial reverse electrodialysis cells for synergistically enhanced power production, Environmental Science & Technology, 45 (2011) 5834-5839.
[57] Y. Kim, B.E. Logan, Hydrogen production from inexhaustible supplies of fresh and salt water using microbial reverse-electrodialysis electrolysis cells, Proceedings of the National Academy of Sciences, 108 (2011) 16176-16181.
[58] R.D. Cusick, Y. Kim, B.E. Logan, Energy Capture from Thermolytic Solutions in Microbial Reverse-Electrodialysis Cells, Science, 335 (2012) 1474-1477.
[59] D.C. Ramato Ashu Tufa, Roman Kodým, Michal Němeček, Efrem Curcio, Karel Bouzek, Hybrid Reverse Electrodialysis-Hydrogen (RED-H2) energy system: performance analysis and optimization, in: Hydrogen days 2015, Prague, Czech Republic, 2015.
[60] J. Veerman, M. Saakes, S.J. Metz, G.J. Harmsen, Electrical power from sea and river water by reverse electrodialysis: A first step from the laboratory to a real power plant, Environmental Science and Technology, 44 (2010) 9207-9212.
[61] M. Tedesco, C. Scalici, D. Vaccari, A. Cipollina, A. Tamburini, G. Micale, Performance of the first Reverse Electrodialysis pilot plant for power production from saline waters and concentrated brines, Journal of Membrane Science, (2015).
[62] N. Boon, R. van Roij, 'Blue energy' from ion adsorption and electrode charging in sea and river water, Molecular Physics, 109 (2011) 1229-1241.
[63] E. Guler, Y. Zhang, M. Saakes, K. Nijmeijer, Tailor-made anion-exchange membranes for salinity gradient power generation using reverse electrodialysis, ChemSusChem, 5 (2012) 2262-2270.
[64] E. Güler, R. Elizen, D.A. Vermaas, M. Saakes, K. Nijmeijer, Performance-determining membrane properties in reverse electrodialysis, Journal of Membrane Science, 446 (2013) 266-276.
[65] M. Tedesco, A. Cipollina, A. Tamburini, G. Micale, J. Helsen, M. Papapetrou, REAPower: use of desalination brine for power production through reverse electrodialysis, Desalination and Water Treatment, (2014) 1-9.
[66] L. Gurreri, A. Tamburini, A. Cipollina, G. Micale, CFD analysis of the fluid flow behavior in a reverse electrodialysis stack, Desalination and Water Treatment, 48 (2012) 390-403.
[67] T. Kim, J. Kang, J.H. Lee, J. Yoon, Influence of attached bacteria and biofilm on double-layer capacitance during biofilm monitoring by electrochemical impedance spectroscopy, Water Research, 45 (2011) 4615-4622.
[68] V. Lindstrand, A.S. Jönsson, G. Sundström, Organic fouling of electrodialysis membranes with and without applied voltage, Desalination, 130 (2000) 73-84.
[69] A. Daniilidis, D.A. Vermaas, R. Herber, K. Nijmeijer, Experimentally obtainable energy from mixing river water, seawater or brines with reverse electrodialysis, Renewable Energy, 64 (2014) 123-131.
[70] D.A. Vermaas, M. Saakes, K. Nijmeijer, Early detection of preferential channeling in reverse electrodialysis, Electrochimica Acta, 117 (2014) 9-17.
[71] S. Pawlowski, J.G. Crespo, S. Velizarov, Pressure drop in reverse electrodialysis: Experimental and modeling studies for stacks with variable number of cell pairs, Journal of Membrane Science, 462 (2014) 96-111.
[72] J.N. WEINSTEIN, F.B. LEITZ, Electric Power from Differences in Salinity: The Dialytic Battery, Science, 191 (1976) 557-559.
[73] D.A. Vermaas, M. Saakes, K. Nijmeijer, Enhanced mixing in the diffusive boundary layer for energy generation in reverse electrodialysis, Journal of Membrane Science, 453 (2014) 312-319.
[74] J.G. Hong, W. Zhang, J. Luo, Y. Chen, Corrigendum to "Modeling of power generation from the mixing of simulated saline and freshwater with a reverse electrodialysis system: The effect of monovalent and multivalent ions" [Appl. Energy 110 (2013) 244–251], Applied Energy, 129 (2014) 398-399.
[75] M. Turek, B. Bandura, P. Dydo, Power production from coal-mine brine utilizing reversed electrodialysis, Desalination, 221 (2008) 462-466.
[76] M. Tedesco, A. Cipollina, A. Tamburini, I.D.L. Bogle, G. Micale, A simulation tool for analysis and design of reverse electrodialysis using concentrated brines, Chemical Engineering Research and Design, 93 (2015) 441-456.

[77] E. Curcio, G. Di Profio, E. Fontananova, E. Drioli, Membrane technologies for seawater desalination and brackish water treatment, Advances in Membrane Technologies for Water Treatment: Materials, Processes and Applications, (2015) 411.
[78] S. Miller, H. Shemer, R. Semiat, Energy and environmental issues in desalination, Desalination, 366 (2015) 2-8.
[79] E. Brauns, Combination of desalination plant and salinity gradient power reverse electrodialysis plant and usethereof, in: United States Patent, Vlaamse Instelling Voor Technologisch Onderzoek (VITO), Mol (BE), United States, 2012.
[80] D. Hou, G. Dai, J. Wang, H. Fan, Z. Luan, C. Fu, Boron removal and desalination from seawater by PVDF flat-sheet membrane through direct contact membrane distillation, Desalination, 326 (2013) 115-124.
[81] S.T. Hsu, K.T. Cheng, J.S. Chiou, Seawater desalination by direct contact membrane distillation, Desalination, 143 (2002) 279-287.
[82] E. Drioli, Y. Wu, V. Calabro, Membrane distillataion in the treatment of aqueous solutions, Journal of Membrane Science, 33 (1987) 277-284.
[83] B. Li, K.K. Sirkar, Novel Membrane and Device for Direct Contact Membrane Distillation-Based Desalination Process, Industrial & Engineering Chemistry Research, 43 (2004) 5300-5309.
[84] S. Al-Obaidani, E. Curcio, F. Macedonio, G. Di Profio, H. Al-Hinai, E. Drioli, Potential of membrane distillation in seawater desalination: Thermal efficiency, sensitivity study and cost estimation, Journal of Membrane Science, 323 (2008) 85-98.
[85] R. Ashu Tufa, E. Curcio, E. Brauns, W. van Baak, E. Fontananova, G. Di Profio, Membrane distillation and reverse electrodialysis for near-zero liquid discharge and low energy seawater desalination, Journal of Membrane Science.
[86] L. Schlapbach, A. Zuttel, Hydrogen-storage materials for mobile applications, Nature, 414 (2001) 353-358.
[87] A.G. Dutton, J.A.M. Bleijs, H. Dienhart, M. Falchetta, W. Hug, D. Prischich, A.J. Ruddell, Experience in the design, sizing, economics, and implementation of autonomous wind-powered hydrogen production systems, International Journal of Hydrogen Energy, 25 (2000) 705-722.
[88] M.C. Hatzell, I. Ivanov, R. D. Cusick, X. Zhu, B.E. Logan, Comparison of hydrogen production and electrical power generation for energy capture in closed-loop ammonium bicarbonate reverse electrodialysis systems, Physical Chemistry Chemical Physics, 16 (2014) 1632-1638.
[89] J.Y. Nam, R.D. Cusick, Y. Kim, B.E. Logan, Hydrogen generation in microbial reverse-electrodialysis electrolysis cells using a heat-regenerated salt solution, Environmental Science and Technology, 46 (2012) 5240-5246.
[90] V.J. Watson, M. Hatzell, B.E. Logan, Hydrogen production from continuous flow, microbial reverse–electrodialysis electrolysis cells treating fermentation wastewater, Bioresource Technology, (2015).
[91] Y. Kim, B.E. Logan, Microbial reverse electrodialysis cells for synergistically enhanced power production, Environmental Science and Technology, 45 (2011) 5834-5839.
[92] D.-K. Kim, C. Duan, Y.-F. Chen, A. Majumdar, Power generation from concentration gradient by reverse electrodialysis in ion-selective nanochannels, Microfluidics and Nanofluidics, 9 (2010) 1215-1224.
[93] Y. Kim, B.E. Logan, Hydrogen production from inexhaustible supplies of fresh and salt water using microbial reverse-electrodialysis electrolysis cells, Proceedings of the National Academy of Sciences of the United States of America, 108 (2011) 16176-16181.
[94] R.D. Cusick, Y. Kim, B.E. Logan, Energy capture from thermolytic solutions in microbial reverse- electrodialysis cells, Science, 335 (2012) 1474-1477.
[95] J.W. Post, C.H. Goeting, J. Valk, S. Goinga, J. Veerman, H.V.M. Hamelers, P.J.F.M. Hack, Towards implementation of reverse electrodialysis for power generation from salinity gradients, Desalination and Water Treatment, 16 (2010) 182-193.
[96] E. Drioli, A. Ali, F. Macedonio, Membrane distillation: Recent developments and perspectives, Desalination, 356 (2015) 56-84.

Chapter 2

Potential of Brackish Water and Brine for Energy Generation by Salinity Gradient Power-Reverse Electrodialysis (SGP-RE)

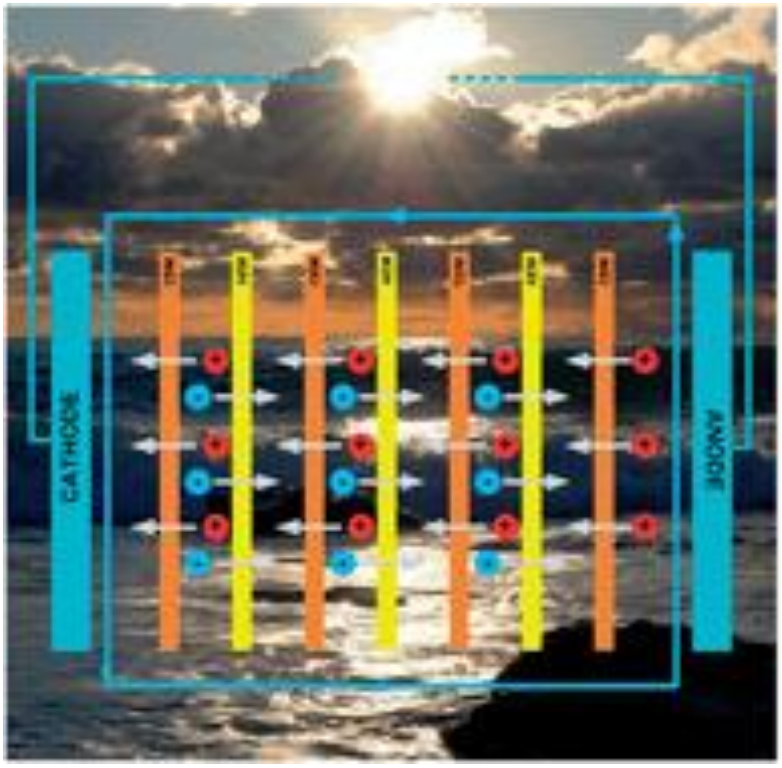

Abstract

In the present work, salinity gradient power-reverse electrodialysis (SGP-RE) unit was tested for the production of electrical energy by exploiting the chemical potential of real brackish water and exhaust brine from solar pond. A cross-flow SGP-RE module (REDstack B.V.), equipped with AEM-80045 and CEM-80050 membranes specifically developed by Fujifilm Manufacturing Europe B.V. within the EU-funded project REAPOWER ("Reverse Electrodialysis Alternative Power Production"), was able to generate a maximum power density (expressed in Watts per m^2 Membrane Pair - MP) of 3.04 W/m^2_{MP} when operated with pure NaCl aqueous solutions (0.1M in Low Concentration Compartment - LCC, 5 M in High Concentration Compartment - HCC) at 20°C and recirculation rate of 20 L/h. However, a drastic reduction to 1.13 W/m^2 (-63%) was observed when feeding SGP-RE unit with artificial multi-ion solutions mimicking real brackish water and exhaust brine. Further experimental activity allowed at identifying Mg^{2+} ions as responsible for the significant increase in stack resistance and consequent depletion of SGP-RE performance. Therefore, specific softening treatment of the real solutions should be considered in order to maintain the process efficiency at practical level.

This chapter has been published as;

R.A. Tufa, E. Curcio, W. van Baak, J. Veerman, S. Grasman, E. Fontananova, G. Di Profio, Potential of brackish water and brine for energy generation by salinity gradient power-reverse electrodialysis (SGP-RE), *RSC Advances*, 4 **(2014)** 42617-42623.

2.1 Introduction

Global demand for energy is increasing at unsustainable rate mainly due to global economic expansion, population growth and increasing living standard in emerging countries. As a result, the extensive utilization of available fossil fuels is causing a progressive depletion of these resources and an increase in global CO_2 emission. Renewable energy sources with limited thermal and environmental pollution, and absence of net emission of greenhouse gases and radioactive wastes, are attracting growing attention. In particular, Reverse Electrodialysis (RE) is an emerging technology having the potential for generating energy from salinity power gradients (SGP). In a typical SGP-RE module, Cation Exchange Membranes (CEM) and Anion Exchange Membranes (AEM) are stacked alternately in a module; driven by a concentration gradient, the diffusive flux of ions generates a electrochemical membrane potential recorded as a voltage across electrodes [1]. From a theoretical point of view, the value of the voltage from unloaded RE stack (Open Circuit Voltage - OCV) is predicted by the Nernst-Plank equation [2]:

$$OCV = \frac{2NRT}{F}\left[\frac{\alpha_{AEM}}{z_a}\ln\left(\frac{\gamma_{a,HCC}\,C_{a,HCC}}{\gamma_{a,LCC}\,C_{a,LCC}}\right)+\frac{\alpha_{CEM}}{z_c}\ln\left(\frac{\gamma_{c,HCC}\,C_{c,HCC}}{\gamma_{c,LCC}\,C_{c,LCC}}\right)\right] \quad (2.1)$$

where R is ideal gas constant (8.314 $J\cdot mol^{-1}K^{-1}$), N is the number of membrane pairs, T is the temperature (K), z is valence, α is the average membrane permselectivity of the ion exchange membrane, F is Faraday constant (96485 C/mol), and γ is the activity coefficient of the ion and C the concentration (mol/l); subscripts a, c, HCC and LCC refer to anion, cation, High Concentration Compartment and Low Concentration Compartment, respectively.

Previous investigations carried out with aqueous NaCl solutions, mimicking seawater and river water salinity, reached a power density around 4 W/m^2MP of membrane [3-7] and energy efficiency around 50% [8]. Vermaas *et al.* (2013) showed that the theoretical obtainable Gibbs free energy of mixing typical seawater (30 g/l NaCl) and river water (1 g/l NaCl), both at flow rate of 1 m^3/s, is 1.39 MW [8].

from SGP-RE operations carried out at high concentration in the HCC have been clearly envisaged in the work of Post *et al*. (2008): if LCC and HCC are fed with 0.05 M and 5 M NaCl, respectively, the theoretically available amount of energy from mixing $1m^3$ of diluted and $1m^3$ of a concentrated solution at 293 K increases to 15 MJ [9].

At present, literature works on RE systems operated under high concentrated solutions like

brine are scarce in number and in large part referred to pure NaCl aqueous solutions. A power density up to 0.87 W/m^2 (all data are referred to total membrane area, unless otherwise specified) has been reported for a RE system operated with a standard grade electrodialysis membrane compartments filled with a coal-mine brine and fresh water [10]. Theoretical models predict that a power density up to 8.5 W/m^2 is achievable through proper optimization and use of specially developed AEM and CEM membranes contacted with brine and seawater solutions [1]. However, the behavior of a RE system might vary significantly when operated with real solutions. From Eq. (1) it is possible to roughly envisage the different levels of influence of monovalent and multivalent ions on the open circuit voltage generated by SGP-RE: assuming apparent membrane permselectivity and activity coefficients constant, the electrochemical potential generated by monovalent ions (almost all investigations in literature focus on Na^+ and Cl^-) is about twice as large as the one produced by divalent ions (Mg^{2+} and Ca^{2+} are among the most abundant in natural environments) when operating at equal ion concentration ratio. Therefore, the sensitivity of SGP-RE system to real feed conditions is crucial for practical applications.

So far, literature lacks systematic and adequate information on the effect of simultaneous presence of ions other than sodium and chloride on SGP-RE performance. Vermaas *et al.* (2014) observed that, when using a mixture with a molar fraction of 10% $MgSO_4$ and 90% of NaCl in both LCC and HCC, experimentally obtained power density in steady state decreased from 29% to 50% compared to the case where the feed solutions contained only NaCl as a salt[11]. An increase of stack resistance due to addition of Mg^{2+} ions into sodium chloride solution was also noticed by Post *et al*. (2009) [12]. More experimental investigation is need in order to better define the potentialities of SGP-RE technology and to move a decisive step towards real applications.

In the present work, with the aim to investigate realistic high-salinity conditions, where sodium, magnesium, calcium, chloride, sulfate, and bicarbonate are among the most common and abundant salt ions in natural waters, experiments have been carried out using brackish water and brine from solar ponds (Sicily, Italy) as sources for low concentration compartment (LCC) and high concentration compartment (HCC) of a SGP-RE unit, respectively. The effect of ionic composition on SGP-RE was evaluated by measurement of current, voltage and power density.

2.2 Materials and methods

2.2.1 Reverse electrodialysis stack

Experimental tests were carried out on a SGP-RE stack (Figure 2.1.a) provided by REDstack B.V. (The Netherlands). The stack, operating in cross-flow configuration, has an active membrane area of 0.01m^2 (10 cm x 10 cm) and 25 cell pairs. The module was equipped with 270 µm poly-ethylene gaskets and PET spacers (Deukum GMBH, Germany). Working electrodes made of inert Ti-Ru/Ir mesh had a dimension of 10cm×10cm (MAGNETO Special Anodes B.V., The Netherlands). All experiments were carried out at 20°C.

a)

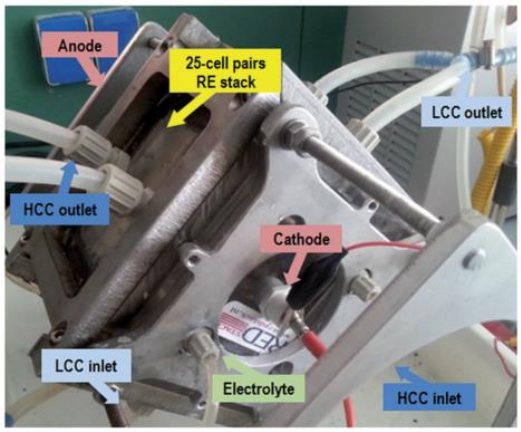

b)

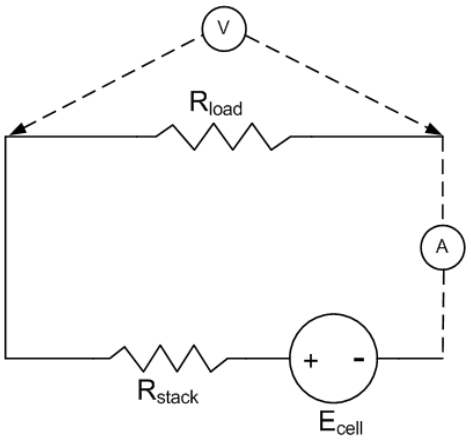

Figure 2.1. a) The cross-flow stack used in SGP-RE experiments (b) Electric circuit diagram of the experimental apparatus. The ammeter (A) is connected in series and voltmeter (V) connecter in parallel with the resistance box (R_{load}).

2.2.2 Membranes

Ion Exchange Membranes (IEM) used are AEM-80045 and CEM-80050 provided by Fujifilm Manufacturing Europe B.V (The Netherlands). The membranes were activated in a 0.1 M NaCl solution before use and stored with the same solution in the stack during intervals of the testing periods. Membrane characteristics are summarized in Table 2.1[13].

2.2.3 Electrolyte and testing solutions

The electrolyte solution, recirculated throughout the electrolytic compartments at 30 l/h by Masterflex L/S digital peristaltic pumps (Cole-Palmer, US), was prepared by dissolving potassium hexacyanoferrate (II), potassium hexacyanoferrate (III) and sodium chloride (Sigma-Aldrich S.r.l., Italy) in de-ionized water (PURELAB, Elga LabWater®, 0.055 uS/cm) up to a final concentration

of 0.3 M $K_4Fe(CN)_6$, 0.3 M $K_3Fe(CN)_6$ and 2.5 M NaCl.

Table 2.1. Relevant properties of ion exchange membranes [13].

Membrane code	Thickness (μm)[a]	Ion exchange capacity (mmol/g membrane)	Density of fixed charges (mol/L)[a]	Membrane areal resistance (Ω cm^2)[b]
Fuji-AEM-80045	129±2	1.4±0.1	3.8±0.2	1.551±0.001
Fuji-CEM-80050	114±2	1.1±0.1	2.4±0.2	2.974±0.001

[a]Measurement conditions: NaCl 0.5 M, 20 °C.

[b]Measurement conditions: NaCl 0.5 M, 20°C, 2.8 cm S^{-1}.

Testing solutions (composition in Table 2.2) were prepared by dissolving in de-ionized water the following salts in reagent grade: $NaHCO_3$, KCl and Na_2SO_4 purchased from Sigma Aldrich S.r.l. (Italy); NaCl, $CaCl_2 \cdot 2H_2O$ and $MgCl_2 \cdot 6H_2O$ from Carlo Erba Reagenti (Italy).

Table 2.2. Ion composition of real brackish water and brine from solar pond (20°C). Source: Ettore Infersa evaporation salt pond (Sicily, Italy).

		Na^+	K^+	Ca^{2+}	Mg^{2+}	Cl^-	HCO_3^-	SO_4^{2-}
Brackish water	Concentration (mg/l)	1,520	49.7	101	323	3,560	0.523	335
	Molar ratio		$[Na^+]/[K^+]$ = 52.1	$[Na^+]/[Ca^{2+}]$ = 26.4	$[Na^+]/[Mg^{2+}]$ = 4.99		$[Cl^-]/[HCO_3^-]$ = 11717	$[Cl^-]/[SO_4^{2-}]$ = 28.8
Brine from Solar Pond	Concentration (mg/l)	66,000	7,740	242	37,400	170,000	50.0	64,400
	Molar ratio		$[Na^+]/[K^+]$ = 14.5	$[Na^+]/[Ca^{2+}]$ = 474	$[Na^+]/[Mg^{2+}]$ = 1.86		$[Cl^-]/[HCO_3^-]$ = 5841	$[Cl^-]/[SO_4^{2-}]$ = 7.15
	Theoretical voltage over membrane [a] (mV)†	84	117	5	61	80	122	42

[a]Calculated from eq. (1). Activity coefficients calculated by PHREEQC v.2.18.00 software[14].

Salt solution were recirculated throughout the SGP-RE system at flowrate of 20 l/h by Masterflex L/S digital peristaltic pumps Mod. N. 7528-10 6-600 rpm (Cole-Palmer, US). Heated circulating baths (PolyScience, US) were used to control the temperature of recirculating streams; temperature at the six inlets of the module was monitored by Multi-channel data logging thermometers type K 800024 with high full scale accuracy of +/-0.5% rdg (Sper Scientific, US). Conductivity of solutions was measured by YSI (US) model 3200 Conductivity Instrument.

2.2.4 Electrochemical measurements

A high dissipation five decade resistance box in the range of 0.1-1000 Ω (CROPICO, Bracken Hill, US) was used to load the SGP-RE system. DC voltage drop across the load resistors was measured by a 3½ digital multimeter with accuracy of ±0.5% in the range of range 200 mV-

200 V (Valleman, DVM760), and the current flowing across the load resistors by Agilent 34422A 6½ Digit Multimeter, according to scheme provided in Figure 2.1.b. All measurements were carried out under continuous operation. The performance of SGP-RE unit was evaluated in terms of voltage (V), current (I) and power density (P_d). The experimental points *V* vs *I* were fit by a straight line having equation:

$$V(I) = OCV - R_{stack} \cdot I \tag{2.2}$$

in which the Open Circuit Voltage (OCV) is evaluated at the intersection of *V(I)* with the voltage axis (I=0), and R_{stack} is the stack resistance (the slope of the straight line). The intercept of *V(I)* with the current axis (V=0) represents the shortcut current $I_{shortcut}$. The calculated electric power density P_d (expressed in terms of W/m^2 of membrane pair) plotted as a function of the current density *i* shows a typical parabolic trend.

It is noteworthy to mention that power density is equal to zero when the current is equal to zero (open circuit condition) or when the voltage is equal to zero (shortcut condition).

Ion chromatography (IC) was used to evaluate the variation in composition of LCC dilute solutions after one hour of SGP-RE operation in batch mode.

Cation and anion analysis was performed by 861 Advanced Compact Ion Chromatography (Metrohom Italiana SrL, Italy) and data processed by ICNet 2.3. For cation analysis, Metrosep A Supp 5 250/4.0 column and Metrosep A Supp 4/5 Guard pre-column were used with eluent solution 2mM HNO_3/0.25 mM Oxalic Acid; for anion analysis, METROSEP C4 - 250/4.0 column and METROSEP C 4 Guard pre-columns were used, with eluent solution 3.2 mM Na_2CO_3/1 mM $NaHCO_3$.

2.3 Results and discussion

2.3.1 Reference test with NaCl

SGP-RE performance was preliminarily checked feeding aqueous NaCl solutions (LCC: 0.1M; HCC: 5M). According to Figure 2.2.a, the measured OCV was 3.4 V and $I_{shortcut}$=0.89 A. The power density curve is shown in Figure 2.2.b. Under these conditions, the system was able to provide a maximum gross power density of 3.04 W/m^2 in correspondence of a current density of 44.7 A/m^2. The maximum gross power density generated under these conditions was assumed as a reference for the system operated with multi-ion solutions.

Kim and Logan (2011) showed an innovative microbial reverse-electrodialysis unit (5-cells stack), when operated with typical seawater (600 mM NaCl) and river water (12 mM NaCl) solutions at 0.85 Wm^{-2}, produced up to 3.6 Wm^{-2} (cathode surface area) and 1.2-1.3 V with acetate as a substrate; a higher flow rate (1.55 $mL.min^{-1}$) resulted in power densities up to 4.3 Wm^{-2} [15].

In a comparative study between reverse electrodialysis and pressure retarded osmosis, both considered for applications on seawater and river water, Post *et al*. (2007) calculated a potential maximum power density for SGP-RE in the range of 2-4 Wm^{-2} [9].

Using a 50-cells stack, a power density of 0.93 Wm^{-2} was obtained by Veerman and colleagues (2009) with artificial river water (1 g/l NaCl) and artificial sea water (30 g/l NaCl) [4].

Daniilidis *et al.* (2014) achieved a power density of 6.7 W/m^2 of total membrane area using 0.01 M NaCl solution against 5 M at 60°C; in general, the power density was found to increase monotonically for high concentrated feed solutions [16].

Theoretical predictions on a 12-cells stack equipped with Fujifilm ion exchange membranes and operated with 0.5 M/5.4 M NaCl diluate/concentrate solutions resulted in a maximum gross power density of 2.4 Wm^{-2} [4]. A maximum gross power density of 2.2 Wm^{-2} was measured in a stack with inter-membrane distance of 100 μm using 0.507 M NaCl as artificial seawater and 0.017 M NaCl as artificial river water [7].

2.3.2 Tests on brackish water/solar pond brine

SGP-RE performance was then evaluated using artificial brackish water (fed to LCC) and exhaust brine from solar pond (fed to HCC) according to composition detailed in Table 2.2. Experimental data reported in Figure 2.2.a-b show a significant reduction of the maximum gross power density generated by the SGP-RE stack; taking as a reference the value of 3.04 W/m^2 (recorded when operating with pure NaCl solutions), it was found that $P_{d,max}$ decreased down to 1.13 W/m^2 in correspondence of a current density of 20.1 A/m^2 when operating with artificial brackish water/brine solutions. Moreover, the -63% power density reduction was accompanied by an increase of stack resistance by 76% (from 3.83 to 6.76 Ω), while OCV and shortcut current fell down to 2.77 V and 0.41 A, respectively.

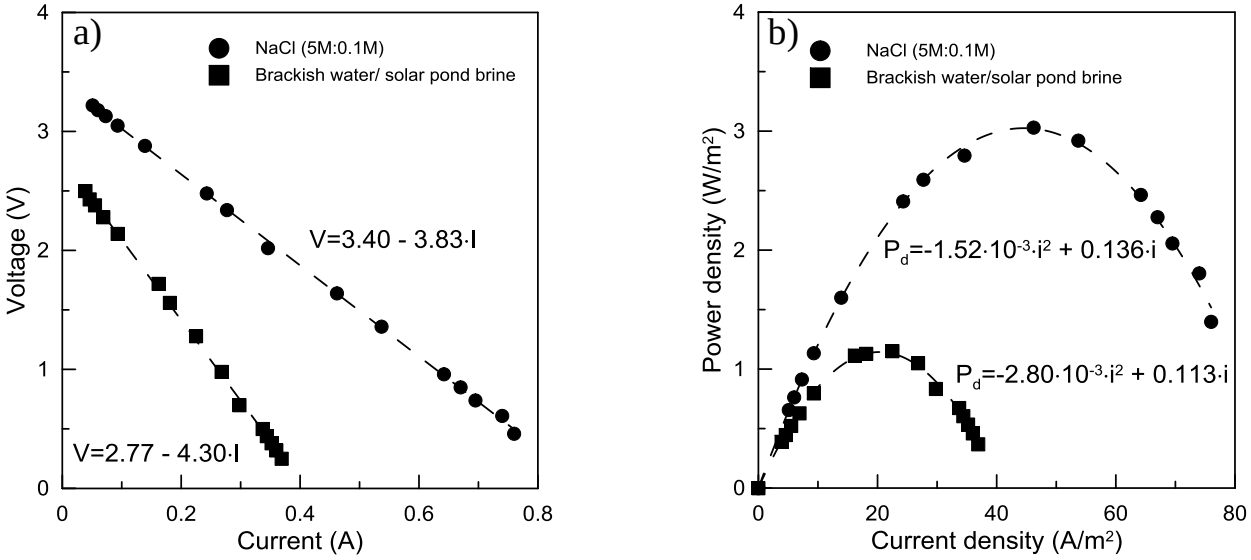

Figure 2.2: a) Voltage vs current; b) gross power density vs current density. Data collected under reference conditions: NaCl solution (0.1M/0.5M). Temperature: 20°C. Margin of error within 10%.

2.3.3 Effect of other ions

In order to discriminate the effect of multiple ions on the drastic reduction of power density generated by SGP-RE unit operated with real solutions, the combined effect of each single cation ($X^{\upsilon+}$) and anion ($Y^{\xi-}$) in presence of NaCl was investigated, and binary solutions were prepared according to compositions reported in Table 2.3. The ratios $[Cl^-]/[Y^{\xi-}]$ and $[Na^+]/[X^{\upsilon+}]$ of solutions fed to LCC and HCC were kept the same as in brackish water and brine, respectively. The trend of voltage, current and power density when SGP-RE was operated with multi-ion solutions is shown in Figure 2.3.a-b. The observed effect of HCO_3^- on SGP-RE performance was negligible due to the very low concentration of bicarbonate ion in both LCC ($8.5 \cdot 10^{-6}$ M) and HCC ($8.5 \cdot 10^{-4}$ M). As a result, the OCV remained substantially unchanged (3.39 V) as well as $I_{shortcut}$ (0.89 A) and $P_{d,max}$ (3.03 W/m^2).

Despite its significant concentration in the brine (0.32 M), the impact of K^+ on the power density was quite limited due to the similar electrochemical properties between Na^+ and K^+ ions: ionic radii of unhydrated Na^+ and K^+ are 1.17 Å and 1.64 Å, respectively; ionic radii of hydrated Na^+ and K^+ are 3.58 Å and 3.32 Å, respectively [17]; ion diffusion coefficients in water for Na^+ and K^+ are $1.334 \cdot 10^{-9}$ m^{2}s^{-1} and $1.957 \cdot 10^{-9}$ m^{2}s^{-1}, respectively[18]. While no appreciable difference in OCV was observed, $I_{shortcut}$ moderately decreased to 0.83 A (-6.7%) and R_{stack} increased to 4.08 Ω (+6.5%). The maximum power density (2.84 Wm^{-2}) was reached for a current density of 41.8

Am^{-2}.

Because its propensity to form sparingly soluble $CaSO_4$ and to precipitate from solution, Ca^{2+} is generally present in natural waters only at relatively low concentration. As a consequence, for the investigated LCC/HCC composition of 0.004M /0.096M $CaCl_2$, both OCV and power density were affected in a limited extent (-4% and -6.6 % with respect to pure NaCl, respectively). Sulfate and magnesium ions typically have the highest concentration after Na^+ and Cl^- in brine, seawater and brackish water. However, the presence of SO_4^{2-} did not change significantly OCV and resulted in a moderate decrease of $I_{shortcut}$ (0.82 A) and $P_{d,max}$ (2.79 W/m^2, - 8.2% with respect to pure NaCl).

On the other hand, the presence of magnesium cations deceased drastically both the OCV (2.73 V, -20% with respect to pure NaCl) and power density (1.11 W/m^2, -64 % with respect to pure NaCl). The value of $i_{P_d,max}$ =20.2 A/m^2 was the lowest measured. The effect of magnesium valence on the reduced electrical potential difference has been already anticipated when introducing the Nernst-Planck Eq. (2.1).

Table 2.3. Molar composition of binary LCC/HCC solutions used to investigate the effect of individual ions in presence of NaCl.

LCC solution composition	HCC solution composition	OCV (V)	R_{stack}
0.1 M NaCl	5 M NaCl	3.40	3.83
0.0999975 M NaCl +8.5·10^{-6} M $NaHCO_3$ *$[Cl^-]/[HCO_3^-]$ = 11717*	4.99915 M NaCl + 8.5·10^{-4} M $NaHCO_3$ *$[Cl^-]/[HCO_3^-]$= 5841*	3.39	3.79
0.098 M NaCl + 0.002 M KCl *$[Na^+]/[K^+]$=52.1*	4.68 M NaCl + 0.32 M KCl *$[Na^+]/[K^+]$= 14.5*	3.40	4.08
0.096 M NaCl + 0.004 M $CaCl_2$ *$[Na^+]/[Ca^{2+}]$=26.4*	4.99 M NaCl + 0.01 M $CaCl_2$ *$[Na^+]/[Ca^{2+}]$= 474*	3.27	3.84
0.0966 M NaCl + 0.0034 M Na_2SO_4 *$[Cl^-]/[SO_4^{2-}]$=28.8*	4.39 M NaCl + 0.61 M Na_2SO_4 *$[Cl^-]/[SO_4^{2-}]$= 7.15*	3.40	4.15
NaCl 0.083 M + $MgCl_2$ 0.017 M *$[Na^+]/[Mg^{2+}]$= 4.99*	NaCl 3.25 M + $MgCl_2$ 1.75 M *$[Na^+]/[Mg^{2+}]$= 1.86*	2.73	6.69

Moreover, the significant enhancement of cell resistance might be ascribed to an increase of membrane resistance in presence of Mg^{2+}. Sata (2004) reported a two to three-fold increase in electrical resistance of different commercial cation exchange membranes (NEOSEPTA CL-25T, AMFion C-310, Ionac MC-3470) when using $MgCl_2$ with respect to NaCl. An enhancement of the electrical resistance of a membrane with the concentration of the electrolyte solution was also due to the increase in Donnan adsorbed salts and shrinking of the membranes [19].

A systematic investigation of this aspect, based on Electrochemical Impedance Spectroscopy [13], will be object of future communications.

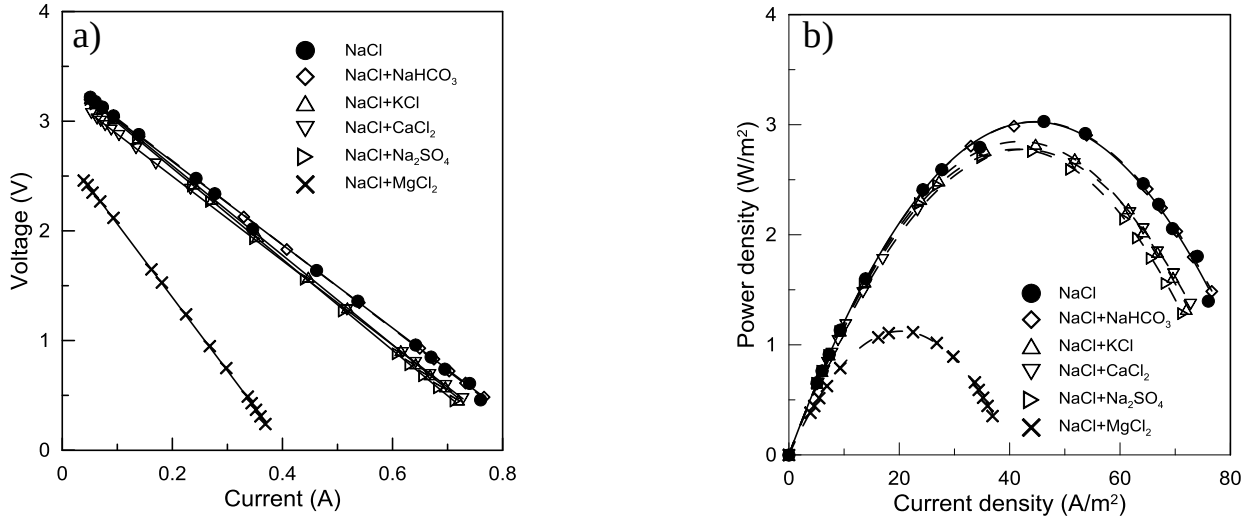

Figure 2.3. a) Voltage vs current; b) gross power density vs current density for multi-ion solutions. Compositions are detailed in Table 2.3. Temperature: 20°C. Margin of error within 10% (average of 3 tests).

2.3.4 Stack resistance

A significant advantage gained when operating SGP-RE at high salt concentration is the reduction of the electrical resistance compared to the extensively studied case of low salt concentration (i.e. combination river water/seawater). The extent of the Internal Area Resistance (IAR) per cell for the different tested solutions is presented in Figure 2.4.

These results show a lower IAR per cell of SGP-RE stack (below 26.8 Ωcm^2) compared to previous investigations on RE operated with river water/seawater solutions pair which was above 50 Ωcm^2 in most cases [3, 4, 20]. With respect to reference NaCl solutions (R_{stack} = 3.83 Ω, IAR= 15.32 Ωcm^2), significant variations in electrical resistance were observed only for NaCl + $MgCl_2$ solutions. In this case, the presence of magnesium increased the resistance of the stack (6.69 Ω) by 75 %, resulting in a drastic decrease of 64 % in power density.

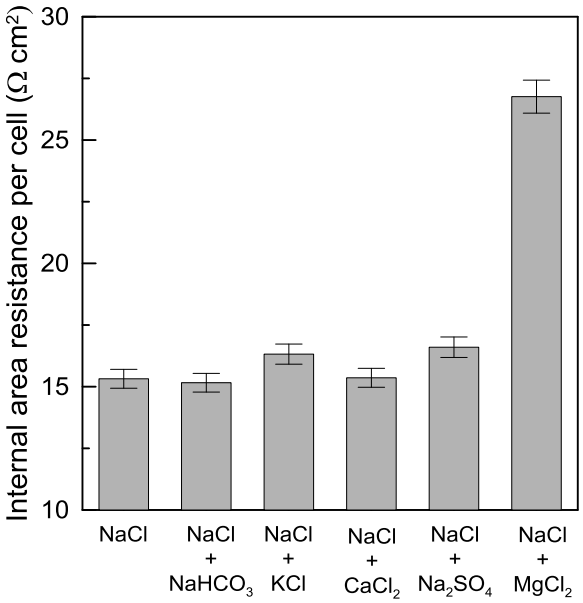

Figure 2.4. Internal area resistance per cell for binary solutions investigated (single membrane area: 100 cm2; number of cell pairs: 25).

2.3.5 Transport of ions

Ion chromatography was used to check the variation of ion composition in feed solutions as a result of the migration of ions through IEM driven by an electrochemical potential. Experimental tests were carried out in batch mode by recycling both artificial brackish water and artificial brine over the stack under open-circuit conditions (absence of net flux of electrical charges) and collecting samples after 1 hour.

Only solution flowing in the low concentration compartment was analyzed because of the large measurement errors related to the small variations in the highly concentrated brine.

Results reported in Table 2.4 show an increase in the overall concentration of LCC in the investigated interval of time, and the total mass of dissolved ions increases by 164% from 6970 to 18400 $meqL^{-1}$. Within a narrow margin of measurement error (2%), the charge balance after migration of ions is satisfied (total positive charge = 329 $meqL^{-1}$; total negative charge = 323 $meqL^{-1}$).

Figure 2.5 illustrates the transport rate of each ion as a function of its concentration in HCC compartment.

Table 2.4. Ion composition (from Ion Chromatography analysis) of the low-concentration stream in SGP-RE batch operation (Low: artificial brackish water; High: artificial brine).

	HCC	LCC		
Ion	Initial concentration (mg/l)	Initial concentration (mg/l)	Concentration after 1 hour (mg/l)	Concentration increase (mmol/l)
Na+	6,6000	1,520	3,870	102
K^+	7,740	49.7	478	11
Mg^{2+}	37,400	323	1,740	58
Ca^{2+}	242	101	115	0.35
Cl^-	170,000	3,560	8,960	152
SO_4^{2-}	64,400	335	3,380	32

Volume of low conc. compartment: 5 L; volume of high conc. compartment: 5 L. Solutions recirculated at 20 l/h. Temperature: 20°C. Data averaged on 3 measurements.

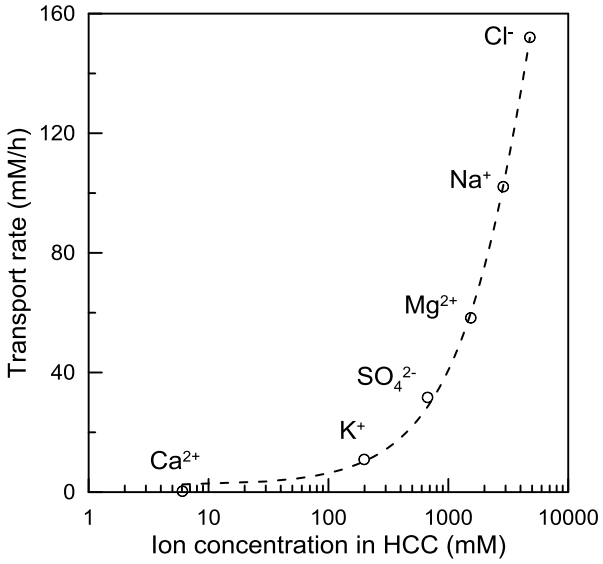

Figure 2.5. Transport rate of single ions versus their concentration in brine compartment.

Because of the non-ideal behavior of membranes, having permselectivity lower than 100%, a combined transport of both cations and anions can occur. It is interesting to compare transport rate and theoretical membrane voltage over membrane for each ion reported in Table 2.2. The measured OCV for the SGP-RE stack operated with brackish water/solar pond brine was 2.77V (Figure 2.2.a), thus implying a membrane voltage of 55 mV. Most of the voltages reported in Table 2.2 are higher than 55 mV, indicating a forward transport. Exceptions are for divalent ions Ca^{2+} and SO_4^{2-}, where expected back-transport is not observed due to the effect of multiple co-ion transport. When considering all ions, the overall electrochemical balance is satisfied within an acceptable confidence interval (7%).

The diffusion of Na^+ resulted in a concentration increase of 155% for an initial HCC/LCC

Na^+ concentration ratio of 34; a similar concentration increase (+152%) was found for chlorine with an initial HCC/LCC Cl^- concentration ratio of 47.8. These data seem to confirm that ion migration through ion exchange membranes is substantially driven by a concentration gradient.

Highlighting experiments with an ion transport carried out by Post *et al.*(2009), in which the LCC solution consisted of 3 mM NaCl + 2 mM $MgSO_4$ and the HCC of 0.45 M NaCl + 0.05 M $MgSO_4$, almost two-fold increase of sodium and chloride content in the LCC was observed after one hour when operating with standard-grade ion-exchange membranes [12].

Moreover, our measurements indicate that sodium and magnesium are transported across CEM with a flux of 2.84 and 3.24 meq $m^{-2}s^{-1}$, respectively, while chlorine and sulfate diffuse across AEM with rate 4.23 and 1.76 meq $m^{-2}s^{-1}$, respectively.

2.4 Conclusions

A cross-flow SGP-RE stack equipped with AEM-80045 and CEM-80050 membranes, when operated with 0.1 M/5M NaCl solutions, reached a maximum gross power density of 3.04 W/m^2 at 20°C and recirculation rate of 20 l/h. However, a remarkable increase of stack resistance (+75%) and a significant loss of maximum power density (-64%) were observed when the SGP-RE was operated with feed solutions containing Mg^{2+} ions (HCC: NaCl 3.25 M + $MgCl_2$ 1.75 M; $[Na^+]/[Mg^{2+}]$ = 1.86; LCC: NaCl 0.083 M + $MgCl_2$ 0.017 M; $[Na^+]/[Mg^{2+}]$ = 4.99). The comparable decrease in power density observed for artificial multi-ion solutions mimicking brackish water and exhaust brine from solar pond (Ettore Infersa site, Sicily), depicts the necessity for specific softening strategies for a better performance of SGP-RE under real conditions. In this respect, the integration of SGP-RE within pre-treatment schemes of typical SWRO desalination plants might represent a feasible and economically viable option for recovering the electrochemical energy intrinsically present into discharged brines.

Moreover, an urgent need for developing specific ion exchange membranes which do not suffer from magnesium effects is envisaged.

References

[1] M. Tedesco, A. Cipollina, A. Tamburini, W. van Baak, G. Micale, Modelling the Reverse ElectroDialysis process with seawater and concentrated brines, Desalination and Water Treatment, 49 (2012) 404-424.
[2] L.F. Weinstein JN, Electric power from differences in salinity: the dialytic battery, 191 (1976) 557-559.
[3] P. Długołęcki, A. Gambier, K. Nijmeijer, M. Wessling, Practical potential of reverse electrodialysis as process for sustainable energy generation, Environmental Science and Technology, 43 (2009) 6888-6894.
[4] J. Veerman, M. Saakes, S.J. Metz, G.J. Harmsen, Reverse electrodialysis: Performance of a stack with 50 cells on the mixing of sea and river water, Journal of Membrane Science, 327 (2009) 136-144.
[5] J.W. Post, C.H. Goeting, J. Valk, S. Goinga, J. Veerman, H.V.M. Hamelers, P.J.F.M. Hack, Towards implementation of reverse electrodialysis for power generation from salinity gradients, Desalination and Water Treatment, 16 (2010) 182-193.
[6] J. Veerman, M. Saakes, S.J. Metz, G.J. Harmsen, Electrical power from sea and river water by reverse electrodialysis: A first step from the laboratory to a real power plant, Environmental Science and Technology, 44 (2010) 9207-9212.
[7] D.A. Vermaas, M. Saakes, K. Nijmeijer, Doubled Power Density from Salinity Gradients at Reduced Intermembrane Distance, Environmental Science & Technology, 45 (2011) 7089-7095.
[8] D.A. Vermaas, J. Veerman, N.Y. Yip, M. Elimelech, M. Saakes, K. Nijmeijer, High Efficiency in Energy Generation from Salinity Gradients with Reverse Electrodialysis, ACS Sustainable Chemistry & Engineering, 1 (2013) 1295-1302.
[9] J.W. Post, J. Veerman, H.V.M. Hamelers, G.J.W. Euverink, S.J. Metz, K. Nymeijer, C.J.N. Buisman, Salinity-gradient power: Evaluation of pressure-retarded osmosis and reverse electrodialysis, Journal of Membrane Science, 288 (2007) 218-230.
[10] M. Turek, B. Bandura, P. Dydo, Power production from coal-mine brine utilizing reversed electrodialysis, Desalination, 221 (2008) 462-466.
[11] D.A. Vermaas, J. Veerman, M. Saakes, K. Nijmeijer, Influence of multivalent ions on renewable energy generation in reverse electrodialysis, Energy & Environmental Science, (2014).
[12] J.W. Post, H.V.M. Hamelers, C.J.N. Buisman, Influence of multivalent ions on power production from mixing salt and fresh water with a reverse electrodialysis system, Journal of Membrane Science, 330 (2009) 65-72.
[13] E. Fontananova, W. Zhang, I. Nicotera, C. Simari, W. van Baak, G. Di Profio, E. Curcio, E. Drioli, Probing membrane and interface properties in concentrated electrolyte solutions, Journal of Membrane Science, 459 (2014) 177-189.
[14] D.L.P.a.C.A.L. Appelo, User's guide to PHREEQC—a computer program for speciation, batch-reaction, one-dimensional transport, and inverse geochemical calculations., US Geol Surv Water Resour Invest Rep 1999.
[15] Y. Kim, B.E. Logan, Microbial reverse electrodialysis cells for synergistically enhanced power production, Environmental Science & Technology, 45 (2011) 5834-5839.
[16] A. Daniilidis, D.A. Vermaas, R. Herber, K. Nijmeijer, Experimentally obtainable energy from mixing river water, seawater or brines with reverse electrodialysis, Renewable Energy, 64 (2014) 123-131.
[17] A.G. Volkov, S. Paula, D.W. Deamer, Two mechanisms of permeation of small neutral molecules and hydrated ions across phospholipid bilayers, Bioelectrochemistry and Bioenergetics, 42 (1997) 153-160.
[18] E. Samson, J. Marchand, K.A. Snyder, Calculation of ionic diffusion coefficients on the basis of migration test results, Mat. Struct., 36 (2003) 156-165.
[19] T. Sata, Ion exchange membranes: preparation, characterization, modification and application, Royal Society of chemistry, 2004.
[20] J.W. Post, H.V.M. Hamelers, C.J.N. Buisman, Energy recovery from controlled mixing salt and fresh water with a reverse electrodialysis system, Environmental Science and Technology, 42 (2008) 5785-5790.

Chapter 3

Membrane Distillation and Reverse Electrodialysis System for Near-Zero Liquid Discharge and Low Energy Seawater Desalination

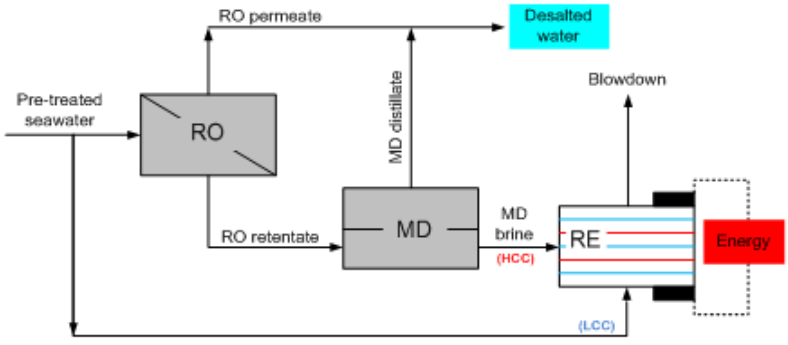

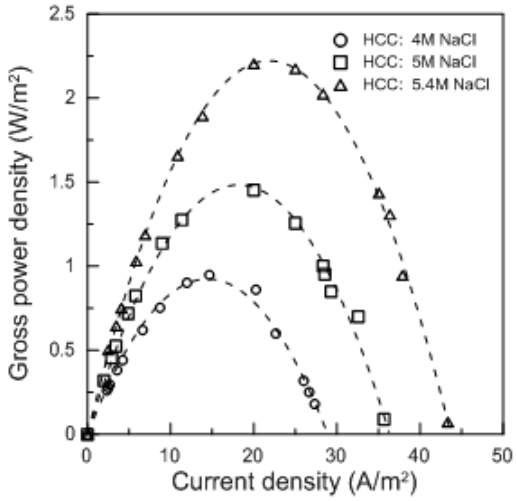

Abstract

With a total capacity of 70 million cubic meters per day, seawater desalination industry represents the most affordable source of drinking water for many people living in arid areas of the word. Seawater Reverse Osmosis (SWRO) technology, driven by the impressive development in membrane materials, modules and process design, currently shows an overall energy consumption of 3-4 kWh per m^3 of desalted water, substantially lower than thermal systems; however, the theoretical energy demand to produce 1 m^3 of potable water from 2 m^3 of seawater (50% recovery factor) is 1.06 kWh. In order to move towards this goal, the possibility to recover the energy content of discharged concentrates assumes a strategic relevance. In this work, an innovative approach combining Direct Contact Membrane Distillation (DCMD) and Reverse Electrodialysis (RE) is tested for simultaneous water and energy production from SWRO brine, thus implementing the concept of low energy and Near-Zero Liquid Discharge in seawater desalination. DCMD applied to 1M NaCl RO retentate fed at 40-50°C resulted in a Volume Reduction Factor (VRF) up to 83.6 % with a flux in the range of 1.15-2.39 kg/m^2h. The performance of RE stack fed with DCMD brine (4-5.4 M) and seawater (0.5M) was investigated at different temperatures (10-45°C) and flow velocities (0.7-1.1 cm/s). Experimental data shows the possibility of obtaining an Open Circuit Voltage (OCV) in the range of 1.5-2.3 V and a gross power density of 0.9 - 2.4 W/m^2_{MP} (membrane pair). In general, optimization is required to find best operating conditions for the proposed system.

This chapter has been published as;

R. A. Tufa, E. Curcio, E. Brauns, W. van Baak, E. Fontananova, G. Di Profio, Membrane Distillation and Reverse Electrodialysis for Near-Zero Liquid Discharge and low energy seawater desalination, *Journal of Membrane Science*, 496 (**2015**) 325-333.

3.1 Introduction

The huge growth in demand for water and energy is a global challenge for a sustainable development. At present, about 33 % of the world's population lives in water-stressed countries, and this value is expected to double by 2025[1]. With a total capacity of 70 million cubic meters per day, desalination is the most affordable source of drinking water. Seawater Reverse Osmosis (SWRO) technology, driven by the impressive development in membrane materials, modules and process design, shows an overall energy consumption of 3-4 kWh per m^3 of desalted water, substantially lower than competing thermal systems [2]. From a thermodynamic point of view, the theoretical energy demand to produce 1m^3 of potable water from 2 m^3 of seawater (50% water recovery factor) is 1.06 kWh; in order to move towards this goal, the possibility of recovering the energy content of discharged concentrates assumes a strategic relevance. Moreover, discharged brine is one of the major environmental problems associated with the extensive practice of desalination technologies, considering that water recovery in SWRO operations generally ranges within 30-50%. Literature studies demonstrate adverse ecological and toxicological impacts of hypersaline brines on soil and groundwater [3], echinoids and ascidians [4], sediment infauna [5, 6], seagrass and epifauna [7-9], planktons [10, 11], fish and clam [12] etc. In addition, the net CO_2 emissions associated with the generation of thermoelectric energy necessary to drive SWRO plants is about 1.4-1.8 kg/m^3 [2, 13, 14] with the perspective of doubling the yearly CO_2 emissions of these projections in two decades.

In this work, an innovative approach combining Membrane Distillation and Reverse Electrodialysis technologies tested for simultaneous water and energy production from SWRO desalination brine, thus implementing the concept of low energy and Near-Zero Liquid Discharge in seawater desalination. In Salinity Gradient Power-Reverse Electrodialyis (SGP-RE), anion (AEM) and cation (CEM) exchange membranes are alternatively stacked in order to create a series of adjacent compartments fed with high and low concentration solutions (High Concentration Compartment: HCC, Low Concentration Compartment: LCC) as illustrated in Figure 3.1. The electrochemical potential, resulting in a voltage drop across the electrodes, is generated from the salinity gradient that drives the selective migration of cations and anions across ion exchange membranes [15, 16]. Details on the operational principles, benefits and challenges of SGP-RE can be found elsewhere [17-23].

The large part of literature studies deal with RE power generation from NaCl solutions mimicking river water (0.015 M) and seawater (0.5 M) fed to LCC and HCC, respectively. In general, results converge towards a power density of about 4 W/m^2_{MP} [24-28] and an energy efficiency of 33-50 % [29, 30]. Further optimization of inter-membrane distance led to a maximum net power density of 4.4 W/m^2_{MP} using a spacer thickness of 60 μm [28].

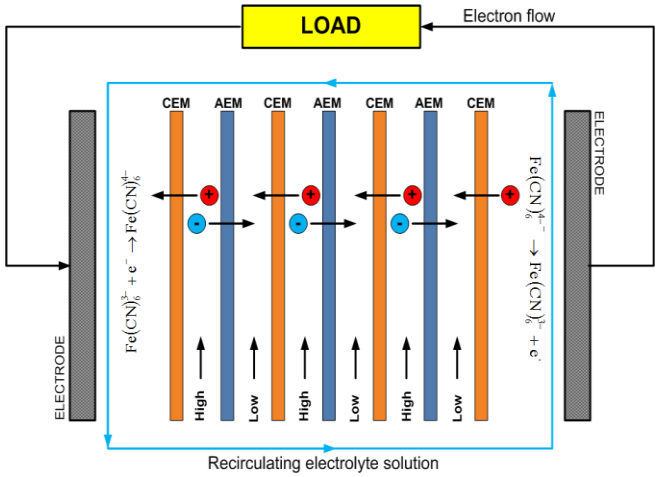

Figure 3.1. Illustration of a SGP-RE stack for electricity generation.

When feeding LCC with NaCl solutions at salinity higher than river water, the consequential depletion in power density can be partially mitigated by using high-concentrated brine in HCC, thus reducing the extent of Ohmic resistances. Theoretical and experimental investigations of Tedesco *et al.* (2012) showed the possibility to obtain a maximum power density of 2.4 W/m^2_{MP} when feeding LCC and HCC with seawater and 5.4M NaCl brine from solar pond, respectively [31]. Tufa *et al.* (2014) achieved a power density up to 3 W/m^2_{MP} using a cross flow RE stack fed with 0.1M/5M NaCl solutions [17]. Technical and economic feasibility of SGP-RE operated with brine was assessed in [32-34].

In the present work, with the aim to obtain highly concentrated NaCl brines (from 4 to 6M) as inlet stream to HCC of a SGP-RE unit, Direct Contact Membrane Distillation (DCMD) was operated on the retentate stream of a typical SWRO desalination unit (1M NaCl) working at 50% water recovery factor. In DCMD, a microporous hydrophobic membrane is in contact with a heated solution on the feed side and with cold pure water on the opposite side ("distillate"). The hydro-repellent nature of the membrane avoids the permeation of the liquid phase while sustaining a vapour-liquid interface at the entrance of each pore. Driven by a partial pressure gradient, water

evaporates from the warm side, diffuses across the membrane, and condenses into the distillate stream. In Membrane Distillation, a modest temperature difference (30-50°C) is generally sufficient to establish a quite satisfactory transmembrane flux (1-10 kg/m^2h), permitting the efficient recycling of low-grade or waste heat streams or the use of alternative renewable sources[35, 36]. The most interesting advantage of DCMD is its small sensitivity to concentration polarization; therefore, integrated RO-DCMD systems have the potential to reduce the volume of disposed brine (by about 90%), thereby increasing significantly the water recovery factor. Permeate fluxes in the range of 2.5-12.5 L $m^{-2}h^{-1}$ were obtained when feeding Capillary Accurel PP S6/2 membranes with 35 g/L NaCl solution in a temperature range of 40-70°C and with distillate at 15 °C [37]. Godino *et al.* (1997) showed a 100% increase in transmembrane flux when shifting feed temperature from 30 to 50 °C, while a 20% flux reduction was observed when feed concentration increased from 0.5 to 2.0 M [38]. A flux of about 30 L m^{-2} h^{-1} was achieved when operating with feed saline solution at 85 °C, distillate temperature of 20 °C and feed flow rate of 0.7 m/s [39].

Combination of SGP technologies with solar-driven desalination for effective conversion of osmotic energy into electrical power with simultaneous production of pure water was envisaged by Brauns (2008, 2010) [40, 41]. An integrated RO-RE system was proposed by Li *et al.* (2013) in order to reduce the high-pressure pump energy at RO stage [42]. Use of RO brine in Pressure Retarded Osmosis (PRO) was found to reduce by 40% the net specific energy consumption of a seawater RO system with respect to state-of-art values [43]. Feinberg *et al.* (2013) showed that the integration of osmotic energy recovery systems (including RE and PRO) in conventional SWRO plant could offset the total capital cost by 42% [44].

The present work experimentally proves the feasibility of simultaneous production of energy and desalted water by exploiting the synergistic combination of DCMD and RE units operated on the retentate stream of a SWRO desalination plant. Starting from separate lab-scale experiments for DCMD and RE, Figure 3.2 conceptually translates the proposed strategy to a continuous process: the brine rejected from the RO stage is further concentrated by DCMD and used to feed HCC of the SGP-RE stack for electrochemical energy generation, while seawater is fed to the LCC of the SGP-RE stack. Reverse Electrodialysis allows to recover the Gibbs free energy of mixing from low and high concentration solutions; therefore, the composition of the outlet stream leaving the SGP-RE unit (having sufficient membrane area to fully accomplish the

operation) is theoretically given by the average of LCC and HCC compositions weighted by the respective volumetric flowrates. On this basis, the outlet stream can be partially recycled back to DCMD unit.

The performance of the integrated system is investigated in terms of DCMD flux and RE gross power density as a function of the most significant operational parameters.

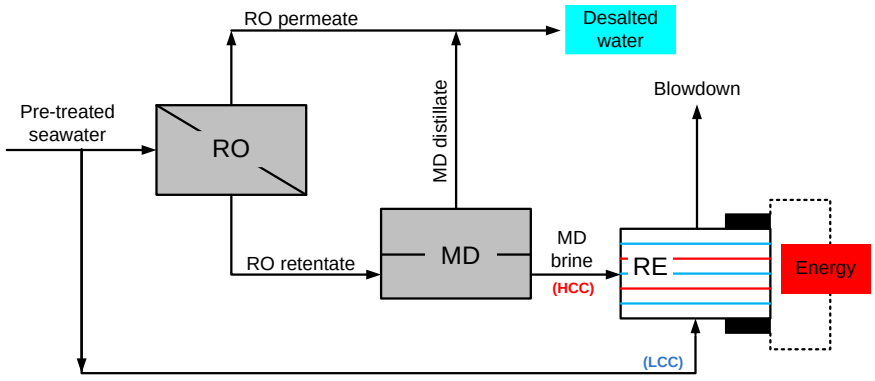

Figure 3.2. Integrated membrane system for simultaneous production of water and renewable energy (RO: Reverse Osmosis; MD: Membrane Distillation; RE: Reverse Electrodialysis; HCC: High Concentration Compartment; LCC: Low Concentration Compartment).

3.2 Theoretical Background

3.2.1 Direct Contact Membrane Distillation

According to the Dusty Gas Model theory, the flux of the i-th volatile component (J_i) through a porous medium driven by a partial pressure gradient between both sides is [36]:

$$J_i = -\frac{D_e}{RT}\nabla p_i \tag{3.1}$$

where D_e is the effective diffusion coefficient, R is the gas constant, T is the absolute temperature, and p_i is the partial pressure. Eq.(1) is valid if surface diffusion and viscous flux is negligible, which is a common assumption in DCMD. At the membrane interface, the vapor-liquid equilibrium for the *i*-th species is generally described by the Raoult equation:

$$p_i = p_i^0 x_i \gamma_i \tag{3.2}$$

where p_i^0 is the vapor pressure of the pure component, and γ_i and x_i are the activity coefficient and molar fraction, respectively. On the distillate side (pure water) x_i=1 and γ_i=1. The Antoine equation is applied to calculate the water vapor pressure as a function of temperature:

$$p_w^0 = 10^{\left(8.07131 - \frac{1730.63}{233.426 + t}\right)} \tag{3.3}$$

with p_w^0 expressed in mmHg and temperature t in °C. Values of NaCl activity coefficient in aqueous solutions are obtained from Ref. [45]. In DCMD, an empirical correlation exists between the transmembrane flux and the partial pressure difference between feed and distillate sides [46];

$$J_i = C_m[p_i^{feed} - p_i^{dist}] \tag{3.4}$$

where C_m is the membrane distillation coefficient.

Membrane Distillation is negatively affected by temperature polarization phenomenon, often causing an important loss in the driving force due to the decrease of temperatures at the membrane interface with respect to values measured in the bulk of the feed and distillate sides. Temperature polarization is quantitatively expressed by the coefficient TPC, that for DCMD is defined as [37]:

$$TPC = \frac{T_{feed}^* - T_{dist}^*}{T_{feed}^{bulk} - T_{dist}^{bulk}} \tag{3.5a}$$

where asterisk defines the interface values. Coupled heat and mass balance gives:

$$TPC_{feed}^* = \frac{\alpha(T_{dist}^{bulk} + \beta\, T_{feed}^{bulk}) + h_{feed}T_{feed}^{bulk} - J\lambda}{\alpha + h_{feed} + \alpha\beta} \tag{3.5b}$$

$$TPC_{dist}^* = \frac{\alpha(T_{feed}^{bulk} + \beta^{-1}\, T_{dist}^{bulk}) + h_{dist}T_{dist}^{bulk} + J\lambda}{\alpha + h_{dist} + \alpha\beta^{-1}} \tag{3.5c}$$

with $\alpha = (k_m/\delta)$ and $\beta = (h_{feed}/h_{dist})$; λ is the latent heat of vaporization, k_m is the thermal conductivity of the polymeric membrane, δ is the membrane thickness and h the heat transfer coefficient estimated by the classical Graetz–Lêvêque equation under laminar flow [35]:

3.2.2 ***Salinity Gradient Power***

As a paradigm of the theoretical potential of energy generation for SGP-RE systems, the free energy of mixing (ΔG_{mix}) is evaluated as a difference between the chemical potential of the mixture and the chemical potentials of the initial solutions. For brine and seawater mixing;

considering constant pressure and temperature operating conditions and no charge transport, the resulting free energy ($\Delta G_{b,s}$) can be calculated as [19, 25]:

$$\Delta G_{mix} = RT[V_m c_m \ln \gamma_m x_m - (V_d c_d \ln \gamma_d x_d + V_b c_b \ln \gamma_b x_b)] \quad (3.6)$$

where V is the volume, c is the concentration, and subscripts m, d and b refer to mixed solution, seawater and brine, respectively. The concentration c_m after mixing is given by:

$$c_m = \frac{V_d c_d + V_b c_b}{V_d + V_b} \quad (3.7)$$

According to Figure 3.3, the theoretically available amount of free energy from mixing 1 m^3 seawater (0.5 M NaCl) and 1 m^3 RO retentate (1 M NaCl) at room temperature is 200 kJ. On the other hand, when mixing 1 m^3 seawater (0.5 M NaCl) and 1 m^3 MD brine (i.e 5 M NaCl) it is about 4500 kJ, with a corresponding equivalent energy of 1.25 kWh, which is a 22-fold increase compared to the amount released by mixing seawater and RO brine. A study of Daniilidis *et al.* (2014) demonstrates the possibility of extracting a significantly higher amount of energy (15 MJ) when mixing same volume of 5 M brine and river water, but experiments carried out at this condition revealed that the maximum power density is strongly limited by the high Ohmic resistance in the low concentration compartment [47].

The electromotive force of a single RE cell (ΔE_{RE}), generated across the CEM and AEM, is:

$$\Delta E_{RE} = \frac{RT}{F}\left[\alpha_{CEM} \ln \frac{c_b \gamma_b^{Na^+}}{c_s \gamma_s^{Na^+}} + \alpha_{AEM} \ln \frac{c_b \gamma_b^{Cl^-}}{c_s \gamma_s^{Cl^-}}\right] \quad (3.8$$

where F is the Faraday constant and α is the permselectivity of the ion exchange membrane; subscripts '*s'* and *'b'* stand for seawater and brine, respectively.

The performance of SPG-RE unit is evaluated in terms of voltage (V), current (I) and gross power density (P_d). The experimental points V vs I align in a straight line described by equation:

$$V = OCV - R_{stack} \cdot I \quad (3.9$$

where OCV is the Open Circuit Voltage representing the intercept at the voltage axis (I=0), and R_{stack} is the stack resistance (the slope of the straight line). The intercept with the current axis is the shortcut current $I_{shortcut}$. The electric power density P_d as a function of the current density i (A/m^2) shows a typical parabolic trend described by a second order equation:

$$P_d = \frac{V \cdot I}{N \cdot A} = -a \cdot i^2 + b \cdot i \qquad (3.10$$

where *a* and *b* are two fitting parameters of the experimental data.

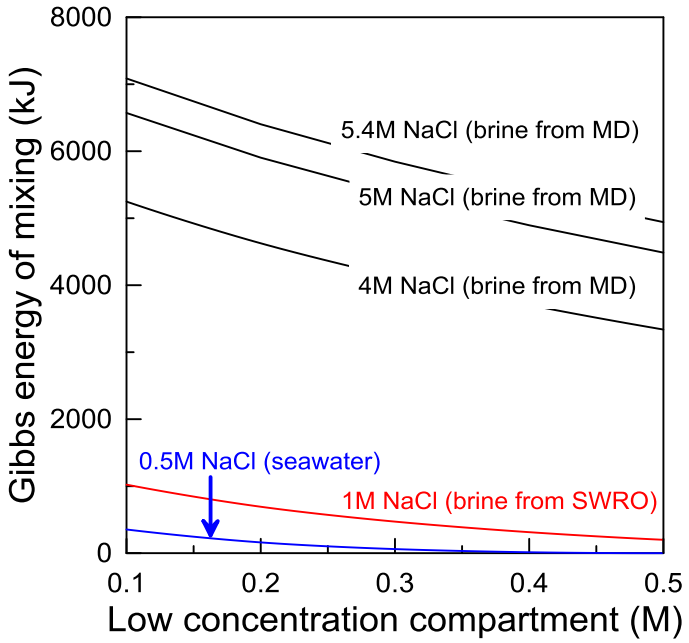

Figure 3.3. The theoretical amount of Gibbs free energy of mixing NaCl solutions (1 m^3 diluate and 1m^3 brine) at different concentrations and 293K.

In order to estimate the energy loss in the SGP-RE system due to pressure drop, the net power density P_{d_net} was calculated by subtracting the theoretical pumping power required to recirculate solutions through HCC and LCC (assuming 100% pump efficiency)-normalized by the total cell pair area of the stack-to the gross power density P_d:

$$P_{d\_net} = P_d - \frac{\Delta p_{HCC} \cdot Q_{HCC} + \Delta p_{LCC} \cdot Q_{LCC}}{N \cdot A} \qquad (3.11)$$

where Δp is the pressure drop along a compartment and Q the volumetric flowrate.

It is noteworthy to mention that P_d is zero when the current is zero (open circuit condition) or when the voltage is zero (shortcut condition). According to Eq.(10), P_d reaches its maximum value $P_{d,max} = b^2/4a$ for a maximum current density $i_{max} = b/2$.

3.3 Materials and methods

3.3.1 Feed and electrolyte solutions

Feed solutions were prepared by using analytical reagent grade NaCl (Carlo Erba, Italy) dissolved in demineralised water (Purelab, ELGA). The conductivity was checked with a conductivity meter (YSI, 3200 Conductivity instruments, USA). Aqueous electrolyte solutions used in SGP-RE unit consisted of 0.1 M $K_3Fe(CN)_6$ (Sigma Aldrich, MKBL8399V), 0.1 M $K_4Fe(CN)_6{\cdot}3H_2O$ (Sigma Aldrich, SZBC1250V), NaCl (2.5 M) with conductivity 261.2 ms/cm.

3.3.2 DCMD setup

The fully automatized DCMD bench-scale setup used in this work (Fig. 4a) is equipped with a membrane module composed of 50 microporous polypropylene hollow fibers (Accurel PP S6/2) having outer diameter of 2.8 mm, thickness of 650 μm, pore size of 0.2 μm, 70% porosity for a total membrane area of 0.35 m^2. In membrane distillation tests, feed solution (1M NaCl, mimicking the SWRO retentate at 50% recovery factor) and distillate (pure water) were recirculated by gear pump SERIE N (Pompe Cucchi, Italy) automated by AC TECH Intelligent Drive, and centrifugal pump BGM5/A (Lowara, Italy), respectively. Flow rates, measured by F14 flow meters (Blue-White Industries Ltd., US), were set to 300 l/h for both streams. Feed and distillate temperatures at the entrance of the membrane module were controlled using a heater Mod. 112A (VWR, USA) and Digital Plus RTE201 thermostatic bath (Neslab, US), respectively. SPER SCIENTIFIC 800012 Pt multi-channel thermocouples with sensitivity ±0.1°C and pressure gauges RF-D201 (DUNGS®, Germany) were used to monitor temperatures and pressures at the inlet and outlet of the membrane module on both feed and distillate streams. The inlet temperature of the distillate stream was set constant at 20°C, while inlet feed temperature was varied within 40 and 50°C. A balance (REFLEX HP 8200) connected to the distillate tank was used to measure the transmembrane flux by measuring the weight variations (± 0.1 g) over time.

3.3.3 SGP-RE setup

The SPG-RE stack (Figure 3.4b), provided by REDStack B.V (The Netherlands), was operated in cross-flow configuration. The module had an active membrane area of 0.01 m^2 (10 cm x 10 cm) per cell and 25 cell pairs. The module was equipped with 270 μm poly-ethylene gaskets and PET spacers (Deukum GMBH, Germany), Ion Exchange Membranes AEM-80045 and CEM-80050 provided by Fujifilm Manufacturing Europe B.V (The Netherlands) and working electrodes

made of inert Ti-Ru/Ir mesh that had dimensions of 10cm×10cm (MAGNETO Special Anodes B.V., The Netherlands). The properties of the ion exchange membranes are reported in Table 3.1.

Table 3.1. Relevant properties of ion exchange membranes [17].

Membrane code	Thickness (μm) †	Ion exchange capacity (mmol/g membrane)	Density of fixed charges (mol/L)†	Membrane areal resistance (Ω cm^2) ‡
Fuji-AEM-80045	129±2	1.4±0.1	3.8±0.2	1.551±0.001
Fuji-CEM-80050	114±2	1.1±0.1	2.4±0.2	2.974±0.001

† Measurement conditions: NaCl 0.5 M, 20°C
‡ Measurement conditions: NaCl 0.5 M, 20°C, 2.8 cm/s

A resistance box (high dissipation five decade) in the range of 0.1-1000 Ω (CROPICO, Bracken Hill, US) was used to load the SGP-RE unit. The resulting DC voltage drop across the resistors was measured by a 3½ digital multimeter (Valleman, DVM760, accuracy of ± 0.5%) in the range of 200 mV-200 V. The current was measured by Agilent 34422A 6½ Digit Multimeter. SGP-RE tests were carried out by fixing the low concentration compartment LCC solution to 0.5M NaCl (mimicking seawater salinity) and varying the main operating parameters (HCC concentration, temperature, flowrate) as detailed in Table 3.2.

Table 3.2. Conditions selected in SGP-RE tests (LCC: 0.5M NaCl, fixed in all experiments).

Operational parameter investigated	Values considered	Other parameters
HCC solution	4/5/5.4 M	20°C; 0.7 cm/s
Temperature	10/20/35/40/45/50 °C	HCC:5M NaCl; 0.7 cm/s
Flow velocity	0.7/0.9/1.1 cm/s	HCC:5M NaCl; 20°C

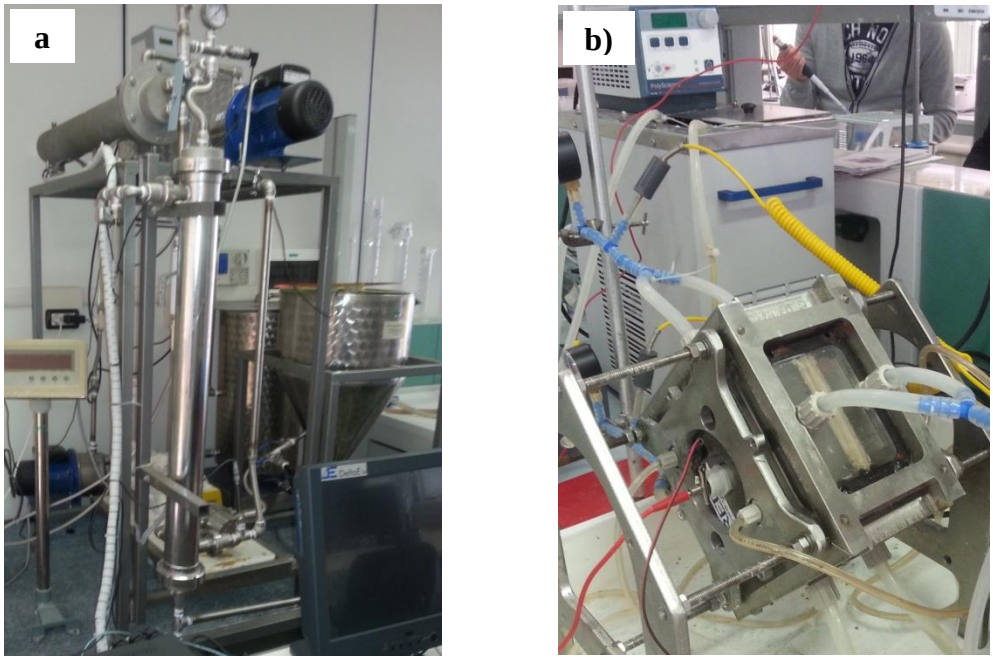

Figure 3.4. Lab-scale experimental setup for a) DCMD; b) SGP-RE.

3.4 Results and Discussion

3.4.1 Membrane distillation tests

Temperature gradient is the main operative parameter affecting the performance of DCMD in terms of transmembrane flux. Figure 3.5 shows three evaporation tests, each one lasting 4 hours, carried out on 1 M NaCl solution fed at a flow rate of 200 L/h and temperatures of 40, 45 and 50°C. The inlet temperature of the distillate is kept constant at 20°C. For a temperature difference of about 20°C, an average water flux of 1.15 kg/m^{2}h was measured, comparable to previous investigations [48]. According to Eq. (2), the value of the activity coefficient for 1 M NaCl solution (γ=0.779) reflects a flux reduction by about 25% with respect to pure water (γ=1).

When increasing feed temperature by 5 °C, the permeate flux enhances by 49.5%, aligning with the well-known exponential correlation between temperature and vapour pressure described by the Clausius-Clapeyron equation. As expected, the highest flux (2.39 kg/m^{2}h) was observed for a feed inlet temperature of 50 °C. A thermo-economic analysis is necessary in order to identify optimal operative conditions. Since an increase in the temperature gradient (and, consequently, the driving force) enhances the distillate flux, the required membrane surface area necessary to achieve a target concentration decreases, thus leading to the reduction of capital costs. Conversely, a higher temperature amplifies the energy demand at the MD stage, so impacting negatively on operating

costs. The study of Al Obaidani *et al.* (2008) identifies an optimal balance of these opposite trends in correspondence of a temperature gradient of 25°C [37]. The membrane distillation coefficient, defined according to Eq. (5), is $9.83 \cdot 10^{-3}$ s/m.

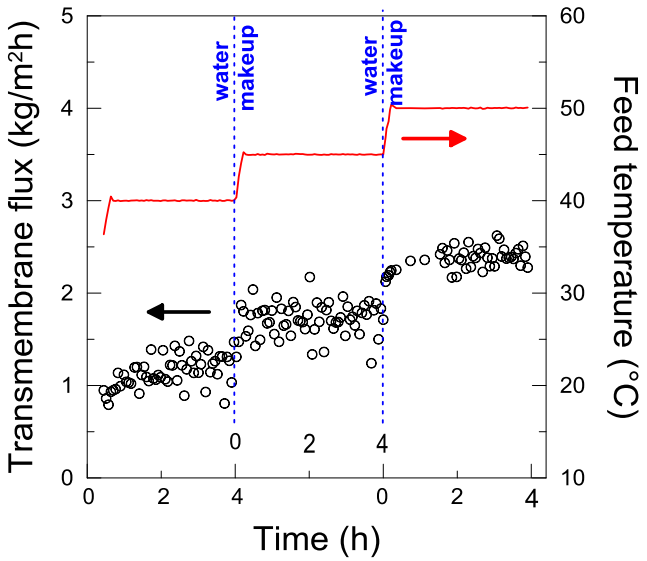

Figure 3.5. Time-variant profile of the transmembrane flux as a function of time and feed inlet temperature (feed: 1 M NaCl, $T_{d,in}$ = 20°C).

Analysis of thermal inefficiency related to temperature polarization reveals that, within the interval of investigated temperature and Reynolds number of 1400-1600, the TPC reduces from 0.71 to 0.62 when heating up the feed stream from 40 to 50 °C, with consequent depletion of the driving force. The progressive decrease of the feed interface temperature with respect to bulk value (the distillate side shows an opposite behavior) is due to the increased heat of vaporization associated to the higher transmembrane flux (term $J \cdot \lambda$ in Eq. 5(b) and (c)). Fluid dynamics significantly affects TPC: higher flowrates enhance the Reynolds number and, consequently, improve the heat transfer coefficients regulating the transport of energy within the boundary layer adjacent to the membrane. Calculations show that, when increasing both feed and distillate flowrates from 200 to 250 l/h (+25%), TPC raises by about 10%.

The ability of DCMD to reach a significant Volume Reduction Factor (VRF) and to increase the concentration of NaCl solution even up to saturation level is illustrated in Figure 3.6. Over 35 hours of operation, starting from 20 L of a solution 1M NaCl, the DCMD process carried out at feed temperature of 40°C and distillate temperature of 20°C, led to a final NaCl concentration of 3.41 M and a 70.7% VRF.

When the temperature gradient was increased to 25°C, a final NaCl concentration of 5.4 M and a VRF of 83.6% were achieved after 28 hours; moreover, transmembrane flux decreased by 21% with respect to the initial value measured (1.7 kg/m^{2}h).

As feed temperature was increased to 50°C, a DCMD test lasting 20 hours was sufficient to attain a final NaCl concentration of 5.4 M, a value close to NaCl saturation (370 g/L). The relatively high stability of DCMD is confirmed by the possibility to extend its operability up to NaCl supersaturation level that is the basis of membrane distillation-crystallization process [48, 49]. When operated with real seawater brine at high volume concentration factors, risk of scaling and fouling contamination is one of the principal challenge for Membrane Distillation. Specifically, detailed analysis on calcium carbonate precipitation rate increased by heterogeneous nucleation taking place at the membrane surface and enhanced by Ca^{2+} complexation with organic contaminants, as well as the impact of natural organic matter on the wettability of the hydrophobic membranes, have been addressed and reviewed in literature [50-52].

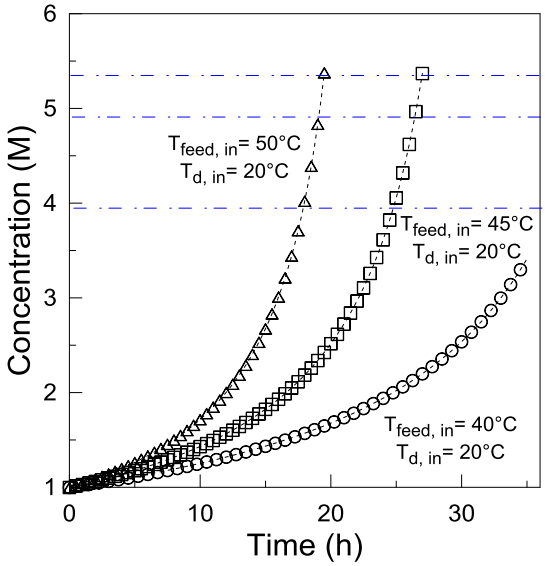

Figure 3.6. Increase of retentate concentration with time from batch evaporation experiments. Initial feed volume: 20 L.

*3.4.2 **SGP-RE tests***

*3.4.2.1 **Effect of brine concentration***

Figure 3.7a shows the linear variation of the voltage with respect to current, coherently with Ohm' law. An open circuit voltage (OCV) of 2.1 V was measured when feeding SGP-RE stack with 0.5 M NaCl/5.4 M NaCl solutions at 0.7 cm/s and 20°C. Under these operative

conditions, a shortcut current ($I_{shortcut}$) of 1.3 A was found. For 5 M NaCl, OCV decreased to 1.7 V (-19%). A further decrease of HCC concentration down to 4 M resulted in a significant reduction of OCV (by 38.5% with respect to 5.4 M NaCl) to 1.23V, and $I_{shortcut}$ was shifted to 0.7 A. These results had a relevant impact on the gross power density that can be produced by the SGP-RE system. The parabolic profiles illustrated in Figure 3.7.b revealed the possibility of obtaining a $P_{d,max}$ of 2.4 W/m^2_{MP} when working with 0.5 M NaCl/5.4 M NaCl solutions; this value was obtained in conjunction with a current density i_{max} of 23.2 A/m^2. The curve is fitted using the following parameters: a= $4.38 \cdot 10^{-3}$, b= 0.203.

A considerable decline of $P_{d,max}$ was observed when reducing the HCC NaCl concentration, specifically: 1.5 W/m^2_{MP} **for** 5M NaCl (-37.5%), and 0.9 W/m^2_{MP} for 4M NaCl (-62.5%). These variations were accompanied by a decrease of i_{max} to 18.6 and 14.5 A/m^2 for 5 M and 4 M NaCl solutions, respectively. While the fitting parameter a appeared substantially independent from HCC NaCl concentration, the parameter b decreased to 0.163 at 5 M NaCl and 0.125 at 4 M NaCl. Although the increase in concentration gradient enhances the power generation, a potential risk of membrane fouling (and, in particular, scaling due to precipitation of sparingly soluble salts such as carbonates and sulphates) when operating SGP-RE with real solutions exists [53].

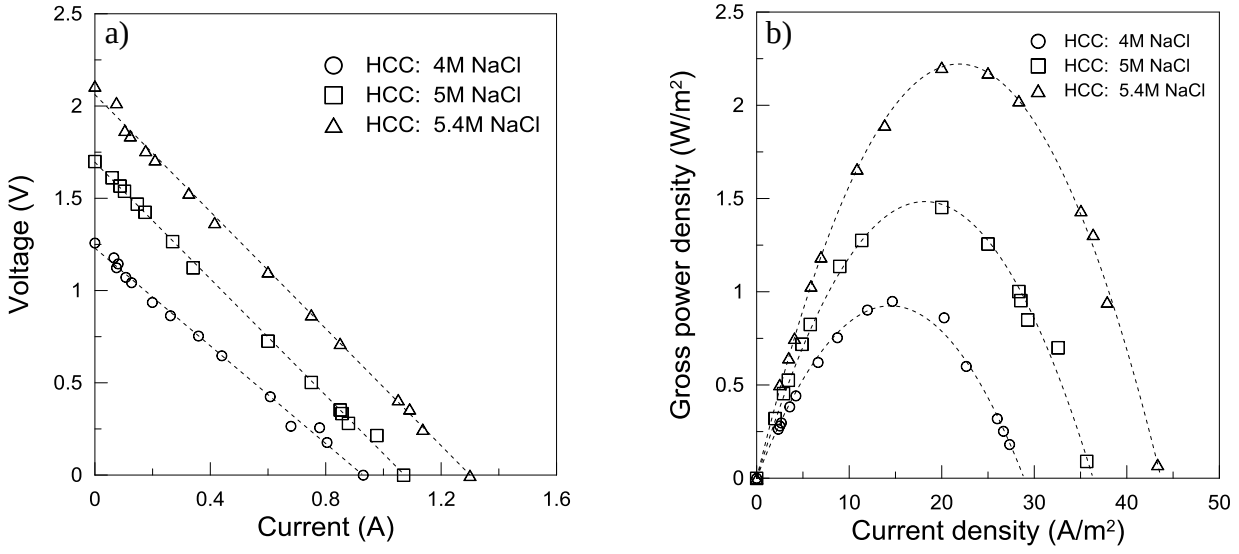

Figure 3.7. Variation of a) voltage vs current, and b) gross power density vs current density, at different HCC concentrations (LCC: 0.5 M NaCl, 20°C).

*3.4.2.2 **Effect of Temperature***

The temperature of brine leaving the DCMD stage depends on that of the feed solution; typically, for the lab-scale setup and operative conditions adopted, the temperature difference between module inlet and outlet is less than 1°C. The impact of temperature on RE performance, considering its influence on the ionic mobility and membrane resistivity, is expected to be significant [54]. As shown in Figure 3.8a, when increasing the temperature from 10 to 50°C, the OCV moderately raises from 1.67 to 1.74 V; this 4% variation is lower than the enhancement predicted by Eq. (8) (+14%). On the other hand, current density enlarges remarkably from 0.74 to 1.44 A/m^2 (+ 95%), thus leading to a positive effect on the power density. A linear trend of $I_{shortcut}$ as a function of temperature, having slope of 0.0171A/°C, was found.

According to Figure 3.8b, the maximum power density almost doubles when warming up the feed solutions from 10 to 50°C, and increases by 44% (from 1.44 to 2.08 W/m$^2_{MP}$) when shifting from room temperature to 50 °C. A linear increase of $P_{d,\,max}$ with temperature, having slope of 0.027 W/°C, was detected; moreover, the value of i_{max} raises from 17.8 A/m^2 (at 20°C) to 23.5 A/m^2 (at 50°C). Daniilidis *et al*. obtained a maximum power density of 13.4 W/m$^2_{MP}$ when using 0.01M NaCl as LCC solution at 60°C [47]. The values of coefficient *b* fitting the parabolic trend of P_d at different temperatures remained substantially stable around the average value of 0.168±0.0045, while coefficient *a* progressively decreased from $6.40\cdot10^{-3}$ to $3.64\cdot10^{-3}$.

These observations agree with our previous Electrochemical Impedance Spectroscopy (EIS) investigations demonstrating that the resistance of the ion transport through the membrane, as well as through the interface, decreased with the temperature, because of the increasing ion mobility. In particular, measurements carried out with 0.5 M NaCl solution and at temperature increasing from 20 to 40°C showed that the membrane areal resistances of Fuji-AEM-80045 and Fuji-CEM-80050 decreased from 0.25 to 0.9 Ωcm^2 and from 3.0 to 1.6 Ωcm^2, respectively [55]. In general, a thermo-economic analysis is necessary to optimize the operative temperatures of both DCMD and RE units, since an increasing temperature negatively affects the overall energy cost of the process, while improving its performance in terms of transmembrane flux and power density.

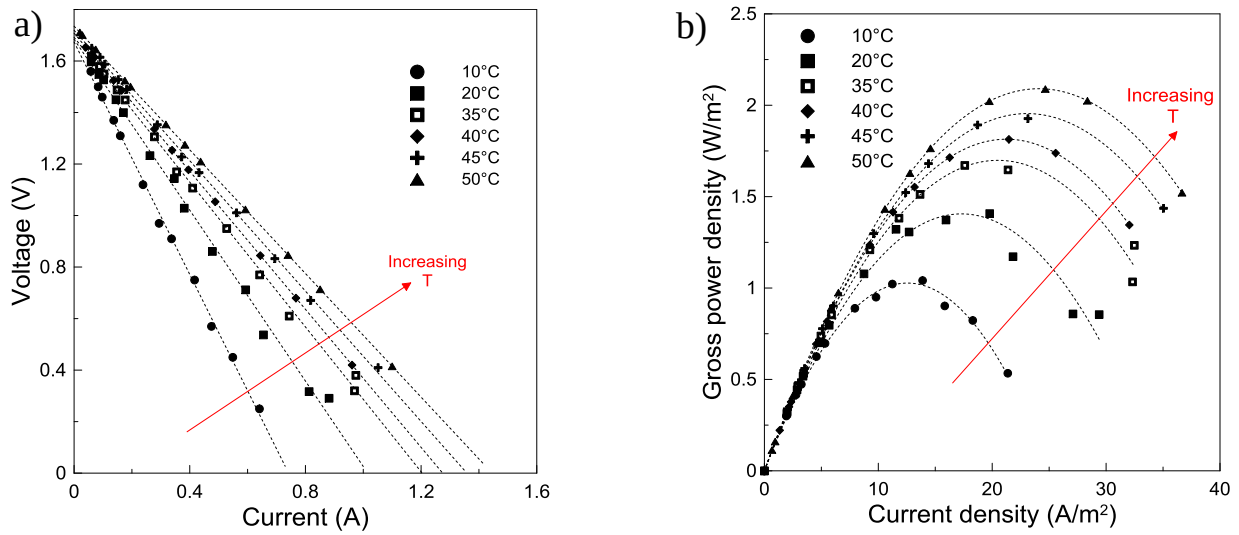

Figure 3.8. Variation of a) voltage vs current, and b) gross power density vs current density, at different temperatures (HCC: 5 M NaCl, LCC: 0.5 M NaCl).

*3.4.2.3 **Effect of Flow Rate***

The flow rate of solutions pumped through the SGP-RE unit is a parameter affecting the mass transfer of changes along the stack. Specifically, an increase of fluid velocity is expected to improve the hydrodynamic distribution of the system and, consequently, reduces the impact of concentration polarization in the boundary layers adjacent to membranes.

Our previous investigations on the interface electrical properties of ion exchange membranes by EIS revealed that increasing solution velocity decreases the interfacial transfer resistance through the diffusion double layer (up to 60% when increasing linear velocity from 1.5 to 4 cm/s) [55].

It was also found that, by increasing flow velocity from 0.7 to 1.1 cm/s, both maximum gross power density (+47%), and the OCV (+35%) enhanced (Table 3.3). Meanwhile, $I_{shortcut}$ appeared less sensitive to hydrodynamic variations within the investigated range.

Table 3.3. Effect of flow velocity on the SGP-RE performance (HCC: 5 M NaCl, LCC: 0.5 M NaCl, temperature: 20°C).

Flow velocity (cm/s)	Δp_{LCC} (bar)	Δp_{HCC} (bar)	OCV (V)	$I_{shortcut}$ (A)	i_{max} (A/m^2)	$P_{d,max}$ (W/m^2)	$P_{dnet,max}$ (W/m^2)
0.7	0.09	0.14	1.7	1.07	18.6	1.5	1.15
0.9	0.11	0.18	1.9	1.25	18.8	1.6	1.02
1.1	0.13	0.22	2.3	1.60	20.5	2.2	1.34

It is worth noting that an increase in the flow rate boosts the pumping energy required to recirculate solutions through the stack; therefore, the net power density achievable by SGP-RE unit declines. Economic optimization is therefore required in order to find optimal operative conditions. The values of pressure drop measured on both LCC and HCC of the RE stack at increasing flow velocity are reported in Table 3.3. The higher density and viscosity of 5 M NaCl (1188 kg/m^3, 1.83 cp) with respect to 0.5 M NaCl (1019 kg/m^3, 1.04 cp) is the reason for values of Δp_{HCC} greater than Δp_{LCC} by 50-60%. The consequent loss of energy, calculated by Eq. (11) and expressed in Table 3.3 in terms of maximum net power density ($P_{d\_net,max}$), raised from 23% to 39% when flow velocity increased from 0.7 to 1.1 cm/s.

3.4.2.3 SGP-RE stack resistance

The properties of the brine retentate coming from DCMD significantly affect the Internal Area Resistance (IAR) per cell of the SGP-RE unit; the trend of IAR with respect to the investigated operative conditions is presented in Figure 3.9.

Tests with increasingly high saline solutions fed to HCC show advantages in terms of reduction of the Ohmic resistance. As reported in Figure 3.9, at constant LCC concentration (0.5M NaCl), IAR decreases by 10% when increasing HCC concentration from 4 to 5.4 M. The modest decrement is probably related to the exacerbation of concentration polarization effects as a consequence of the higher diffusional flux of ions through IEMs.

For the same stack operated with 0.1 M:5 M NaCl solutions, Tufa *et al*. (2014) reported a IAR value of 15.32 Ωcm^2 [17]; interestingly, an increase of resistance by 75% was experienced when using NaCl/$MgCl_2$ solutions. Moreover, the stack resistance operated with 0.5M/5M NaCl solutions simulating seawater/MD brine composition (1.6 Ω) is significantly lower with respect to seawater/river water combination (6Ω) [24].

Tests carried out at increasing feed temperature revealed the possibility to decrease IAR by about 0.1 Ωcm^2/°C, so resulting in overall reduction of the internal area resistance of 47% when warming up solutions from 10 to 50°C. As previously mentioned, since the operative temperature in the integrated DCMD/SGP-RE system strongly affects both the energy input and output, a thermo-economic analysis is required to optimize this critical operative parameter.

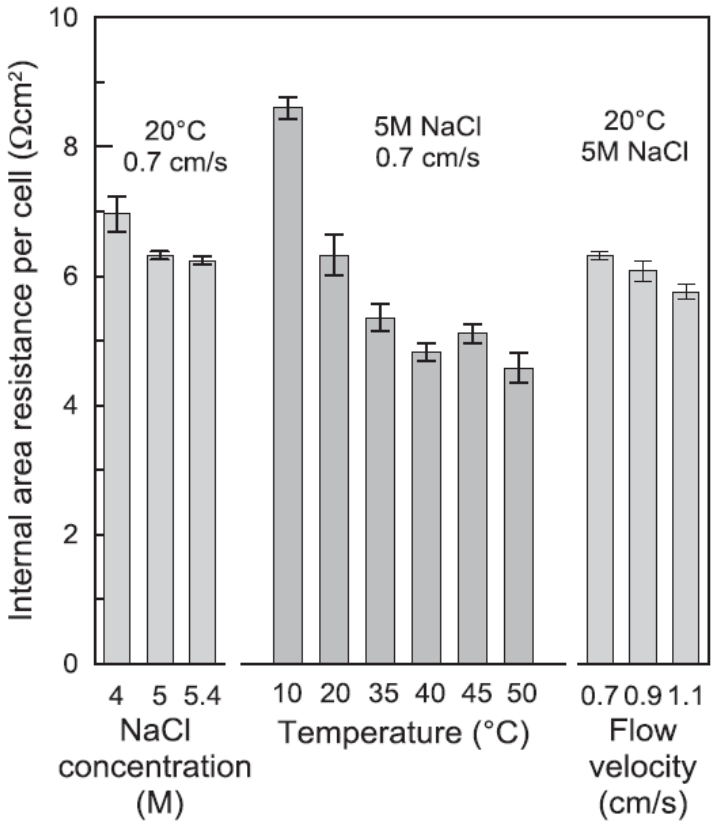

Figure 3.9. Effect of operational parameters on the internal areal resistance of the stack (single membrane area: 100 cm^2; number of cell pairs: 25).

Improvement of the mixing degree and hydrodynamics of the cells due to higher solution velocity resulted in IAR decrease of 0.14 Ωcm^2 per 0.1 cm/s increase in fluid velocity. However, the improved efficiency is counter-balanced by a decrease in the net power density due to additional pumping energy required.

3.5 Conclusions

The concept of an integrated Membrane Distillation – Reverse Electrodialysis system is a promising approach for simultaneous production of desalted water and electrical energy. In principle, when applied to Reverse-Osmosis based seawater desalination plants (SWRO), this technological solution might represent a step towards low energy desalination and Near-Zero Liquid Discharge paradigm. Moreover, benefits in terms of minimization of adverse effects of brine discharge on aquatic life and reduction of greenhouse gas emissions associated to power

plants serving huge desalination facilities can be envisaged. The exploitation of potential advantages related to the synergistic effects coming from the integration of different membrane technologies is coherent with the Process Intensification strategy [56].

Combining the hot brine produced by DCMD (that can be concentrated up to 5.4 M, leading to a volume reduction factor of 83.6%) with a SGP-RE unit might potentially result in overall water recovery factor approaching 92% and a gross power density up to 2.4 W/m^2_{MP} at 20°C and susceptible of further increase at higher temperature.

Implementation of DCMD and SGP-RE at industrial level will require significant efforts in the near future, and accurate thermo-economic analysis is required to optimize the energy input and power output. Use of renewable energy sources (i.e. solar thermal energy) or waste heat streams might contribute to supply the necessary evaporation heat at the membrane distillation stage, thus making the dehydration of RO retentate affordable [57].

Power losses observed in SGP-RE units operated with real seawater and brine solutions claim for further investigations in order to deeply understand the effect of different ions (especially divalent ones) and to efficiently implement appropriate softening methods.

The limited availability of ion-exchange membranes optimized for SGP-RE operations, in conjunction with the relatively high cost of ion exchange membrane manufacturing processes, still constrict the expansion of this market segment. Extensive research efforts have to be directed towards the improvement of stack design (including spacers and electrodes) and the achievement of long-term stability of IEM operated in a hypersaline environment. Thermo-economic analysis and cost optimization, as well as development and validation of appropriate model predicting process performance for scale-up applications, are key issues to balance benefits from enhanced performance and drawbacks from higher energy demand.

References

[1] U.E.I. Administration, International Energy Outlook 2013, in, Washington, DC 20585, 2013, pp. 9-19.
[2] M. Elimelech, W.A. Phillip, The Future of Seawater Desalination: Energy, Technology, and the Environment, Science, 333 (2011) 712-717.
[3] A.M.O. Mohamed, M. Maraqa, J. Al Handhaly, Impact of land disposal of reject brine from desalination plants on soil and groundwater, Desalination, 182 (2005) 411-433.
[4] R.H. Chesher, . Biological Impact of a Large-Scale Desalination Plant at Key West, Florida, Elsevier oceanography series, 12 (1975) 99-153.
[5] Y.D.P. Ruso, J.A.D. la Ossa Carretero, F.G. Casalduero, J.L.S. Lizaso, Spatial and temporal changes in infaunal communities inhabiting soft-bottoms affected by brine discharge, Marine Environmental Research, 64 (2007) 492-503.

[6] Y. Del-Pilar-Ruso, J.A. De-la-Ossa-Carretero, F. Giménez-Casalduero, J.L. Sánchez-Lizaso, Effects of a brine discharge over soft bottom Polychaeta assemblage, Environmental Pollution, 156 (2008) 240-250.
[7] Y. Fernández-Torquemada, J.L. Sánchez-Lizaso, J.M. González-Correa, Preliminary results of the monitoring of the brine discharge produced by the SWRO desalination plant of Alicante (SE Spain), Desalination, 182 (2005) 395-402.
[8] M. Latorre, Environmental impact of brine disposal on Posidonia seagrasses, Desalination, 182 (2005) 517-524.
[9] E. Gacia, O. Invers, M. Manzanera, E. Ballesteros, J. Romero, Impact of the brine from a desalination plant on a shallow seagrass (< i> Posidonia oceanica</i>) meadow, Estuarine, Coastal and Shelf Science, 72 (2007) 579-590.
[10] S. Lattemann, T. Höpner, Environmental impact and impact assessment of seawater desalination, Desalination, 220 (2008) 1-15.
[11] N. Raventós, E. Macpherson, A. García-Rubies, Effect of brine discharge from a desalination plant on macrobenthic communities in the NW Mediterranean, Marine Environmental Research, 62 (2006) 1-14.
[12] S. Iso, S. Suizu, A. Maejima, The lethal effect of hypertonic solutions and avoidance of marine organisms in relation to discharged brine from a destination plant, Desalination, 97 (1994) 389-399.
[13] C. Fritzmann, J. Löwenberg, T. Wintgens, T. Melin, State-of-the-art of reverse osmosis desalination, Desalination, 216 (2007) 1-76.
[14] V.G. Gude, N. Nirmalakhandan, S. Deng, Renewable and sustainable approaches for desalination, Renewable and Sustainable Energy Reviews, 14 (2010) 2641-2654.
[15] J.W. Post, H.V.M. Hamelers, C.J.N. Buisman, Energy recovery from controlled mixing salt and fresh water with a reverse electrodialysis system, Environmental Science and Technology, 42 (2008) 5785-5790.
[16] S. Pawlowski, P. Sistat, J.G. Crespo, S. Velizarov, Mass transfer in reverse electrodialysis: Flow entrance effects and diffusion boundary layer thickness, Journal of Membrane Science, 471 (2014) 72-83.
[17] R.A. Tufa, E. Curcio, W. van Baak, J. Veerman, S. Grasman, E. Fontananova, G. Di Profio, Potential of brackish water and brine for energy generation by salinity gradient power-reverse electrodialysis (SGP-RE), RSC Advances, 4 (2014) 42617-42623.
[18] J.N. WEINSTEIN, F.B. LEITZ, Electric Power from Differences in Salinity: The Dialytic Battery, Science, 191 (1976) 557-559.
[19] G.Z. Ramon, B.J. Feinberg, E.M.V. Hoek, Membrane-based production of salinity-gradient power, Energy & Environmental Science, 4 (2011) 4423-4434.
[20] Z. Jia, B. Wang, S. Song, Y. Fan, Blue energy: Current technologies for sustainable power generation from water salinity gradient, Renewable and Sustainable Energy Reviews, 31 (2014) 91-100.
[21] M.G. Buonomenna, J. Bae, Membrane processes and renewable energies, Renewable and Sustainable Energy Reviews, 43 (2015) 1343-1398.
[22] L. Cao, W. Guo, W. Ma, L. Wang, F. Xia, S. Wang, Y. Wang, L. Jiang, D. Zhu, Towards understanding the nanofluidic reverse electrodialysis system: Well matched charge selectivity and ionic composition, Energy and Environmental Science, 4 (2011) 2259-2266.
[23] D.A. Vermaas, S. Bajracharya, B.B. Sales, M. Saakes, B. Hamelers, K. Nijmeijer, Clean energy generation using capacitive electrodes in reverse electrodialysis, Energy and Environmental Science, 6 (2013) 643-651.
[24] P. Długołęcki, A. Gambier, K. Nijmeijer, M. Wessling, Practical potential of reverse electrodialysis as process for sustainable energy generation, Environmental Science and Technology, 43 (2009) 6888-6894.
[25] J. Veerman, M. Saakes, S.J. Metz, G.J. Harmsen, Reverse electrodialysis: Performance of a stack with 50 cells on the mixing of sea and river water, Journal of Membrane Science, 327 (2009) 136-144.
[26] J.W. Post, C.H. Goeting, J. Valk, S. Goinga, J. Veerman, H.V.M. Hamelers, P.J.F.M. Hack, Towards implementation of reverse electrodialysis for power generation from salinity gradients, Desalination and Water Treatment, 16 (2010) 182-193.
[27] J. Veerman, M. Saakes, S.J. Metz, G.J. Harmsen, Electrical power from sea and river water by reverse electrodialysis: A first step from the laboratory to a real power plant, Environmental Science and Technology, 44 (2010) 9207-9212.
[28] D.A. Vermaas, M. Saakes, K. Nijmeijer, Doubled Power Density from Salinity Gradients at Reduced Intermembrane Distance, Environmental Science & Technology, 45 (2011) 7089-7095.
[29] D.A. Vermaas, J. Veerman, N.Y. Yip, M. Elimelech, M. Saakes, K. Nijmeijer, High Efficiency in Energy Generation from Salinity Gradients with Reverse Electrodialysis, ACS Sustainable Chemistry & Engineering, 1 (2013) 1295-1302.

[30] N.Y. Yip, D.A. Vermaas, K. Nijmeijer, M. Elimelech, Thermodynamic, energy efficiency, and power density analysis of reverse electrodialysis power generation with natural salinity gradients, Environmental Science & Technology, 48 (2014) 4925-4936.
[31] M. Tedesco, A. Cipollina, A. Tamburini, W. van Baak, G. Micale, Modelling the Reverse ElectroDialysis process with seawater and concentrated brines, Desalination and Water Treatment, 49 (2012) 404-424.
[32] D.A. Vermaas, J. Veerman, M. Saakes, K. Nijmeijer, Influence of multivalent ions on renewable energy generation in reverse electrodialysis, Energy & Environmental Science, 7 (2014) 1434-1445.
[33] J.G. Hong, W. Zhang, J. Luo, Y. Chen, Modeling of power generation from the mixing of simulated saline and freshwater with a reverse electrodialysis system: The effect of monovalent and multivalent ions, Applied Energy, 110 (2013) 244-251.
[34] A. Daniilidis, R. Herber, D.A. Vermaas, Upscale potential and financial feasibility of a reverse electrodialysis power plant, Applied Energy, 119 (2014) 257-265.
[35] E. Drioli, A. Criscuoli, E. Curcio, Membrane Contactors: Fundamentals, Applications and Potentialities: Fundamentals, Applications and Potentialities, Elsevier, 2011.
[36] E. Curcio, E. Drioli, Membrane distillation and related operations—a review, Separation and Purification Reviews, 34 (2005) 35-86.
[37] S. Al-Obaidani, E. Curcio, F. Macedonio, G. Di Profio, H. Al-Hinai, E. Drioli, Potential of membrane distillation in seawater desalination: Thermal efficiency, sensitivity study and cost estimation, Journal of Membrane Science, 323 (2008) 85-98.
[38] M.P. Godino, L. Peña, C. Rincón, J.I. Mengual, Water production from brines by membrane distillation, Desalination, 108 (1997) 91-97.
[39] M. Gryta, Concentration of nacl solution by membrane distillation integrated with crystallization, Separation Science and Technology, 37 (2002) 3535-3558.
[40] E. Brauns, Towards a worldwide sustainable and simultaneous large-scale production of renewable energy and potable water through salinity gradient power by combining reversed electrodialysis and solar power?, Desalination, 219 (2008) 312-323.
[41] E. Brauns, An alternative hybrid concept combining seawater desalination, solar energy and reverse electrodialysis for a sustainable production of sweet water and electrical energy, Desalination and Water Treatment, 13 (2010) 53-62.
[42] W. Li, W.B. Krantz, E.R. Cornelissen, J.W. Post, A.R.D. Verliefde, C.Y. Tang, A novel hybrid process of reverse electrodialysis and reverse osmosis for low energy seawater desalination and brine management, Applied Energy, 104 (2013) 592-602.
[43] J.L. Prante, J.A. Ruskowitz, A.E. Childress, A. Achilli, RO-PRO desalination: An integrated low-energy approach to seawater desalination, Applied Energy, 120 (2014) 104-114.
[44] B.J. Feinberg, G.Z. Ramon, E.M. Hoek, Thermodynamic analysis of osmotic energy recovery at a reverse osmosis desalination plant, Environmental Science & Technology, 47 (2013) 2982-2989.
[45] X. Ji, X. Lu, S. Li, L. Zhang, Y. Wang, J. Shi, Determination of the Activity Coefficients of NaCl in the System NaCl–NH4Cl–H2O, J Solution Chem, 30 (2001) 463-473.
[46] A. Alkhudhiri, N. Darwish, N. Hilal, Membrane distillation: A comprehensive review, Desalination, 287 (2012) 2-18.
[47] A. Daniilidis, D.A. Vermaas, R. Herber, K. Nijmeijer, Experimentally obtainable energy from mixing river water, seawater or brines with reverse electrodialysis, Renewable Energy, 64 (2014) 123-131.
[48] E. Curcio, A. Criscuoli, E. Drioli, Membrane Crystallizers, Industrial & Engineering Chemistry Research, 40 (2001) 2679-2684.
[49] X. Ji, E. Curcio, S. Al Obaidani, G. Di Profio, E. Fontananova, E. Drioli, Membrane distillation-crystallization of seawater reverse osmosis brines, Separation and Purification Technology, 71 (2010) 76-82.
[50] E. Curcio, X. Ji, G. Di Profio, E. Fontananova, E. Drioli, Membrane distillation operated at high seawater concentration factors: role of the membrane on CaCO 3 scaling in presence of humic acid, Journal of Membrane Science, 346 (2010) 263-269.
[51] L.D. Tijing, Y.C. Woo, J.-S. Choi, S. Lee, S.-H. Kim, H.K. Shon, Fouling and its control in membrane distillation—A review, Journal of Membrane Science, 475 (2015) 215-244.
[52] D.M. Warsinger, J. Swaminathan, E. Guillen-Burrieza, H.A. Arafat, J.H. Lienhard V, Scaling and fouling in membrane distillation for desalination applications: A review, Desalination, 356 (2015) 294-313.
[53] D.A. Vermaas, D. Kunteng, M. Saakes, K. Nijmeijer, Fouling in reverse electrodialysis under natural conditions, Water Research, 47 (2013) 1289-1298.

[54] E. Brauns, Salinity gradient power by reverse electrodialysis: effect of model parameters on electrical power output, Desalination, 237 (2009) 378-391.
[55] E. Fontananova, W. Zhang, I. Nicotera, C. Simari, W. van Baak, G. Di Profio, E. Curcio, E. Drioli, Probing membrane and interface properties in concentrated electrolyte solutions, Journal of Membrane Science, 459 (2014) 177-189.
[56] E. Drioli, E. Curcio, Membrane engineering for process intensification: a perspective, Journal of Chemical Technology and Biotechnology, 82 (2007) 223-227.

Renewable Energy from Aqueous Sulfate Wastes by Reverse Electrodialysis

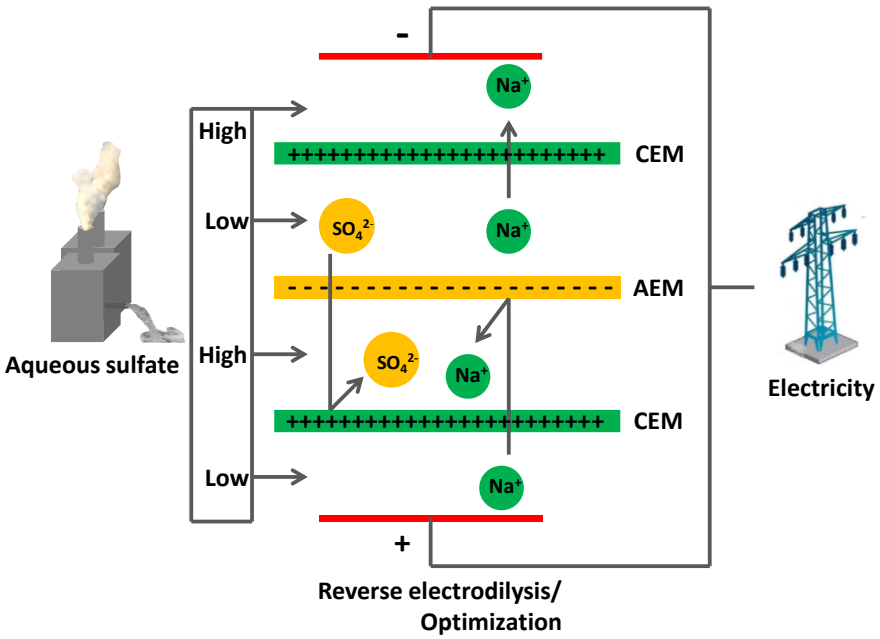

Abstract

In the present work, the potential applicability of Reverse Electrodialysis (RE) for renewable energy generation from aqueous sulfate wastes is presented. Initially, Ion Exchange Membranes (IEMs) were characterized in sulfate solution for comparison of the properties in a typically used NaCl test solution. Results indicate membrane resistance in Na_2SO_4 test solutions are higher (about 2-fold) in comparison to NaCl test solutions. In sulfate solutions, membrane area resistance decreased by about 9-12 % per 5 ^oC rise of temperature: flow dynamics have a slight influence on the membrane resistance at higher concentrations (above 0.5 M). Permselectivites determined in sulfate solution were quite low (-10%) compared to the results in NaCl test solution. RE tests with 0.035 M Na_2SO_4//1 M Na_2SO_4 solutions revealed the maximum achievable power density of about 0.3 W/m^2_{MP} (Watt per square meter membrane pair) at room temperature. Model predictions based on experimental data show a 50 % reduction in internal stack resistance results in an eight-fold increase in power density for a RE operated in sulfate solutions. Successful application of the proposed technology enables conversion of chemical potential of sulfate wastes into renewable energy, thereby reducing potential environmental impact, waste treatment and disposal costs.

This Chapter is pending for submission to the *Journal of Membrane Science*.

10.1. Introduction

Sulfate commonly occurs at high concentrations in wastewaters from sewage treatment plants and industrial processes like tanneries, pulp mills, textile mills and manufacturing processes of rechargeable batteries. Agricultural runoffs also contribute to high level of sulfate in surface water. Other source is that it can be produced as a byproduct from chemical and metallurgical processes [1]. The amount of sulfate discharged into natural water bodies is increasing from time to time due to an increased practice of these technological activities. This can lead to an acute and chronic toxicity to aquatic environments [2]. For example, one of the issues related to this is ionic imbalance due to salinity changes in natural water bodies resulting in toxicity when ionic concentrations exceed or do not meet the physiological tolerance limit of an aquatic organism [3]. Sulfate toxicity may also dependent on concentrations of other major ions, for example, with a general reduction in toxicity observed for an increasing water hardness [2]. In general, there is no well-established water quality guidelines for limiting the threshold values of the sulfate ion in various discharges implying the requirements of possible mitigation strategies to manage effluents with high load of sulfate ion.

The global potential of salinity gradient power (SGP) is estimated to be ~2.4-2.6 TW of which 980 GW is extractable [4]. In addition, up to 18 GW of SGP can be harnessed from wastewater that is discharged into an ocean [5] of which sulfate is expected to have a significant contribution. Capturing part of the chemical potential of these effluents would provide a new source of electricity, opening technological opportunities for renewable energy generation from mixing sulfate wastes of different concentration. This has a double advantage in terms of energy and environment in the process of sulfate waste management.

Reverse electrodialysis (RE) is an emerging membrane based technology used to extract SGP from mixing dilute and concentrated solutions. Simply, electricity is generated as a result of diffusion of ions (driven by salinity gradient) across alternatively aligned ion exchange membranes between two electrodes. Figure 4.1 presents a RE system operated with sulphate solution for energy generation. Level of output power and efficiency depends on stack design [6-8], membrane and cell properties [9-11], operating conditions like flow rate, temperature and concentrations [12, 13], and quality of feed streams [12, 14-16]. The total potential obtained from the stack i.e open circuit voltage (OCV) will be the sum of the Nernst potential across each membrane. Theoretically, the OCV obtained when using sulfate solutions is expected to be lower than that of NaCl due to the valence of SO_4^{2-} ion, which have a lowering effect on the Nernst potential across anion exchange membrane, as shown in the following

equation [17];

$$OCV = \frac{NRT}{F}\left(\frac{\alpha_{AEM}}{2}\ln\left(\frac{\gamma_{SO_4^{2-},c}C_{SO_4^{2-},c}}{\gamma_{SO_4^{2-},d}C_{SO_4^{2-},d}}\right)+\alpha_{CEM}\ln\left(\frac{\gamma_{Na^+,c}C_{Na^+,c}}{\gamma_{Na^+,d}C_{Na^+,d}}\right)\right) \quad (4.1)$$

where R is ideal gas constant (8.31432 J/mol.K), N is the number of membrane pairs, T is temperature (K), α is the permselectivity of the ion exchange membranes, F is Faraday constant (96485 C/mol), γ the activity coefficient of the ion and *C* is the concentration (mol/l); subscripts *c* and *d* refer to concentrated and dilute feed, respectively. The valence of SO_4^{2-} (v=2) implies that the theoretical Nernst potential across the anion exchange membrane (AEM) is reduced by half compared NaCl feed stream. According to Nernst equation, an OCV of about 0.22 V per membrane pair can be obtained from sea mixing seawater and river water (100 % selective IEMs at 298 K and neglecting electrode losses). When using sulfate feed streams (Na_2SO_4), up to 0.12 V OCV can be obtained theoretically from mixing 0.07 M//1M solutions. This value is comparable to an OCV (0.14 V) that can be obtained from brine (5 M NaCl) and seawater feeds (0.5 M NaCl).

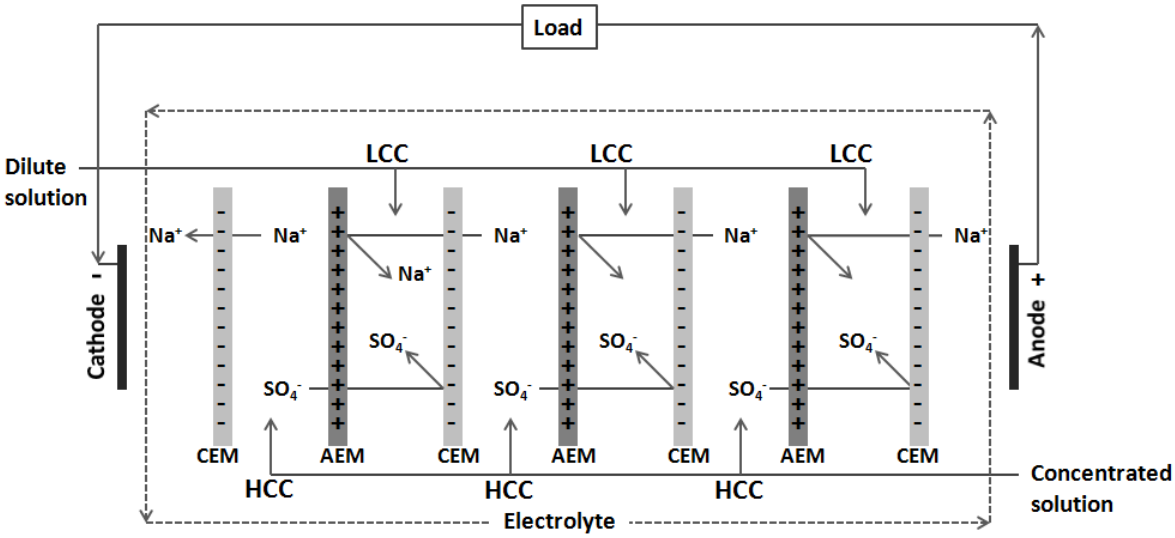

Figure 4.1. Scheme of a crossflow RE stack operated with aqueous sodium sulfate stream; AEM: anion exchange membranes, CEM: cation exchange membranes, LCC: low compartment concentration, HCC: high compartment concentration.

The RE technique was first proposed by Pattle [18] with initial power density record of about 0.05 W/m^2. A promising research progress in terms of power density improvement have been observed in the past years. So far, Vermaas *el al.* (2011) reported the highest power density (4.4 W/m$^2_{MP}$) from mixing seawater and river water at ambient temperature. Recently, Tedesco *et al.* (2015) reported higher power density of up to 12 W/m$^2_{MP}$ by working at higher

with 0.1 M//5 M) NaCl solutions and temperature of 40 ºC [19]. Much higher power density (above 13 W/m^2_{MP}) was reported by Deniilidis *et al*. (2014) using feed solutions of 0.01 M//5 M NaCl and temperature of 60 ºC [13].

Literatures report a negative impact of the presence of SO_4^{2-} ion on SGP-RE system operated with NaCl solutions. Post *et al*. (2009) have shown that the presence of SO_4^{2-} in the LCC indicated a lowering effect (up to 7 %) on OCV when the LCC compartment (3 mmol/L) is dosed with Na_2SO_4 solution at a rate in the range of 0.2 - 0.4 mmol/L.min, with an HCC solution kept at 0.4 mol/L [20]. Recently, Tufa *el al.* (2014) observed that the addition of only 3.4% Na_2SO_4 in LCC feed and 12% in HCC feed of a RE system operating with NaCl solution (0.1 M vs. 5 M) results in 8.3% increase in internal stack resistance [16]. The reasons behind the negative impact of presence of SO_4^{2-} is mainly explained in terms of higher ionic charge influencing the Nernst voltage drop over membranes, increase in membrane resistance and lowering of feed conductivity.

The possibility to exploit the chemical potential of sulfate wastes by RE was not reported so far. The main objective of this work is evaluation of potential applicability of RE for renewable energy generation from sulfate wastes. Proper experimental design and optimization technique is implemented to predict the optimal feed concentration range were the hydrodynamic and Ohmic losses at high feed flow rate and LCC concentrations can be compromised for high performance. Electrochemical characterization of IEMs was performed in terms of membrane resistance and permslectivity. In addition, the effect of operating parameters like flow rate and temperature on electrochemical membrane properties and stack power density is evaluated based on experiments and modeling. Success in conversion of sulfate wastes into renewable energy will not only be beneficial in terms of clean energy generation and waste management, but also helps in extending the application of RE to a variety of feed samples and hence further initiative for R & D in the field of blue energy.

10.2. Materials and Methods

10.2.1. Electrolyte and feed solutions

The electrolyte solution used was prepared by dissolving Na_2SO_4 (Sigma Aldrich) in deionized water (Milli Q, 18.2 mΩ cm) to 5 M, recirculated at a flow rate of 25 L/h and refreshed every week. Feed solutions of Na_2SO_4 prepared in deionized water in the concentration range of 0.035-0.1 M and 0.5-1 M were used as HCC solution and LCC solution, respectively; both solutions were recirculated at a flow velocity of 0.25-1 cm/s. A four-

electrode TetraCon 325 Conductivity Cell was used for measuring conductivity of solutions (WTW GmbH, Germany).

10.2.2. Membranes

Homogenous reinforced Fuji RP1-AEM, Fuji RP1-CEM membranes provided by Fujifilm Manufacturing Europe B.V. (The Netherlands) and commercially available homogenous CMX and AMX membranes (Neosepta, Japan) were used for experimental tests in membrane characterization and RE stack performance evaluations. Before use, membranes were equilibrated with 0.5 M Na_2SO_4 solution overnight. Properties of the ion exchange membranes in NaCl test solutions are presented Table 4.1 for comparative purposes to the properties determined in Na_2SO_4 test solutions.

10.2.3. Electrochemical membrane characterization

Permselectivity of the membrane was determined by a two compartment cell having two reference calomel electrodes separated by membrane. Details of the materials and set-up when using KCl as a test solution is described elsewhere [22]. Here, a solution of 0.1 M Na_2SO_4 is recirculated in one chamber and 0.5 M Na_2SO_4 solution is recirculated in the other chamber at room temperature. An electrical potential i.e. the Nernst potential results due to the concentration difference across the chambers. The apparent permselectivity (α) was obtained as the ratio of the measured potential (E_m) to the calculated theoretical potential of an ideally permselective (100 %) membrane (E_t);

$$\alpha = \frac{E_m}{E_t} \tag{4.2}$$

Table 4.1. Properties of the ion exchange membrane in NaCl test solution (concentration of 0.5 M) [9, 16, 23].

Membranes	IEC (mequiv./g dry membrane)	Permselectivity (%)	Area resistance ($\Omega.cm^2$)	Charge density (mol/L)
Fuji RP1 AEM	1.4±0.1	Above 95 %*	1.551±0.001	3.8±0.2
Fuji RP1 CEM	1.1±0.1		2.974±0.001	2.4±0.2
AMX	1.30 ± 0.02	91	2.65±0.04	7.8
CMX	1.64 ± 0.01	99	3.43±0.16	4.5

*Based on apparent permselectivity with in RE stack operated with seawater and river water [12].

Areal resistance determination in 0.5 M Na_2SO_4 was performed based on the direct current measurement using a Plexiglas membrane cell with six-compartments. Figure 4.2 illustrates the six compartment membrane cell used to evaluate the membrane resistance.

Experimental measurements were performed similar to the general protocol for determining membranes area resistance in NaCl test solution. Membrane area resistance measurements were performed under varying operating conditions: Na_2SO_4 concentration from 0.07 to 1M, temperatures from 10 to 35 ^oC and flow velocity from 0.5-5 cm/s. The temperature of the feed compartments was controlled with an external water bath connected with heat exchanger spiral of recirculated streams. Electrochemical measurements were performed using an Autolab PGSTAT302N (Metrohm Autolab B.V., The Netherlands). Fast step DC current was applied in the Ohmic region, in the range of 3-47 mΩ/cm^2 for 30 s. The resistance is determined from the slope of the voltage-current (V-I) curve in accordance with the Ohm's law. The area resistance of the membrane (R_m, Ω.cm^2) is obtained as the difference between the experimental runs with membranes and solutions (R_{m+s}, Ω.cm^2) and without membranes or blank solution determination (R_s, Ω.cm^2) as follows;

$$R_m = R_{m+s} - R_s \tag{4.3}$$

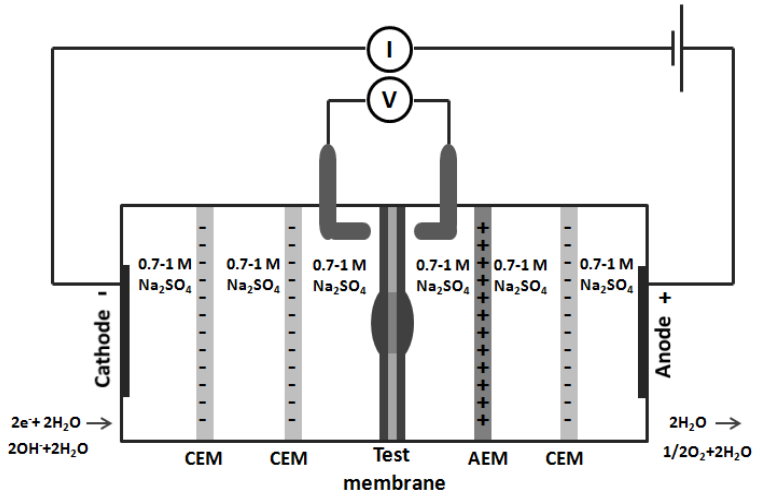

Figure 4.2. Experimental set-up of the six-compartment cell used for membrane area resistance measurements.

10.2.4. RE stack

The RE setup used in our study is described elsewhere [16]. Two stacks of 10 cell pairs and 25 cell pairs were used, each equipped with Neocepta and Fuji ion exchange membranes, respectively. The membranes had an active area of 0.01m^2 (10 cm x 10 cm) and thickness in the range of 114-181 μm. Working electrodes made of inert Ti-Ru/Ir mesh had a dimension of 10×10 cm^2 (MAGNETO Special Anodes B.V., The Netherlands). Woven nylon spacer materials with a thickness of 200 μm were used to keep distance between the membranes and allow a uniform flow distribution and turbulence promotion [24].

10.2.5. RE performance evaluation

RE stack performance analysis was evaluated mainly by electrochemical determination following a chronopotentiometric application of current density steps in the range of 0-40 A/m^2 for a minimum of 60 s to a RE stack by Autolab PGSTAT204 (Ivium Technologies, the Netherlands). Besides, V-I characterisitics of the RE was analysed by loading the system with a high dissipation five-decade resistance box in the range of 0.1-1000 Ω (CROPICO, Bracken Hill, US). The measurement of the DC voltage drop in the range of 200 mV to 200 V was done by a 3½ digital multimeter with an accuracy of 0.5% (Valleman, DVM760). The performance of the RE stack was evaluated by determinations of *OCV* (V), stack internal resistance R_{stack} (Ω) and power density P_d (W/m$^2_{MP}$). The experimentally measured potential V (V) and Current I (A) can be related as;

$$V(I) = OCV - R_{stack} I \tag{4.4}$$

The electric power density P_d as a function of the current density i (A/m^2) follows a parabolic trend fitted by a second order equation:

$$P_d = -a \cdot i^2 + b \cdot i \tag{4.5}$$

Where a and b are two fitting parameters of the experimental data. The P_d reaches its maximum value at b^2/4a for current density at b/2a.

A Box-Behnken design [25] combined with the response surface (Design-Expert® Software) methodology was employed for identification of the optimal conditions.

10.3. Results and discussion

10.3.1. Membrane resistance

Determination of membrane resistance is useful in investigation of the overall internal losses and hence the performance of SGP-RE system. Table 4.2 presents the membrane area resistance determined in Na_2SO_4 test solutions. The membrane area resistance determined in 0.5 M Na_2SO_4 test solution reached 3.99 Ω.cm^2 and 4.49 Ω.cm^2 for CMX and AMX membranes, respectively. In general, the cation exchange membranes (Fuji RP1 CEM and CMX) show slightly higher area resistance compared to anion exchange membranes (Fuji RP1 AEM and AMX). The high area resistance of cation exchange membranes is attributed to their larger membrane thickness (50-100 μm) and lower charge density compared to anion exchange membranes. The resistance values in Na_2SO_4 test solutions are about 2-fold higher when compared to the results reported for NaCl test solution [26]; for example, in Na_2SO_4 test

solution of 0.5 M concentration, the measured area resistance of AMX in Na_2SO_4 (4.49 $\Omega.cm^2$) is more or less twice as that of NaCl test solution (2.65 $\Omega.cm^2$). High membrane resistance in sulphate test solution can be explained by the lower ionic mobility of the bulky SO_4^{2-} ion compared to Cl^- ion and low specific solution conductivity of Na_2SO_4 solution in general.

Figure 4.3 presents the variation of the membrane area resistance determined in different concentrations of Na_2SO_4 test solution. A concentration mark of 0.5 M can be noted from the results. The membrane resistance doesn't depend on concentration when working with Na_2SO_4 solution at concentrations above 0.5 M indicating that Ohmic resistance (mainly due to the membrane) dominates in this region. The membrane resistance is sensitive to changes in concentration when working at concentrations below 0.5 M. This sensitivity is higher for CEMs compared to AEMs due to the difference in the ionic mobility of the cations and anions in the membrane phase [27]. This changes in membrane resistance with concentrations is more visible at concentrations below 0.5 M which is lower than the case of NaCl solution, which was reported to be below 0.1 M for Neocepta membranes [27]. Increasing the concentration of Na_2SO_4 from 0.1 M to 0.07 M results in a marked increase of membrane resistance: from 24.2 Ωcm^2 to 89.2 Ωcm^2 (about 4-fold), and from 20 Ωcm^2 to 60 Ωcm^2 (3-fold) for Neocepta and Fuji membranes, respectively. Under similar conditions, the increase in membrane resistance doesn't go beyond ~22.5 Ωcm^2 in the case of NaCl test solution [22]. The higher resistance when using Na_2SO_4 at low concentration (below 0.1 M) is due to the higher non-Ohmic resistances as a result of the concentration polarization at the membrane-solution interface and a lower specific conductivity of Na_2SO_4 compared to NaCl.

Table 4.2. Properties of ion exchange membranes in 0.5 M Na_2SO_4 test solution as determined by experiments carried out on a six compartment cell at flow velocity of 2 cm/s and temperature 25 ^oC.

Membrane	Area resistance ($\Omega.cm^2$)	Permselectivity (%)
Fuji RP1 CEM	4.70 ± 0.01	80
Fuji RP1 AEM	4.33 ± 0.067	80
AMX	3.99 ± 0.77	82
CMX	4.49 ± 0.12	90

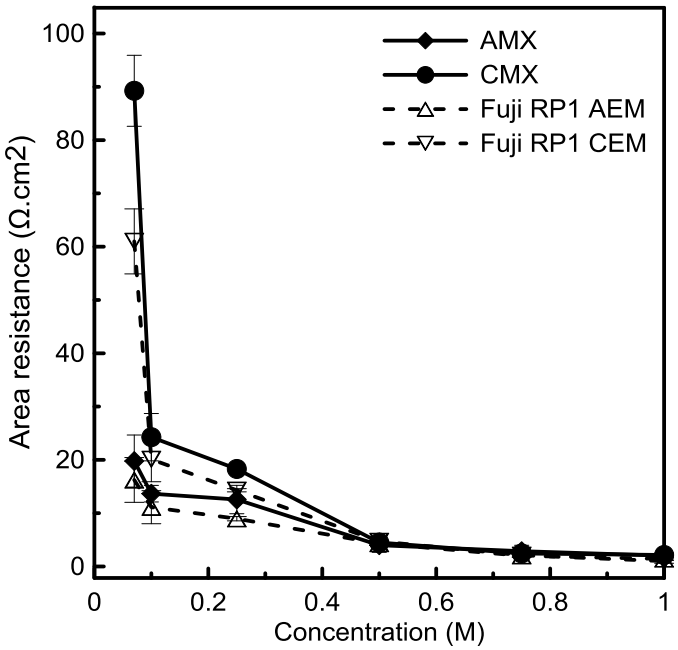

Figure 4.3. Variation of membrane area resistance with concentration changes for Na_2SO_4 test solution; experiments performed at flow velocity of 2 cm/s and temperature 25 ^oC.

Flow velocity does not have a significant influence on the membrane resistance as shown in Figure 4.4 for experiments performed in 0.5 M Na_2SO_4 test solution, a similar trend to that of NaCl solution [22]. Membrane resistance (Ohmic one) dominates here whereas the non-Ohmic part is insignificant to be influenced by the change in the hydrodynamics occurring at the membrane solution interface.

Membrane area resistance drops with increasing temperature as shown in Figure 4.5. Temperature has a direct effect on ionic mobility and solution conductivity [28], and to a less extent on the reduction of electrode over-potential. A synergetic effect of high solution conductivity and increased ionic migration across the membrane results in a lowering effect of the temperature factor on membrane area resistance. On average, membrane area resistance decreases by 11.6 % per 5 ^oC rise of temperature for the investigated membranes. Although the area resistance decreases with increase in temperature, current ion exchange membranes are reported to suffer from application at high temperature (above 40 ^oC) due to increased ionic shortcuts and electro-osmosis effect [13]. In general, benefits obtained from elevated temperature should be balanced with the cost of input energy during RE optimization procedure for scaled-up applications.

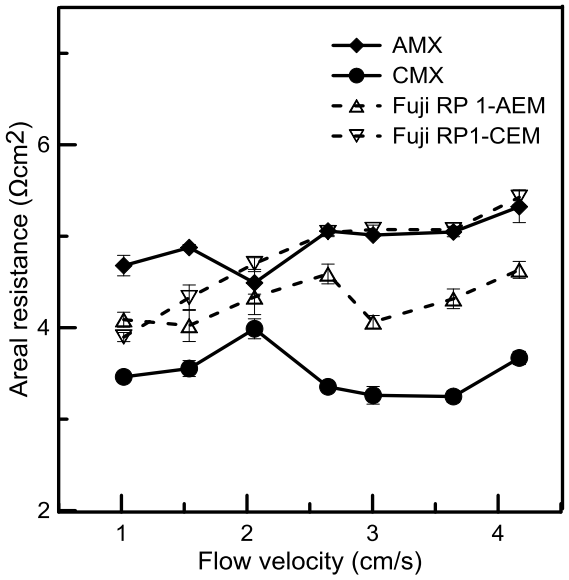

Figure 4.4. Effect of feed flow velocity on membrane areal resistance in 0.5 M Na_2SO_4 test solution at temperature 25 ^oC.

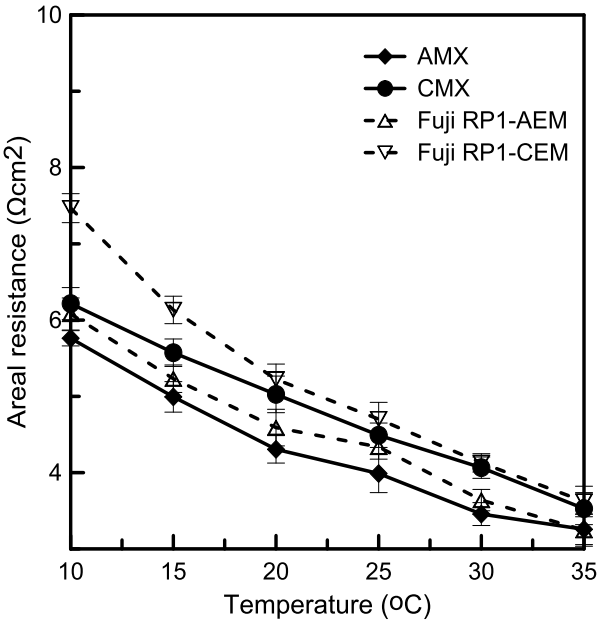

Figure 4.5. Effect of temperature parameters on membrane area resistance in 0.5 M Na_2SO_4 test solution at 2 cm/s flow velocity.

10.3.2. Permselectivity

Permselectivity is an important parameter in evaluating the performance of IEMs in RE, particularly determining the level of OCV. It is generally dependent on the transport of electric charges by the counter-ions and the total electrical current through ion exchange membranes. Since transport rate of different species of the same charge varies, it also depends on kinetic parameters of a species like ionic size [28]. This is one of the reasons for the challenges in permeability of the bulky SO_4^{2-} ions through ion exchange membranes [29]. On average, about 10 % lower permselectivity was observed for the investigated ion exchange

membranes tested in Na_2SO_4 solution compared to the standard NaCl solution (see Table 4.1). Higher permselectivity of Neocepta membranes (82-90%) compared to Fuji membranes (80-86 %) membranes could be explained by the higher fixed change density and swelling degree; higher fixed charge density of membrane increases efficiency of co-ion exclusion while moderate free volume due to higher swelling facilitates counter-ions transport and blockage of co-ions transport though the membrane layer [28, 30]. Proper membrane design could solve the permeation problems associated with SO_4^{2-} ions and concentration polarization effects for efficient application of RE system.

10.3.3. RE tests

Figure 4.6a shows the V-I (polarization) curve for the tested RE stacks. An OCV of about 1.60 V (25 cells) and 0.43 V (10 cells) was obtained when working with 0.035 M/1 M Na_2SO_4 solution. This was accompanied by 70% (from 1.6 A to 0.5 A) reduction in ionic shortcut currents ($I_{shortcut}$). In general, the OCV increases proportionally with number of cell pairs. However, there are problems with the enhancement of shortcut currents limiting the performance of RE, in particular the energy efficiency [13].

The change in OCV has a direct impact on power density [12, 17]. As shown in Figure 4.6b, a $P_{d,max}$ of 0.26 W/m$^2_{MP}$ (25 cells) and 0.3 W/m$^2_{MP}$ (10 cells) was obtained at i_{max} of 12.7 A/m^2 and 8.5 A/m^2, respectively, when working with 0.035 M//1 M Na_2SO_4 solution. When reducing the number of cell pairs from 10 to 25, the fitting parameters *a* and *b* increased by 95 % (from 0.019 to 0.037) and 46 % (0.043 to 0.063), respectively. The power densities are quite low, which could be attributed to sulphate streams basically due to low conductance of sulphate solutions resulting in high Ohmic losses in the feed compartment. In addition, suppression of the Nernst potential due to high valence of SO_4^{2-} ion, and permeation problems associated with strongly hydrated and bulky SO_4^{2-} ion accounts for the low performance of RE with sulphate solutions at this stage. The power liming problems associated with these factors can be reduced to some extent by working at high salinity gradient. More importantly, optimal membranes for sulphate solution need to be designed.

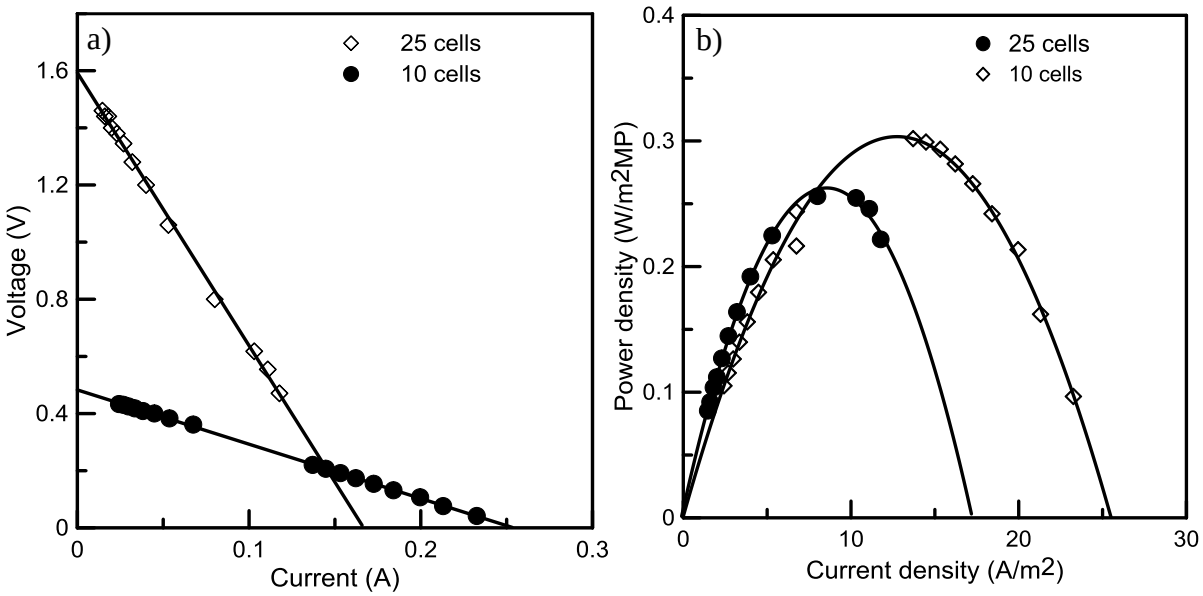

Figure 4. 6. a) Voltage-current curves, and b) power curves for the tested RE stacks; experiments at flow velocity 1 cm/s, temperature 25 ºC, LCC : 0.035 M Na_2SO_4, HCC : 1 M Na_2SO_4, error margins below 5 %.

Figure 4.7 presents a comparison of the performance of RE stacks operated with NaCl and Na_2SO_4 feed streams. It has been reported that the performance (OCV and power density) of RE with NaCl solutions increases with an increase in salinity gradient and cell size [13, 31]. This trend for Na_2SO_4 is similar to that of NaCl as mentioned earlier. Increase of OCV at the extreme salinity gradients for a RE stack operated with sulphate solution is mainly attributed to the reduction in specific conductivity of the solution, and to some extent the presence of singly charged $NaSO_4^{1-}$ ion pairs [32, 33]. However, the overall stack performance is low in the case of Na_2SO_4 solution.

A comparative assessment of the performance of RE for NaCl and NaCl solutions is presented in Figure 4.7. At the extreme salinity gradient (0.017 M//1 M Na_2SO_4), up to 23 % difference in OCV is recorded for Na_2SO_4 solutions (OCV = 0.58 V) and NaCl solutions (OCV = 0.76 V). The OCV (0.46 V) obtained for Na_2SO_4 streams when working with 0.035 M//1 M solutions and 10 cell pairs is in general lower compared to the previously reported OCV for sea-river streams; for example, Długołecki *et al.* (2009) as ~ 0.78 V (5 cells) [12] and Vermaas *et al.* (2009) as ~0.80 V (5 cells) [33]. The bulky and strongly hydrated nature of SO_4^{2-} ion [17, 34] results in lower diffusion coefficients compared to Cl^- ion (at about 0.35 M, $D_{SO_4^{2-}} = 7x10^{-6} cm^2/s$ and $D_{Cl^-} = 17.3x10^{-6} cm^2/s$) [35] which leads to the pronounced performance loss of the RE stack due to transport limitation associated with inefficient mobility of ions. In addition, the ionic fluxes and bulk transport numbers of SO_4^{2-} ion ($J_{SO_4^{2-}} = 5.58x10^{-8} mol/cm^2 s$ and $t_{SO_4^{2-}} = 0.449$) across AMX are lower than that of Cl^- ($J_{Cl^-} = 6.56x10^{-8} mol/cm^2 s$ and $t_{Cl^-} = 0.519$)

[36].

The reduction in LCC concentration also improved the performance in terms of OCV. As shown in Figure 4.7, up to 87 % and 77 % increase in OCV is recorded when LCC concentration is reduced by 83 % keeping the HCC concentration at 1 M for Na_2SO_4 and NaCl solutions, respectively.

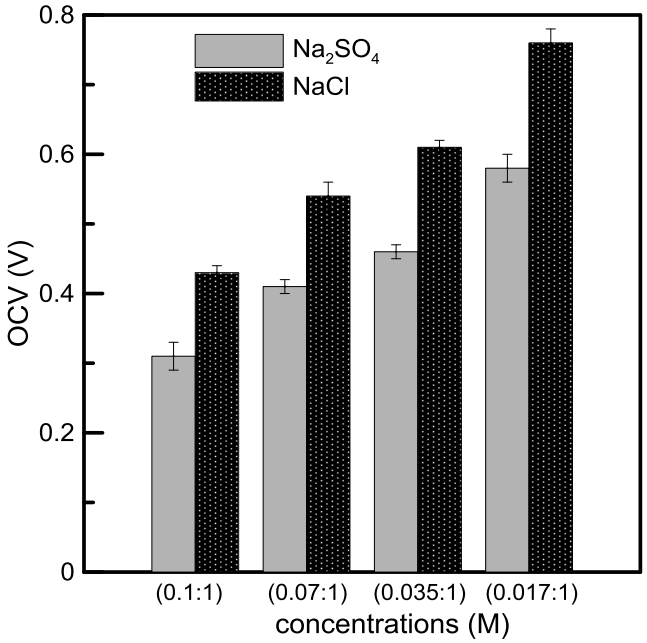

Figure 4.7. Comparison of the RE performance for Na_2SO_4 and NaCl streams (10 cells, flow velocity 1 cm/s); all measurements at temperature of 20 ^oC, error margins below 5 %.

10.3.4. Stack resistance

Internal stack resistance is a key parameter determining the overall performance of RE. In this study, RE stack equipped with Neocepta membranes tested by Na_2SO_4 feed solution resulted in internal areal resistance (IAR) per cell value in the range of 45-80 $\Omega.cm^2$ for the tested feed solutions as shown in Figure 4.8. This values are a bit higher than the typical sea/river operations which usually results in IAR of up to 40 $\Omega.cm^2$ [33]. Again, the low specific conductivity of the Na_2SO_4 solution and limited transport of ions particularly SO_4^{2-} is accountable for this phenomenon.

Although the specific conductivity of both LCC solution and HCC solution affect the level of IAR, the LCC concentrations is much more determinant. As shown in Figure 4.8, IAR is quite large (up to 80 $\Omega.cm^2$) when working in the low concentration region (0.035 M). This is correlated with the significant increase in membrane resistance at lower salt concentration (see Figure 4.3) due to the pronounced effect of the boundary layer resistance [37].

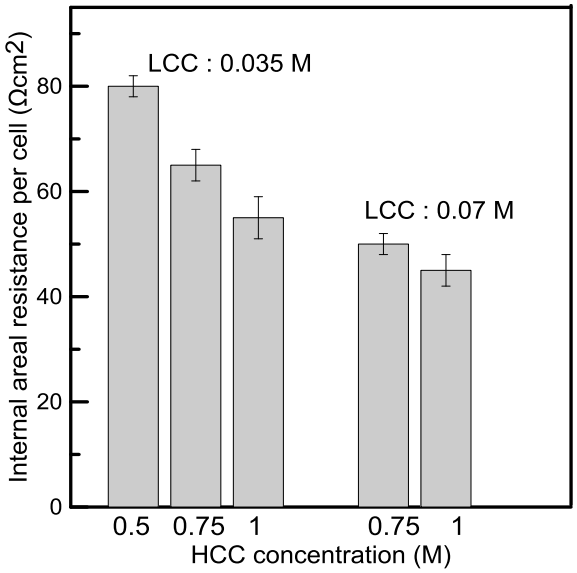

Figure 4.8. Internal area resistance plot with varying feed concentrations; LCC:0.035-0.1 M, HCC:0.5-1 M) and flow velocity 1 cm/s. All experiments were performed at 20 ^oC.

The IAR of the larger stack (25 cells) was significantly higher (up to 50 %) than that of the smaller stack (25 cells), evident from the huge internal loss revealed by the sloppy I-V curves of shown in Figure 4.6a. This indicates magnification of internal losses with increase in number of cell pairs (scale-up) although the output voltage increases.

Further enhancement of the P_d is possible by reduction of IAR either by designing suitable ion exchange membranes for sulphate solution or stack optimization for high output increasing the performance in the hydrodynamics of SGP channel through control of operating parameters like temperature and flow velocity. Figure 4.9 shows a simple linear regression model developed from the relationship between P_d and R_{stack} at different temperatures, and curve fitting was done by input parameters based on the experimental value determined in the present study. The result shows that the reduction of R_{stack} by half (e.g. from about 4.2 Ω to 2.1 Ω, at current density in the range of 5-10 A/m^2, at 20 ^oC) results in eight-fold increase of P_d (from about 0.27 to 2.2 W/m^2).

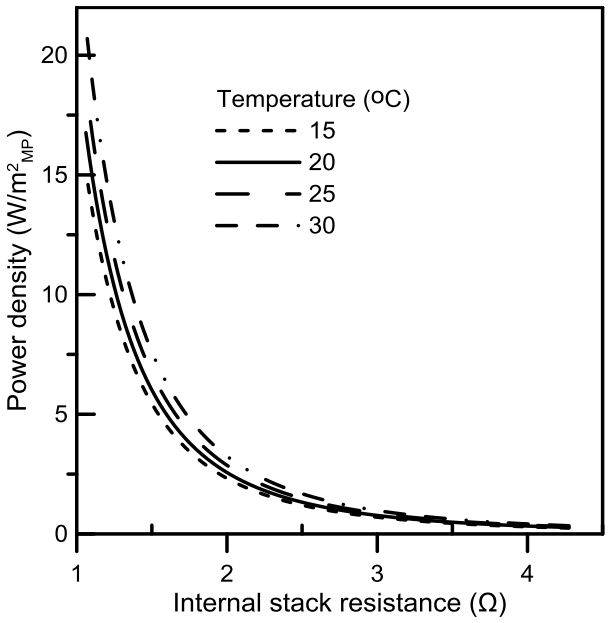

Figure 4.9. Predictions of power outputs as a function of R_i by a simple linear regression from RE system (10 cells) operated with sulfate streams; LCC: 0.035, HCC: 1 M, 1 cm/s flow velocity, and temperature variations in the range of 15-30 ºC.

10.3.5. Depiction of optimal point

A response surface model allows the prediction of optimal working conditions with a specified range of experimental variables. Systematic experimental plan based on three chosen variables (HCC concentration, LCC concentration and flow velocity) allows the prediction of the spectrum of response parameters of the RE stack (like P_d and OCV). Figure 4.10 shows the response surface plot obtained for fifteen experimental runs in the experimental boundaries of the chosen factors for the smaller stack. The results indicate the shift of optimal P_d to the region of higher salinity gradient. The maximum P_d achieved at the depicted optimal point was about 0.3 W/m^2_{MP} at 0.035 M//1 M Na_2SO_4 solutions (flow velocity 1 cm/s, temperature 20 ºC) for the small stack. For the larger stack, $P_{d,max}$ reached 0.27 $W/m^2_{MP.}$ These power densities can be increased further by increasing temperature and salinity gradient (feed concentrations)

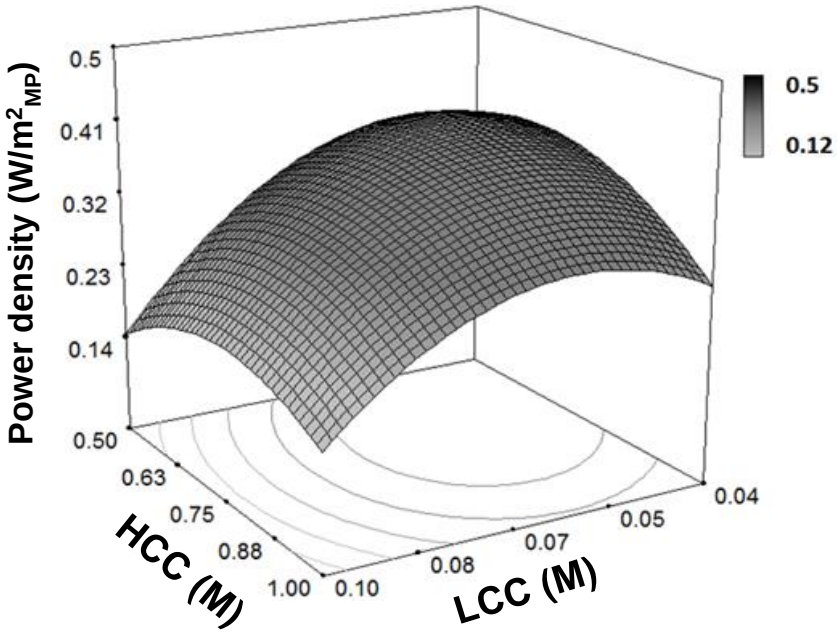

Figure 4.10. Response surface plot for experimental runs under varying feed concentrations (LCC : 0.035-0.1 M, HCC : 0.5-1 M) and flow velocity (0.25-1 cm/s); stack with10 cells. All experiments were performed at ambient temperature.

10.3.6. Response time

The stack response time indicates the time required to turn back to the blank OCV of the RE stack (~10 mV with distilled water) after experiments with salt solutions. Figure 4.11 shows the OCV vs. time plot for the experiments involving RE stack operated with Na_2SO_4 and getting back to a stable blank OCV reading. In consecutive experiments that involve switching between Na_2SO_4 and NaCl feed streams, at least 0.4 h is required for stable OCV measurements. The larger response time due to the presence of SO_4^{2-} can be attributed to the fact that SO_4^{2-} ion with high valence (z=2) binds strongly to the positive fixed charge groups of the AEMs as well as the its lower diffusivity. A similar phenomenon have been reported by Vermaas *et al.* (2014) for a RE stack operated with mixtures of NaCl and $MgSO_4$ feed solutions; RE stack equipped with Fuji membranes operating with NaCl feed solutions containing 10 % of $MgSO_4$ required a response time of about 0.5 h for a stable power density [33].

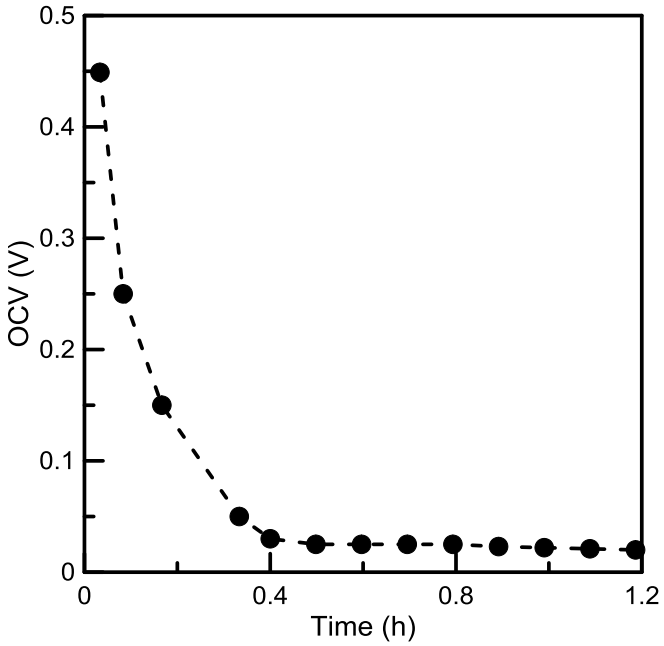

Figure 4.11. Variation of OCV with time between experiments that involve switching between Na_2SO_4 and NaCl feed solutions.

10.3.7. Conclusions and outlook

RE can be used for renewable energy generation from mixing aqueous waste resources, particularly sulfate wastes which are abundant in industrial and agricultural discharges. Membranes properties play a crucial role for the these applications. Characteristics trend of membranes in sulfate streams were similar to the trends in NaCl solution, however, with membrane conductivity and permeability observed to be low in the case of sulfate streams. Membrane area resistance increased by 2-fold whereas the permselectivity decreased by about 10 % in Na_2SO_4 compared to NaCl solution. The $P_{d,max}$ obtained was about 0.3 W/m^2_{MP} when working with 0.035 M Na_2SO_4//1 M Na_2SO_4 solutions at room temperature. Highly hydrated, bulky and doubly charged SO_4^{2-} ion with limited duffusivity in the membrane phase suppresses the Nernst potential over the membranes thereby reducing the RE performance in general.

The main challenges involve low permeability of sulfate ions through ion exchange membranes, the low specific conductivity of Na_2SO_4 solution and increase of membrane resistance. Increasing the permselectivity and reducing the membrane resistance through appropriate polymerization and structural modification is suggested as a good strategy to enhance membrane permeability for SO_4^{2-} ion [29, 38]. Investigations on the effect of blend ratios and cross linking degree [39] on one or more of electrochemical properties of membranes is also important.

Successful application of RE for energy generation from waste resources is helpful in tackling the environmental and ecological problems associated with continuous disposal of

sulphate waste resources. This also enables implementation of renewable energy based waste treatment plants or grid power supply from SGP captured from mixing sulfate waste streams.

References

[1] S.S. Chadwick, Ullmann's Encyclopedia of Industrial Chemistry, Reference Services Review, 16 (1988) 31-34.

[2] J.R. Elphick, M. Davies, G. Gilron, E.C. Canaria, B. Lo, H.C. Bailey, An aquatic toxicological evaluation of sulfate: The case for considering hardness as a modifying factor in setting water quality guidelines, Environmental Toxicology and Chemistry, 30 (2011) 247-253.

[3] W.L. Goodfellow, L.W. Ausley, D.T. Burton, D.L. Denton, P.B. Dorn, D.R. Grothe, M.A. Heber, T.J. Norberg-King, J.H. Rodgers, Major ion toxicity in effluents: A review with permitting recommendations, Environmental Toxicology and Chemistry, 19 (2000) 175-182.

[4] J.W. Post, J. Veerman, H.V.M. Hamelers, G.J.W. Euverink, S.J. Metz, K. Nymeijer, C.J.N. Buisman, Salinity-gradient power: Evaluation of pressure-retarded osmosis and reverse electrodialysis, Journal of Membrane Science, 288 (2007) 218-230.

[5] B.E. Logan, M. Elimelech, Membrane-based processes for sustainable power generation using water, Nature, 488 (2012) 313-319.

[6] J. Veerman, M. Saakes, S.J. Metz, G.J. Harmsen, Electrical power from sea and river water by reverse electrodialysis: A first step from the laboratory to a real power plant, Environmental Science and Technology, 44 (2010) 9207-9212.

[7] J. Veerman, J.W. Post, M. Saakes, S.J. Metz, G.J. Harmsen, Reducing power losses caused by ionic shortcut currents in reverse electrodialysis stacks by a validated model, Journal of Membrane Science, 310 (2008) 418-430.

[8] D.A. Vermaas, M. Saakes, K. Nijmeijer, Doubled Power Density from Salinity Gradients at Reduced Intermembrane Distance, Environmental Science & Technology, 45 (2011) 7089-7095.

[9] E. Güler, R. Elizen, D.A. Vermaas, M. Saakes, K. Nijmeijer, Performance-determining membrane properties in reverse electrodialysis, Journal of Membrane Science, 446 (2013) 266-276.

[10] D.A. Vermaas, M. Saakes, K. Nijmeijer, Power generation using profiled membranes in reverse electrodialysis, Journal of Membrane Science, 385-386 (2011) 234-242.

[11] J. Veerman, M. Saakes, S.J. Metz, G.J. Harmsen, Reverse electrodialysis: Performance of a stack with 50 cells on the mixing of sea and river water, Journal of Membrane Science, 327 (2009) 136-144.

[12] P. Długołęcki, A. Gambier, K. Nijmeijer, M. Wessling, Practical potential of reverse electrodialysis as process for sustainable energy generation, Environmental Science and Technology, 43 (2009) 6888-6894.

[13] A. Daniilidis, D.A. Vermaas, R. Herber, K. Nijmeijer, Experimentally obtainable energy from mixing river water, seawater or brines with reverse electrodialysis, Renewable Energy, 64 (2014) 123-131.

[14] E. Brauns, Salinity gradient power by reverse electrodialysis: effect of model parameters on electrical power output, Desalination, 237 (2009) 378-391.

[15] K.S. Kim, W. Ryoo, M.S. Chun, G.Y. Chung, S.O. Lee, Transport analysis in reverse electrodialysis with pulsatile flows for enhanced power generation, Korean Journal of Chemical Engineering, 29 (2012) 162-168.

[16] R.A. Tufa, E. Curcio, W. van Baak, J. Veerman, S. Grasman, E. Fontananova, G. Di Profio, Potential of brackish water and brine for energy generation by salinity gradient power-reverse electrodialysis (SGP-RE), RSC Advances, 4 (2014) 42617-42623.

[17] J.N. WEINSTEIN, F.B. LEITZ, Electric Power from Differences in Salinity: The Dialytic Battery, Science, 191 (1976) 557-559.

[18] R. Pattle, Production of electric power by mixing fresh and salt water in the hydroelectric pile, (1954).

[19] M. Tedesco, E. Brauns, A. Cipollina, G. Micale, P. Modica, G. Russo, J. Helsen, Reverse Electrodialysis with saline waters and concentrated brines: a laboratory investigation towards technology scale-up, Journal of Membrane Science, (2015).

[20] J.W. Post, H.V.M. Hamelers, C.J.N. Buisman, Influence of multivalent ions on power production from mixing salt and fresh water with a reverse electrodialysis system, Journal of Membrane Science, 330 (2009) 65-72.

[21] J.G. Hong, W. Zhang, J. Luo, Y. Chen, Modeling of power generation from the mixing of simulated saline and freshwater with a reverse electrodialysis system: The effect of monovalent and multivalent ions, Applied Energy, 110 (2013) 244-251.

[22] P. Długołęcki, P. Ogonowski, S.J. Metz, M. Saakes, K. Nijmeijer, M. Wessling, On the resistances of membrane, diffusion boundary layer and double layer in ion exchange membrane transport, Journal of Membrane Science, 349 (2010) 369-379.

[23] E. Fontananova, W. Zhang, I. Nicotera, C. Simari, W. van Baak, G. Di Profio, E. Curcio, E. Drioli, Probing membrane and interface properties in concentrated electrolyte solutions, Journal of Membrane Science, 459 (2014) 177-189.
[24] P. Długołecki, J. Dabrowska, K. Nijmeijer, M. Wessling, Ion conductive spacers for increased power generation in reverse electrodialysis, Journal of Membrane Science, 347 (2010) 101-107.
[25] S.L.C. Ferreira, R.E. Bruns, H.S. Ferreira, G.D. Matos, J.M. David, G.C. Brandão, E.G.P. da Silva, L.A. Portugal, P.S. dos Reis, A.S. Souza, W.N.L. dos Santos, Box-Behnken design: An alternative for the optimization of analytical methods, Analytica Chimica Acta, 597 (2007) 179-186.
[26] P. Długołęcki, K. Nymeijer, S. Metz, M. Wessling, Current status of ion exchange membranes for power generation from salinity gradients, Journal of Membrane Science, 319 (2008) 214-222.
[27] P. Długołęcki, B. Anet, S.J. Metz, K. Nijmeijer, M. Wessling, Transport limitations in ion exchange membranes at low salt concentrations, Journal of Membrane Science, 346 (2010) 163-171.
[28] H. Strathmann, Ion-exchange membrane separation processes, Elsevier, 2004.
[29] T. Sata, K. Mine, M. Higa, Change in permselectivity between sulfate and chloride ions through anion exchange membrane with hydrophilicity of the membrane, Journal of Membrane Science, 141 (1998) 137-144.
[30] E. Güler, R. Elizen, D.A. Vermaas, M. Saakes, K. Nijmeijer, Performance-determining membrane properties in reverse electrodialysis, Journal of Membrane Science, 446 (2013) 266-276.
[31] J. Kim, S.J. Kim, D.K. Kim, Energy harvesting from salinity gradient by reverse electrodialysis with anodic alumina nanopores, Energy, (2013).
[32] R. Buchner, S.G. Capewell, G. Hefter, P.M. May, Ion-pair and solvent relaxation processes in aqueous Na2SO4 solutions, The Journal of Physical Chemistry B, 103 (1999) 1185-1192.
[33] D.A. Vermaas, J. Veerman, M. Saakes, K. Nijmeijer, Influence of multivalent ions on renewable energy generation in reverse electrodialysis, Energy & Environmental Science, (2014).
[34] J. Jörissen, K.H. Simmrock, The behaviour of ion exchange membranes in electrolysis and electrodialysis of sodium sulphate, Journal of Applied Electrochemistry, 21 (1991) 869-876.
[35] J.M. Nielsen, A.W. Adamson, J.W. Cobble, The Self-diffusion Coefficients of the Ions in Aqueous Sodium Chloride and Sodium Sulfate at 25°, Journal of the American Chemical Society, 74 (1952) 446-451.
[36] E. Güler, W. van Baak, M. Saakes, K. Nijmeijer, Monovalent-ion-selective membranes for reverse electrodialysis, Journal of Membrane Science, 455 (2014) 254-270.
[37] J.-S. Park, J.-H. Choi, J.-J. Woo, S.-H. Moon, An electrical impedance spectroscopic (EIS) study on transport characteristics of ion-exchange membrane systems, Journal of Colloid and Interface Science, 300 (2006) 655-662.
[38] T. Sata, T. Yamaguchi, K. Matsusaki, Effect of Hydrophobicity of Ion Exchange Groups of Anion Exchange Membranes on Permselectivity between Two Anions, The Journal of Physical Chemistry, 99 (1995) 12875-12882.
[39] E. Guler, Y. Zhang, M. Saakes, K. Nijmeijer, Tailor-Made Anion-Exchange Membranes for Salinity Gradient Power Generation Using Reverse Electrodialysis, ChemSusChem, 5 (2012) 2262-2270.

Chapter 5

Fouling Tendency and Stability of Ion Exchange Membranes for Reverse Electrodialysis Operated with Concentrated Brine

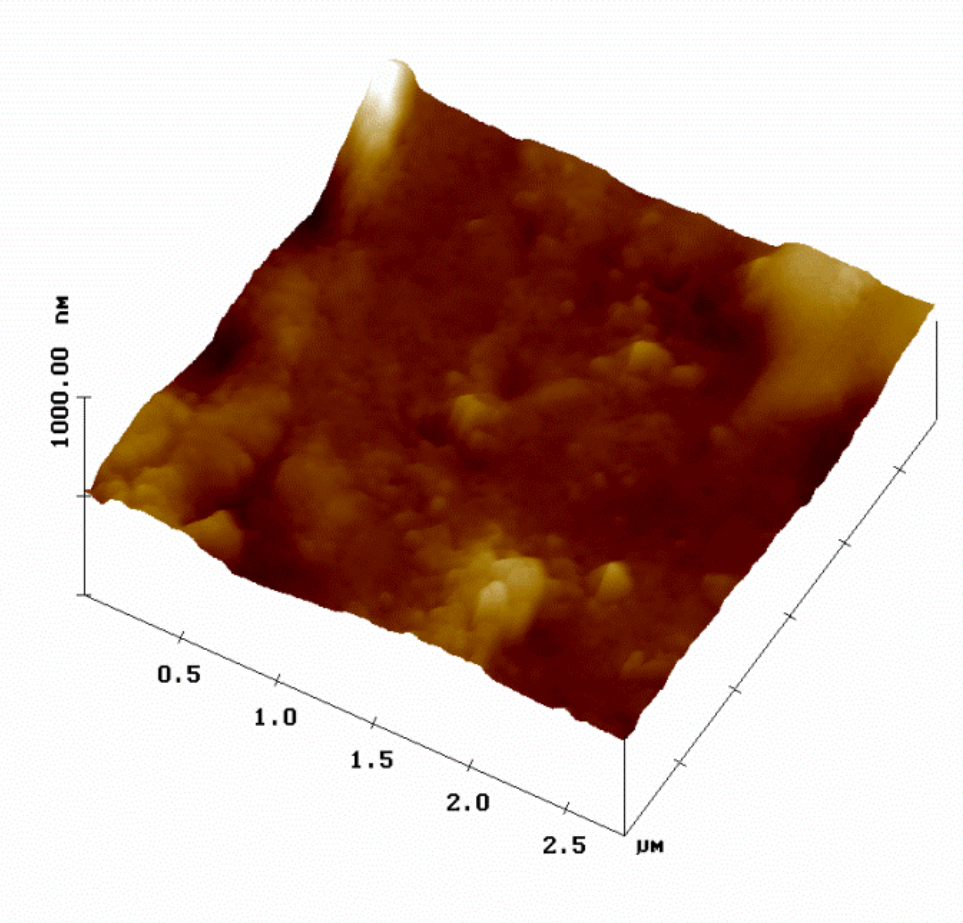

Abstract

Reverse Electrodialysis (RE) is a renewable energy technology for converting salinity gradient energy into electricity. Ion exchanging membranes (IEMs) are key components in RE which require clear understanding in fouling behaviour and stability in order to evaluate its performance and life time. In this work, the fouling propensity of commercial IEMs for potential use in RE system are evaluated in real brine and seawater samples (Sicily, Italy) considered under the EU-FP7 REAPower project. A theoretical model based on surface energy and morphology parameters of IEMs is developed and implemented for prediction of scaling, colloidal and organic fouling propensity of the membranes. Results show higher fouling tendency of IEMs contacted with concentrated brine than seawater. In a stability studies, ATR-FTIR results show no significant decrease in the band intensity and no band shifts for IEMs aged in seawater and brine over six months. An overall low mechanical strength of IEMs shows low cross linking degree for better ion transport. In SGP-RE testes, presence of organic components in feed doesn't have a significant influence on the power output during short term experiments. A drastic reduction (-78 %) in power (from 2.25 to 0.48 W/m^2_{MP}, MP: Membrane pair) density was observed for the tests with feed solutions mimicking real seawater and brine compared to operations with pure NaCl solutions (2.2 W/m^2_{MP} at current density of 29 A/cm^2). This indicates the requirement of a pre-treatment step for optimal power output for RE operations under real conditions.

This Chapter is submitted to the *Journal of Membrane Science*.

5.1 Introduction

Reverse electrodialysis is a promising membrane based technology for conversion of salinity gradient power (SGP) into electricity. RE is more often applied to seawater and river water. However, under this condition, the high Ohmic resistance due to river water compartment is limits the RE performance. This can be overcomed by the use of concentrated solutions like brine which can be from salt mines, salt-works, discharge from desalination plants and various industrial effluents. Recently, we demonstrated that the use of brine and brackish water significantly reduces internal areal resistance in a RE stack by up to 50 % compared to the operations with river/seawater solutions [1, 2].

Ion exchange membranes (IEMs) which are widely used in electrochemical processes like electrodialysis [3, 4], fuel cells [5-7], electrolysers [8, 9], redox flow batteries [10, 11], bioelectrochemical systems [12, 13], are regarded as the heart of RE. Their properties determine the overall performance of the RE system [14]. The main desirable characteristics of IEMs for reverse electrodialysis application involve low membrane resistance and high permeability. Other properties like good mechanical strength and stability are important, in particular when operating RE in highly saline solution like brine over a long period of time. Membranes may lose their performance due to physical damage or deterioration when operated over a long-term period time. For example, there may be a loss in properties like ion-exchange capacity and conductivity as demonstrated by Ghalloussi *et al.* (2013) for IEMs operated in organic acid media [15]. Thus, membranes with good mechanical and chemical stability are required for longer membrane life time.

Operational efficiency of RE is also dependent on availability of high quality feed streams, particularly, the fouling propensities and the composition of feed streams need to be addressed in order to evaluate the impact of raw feed composition on the process performance. Relevant feed quality parameters involve total hardness (TH), total dissolved solids (TDS), total suspended solids (TSS), total organic matter (TOM), and alkalinity. In addition to Cl^- and Na^+ ions, natural seawater and anthropogenic brines also display a high concentration of Ca^{2+}, Mg^{2+}, SO_4^{2-} and HCO_3^- ions. In particular, the presence of multivalent ions in RE feed solutions have a negative impact on the performance [1, 16, 17]. Loss in SGP-RE performance due to the presence of multivalent ions is more significant compared to the fouling effect. For RE operated with seawater and river water,

the addition of 10 % $MgSO_4$ in both feed compartments resulted in a 29-50% reduction of power density [17]. On the other hand, RE operation with brine (35 % $MgCl_2$) and brackish water (17 % $MgCl_2$) simulated to the real feed compositions originating from solar ponds resulted in significant power reduction (-63 %). This is directly related to the reduction of stack voltage and enhancement of internal stack resistance (major contribution from membranes) due to the presence of multivalent ions.

Besides, there is a huge fouling potential of IEMs when operating RE under realistic salinity environments. Fouling may occur due to particulate, colloidal and microbial matters on the membrane surface depending on the employed feed quality [18, 19]. In RE operating with highly concentrated brines solutions, scaling is the type of fouling most likely to occur. Scaling results when the concentration of sparingly soluble salts (divalent and multivalent) overcomes the solubility limits, on the membrane surface causing a decrease of mass transfer efficiency. Continuous operation of RE with feeds containing ions with high potential to form sparingly soluble salts like $CaCO_3$, $Ca_3(PO_4)_2$ results in membrane scaling. This phenomenon is controlled by both solution chemistry and membrane morphology. In a recent study, Kang *et al*. (2011) reported that membrane roughness increases significantly the extent of calcium carbonate scaling on reverse osmosis membranes [20]. Curcio *et al.*(2010) investigated the precipitation of calcium carbonate on microporous polypropylene membranes as a function of the Gibbs free energy barrier for the formation of critical nuclei [21]. In RE operated under natural saline water, particulate fouling may also occur due to the deposition of suspended solids and colloidal matters such as clay minerals, organic particulates, algae, non-growing bacteria, etc. The presence of particulate matter is commonly monitored by the Silt Density Index (SDI) [22].

So far, investigations on the impact of membrane fouling on SGP-RE performance and aging testes for IEMs stability are scarce. In an experiment with accelerated biofilm formation, Post demonstrated that biofilm accumulation over the membrane surface is observed to increases pressure drop over the feed compartments with longer time (13 days) for the sea side compared to the river side (8 days), before the rise in pressure drop occurs [23]. Periodic reversal of feed streams and flow directions were suggested promising control strategies compared to stack cleaning. Vermaas *et al.* (2013) studied the effect of fouling on the performance of SGP-RE stacks operated for 25 days with natural feed waters without cleaning [18]. They CEMs indicated a pronounced scaling (due to formation of sparingly soluble salts at the membrane interface like calcium

phosphate) compared to AEMs similar to the case of electrodialysis [18, 24]. In relation to the stack performance, pressure drop in the stack with spacers increased rapidly compared to the spacerless stacks. The observed decrease in permselectivity was less (about 10 %) compared to the power density (above 40 %) and the electrical resistance (in the range of 40-70%) in the first day of the experiment. The generalization is the performance loss of RE system during operation under natural condition.

The present work performed under EU-FP7 REAPower project was particularly devoted to SGP generation from seawater and concentrated brines [25]. Thus**,** fouling propensity of IEMs in concentrated brine and seawater within the vicinity of SGP-RE channel is investigated systematically. For concentrated brines and seawater, particulate fouling tendency was predicted by Saturation Index (SI) determinations. TOC determinations of the raw feeds were used to assess the organic fouling and its effect on SGP-RE performance. With the aim to clarify the effect of surface chemistry and morphology of IEMs on the kinetics of salts precipitation, a theoretical model has been implemented; input parameters to the model (experimentally measured contact angles and roughness) allow evaluating the scaling tendency of a set of IEMs. Finally, proper pre-treatment strategies for real feed streams under constrain of low-energy consumption is identified.

5.1 Theoretical Modelling

In saline solutions like seawater and brine, the solution chemistry in relation to the solubility limits of different salts and other factors like the membrane morphology and properties of the surrounding fields with in the solution influence scale formation over IEMs. In the process of kinetics of nucleation during scaling, moderately supersaturated solutions might show a high lag time or induction time (i.e. the time elapsed between the achievement of supersaturation and the nucleation of first particles) for scale formation. On the other hand, induction time is drastically decreased if nucleation occurs in the presence of solid surfaces or membranes (heterogeneous nucleation).

The variations in contact angle of membranes in different feeds and membrane roughness can be used to develop a model for prediction of fouling propensities of IEMs. In order to implement this, a cluster nucleating from a solution in contact with a membrane is assumed to be spherical cap shaped as shown in Figure 5.1 below;

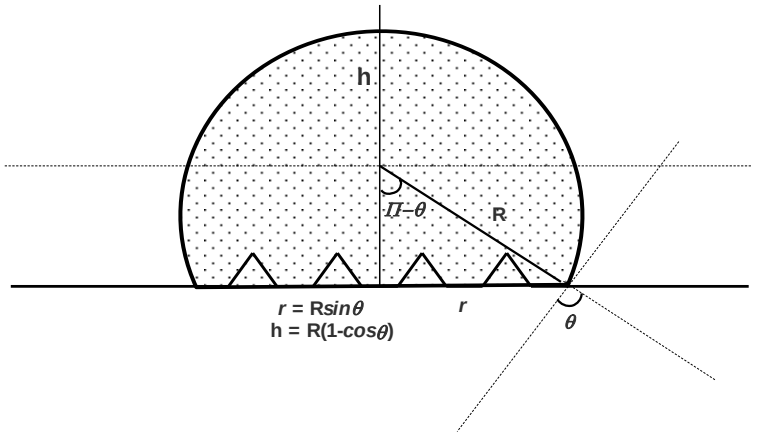

Figure 5.1. Geometry of a sphere cap on a rough membrane surface. θ is the contact angle; R, r, and h are the main radius, the contact radius, and the height of the cap, respectively.

According to the geometry of the system:

$$A_{SL} = \pi R^2 \sin^2\theta \qquad 5.1a$$

$$A_L = 2\pi R^2(1-\cos\theta) \qquad 5.1b$$

$$V = \pi\frac{R^3}{3}(1-\cos\theta)^2(2+\cos\theta) \qquad 5.1c$$

where A_{SL} is the solid-liquid interfacial area generated by spherical nucleus, A_L is the surface area and V is the volume.

The change of Gibbs free energy ΔG_{het} of formation for a critical nucleus (having, by definition, 50% probability to grow or dissolve in solution) on a solid surface (membrane) is a crucial parameter in crystals nucleation and growth. ΔG_{het} is quantified by energy balance that includes positive contributions from nucleus-solution (γ_L), nucleus-membrane (γ_i), and a negative contribution from solution-membrane (γ_s) interfacial energies:

$$\Delta G_{het} = -\frac{\Delta\mu}{\Omega}\frac{\pi R^3}{3}(1-\cos\theta)^2(2+\cos\theta) + 2\pi R^2\gamma_L(1-\cos\theta) - \pi R^2(\gamma_s-\gamma_i)\sin^2\theta \qquad 5.2$$

In order to investigate the effect of membrane morphology and solution-membrane interaction, we used the Wenzel equation to correlate contact angle and roughness coefficient *r* to the surface energies [26]:

$$(\gamma_s-\gamma_i) = r\gamma_L\cos\theta \qquad 5.3$$

where *r* is defined as the ratio between the actual membrane surface and its projection on an ideally smooth plane ($r > 1$).

From Eq. (5.2) and (5.3):

$$\Delta G_{het} = -\frac{\Delta\mu}{\Omega}\frac{\pi R^3}{3}(1-\cos\theta)^2(2+\cos\theta) + 2\pi R^2\gamma_L(1-\cos\theta) - \pi R^2 r\gamma_L \sin^2\theta \qquad 5.4$$

The energy barrier ΔG^*_{het} corresponding to the maximum value of the Gibbs free energy of heterogeneous ΔG_{het} nucleation is obtained by:

$$\frac{d\Delta G_{het}}{dR} = 0 \qquad 5.5$$

The radius *R* of the nucleus in correspondence of ΔG^*_{het} is known as "critical radius"; solving (5.5):

$$R^*_{het} = R^*_{\text{hom}}\frac{r\cos\theta(1+\cos\theta)-2}{\cos\theta(1+\cos\theta)-2} \qquad 5.6$$

where R^*_{hom} is the critical radius for a homogeneous nucleation (occurring in the bulk of the solution); according to the Classical Nucleation Theory:

$$R^*_{\text{hom}} = \frac{2\Omega\gamma_L}{\Delta\mu} \qquad 5.7$$

To simplify the notation, we define *Y* as:

$$Y = \frac{r\cos\theta(1+\cos\theta)-2}{\cos\theta(1+\cos\theta)-2} \qquad 5.8$$

and

$$R^*_{het} = R^*_{\text{hom}}Y \qquad 5.9$$

Substituting Eq. (5.9) in Eq. (5.4) and dividing for ΔG^*_{het} (the Gibbs free energy barrier for homogeneous nucleation obtained at θ =180°):

$$\Delta G_{\text{hom}} = \frac{16}{3}\pi\gamma_L^3\left(\frac{\Omega}{\Delta\mu}\right)^2 \qquad 5.10$$

$$\frac{\Delta G^*_{het}}{\Delta G^*_{\text{hom}}} = \frac{1}{4}Y^3(\cos^3\theta - 3\cos\theta + 2) \qquad 5.11$$

For an ideally smooth surface (r=1 and, consequently, $Y=1$) Eq. (5.11) reduces to the output provided by the Classical Nucleation Theory. Eq. (5.11) is plotted in Figure 5.2 as a function of contact angle and membrane roughness.

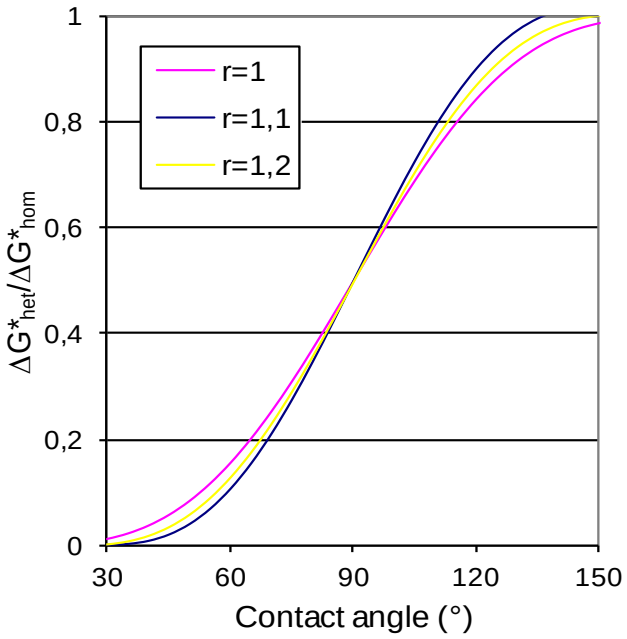

Figure 5.2. Reduction of Gibbs energy barrier of nucleation on membrane as a function of contact angle and roughness.

5.2 Material and Methods

5.2.1 Raw Feed Analysis

Samples of raw feed streams were collected at an exhaust point of desalination plant in Trapani (received from University of Palermo). All samples were stored at 4°C; samples were brought at room temperature for 2 hours before analysis. The samples were pre-filtered through 0.45 μm polyethersulfone membrane before analysis.

5.2.1.1 Ion chromatography

Cation and anion analysis was performed by 861 Advanced Compact Ion Chromatograph (Metrohom Italiana SrL, Italy) and data processed by ICNet 2.3. For cation analysis, Metrosep A Supp 5 250/4.0 column and Metrosep A Supp 4/5 Guard pre-column were used with eluent solution 2mM HNO_3/0.25 mM oxalic acid; for anion analysis, METROSEP C4 - 250/4.0 column and METROSEP C 4 Guard pre-columns were used, with eluent solution 3.2 mM Na_2CO_3/1 mM

$NaHCO_3$.

5.2.1.2 Optical emission spectrometer

Calcium and magnesium ion concentrations were evaluated by Optical Emission Spectrometer - Optima 2100DV (PerkinElmer Inc.). For ICP analysis all samples, pre-filtered through 0.45 μm PVDF membrane, were properly diluted in bi-distilled water at 0.055 μS/cm (Milli-Q Water Purification System, Millipore Corporation) in order to fit the optimal sensitivity range of the instrument; 2% v/v of HNO_3 (65%, Sigma Aldrich) was added to each sample.

5.2.1.3 Contact angle

Contact angles of the different feed samples in different membranes were measured by sessile drop method using a CAM 200 contact angle meter (KSV Instruments Ltd.) equipped with a microsyringe, automatic dispenser, and software for image acquisition and processing.

5.2.1.4 Speciation of ions

Speciation of ions in solutions and Saturation Index (SI) were calculated by PHREEQC software (version 2.18.00.). A positive value of SI indicates that the solution is supersaturated and precipitation of solid phase is likely to occur. Results for determination of raw feed quality parameters are presented in Table 5.1.

5.2.2 Membrane Characterization

5.2.2.1 AFM measurements: Scaling

Four membrane samples (the ones showing a compatible surface homogeneity and roughness, no wearing or breakage of the tips) were selected for AFM Characterization. Surface morphology of IEMs influence the process of nucleation accountable for scale formation in membranes contacted with concentrated brines. Membrane surface was characterized by Nanoscope III atomic force microscope (AFM, Digital Instruments, VEECO Metrology Group) in air, a tapping mode AFM imaging (average of 3 samples 5x5 μm^2); roughness analyses of surfaces were performed by SPIP 6.0 software (Image Metrology). Wenzel roughness factor was calculated as the ratio of the actual area of the rough surface to that of the projected area.

5.2.2.2 FT-IR analysis: Aging

Deterioration and hence physicochemical changes with time in membranes operated with

brine for a long time can be analyzed by FT-IR. Six commercially available membranes (FujiCEM80050, FumatechAEM, FujAEM80045, KratonCEM2, FujiCEM and FujiAEM) were cut in a square form (2 cm^2) and initially activated with MilliQ water for half a day. For aging test, the membranes were kept in a 2 mL vial containing 15 mL of water samples (Brine Ettore Infersa and Seawater Ettore Infersa) for three weeks at room temperature. FT-IR measurements were then taken at an interval of six months from the day of activation. Spectra were collected on a Thermo Scientific Nicolet™ iS™ 10 FT-IR spectrometer using Smart iTR™ diamond ATR accessory (Nicolet Instruments Corporation, Madison, WI). The spectra were obtained by collecting 100 scans. The ATR accessory contained a ZnSe crystal (2552 mm) at a nominal incident angle of 45° which yields 12 internal reflections at the sample surface. All spectra (100 scan at 4.0 cm-1 resolution and rationed to the appropriate background spectra) were recorded at 25°C. A desiccant (DESI PAK, MIL-D-3464) was used to prevent the interference of atmospheric moisture with the spectra. The spectrum was processed in OMNIC Specta using Advanced ATR Correction Algorithm.

5.2.2.3 Mechanical strength: Cross linking degree

High cross-linking in membranes as well as thickness is directly correlated with membrane mechanical strength [27]. Tensile tests on the membranes were carried out at room temperature on a Zwick/Roell Single Column Universal Testing Machine (model Z2.5) equipped with a 50N load cell and flat pneumatic clamps. The clamp surface was covered with adhesive rubber to avoid slipping. Specimens with an effective length of 40 mm (distance between the clamps) and a width of 10 mm were tested at a deformation rate of 50 mm min^{-1}. Tensile testing provides data regarding the yield point, break properties and the stiffness of the material as elastic modulus.

5.2.3 Fouling studies

5.2.3.1 Scaling

Systematic induction of $CaCO_3$ precipitation on the membrane surface was used for evaluation of scaling tendency of the membranes. Four IEMs (Fuji AEM 80045, FumaSep-FAS AEM, Fuji-CEM 80050, Kraton CEM 2-Nexar MD9100-T/P) were placed in a closed desiccator containing a 20 ml vial of solid ammonium carbonate (Figure 5.3). 10 µl of calcium chloride testing solution (10 mM) were deposited on each membrane surface; experiments were carried out at room temperature for 24 hours. Precipitation of $CaCO_3$ resulted from sublimation of $(NH_4)_2CO_3$

(solid) and diffusion of CO_2 (gas) into $CaCl_2$ solution (liquid) according to the following reactions:

$$(NH_4)_2CO_3(s) \rightarrow 2NH_3(g) + CO_2(g) + H_2O \quad \text{(R1)}$$

$$CO_2 + Ca^{2+} + H_2O \rightarrow CaCO_3(s) + 2H^+ \quad \text{(R2)}$$

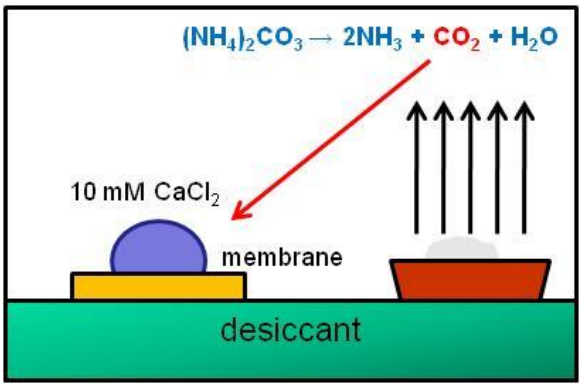

Figure 5.3. Schematic representation of the laboratory setup for $CaCO_3$ precipitation experiments.

5.2.3.2 Colloidal fouling

UHP-43 stirred filtration cell (Advantec MFS Inc., Japan) with capacity of 70 ml and effective permeation area of 1150 mm^2 was used to evaluate the silt density (SDI) index, the most widely applied fouling indicator to measure the particulate fouling potential of feed water. Experiments were carried out by plugging of a membrane filter BA85 Schleichers & Schuell BioScience GmbH (Germany) with 0.45 μm at a pressure of 210 kPa (30 psi).

Quantitative determinations of SDI_{15} were done using the following mathematical equation;

$$SDI_{15} = \frac{1 - \frac{t_1}{t_2}}{T_{15}} * 100 \ [\%\,\mathrm{min}^{-1}] \quad 5.12$$

where SDI_{15} corresponds to SDI obtained at elapse time of 15 minutes, t_1 is the time required filtering the first 500 ml portion of seawater, t_2 is the time required to filter the second 500 ml portion of seawater, and T_{15} is the time elapsed between the starting of first filtration and the starting of the second filtration (in this case 15 minutes). The value of SDI_{15} index (usually used in RO feed water evaluations), according to Eq. (16), varies between a minimum of 0 (no particulate fouling, $t_1=t_2$) and a maximum of 6.67 (complete pore blocking, $t_2=0$).

5.2.3.3 Organic fouling

The characterization of organic matter present in feed solutions is essential to predict and control the organic fouling because this type of fouling is generally irreversible and involved in the first stage of biofouling establishment. Dissolved organic matter typically includes biopolymers (polysaccharides, proteins, aminosugars), humic substances, building blocks (mostly breakdown products of humics), neutrals (mono-oligosaccharides, alcohols, aldehydes, ketones and amino acids), and monoprotic organic acids. Total Organic Carbon (TOC) analysis was used for evaluating the dissolved organic matter content in real seawater and brine solutions. There is high tendency of organic fouling for TOC values above 2 mg/L. Moreover, it has been noted in previous experiences that TOC parameter seems to vary as function of the season for the raw water, with an increasing trend during summer season [28].

5.2.4 SGP-RE tests

A counter-flow RE stack (PC cell, GmbH, Germany) consisting of 25 cell pairs was used to test the performance of ion exchange membranes operated by artificial salt solutions (composition similar to Ettore infers brine and seawater, see Table 5.1) and varying humic acid content. The stack is packed with alternatively aligned cation exchange membranes and anion exchange membranes (PC-SA AEM, and PC-SK CEM, Germany) with an active membrane area of 0.03 m^3. The electrodes system is composed of Titanium with a Ruthenium/Iridium mixed metal oxide coating. The electrode rinse solution was composed of 0.1 M $K_3Fe(CN)_6$ (Sigma Aldrich, MKBL8399V), 0.1 M $K_4Fe(CN)_6.3H_2O$ (Sigma Aldrich, SZBC1250V) and NaCl (2.5M), with conductivity 261.2 ms/cm.

SGP-RE performance evaluations were done by loading the system using a resistance box (high dissipation five decade) in the range of 0.1-1000 Ω (CROPICO, Bracken Hill, US), and measuring the corresponding DC voltage drop across the load resistors by a 3½ digital multimeter (Valleman, DVM760, accuracy of ± 0.5%) in the range of range 200 mV-200 V. The value at the steady state voltage without loading the system was recorded as an open circuit voltage (OCV). The current across the load resistors was measured by Agilent 34422A 6½ Digit Multimeter. The electrical circuit diagram for the measurement of the voltage and current from the RE stack is described in our previous work [29]. A four SPER SCIENTIFIC 800024 Pt multi-channel thermocouples (T) with sensitivity of ±0.1 ˚C was used for monitoring temperature of the feed and

a manometer (RF-D201, DUNGS®, Germany) was used to control the pressure, at the inlet and outlet of the RE stack. Performance of the system is mainly evaluated by open circuit, power density and internal stack determinations.

Table 5.1. Composition of artificial seawater and brine solutions prepared mimicking real solutions (Ettore Infersa brine and seawater, Sicilia, Italy).

Ions	Seawater (mg/L)	Brine (mg/L)
Ca^{2+}	705	242
Mg^{2+}	2260	37350
Na^{+}	10664	65900
K^{+}	348	7740
Cl^{-}	24950	170169
SO_4^{2-}	2344	64700

5.2.5 Pretreatment tests

In a membrane pre-treatment step, two commercial membranes for microfiltration (BA85 - 0.45 μm) and ultrafiltration (SEPA CF TF UF-type GK-MWCO: 3 kDa.) were tested for TOC removal from seawater and brine samples.

Preliminary softening tests were carried out on Ettore Infersa brine. In a typical test, sodium carbonate and sodium hydroxide (Sigma Aldrich, Italy) are mixed in an appropriate amount in 100 ml of raw solution and vigorously stirred at room temperature. Both pH and conductivity (YSI Model 3200 Conductivity Instrument, YSI Inc. USA) of solutions were monitored in order to evaluate the apparent softening of the brine sample.

5.3 Result and Discussions

5.3.1 Contact angle measurements

In order to investigate the extent of physico-chemical interactions between the polymeric membranes and the three brine samples, contact angles were measured for 9 IEMs. As shown in Figure 5.4, membranes exhibit (with different extent) a hydrophilic behavior ($\theta<90°$). This is not actually an advantage with respect to application membranes in concentrated brines as IEMs are designed to selectively pass charged ion while retaining the osmotic flow of water. Contact angles to Trapani brine, having the lowest TH (2849 mg/l) and lowest Total Organic Carbon TOC (1.85 mg/l) among the three brines, are generally lower with respect to values measured for Margi exhaust brine (TH=64466 mg/l; TOC=184.3 mg/l) and E. Infersa brine (TH=37592 mg/l,

TOC=159.8 mg/l). The natural organic matter present in water could be adsorbed into the membranes which can affect the surface energy and morphology of the membranes. The low content of TOC and TH results in a low effect on surface chemistry of the membranes with the insignificant change in contact angle expected for IEMs. In a taste conducted by Kim *et al*.(2009) with ultrafiltration and nanofiltration membranes, it was observed that contact angle of NOM fouled membranes were higher than the respective clean membranes implying larger hydrophobicity of the fouled membranes compared to clean ones [30]. Moreover, contact angles measured for commercial and tailored nanofiltration membranes increased after permeation of water containing NOM [31]. In addition, the membranes FujiAEM and FujiAEM90025 display the least contact angle ($\theta < 41$ ^{o}C) compared to other membranes in Trapani brine. This shows more hydrophilic nature of these membranes compared to others, and in terms of membrane performance, this behavior may not be favorable as it may enhance the osmotic losses with in SGP-RE stack when operated with concentrated brines.

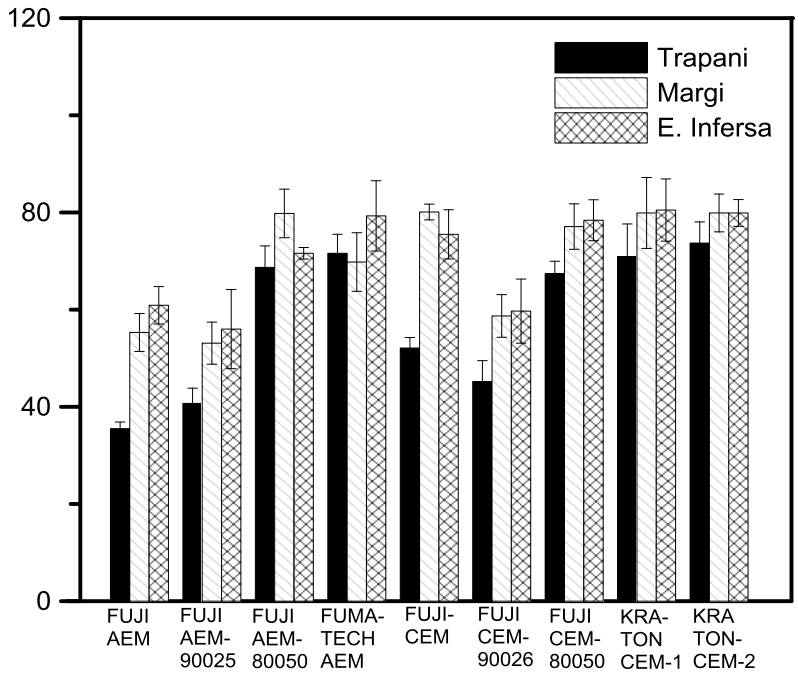

Figure 5.4. Contact angles for the different IEMs (measurements taken in for feed samples; Trapani, Margi and E. Infersa).

5.3.2 AFM measurements

The spread when a drop of water rest on a hydrophilic membrane surface is correlated with the specific energy derive created between the wetted membranes surface and dry side. In the process, a rough membrane surface is wetted more rapidly than smooth ones. This phenomenon will remain the same for hydrophilic membranes too. This is governed by the roughness coefficient r as determined by the radiation of actual surface and rough surface, considering surface tensions as one unit of actual surface. A value of r beyond 1.2 implies a high resistance to wetting with greater effective adhesion tension than interfacial tensions [26].

Results from the AFM images are indicated in Figure 5.5. The membrane surface morphology varies; Root mean square roughness R_{MS} was determined in the range of 9.7 - 30 nm. Fuji membranes show rougher surface (R_{MS}=20-30 nm) compared to Kraton-CEM-2 and Fumatech-AEM. Though FujiCEM-80050 and Kraton-CEM-2 have a comparable contact angle values in all feed samples, AFM measurement shows FujiCEM-80050 has rougher surface. At the same time, Fuji-AEM (R_{MS} = 20.8 nm) and FujiCEM-80050 (R_{MS} = 30.6 nm) show a comparable surface roughness while the difference in contact angle is high (Fuji-AEM, θ = 35.5 - 60.9, Fuji-AEM, θ = 67.4 - 78.4). It's difficult to see a general trend between contact angle and membrane roughness. However, from the roughness tests obtained for the limited number of membranes here, results show that an increased contact angle of membranes in brine and seawater samples is accompanied by lower roughness coefficient.

5.3.3 Scaling tendency

5.3.3.1 Model predictions

During scale formation over the membrane surface, small ions of sparingly soluble salts start to nucleate and energy changes occur due to heterogeneous nucleation at the membrane surface (ΔG_{het}) and bulk nucleation (ΔG_{hom}); reduction of the energy barrier to ΔG_{het} with respect to ΔG_{hom} varies depending on the surface chemistry of the membranes. This can be used for qualitative assessment of scaling tendency with the respective model calculations involving parameters related to surface roughness and contact angle, as described earlier where theoretical model development is demonstrated for this phenomenon.

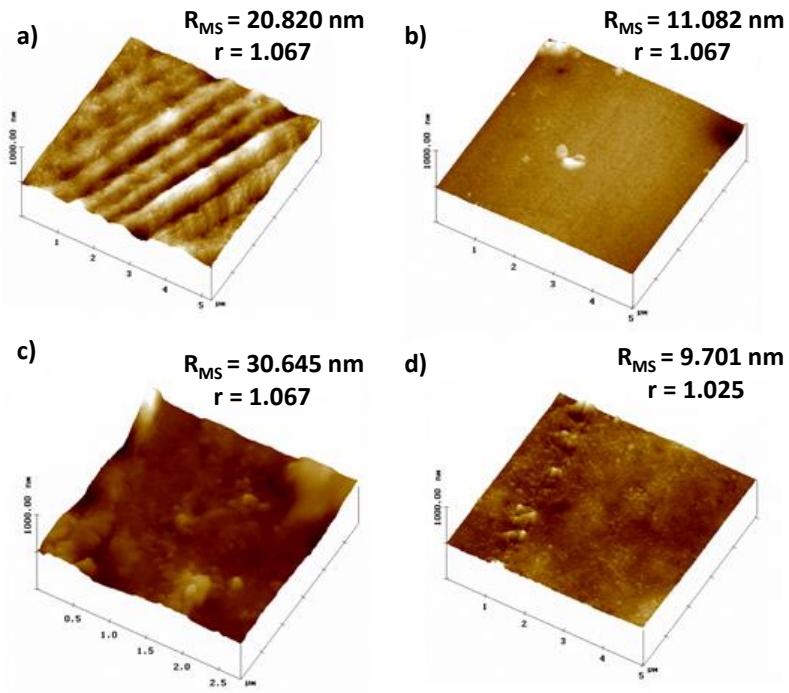

Figure 5.5 AFM images (100 nm) with roughness analysis for the tested membrane samples; a) FujiAEM, b) Fumatech AEM, c) FujiCEM80050, d) Kraton-CEM-2.

The scaling propensity of different IEMs in different feed samples is shown in Figure 5.6. FujiAEM has high fouling tendency compared to other membranes in all the feeds, coherent with its high roughness coefficient. Moderate scaling tendency is observed for other membranes. For the investigated feed solutions, brine from Ettore Infersa (TH=37592 mg/L) has high scaling tendency to IEMs as shown in Table 5.1; high concentration of Ca^{2+} (242 mg/L) ion and a positive value of saturation indexes indicate high potential precipitation of sparingly soluble salts from this ion; anhydrite ($CaSO_4$), dolomite ($CaMg(CO_3)$, gypsum ($CaSO_4.2H_2O$) and halite ($NaCl.2H_2O$) supersaturations are expected to precipitate (Appendix 5.1). Generally, the membrane fouling is higher in concentrated brines than in seawater.

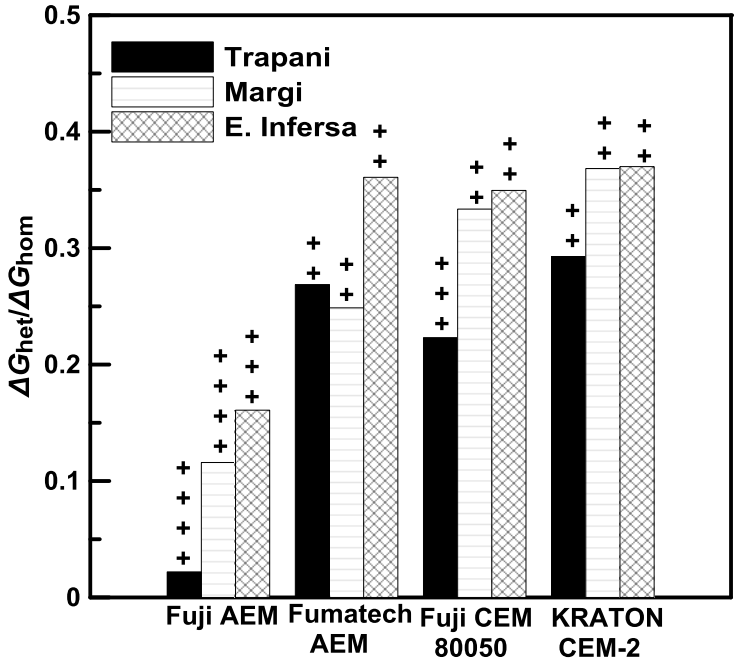

Figure 5.6. Reduction of the energy barrier to heterogeneous nucleation at the membrane surface (ΔG_{het}) with respect to bulk nucleation (ΔG_{hom}) and qualitative assessment of scaling tendency; $\Delta G_{het}/\Delta G_{hom}$= 0.5-0.75, 0.25-0.5, 0.15-0.25 and < 0.15 implies poor (+), moderate (++), high (+++) and very high (++++) scaling tendency, respectively.

Table 5.1. Fouling potential of feed solutions.

Feed	Scaling Potential	Colloidal Fouling	Organic Fouling
Seawater Ettore Infersa	++	++	+
Seawater Margi	+	++	+++
Brine Ettore Infersa	++++	++++	++++
Brine Margi	+++	+++++	+++++

5.3.3.2 $CaCO_3$ precipitation tests

The sensitivity of IEMs to calcium carbonate scaling can be correlated to the density of $CaCO_3$ crystals nucleated at the membrane surface. As already discussed in the previous section, the scaling potential strongly depends both on the chemistry of solution (supersaturation) and on the physico-chemical properties of IEMs. Figure 5.7 shows the surface images of three IEM membranes at the end of $CaCO_3$ crystallization test as per optical microscopy; crystals exhibit a rhombohedral shape typical of calcite. The highest $CaCO_3$ crystal density is observed on Fuji CEM 80050 membrane as shown in Figure 5.8. This is consistent with its highest value of surface

roughness (Wenzel coefficient r = 1.067) and ion exchange capacity (1.1 mmol/$g_{membrane}$) as shown in Figure 5.6. This shows that factors like solution chemistry and membrane morphology play a role in the scaling of IEMs although the fouling in RE is generally expected to be less articulated compared to other membrane processes. The ion exchange membrane tested so far for scaling in RE involve Ralex membrane; Vermaas *et al.* (2013) observed scaling phenomenon on cation exchange membrane after 25-days of RE operation with a pre-treatment step involving only 20 μm filter [18].

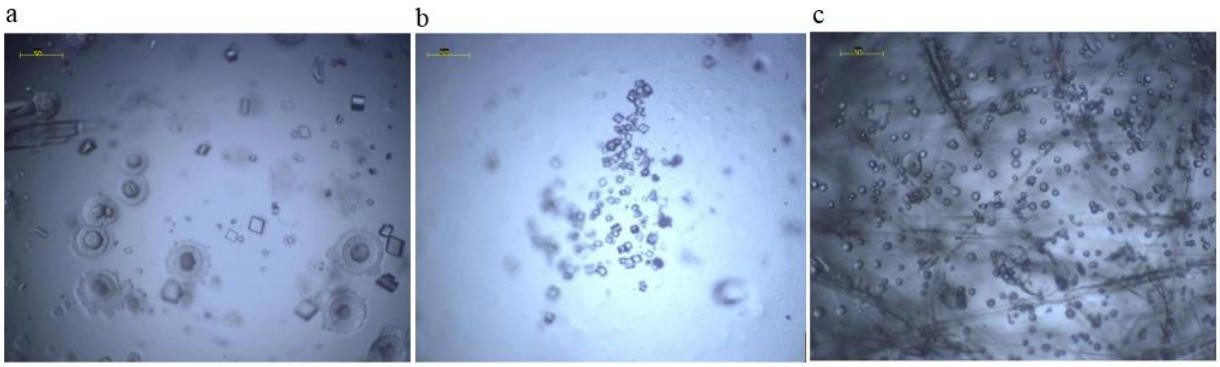

Figure 5.7. Light microscope image of calcite deposits on the surfaces of: a) Kraton CEM 2-Nexar MD9100-T/P; b) FumaSep-FAS AEM; c) Fuji-CEM 80050.

5.3.4 Colloidal fouling: SDI tests

For brine solutions, due to high viscosity and huge particulate content, it was not possible to prolong SDI filtration tests up to a permeate volume of 500 ml. However, in order to provide a preliminary indication of the colloidal fouling potential, the SDI index was measured with respect to a filtration volume of 10 mL. The term $(1-t_1/t_2)*100$ allows estimating the percentage of membrane pore blocking. Table 5.2 summarizes SDI filtration data of the tested feed samples.

No significant difference in SDI value is noticed for Ettore Infersa and Margi seawater. The pore-blocking potential of brine from Margi solar pond is extremely high; moreover, visual inspection reveals a brown-red colored solution consistent with the highest TOC values compared to other feeds. Figure 5.9 shows that the surfaces of BA85 reference membranes after SDI tests with seawater Margi had more colloidal concentrates compared to seawater Ettore Infersa and brine from Trapani Desalinator. In general, membranes contacted with seawater samples are less susceptible to colloidal fouling compared to the ones contacted with brine samples (Table 5.2). So far, there are no literatures that provide specific correlations between a value of SDI and the cleaning frequency of IEM for RE process. However, analogy with reverse osmosis processes

might offer a preliminary and rough indication on the impact of feed quality on the fouling phenomenon in RE process (Figure 5.10) [28]. Based on these, the use of brine samples from Ettore Infersa and Margi requires extensive pre-treatment.

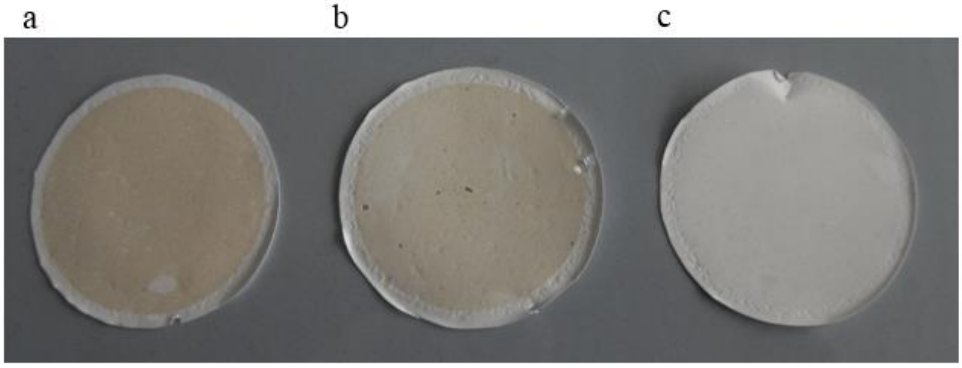

Figure 5.9. Surfaces of BA85 reference membranes after SDI tests; a) seawater from Margi b) seawater from Ettore Infersa, and c) brine from Trapani Desalinator.

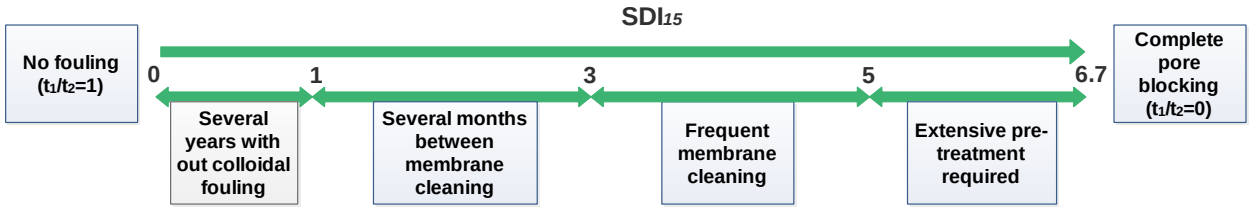

Figure 5.10. Correlation between SDI_{15} value and cleaning frequency in seawater Reverse Osmosis desalination.

5.3.5 Organic fouling: TOC measurements

Natural organic matter present in natural waters is undesirable because it is responsible for color in the water, formation of by products during water disinfection, complexation with heavy metals, etc. Interaction of organic compounds dissolved in feed streams (commonly: humic acids, proteins, carbohydrates and tannins) with membrane surface is referred as organic fouling. The content of organics present in feed water has been evaluated by TOC (Total Organic Matter) analysis. Considering that the fouling risk for raw seawater is high for TOC>2 mg/L, seawater from Margi and brines from E. Infersa and Margi would require extensive pre-treatment operations. Results for feed quality parameters are presented in Table 5.3. Operation with seawater from Ettore Infersa can last several years without fouling with potentially less fouling propensity. In general, organic fouling can alter the electrochemical property of ion exchange membranes and this can be overcomed by designing suitable IEM.

Table 5.3. Characterization of feed samples (brackish water and brine) obtained from solar ponds (Sicily, Italy); all measurements were done at 20 ºC.

Sample*	TOC (mg/L)		TIC**, mg/L	pH***	Ca^{2+}, mg/L	Mg^{2+}, mg/L	Na^{+} mg/L	K^{+} mg/L	Cl^{-} mg/L	SO_4^{2-} mg/L	TH****, mg/L	Alkalinity, mg/Las $CaCO_3$
	August 2012	February 2013										
MARGI, seawater	37.1	18.3	1.2	7.9	582	3160	9922	844	25343	2982	3742	1.0
MARGI, exhaust brine	184.3	92.8	107.6	6.5	166	64300	21230	9970	164151	87970	64466	88.2
ETTORE INFERSA, brine	159.8	5.3	50.2	6.9	242	37350	65900	7740	170169	64700	37592	41.2
ETTORE INFERSA, seawater	5.3	3.1	18	8.2	705	2260	10664	348	24950	2344	2965	15

*Samples are quoted by the name of the local site they were obtained
**Total Inorganic Carbon (TIC) = $[HCO_3^-] + [CO_3^{2-}]$ (measured on CO_2 free solutions)
****Total hardness (TH) = $[Ca^{2+}] + [Mg^{2+}]$ (sum of calcium and magnesium ions, preponderant in these waters with respect to other divalent metal ion

5.3.6 Stability and mechanical strength

5.3.6.1 FT-IR measurements

FT-IR has been widely applied for the characterization of components in natural water that cause fouling, and aging and satiability of IEMs for different application [15, 32, 33]. For the membranes investigated in our study, results from the FT-IR analysis show no significant alteration in membrane fictional groups, after 6 months of preservation in the brine and seawater samples. FT-IR spectra for two of the IEMs (FujiAEM80045 and FujiCEM80050) are presented in Figure 5.11. For confidential reasons, the structural details of Fuji membranes cannot be given. However, a general peak assignment can be done. Medium absorptions in the region of 1400 - 1700 cm^{-1} and broad absorption around 3400 cm^{-1} for CEM could be attributed to the amide and hydroxyl groups, respectively. The bands at higher wave numbers (1672 and 1682 cm^{-1}) indicate strong hydrogen-bonding interactions between hydrophilic groups of the membrane and the water molecules, while the bands at lower wave numbers (1647 and 1649 cm^{-1}) reveal weak hydrogen-bonding interactions between the hydrophilic groups and the water molecules. This phenomenon is observed for the case of AEM. In the case of CEM, a strong band at 1060 cm^{-1} is observed which probably corresponds to the symmetric stretching vibration of SO_3^-. The bands around 1200 and 1034 cm^{-1} correspond to the bands of the sulfonic acid groups which splits to higher wave number (1350 - 1175 cm^{-1}) due to lowering of free water (drying of membranes)[34].

In general, there was no significant decrease in the band intensity as well as band shifts for the membranes in seawater and brine compared to the virgin ones. There was no significant observation in the loss of polymer rigidity and damage in the chain for this membrane over 6 months. Thus, organic foulants rather have an effect on chemical property than the structural modification of the ion exchange membranes. ATR-FTIR analysis of humate fouled anion exchange membranes by Lee *et al*. (2009) showed that the organic foulant altered the membrane functional group in a small degree [33]. With respect to swelling, AEM shows more water retention (hydrophilic nature) with time compared to the CEM[15]. The stability trend is that the water retention and stability of the membranes is quite high for the membranes aged in saline water compared to virgin ones as observed from the few band shifts in the ATR-FTIR spectra of these membranes.

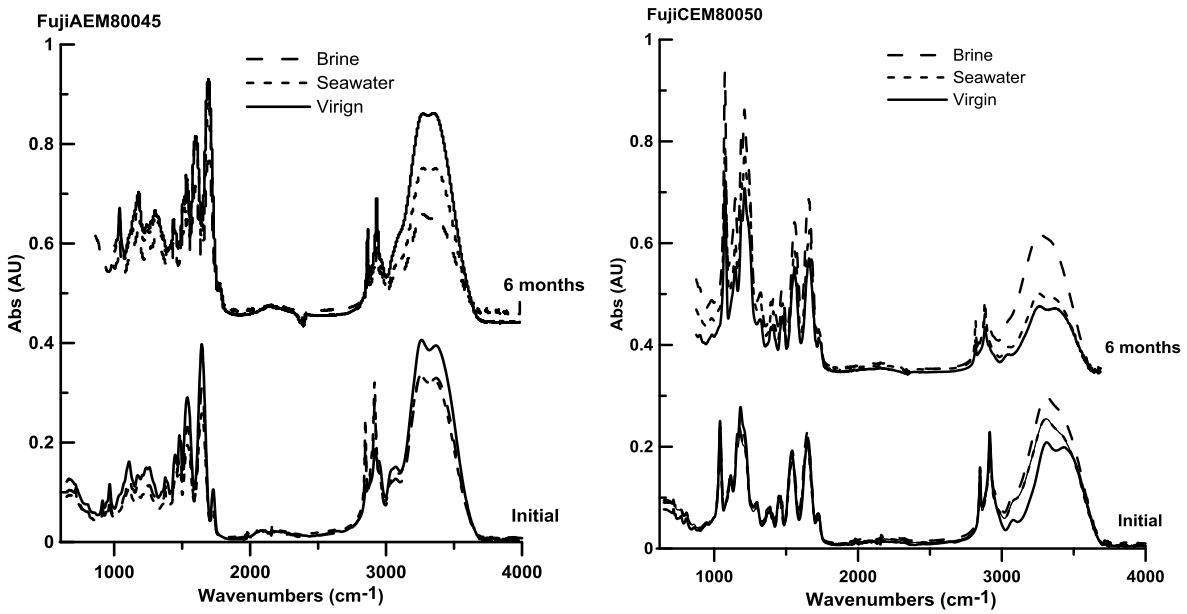

Figure 5.11. ATR-FTIR spectra of IEMs; a) FujiAEM80045 b) FujiCEM80050 membranes activated in distilled water (virgin), seawater and brine; initial spectra indicate measurements taken three days after activation.

5.3.6.2 Mechanical properties

The mechanical properties of ion exchange membranes are determined by many properties like polymer molecular weight, chemical structure of polymer main chain, polymer morphology and test conditions. During mechanical tests, high tensile strength and longer elongation at break indicate good mechanical properties of membranes.

Table 5.4 presents results from the test on mechanical properties of different IEMs. Comparison is made between virgin and membranes aged in seawater and concentrated brine sample for 6 months. In general, CEMs showed good mechanical properties compared to AEMs both in virgin state and after aging: tensile strength 15-31 MPa) and elongation at break (20.9-52.6%) for CEMs were higher than that of AEMs with tensile strength (13-28 MPa) and elongation at break (11.3-40.3%).

Mechanical properties of IEMS have a direct link with durability in terms of polymer rigidity and lifetimes [35]. For long-term use IEMs in electrochemical membrane processes, membranes with good mechanical properties are required. Membranes with low mechanical properties or poor hold of polymer rigidity will have a shorter life time. Ghalloussi *et al*. (2013) observed dramatic loss of polymer rigidity (above 93 %) for IEMs after two years of operation in ED, with the effect more noticeable on AEM than CEM [15].

In general, good mechanical property account positively for long term stability of membranes. However, higher mechanical and dimensional stability could lead to higher resistances [36]. Also, the design of ion exchange membranes with good mechanical properties counteracts with other properties like permselectivity. For example, ion exchange membrane with high crosslinking degree enable effective ion transport of the membranes (good permselectivity) but this is at cost of low mechanical strength. Thus, the design of suitable ion exchange membranes for RE, in particular highly selectivity, stable and low resistance membranes is a complex situation requiring intensive research.

Table 5.4. Results from mechanical test of ion exchange virgin and membranes preserved in seawater and brine for six months.

Membranes	Young's modulus (MPa)			Tensile stress (MPa)			Elongation at break (%)		
	Virgin	Seawater	Brine	Virgin	Seawater	Brine	Virgin	Seawater	Brine
Fuji AEM0051	392.4±6.6	139.5±20.3	144.7±4.2	28.4±6.1	6.2±1.1	17.5±7.5	40.3±1.8	35.3±9.7	26.1±3.5
Fuji CEM0051	631.3±16.0	318.2±9.1	225.7±7.7	31.1±9.5	20.6±7.9	19.0±8.7	52.6±4.1	38.3±9.8	28.7±3.8
Fuji AEM 80045	193.0±6.4	175.2±1.2	79.4±5.0	13.1±1.0	5.8±0.9	11.3±1.7	11.3±1.9	8.0±1.8	22.6±6.8
Fuji CEM 80045	1099.4±5.1	371.9±2.0	398.8±4.9	15.3±1.6	8.0±1.2	11.2±2.9	20.9±2.4	16.0±2.4	23.7±2.0

5.3.7 SGP-RE tests

Figure 5.12 shows the V-I curve and power curves for the RE tested with artificial solutions mimicking real seawater and brine, and reference NaCl solutions. Results reveal a drastic reduction (-78 %) in power density (0.48 W/m^2_{MP}) compared to operations with pure NaCl solutions (2.2 W/m^2_{MP}). This was accompanied by a significant reduction (-61%) of OCV (from 1.8 V to 0.7 V). This is coherent with our previous investigation on SGP-RE tested with artificial brine and brackish water: the presence of Mg^{2+} in feed samples resulted in up to 63% reduction in maximum power density compared to reference solution (pure NaCl solution).

Vermaas *et al*. (2013) operated a RE with a mixture of NaCl solution containing multivalent ions like Mg^{2+} and SO_4^{2-} with the total salt concentration simulating seawater and river water [37]. They observed 29-50% reduction in power density when using a mixture with a molar fraction of 10% $MgSO_4$ and 90% of NaCl in feed water. Besides, about 40% decrease of power density was observed on the first 24 h operation of RE with natural feed water [18]. Besides the alteration of membrane properties (permselectivity and resistance) in presence of multivalent ions, the reduction in power density with real solutions can also be attributed to fouling phenomenon, for example, scaling of thin film salt deposits on the surface with a potentially negative impact on electrochemical membrane properties.

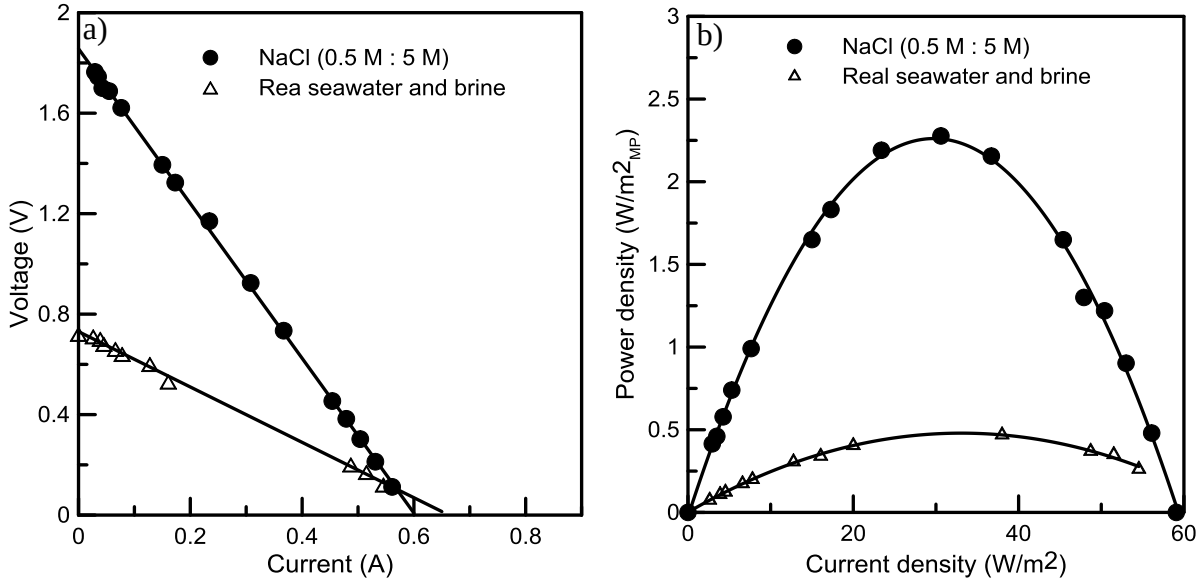

Figure 5.12. a) V-I and b) power curves for SGP-RE test pure NaCl solutions and artificial solutions mimicking seawater and brine.

Figure 5.13 shows the effect of presence of humic acid in SGP-RE performance. There is no significant effect (below 10% change compared to pure NaCl solutions) on OCV and power densities obtained from short term experimental test. This implies quite low effect of organic matter on SGP-RE performance when working with concentrated solutions like brine.

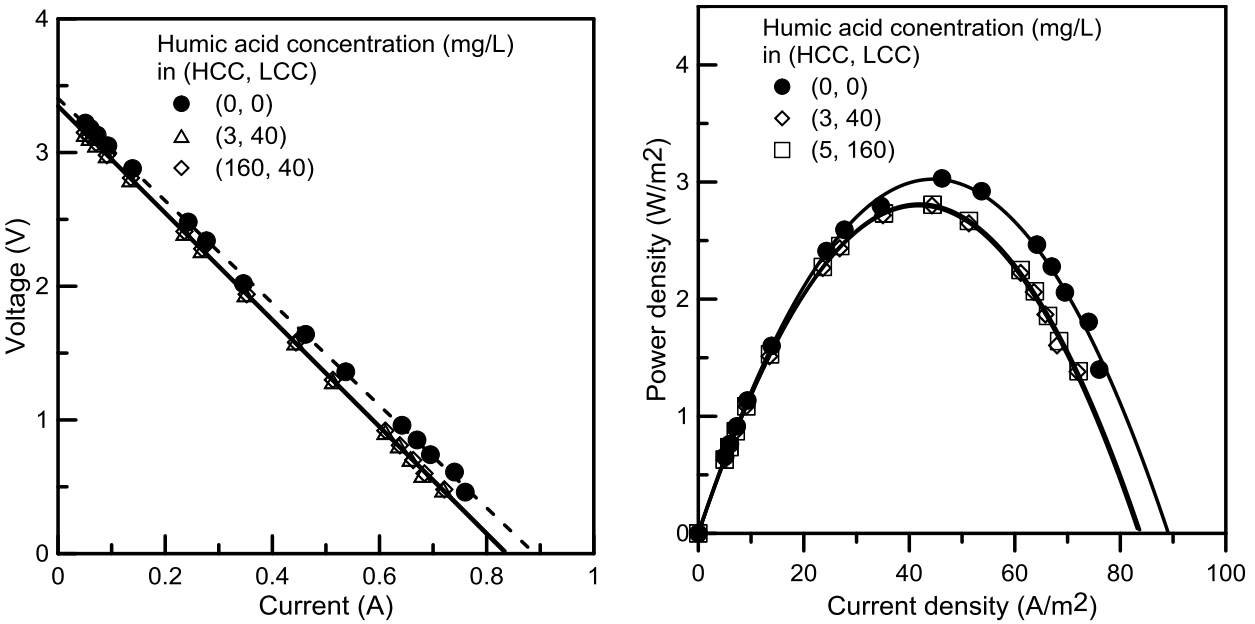

Figure 5.13. Effect of humic acid on salinity gradient power-reverse electrodialysis performance; a) I-V curve and b) power curves for the tested solutions with different humic acid content.

Figure 5.14. Shows the variation of power densities with time for the RE stack operated over 24 months alternatively with pure NaCl solution and artificial solutions prepared by mimicking real brackish water and brine. In the first three months, the change in power density is quite low (below 10 %). At this time, any risk of fouling or other potential effects that can alter electrochemical membrane properties is not so significant. However, the change in power density is visible after operations over the six months. This can be attributed different effects related to membrane, for example, formation of insoluble species over the membranes operated in highly concentrated solutions. This can potentially affect the membrane permselectivity and resistivity which impact the power density. Electrolyte leakage may also occur over a long operational period resulting in membrane poisoning. After about 18 months, the power density comes to its minimum value and continues with relatively small change again.

For a stack operated with natural seawater and river water, the apparent permselectivity of membranes have been observed to decrease sharply by about 10% which is accompanied by a significant increase in stack internal resistance (40-70 %)[18].

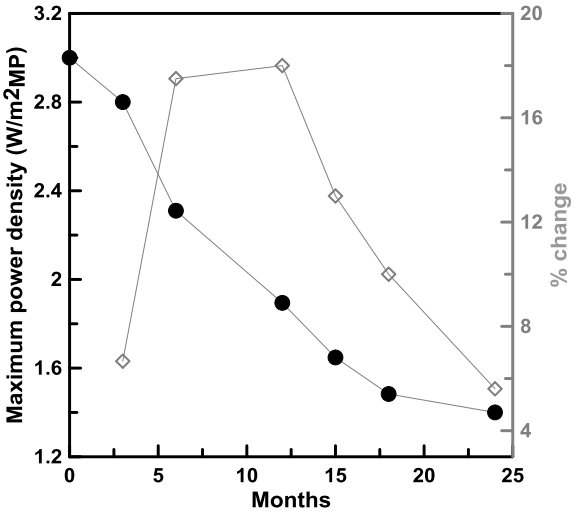

Figure 5.14. Variation of power densities with time for SGP-RE operated alternatively with pure NaCl solutions; LCC: 0.1 M NaCl, HCC: 5 M NaCl. The stack is operated with artificial solutions mimicking real brackish water and brine at some time interval but in a comparatively few experiments compared to pure solutions; experiments performed over 24 months at room temperature.

5.3.8 Pretreatment strategies

The impact of fouling on the performance of RE is an important issue requiring careful investigation. However, analogies with membrane operations on raw salt solutions allow at identifying general pre-treatment strategies to be implemented in order to preserve performance and lifetime of IEMs. Moreover, the efficiency of pre-treatment system directly affects cleaning frequency and cost of RE units. In analogy to membrane processes for desalination, two strategies can be envisaged for RE process: membrane pre-treatment and chemical softening.

Due to the progressive decrease of membrane costs, membrane pre-treatment is being considered as a reliable alternative to conventional pre-treatment. Mostly Microfiltration (MF) and Ultrafiltration (UF) are used as pre-treatment units; in RO desalination, the combination of all these different membrane operations is termed “Integrated Membrane System”. In this respect, there also a possibility to combine RE in an integrated membrane desalination system which might represent an interesting opportunity due to availability of pre-treated seawater and brine from reverse osmosis technology.

MF acts as a barrier against suspended particles, colloidal materials and bacteria, with stable performance (SDI<2.5, turbidity<0.1 NTU) even under significant fluctuation of raw water quality. UF membranes provide an effective barrier to pathogens (removal: bacteria>5 log, Giardia>4 log, virus > 4 log). It is also reported that plant footprint can be reduced by about 30-50

% using membrane pretreatment with respect to conventional sedimentation/flocculation/dual media filtration systems [1]. MF and UF guarantee simplicity of operation and maintenance, easy automation and scale-up, and very low consumption of chemicals.

Energy and economic aspects related to membrane pretreatment need to be carefully considered. Capital costs of MF or UF are higher up to 25% than conventional pretreatment, in large part recovered by an increase of membrane lifetime and by a decrease of cleaning frequency. Moreover, MF and UF require pumping energy to pressurize feed solutions. Table 5.4 compares performance of MF and UF in terms of TC and TOC removal, when operated at 2 bars on Margi seawater and Ettore Infersa seawater; pressure is kept low in order to limit energy consumption.

Table 5.4. Removal of Total Organic Carbon (TOC) and Total Carbon (TC) by Microfiltration (MF) or Ultrafiltration (UF).

			% reduction			
Initial			Microfiltration* BA85 - 0.45 μm		Ultrafiltration* SEPA CF TF UF, type GK (MWCO: 3 kDa)	
Raw water	TOC (mg/l)	TC (mg/l)	TOC (%)	TC (%)	TOC (%)	TC (%)
Seawater Margi	37.0±3	40.3±3	-0.65	-0.49	-32.7	-20.1
Seawater Ettore Infersa	5.3±2	24.7±9	-2.9	-0.70	-20.6	-14.0

*Measured at 2 bar room temperature.

Another strategy to prevent precipitation of calcium carbonate, magnesium carbonate and other sparingly soluble salts is chemical softening. The selection of the proper chemicals (typically caustic soda-NaOH, lime or hydrated lime-$Ca(OH)_2$, quickline-CaO, soda ash - Na_2CO_3) can be determined by the quality of the raw solution. The ions (Ca^{2+} and Mg^{2+}) can be removed by a level up to 92 % through proper treatment of solutions according to strategic chemical treatment mechanism.

5.4 Conclusion

Fouling of IEMs one of the challenges in separation technologies as well as energy conversion technologies like RE. There is still lack of highly stable and fouling resistance membranes, specially designed for RE application in concentrate solutions like brine. The challenges remain when working in concentrated brine solutions which may result in potential scaling of sparingly soluble salts over membrane. As demonstrated in the presented study, not only

the chemistry, but also the morphology of ion exchange membranes comes in to effect in the process of scaling. In general, FujiAEM showed high scaling tendency compared to other membranes in the concentrated brine and seawater, confirmed by the highest roughness coefficient observed from AFM characterizations. The variation of TOC and TH of feed samples depending on the sources impact the membranes physico-chemical interaction with feeds; for example, low TOC and TH result in a very low alteration of surface energies and morphology of IEMs. However, for the feed samples with high TOC and TH content, extremely high pore-blocking is observed. In general, the threshold value (TOC>2) for high fouling risk assignment indicate the requirement of pre-treatment operations for real solutions. However, promising results were obtained with respect to stability of IEMs aged in brine and seawater samples over 6 months.

Further research is required for selection or design of suitable IEMs for RE application in concentrated brine. Development of anti-fouling and stable IEMs will not only reduce the cost related to the membrane replacement and energy consumption, but also have a significant contribution to a stable performance and better efficiency of the SGP-RE system. This will be helpful for implementation of efficient pre-treatment methods in RE. Identification of the pre-treatment requirements is crucial for establishing reliable data for techno-economic evaluations and scale-up of RE system.

References

[1] R.A. Tufa, E. Curcio, W. van Baak, J. Veerman, S. Grasman, E. Fontananova, G. Di Profio, Potential of brackish water and brine for energy generation by salinity gradient power-reverse electrodialysis (SGP-RE), RSC Advances, 4 (2014) 42617-42623.

[2] Ramato A. Tufa, E. Curcio, E. Brauns, W. van Baak, E. Fontananova, G. Di Profio, Membrane Distillation and Reverse Electrodialysis for Near-Zero Liquid Discharge and low energy seawater desalination, Journal of Membrane Science, 496 (2015) 325-333.

[3] Y. Tanaka, Mass transport and energy consumption in ion-exchange membrane electrodialysis of seawater, Journal of Membrane Science, 215 (2003) 265-279.

[4] M. Kariduraganavar, R. Nagarale, A. Kittur, S. Kulkarni, Ion-exchange membranes: preparative methods for electrodialysis and fuel cell applications, Desalination, 197 (2006) 225-246.

[5] L. Gubler, G.G. Scherer, Trends for fuel cell membrane development, Desalination, 250 (2010) 1034-1037.

[6] K. Bouzek, Z. Cílová, P. Podubecká, M. Paidar, J. Schauer, Homogeneous vs. heterogeneous membranes for the application in PEM type fuel cells, Desalination, 200 (2006) 650-652.

[7] V. Sproll, G. Nagy, U. Gasser, S. Balog, S. Gustavsson, T.J. Schmidt, L. Gubler, Structure–property correlations of ion-containing polymers for fuel cell applications, Radiation Physics and Chemistry, (2015).

[8] D. Aili, M.K. Hansen, R.F. Renzaho, Q. Li, E. Christensen, J.O. Jensen, N.J. Bjerrum, Heterogeneous anion conducting membranes based on linear and crosslinked KOH doped polybenzimidazole for alkaline water electrolysis, Journal of Membrane Science, 447 (2013) 424-432.

[9] R. Holze, J. Ahn, Advances in the use of perfluorinated cation exchange membranes in integrated water electrolysis and hydrogen/oxygen fuel cell systems, Journal of Membrane Science, 73 (1992) 87-97.

[10] A. Chromik, A.R. dos Santos, T. Turek, U. Kunz, T. Häring, J. Kerres, Stability of acid-excess acid–base blend membranes in all-vanadium redox-flow batteries, Journal of Membrane Science, 476 (2015) 148-155.

[11] X. Li, H. Zhang, Z. Mai, H. Zhang, I. Vankelecom, Ion exchange membranes for vanadium redox flow battery (VRB) applications, Energy & Environmental Science, 4 (2011) 1147-1160.

[12] B.E. Logan, Microbial fuel cells, John Wiley & Sons, 2008.

[13] Y. Kim, B.E. Logan, Microbial reverse electrodialysis cells for synergistically enhanced power production, Environmental Science & Technology, 45 (2011) 5834-5839.

[14] P. Długołęcki, K. Nymeijer, S. Metz, M. Wessling, Current status of ion exchange membranes for power generation from salinity gradients, Journal of Membrane Science, 319 (2008) 214-222.

[15] R. Ghalloussi, W. Garcia-Vasquez, L. Chaabane, L. Dammak, C. Larchet, S. Deabate, E. Nevakshenova, V. Nikonenko, D. Grande, Ageing of ion-exchange membranes in electrodialysis: a structural and physicochemical investigation, Journal of Membrane Science, 436 (2013) 68-78.

[16] J.W. Post, H.V. Hamelers, C.J. Buisman, Influence of multivalent ions on power production from mixing salt and fresh water with a reverse electrodialysis system, Journal of Membrane Science, 330 (2009) 65-72.

[17] D.A. Vermaas, J. Veerman, M. Saakes, K. Nijmeijer, Influence of multivalent ions on renewable energy generation in reverse electrodialysis, Energy & Environmental Science, (2014).

[18] D.A. Vermaas, D. Kunteng, M. Saakes, K. Nijmeijer, Fouling in reverse electrodialysis under natural conditions, Water Research, 47 (2013) 1289-1298.

[19] H.-J. Lee, M.-K. Hong, S.-D. Han, S.-H. Cho, S.-H. Moon, Fouling of an anion exchange membrane in the electrodialysis desalination process in the presence of organic foulants, Desalination, 238 (2009) 60-69.

[20] N.W. Kang, S. Lee, D. Kim, S. Hong, J.H. Kweon, Analyses of calcium carbonate scale deposition on four RO membranes under a seawater desalination condition, Water Science & Technology, 64 (2011) 1573-1580.

[21] E. Curcio, X. Ji, G. Di Profio, E. Fontananova, E. Drioli, Membrane distillation operated at high seawater concentration factors: role of the membrane on CaCO 3 scaling in presence of humic acid, Journal of Membrane Science, 346 (2010) 263-269.

[22] S.F.E. Boerlage, M.D. Kennedy, M.R. Dickson, D.E.Y. El-Hodali, J.C. Schippers, The modified fouling index using ultrafiltration membranes (MFI-UF): characterisation, filtration mechanisms and proposed reference membrane, Journal of Membrane Science, 197 (2002) 1-21.

[23] J.W. Post, Blue Energy: electricity production from salinity gradients by reverse electrodialysis, publisher not identified, 2009.

[24] E. Korngold, F. de Körösy, R. Rahav, M.F. Taboch, Fouling of anionselective membranes in electrodialysis, Desalination, 8 (1970) 195-220.
[25] K. Scott, 10 - Microbial fuel cells: transformation of wastes into clean energy, in: A. Gugliuzza, A. Basile (Eds.) Membranes for Clean and Renewable Power Applications, Woodhead Publishing, 2014, pp. 266-300.
[26] R.N. Wenzel, RESISTANCE OF SOLID SURFACES TO WETTING BY WATER, Industrial & Engineering Chemistry, 28 (1936) 988-994.
[27] H. Strathmann, Ion Exchange Membrane Separation Processes, 1st ed., Elsevier, 2004.
[28] S.G. Yiantsios, D. Sioutopoulos, A.J. Karabelas, Colloidal fouling of RO membranes: an overview of key issues and efforts to develop improved prediction techniques, Desalination, 183 (2005) 257-272.
[29] R.A. Tufa, E. Curcio, W. van Baak, J. Veerman, S. Grasman, E. Fontananova, G. Di Profio, Potential of brackish water and brine for energy generation by salinity gradient power-reverse electrodialysis (SGP-RE), RSC Advances, (2014).
[30] S. Kim, N. Park, S. Lee, J. Cho, Membrane characterizations for mitigation of organic fouling during desalination and wastewater reclamation, Desalination, 238 (2009) 70-77.
[31] A.R. Roudman, F.A. DiGiano, Surface energy of experimental and commercial nanofiltration membranes: effects of wetting and natural organic matter fouling, Journal of Membrane Science, 175 (2000) 61-73.
[32] K.J. Howe, K.P. Ishida, M.M. Clark, Use of ATR/FTIR spectrometry to study fouling of microfiltration membranes by natural waters, Desalination, 147 (2002) 251-255.
[33] H.-J. Lee, M.-K. Hong, S.-D. Han, S.-H. Cho, S.-H. Moon, Fouling of an anion exchange membrane in the electrodialysis desalination process in the presence of organic foulants, Desalination, 238 (2009) 60-69.
[34] C. Heitner-Wirguin, Infra-red spectra of perfluorinated cation-exchanged membranes, Polymer, 20 (1979) 371-374.
[35] S. Kundu, L.C. Simon, M. Fowler, S. Grot, Mechanical properties of Nafion™ electrolyte membranes under hydrated conditions, Polymer, 46 (2005) 11707-11715.
[36] H. Strathmann, Ion-exchange membrane separation processes, Elsevier, 2004.
[37] D.A. Vermaas, J. Veerman, M. Saakes, K. Nijmeijer, Influence of multivalent ions on renewable energy generation in reverse electrodialysis, Energy & Environmental Science, 7 (2014) 1434-1445.

Appendix 5.1

Speciation Analysis

For a given compound, a positive value of SI indicates that the solution is supersaturated with and precipitation of a solid phase may occur. Detailed results of the speciation analysis are reported below:

SEAWATER - ETTORE INFERSA

Ionic strength = 8.456×10^{-1}
Total carbon (mol/kg) = 2.098×10^{-4}
Electrical balance, percent error, 100*(Cat-|An|)/(Cat+|An|) = -4.21%

----------Distribution of species----------

Species	*Molality*	*Activity*	*Log Molality*	*Log Activity*	*Log Gamma*
OH^-	2.619×10^{-6}	1.550×10^{-6}	-5.582	-5.810	-0.228
H^+	8.433×10^{-9}	6.310×10^{-9}	-8.074	-8.200	-0.126
H_2O	5.551e+01	9.770×10^{-1}	1.744	-0.010	0.000
HCO_3^-	1.295×10^{-4}	8.594×10^{-5}	-3.888	-4.066	-0.178
$MgHCO_3^+$	3.358×10^{-5}	2.578×10^{-5}	-4.474	-4.589	-0.115
$NaHCO_3$	1.355×10^{-5}	1.646×10^{-5}	-4.868	-4.783	0.085
$MgCO_3$	1.286×10^{-5}	1.563×10^{-5}	-4.891	-4.806	0.085
$CaHCO_3^+$	6.972×10^{-6}	4.627×10^{-6}	-5.157	-5.335	-0.178
$NaCO_3^-$	5.278×10^{-6}	4.052×10^{-6}	-5.278	-5.392	-0.115
$CaCO_3$	3.727×10^{-6}	4.528×10^{-6}	-5.429	-5.344	0.085
CO_3^{2-}	3.293×10^{-6}	6.388×10^{-7}	-5.482	-6.195	-0.712
CO_2	1.027×10^{-6}	1.248×10^{-6}	-5.988	-5.904	0.085
Ca^{2+}	1.707×10^{-2}	4.220×10^{-3}	-1.768	-2.375	-0.607
$CaSO_4$	1.265×10^{-3}	1.537×10^{-3}	-2.898	-2.813	0.085
$CaHCO_3^+$	6.972×10^{-6}	4.627×10^{-6}	-5.157	-5.335	-0.178
$CaCO_3$	3.727×10^{-6}	4.528×10^{-6}	-5.429	-5.344	0.085
$CaOH^+$	1.412x10-7	1.084×10^{-7}	-6.850	-6.965	-0.115
$CaHSO_4^+$	7.399×10^{-11}	5.681×10^{-11}	-10.131	-10.246	-0.115

Cl^-	$7.341x10^{-1}$	$4.474x10^{-1}$	-0.134	-0.349	-0.215
H_2	2.320e-22	2.818e-22	-21.635	-21.550	0.085
K^+	$9.189x10^{-3}$	$5.601x10^{-3}$	-2.037	-2.252	-0.215
KSO_4^-	$9.356x10^{-5}$	$7.183x10^{-5}$	-4.029	-4.144	-0.115
KOH	$2.475x10^{-9}$	$3.007x10^{-9}$	-8.606	-8.522	0.085
Mg^{2+}	$8.787x10^{-2}$	$2.563x10^{-2}$	-1.056	-1.591	-0.535
$MgSO_4$	$9.028x10^{-3}$	$1.097x10^{-2}$	-2.044	-1.960	0.085
$MgHCO_3^+$	$3.358x10^{-5}$	$2.578x10^{-5}$	-4.474	-4.589	-0.115
$MgOH^+$	$1.877x10^{-5}$	$1.441x10^{-5}$	-4.727	-4.841	-0.115
$MgCO_3$	$1.286x10^{-5}$	$1.563x10^{-5}$	-4.891	-4.806	0.085
Na^+	$4.798x10^{-1}$	$3.406x10^{-1}$	-0.319	-0.468	-0.149
$NaSO_4^-$	$4.059x10^{-3}$	$3.116x10^{-3}$	-2.392	-2.506	-0.115
$NaHCO_3$	$1.355x10^{-5}$	$1.646x10^{-5}$	-4.868	-4.783	0.085
$NaCO_3^-$	$5.278x10^{-6}$	$4.052x10^{-6}$	-5.278	-5.392	-0.115
NaOH	$2.868x10^{-7}$	$3.485x10^{-7}$	-6.542	-6.458	0.085
O_2	0.000	0.000	-49.385	-49.300	0.085
SO_4^{2-}	$1.101x10^{-2}$	$1.825x10^{-3}$	-1.958	-2.739	-0.780
$MgSO_4$	$9.028x10^{-3}$	$1.097x10^{-2}$	-2.044	-1.960	0.085
$NaSO_4^-$	$4.059x10^{-3}$	$3.116x10^{-3}$	-2.392	-2.506	-0.115
$CaSO_4$	$1.265x10^{-3}$	$1.537x10^{-3}$	-2.898	-2.813	0.085
KSO_4^-	$9.356x10^{-5}$	$7.183x10^{-5}$	-4.029	-4.144	-0.115
HSO_4^-	$1.458x10^{-9}$	$1.120x10^{-9}$	-8.836	-8.951	-0.115
$CaHSO_4^+$	7.399e-11	5.681e-11	-10.131	-10.246	-0.115

----------Saturation indexes ----------

Phase	*SI*	*log IAP*	*log KT*	
Anhydrite	-0.75	-5.11	-4.36	$CaSO_4$
Aragonite	-0.23	-8.57	-8.34	$CaCO_3$
Calcite	-0.09	-8.57	-8.48	$CaCO_3$
Dolomite	0.73	-16.36	-17.09	$CaMg(CO_3)_2$
Gypsum	-0.55	-5.13	-4.58	$CaSO_4{:}2H_2O$
Halite	-2.40	-0.82	1.58	NaCl

SEAWATER – MARGI

Ionic strength = 9.073x10-1
Total carbon (mol/kg) = 2.504x10-6
Electrical balance, percent error, 100*(Cat-|An|)/(Cat+|An|) = -2.39%

----------Distribution of species----------

Species	*Molality*	*Activity*	*Log Molality*	*Log Activity*	*Log Gamma*
OH^-	$1.324x10^{-6}$	$7.765x10^{-7}$	-5.878	-6.110	-0.232
H^+	$1.687x10^{-8}$	$1.259x10^{-8}$	-7.773	-7.900	-0.127
H_2O	$5.551x10^{1}$	$9.765x10^{-1}$	1.744	-0.010	0.000
HCO_3^-	$1.543x10^{-6}$	$1.019x10^{-6}$	-5.812	-5.992	-0.180
$MgHCO_3^+$	$5.490x10^{-7}$	$4.264x10^{-7}$	-6.260	-6.370	-0.110
$NaHCO_3$	$1.478x10^{-7}$	$1.822x10^{-7}$	-6.830	-6.740	0.091
$MgCO_3$	$1.051x10^{-7}$	$1.295x10^{-7}$	-6.978	-6.888	0.091
$CaHCO_3^+$	$6.817x10^{-8}$	$4.500x10^{-8}$	-7.166	-7.347	-0.180
$NaCO_3^-$	$2.894x10^{-8}$	$2.247x10^{-8}$	-7.539	-7.648	-0.110
CO_2	$2.396x10^{-8}$	$2.952x10^{-8}$	-7.621	-7.530	0.091
CO_3^{2-}	$1.999x10^{-8}$	$3.794x10^{-9}$	-7.699	-8.421	-0.722
$CaCO_3$	$1.791x10^{-8}$	$2.207x10^{-8}$	-7.747	-7.656	0.091
Ca^{2+}	$1.402x10^{-2}$	$3.463x10^{-3}$	-1.853	-2.461	-0.607
$CaSO_4$	$1.154x10^{-3}$	$1.422x10^{-3}$	-2.938	-2.847	0.091
$CaHCO_3^+$	$6.817x10^{-8}$	$4.500x10^{-8}$	-7.166	-7.347	-0.180
$CaOH^+$	$5.740x10^{-8}$	$4.457x10^{-8}$	-7.241	-7.351	-0.110
$CaCO_3$	$1.791x10^{-8}$	$2.207x10^{-8}$	-7.747	-7.656	0.091
$CaHSO_4^+$	$1.351x10^{-10}$	$1.049x10^{-10}$	-9.869	-9.979	-0.110
Cl^-	$7.468x10^{-1}$	$4.521x10^{-1}$	-0.127	-0.345	-0.218
H_2	$9.105x10^{-22}$	$1.122x10^{-21}$	-21.041	-20.950	0.091
K^+	$2.230x10^{-2}$	$1.350x10^{-2}$	-1.652	-1.870	-0.218
KSO_4^-	$2.514x10^{-4}$	$1.953x10^{-4}$	-3.600	-3.709	-0.110
KOH	$2.946x10^{-9}$	$3.630x10^{-9}$	-8.531	-8.440	0.091
Mg^{2+}	$1.218x10^{-1}$	$3.577x10^{-2}$	-0.914	-1.446	-0.532
$MgSO_4$	$1.401x10^{-2}$	$1.727x10^{-2}$	-1.854	-1.763	0.091
$MgOH^+$	$1.297x10^{-5}$	$1.007x10^{-5}$	-4.887	-4.997	-0.110
$MgHCO_3^+$	$5.490x10^{-7}$	$4.264x10^{-7}$	-6.260	-6.370	-0.110

$MgCO_3$	$1.051x10^{-7}$	$1.295x10^{-7}$	-6.978	-6.888	0.091
Na^+	$4.467x10^{-1}$	$3.181x10^{-1}$	-0.350	-0.497	-0.147
$NaSO_4^-$	$4.226x10^{-3}$	$3.282x10^{-3}$	-2.374	-2.484	-0.110
$NaHCO_3$	$1.478x10^{-7}$	$1.822x10^{-7}$	-6.830	-6.740	0.091
NaOH	$1.323x10^{-7}$	$1.630x10^{-7}$	-6.879	-6.788	0.091
$NaCO_3^-$	$2.894x10^{-8}$	$2.247x10^{-8}$	-7.539	-7.648	-0.110
O_2	0.000	0.000	-50.591	-50.501	0.091
$MgSO_4$	$1.401x10^{-2}$	$1.727x10^{-2}$	-1.854	-1.763	0.091
SO_4^{2-}	$1.279x10^{-2}$	$2.059x10^{-3}$	-1.893	-2.686	-0.793
$NaSO_4^-$	$4.226x10^{-3}$	$3.282x10^{-3}$	-2.374	-2.484	-0.110
$CaSO_4$	$1.154x10^{-3}$	$1.422x10^{-3}$	-2.938	-2.847	0.091
KSO_4^-	$2.514x10^{-4}$	$1.953x10^{-4}$	-3.600	-3.709	-0.110
HSO_4^-	$3.245x10^{-9}$	$2.520x10^{-9}$	-8.489	-8.599	-0.110
$CaHSO_4^+$	1.351e-10	1.049e-10	-9.869	-9.979	-0.110

----------Saturation indexes----------

Phase	*SI*	*log IAP*	*log KT*	
Anhydrite	-0.79	-5.15	-4.36	$CaSO_4$
Aragonite	-2.55	-10.88	-8.34	$CaCO_3$
Calcite	-2.40	-10.88	-8.48	$CaCO_3$
Dolomite	-3.66	-20.75	-17.09	$CaMg(CO_3)_2$
Gypsum	-0.59	-5.17	-4.58	$CaSO_4:2H_2O$
Halite	-2.42	-0.84	1.58	NaCl

BRINE - ETTORE INFERSA

Ionic strength = 9.016e+00
Total carbon (mol/kg) = 9.828x10-4
Electrical balance, percent error, 100*(Cat-|An|)/(Cat+|An|) = 0.02%

----------Distribution of species----------

Species	*Molality*	*Activity*	*Log Molality*	*Log Activity*	*LogGamma*
H^+	$1.798x10^{-7}$	$1.259x10^{-7}$	-6.745	-6.900	-0.155
OH^-	$1.323x10^{-7}$	$5.997x10^{-8}$	-6.878	-7.222	-0.344
H_2O	5.551e+01	$7.541x10^{-1}$	1.744	-0.123	0.000
$MgHCO_3^+$	$7.616x10^{-4}$	$7.537x10^{-3}$	-3.118	-2.123	0.995
HCO_3^-	$1.120x10^{-4}$	6.420x10-^{5}	-3.951	-4.192	-0.242
$NaHCO_3$	$4.603x10^{-5}$	$3.669x10^{-4}$	-4.337	-3.435	0.902
$CaHCO_3^+$	$3.065x10^{-5}$	$1.756x10^{-5}$	-4.514	-4.755	-0.242
$MgCO_3$	$2.872x10^{-5}$	$2.290x10^{-4}$	-4.542	-3.640	0.902
CO_2	$3.023x10^{-6}$	$2.410x10^{-5}$	-5.520	-4.618	0.902
$NaCO_3^-$	$4.574x10^{-7}$	$4.526x10^{-6}$	-6.340	-5.344	0.995
CO_3^{2-}	$2.219x10^{-7}$	$2.392x10^{-8}$	-6.654	-7.621	-0.967
$CaCO_3$	$1.081x10^{-7}$	$8.614x10^{-7}$	-6.966	-6.065	0.902
Ca^{2+}	$7.505x10^{-3}$	$2.144x10^{-2}$	-2.125	-1.669	0.456
$CaSO_4$	$1.698x10^{-3}$	$1.354x10^{-2}$	-2.770	-1.868	0.902
$CaHCO_3^+$	$3.065x10^{-5}$	$1.756x10^{-5}$	-4.514	-4.755	-0.242
$CaCO_3$	$1.081x10^{-7}$	$8.614x10^{-7}$	-6.966	-6.065	0.902
$CaOH^+$	$2.154x10^{-9}$	$2.132x10^{-8}$	-8.667	-7.671	0.995
$CaHSO_4^+$	$1.009x10^{-9}$	$9.984x10^{-9}$	-8.996	-8.001	0.995
Cl^-	7.341	4.543	0.866	0.657	-0.208
H^2	$1.407x10^{-20}$	$1.122e^{-19}$	-19.852	-18.950	0.902
K^+	$3.023x10^{-1}$	$1.871x10^{-1}$	-0.520	-0.728	-0.208
KSO_4^-	$4.203x10^{-4}$	$4.160x10^{-3}$	-3.376	-2.381	0.995
KOH	4.874e-10	$3.886x10^{-9}$	-9.312	-8.411	0.902
Mg^{2+}	1.415e+00	1.003e+01	0.151	1.001	0.851
$MgSO_4$	$9.336x10^{-1}$	7.442e+00	-0.030	0.872	0.902
$MgHCO_3^+$	$7.616x10^{-4}$	$7.537x10^{-3}$	-3.118	-2.123	0.995
$MgCO_3$	$2.872x10^{-5}$	$2.290x10^{-4}$	-4.542	-3.640	0.902
$MgOH^+$	$2.205x10^{-5}$	$2.182x10^{-4}$	-4.657	-3.661	0.995

Na^+	4.368e+00	1.016e+01	0.640	1.007	0.367
$NaSO_4^-$	$1.629x10^{-2}$	$1.612x10^{-1}$	-1.788	-0.793	0.995
$NaHCO_3$	$4.603x10^{-5}$	$3.669x10^{-4}$	-4.337	-3.435	0.902
$NaCO_3^-$	$4.574x10^{-7}$	$4.526x10^{-6}$	-6.340	-5.344	0.995
NaOH	$5.046x10^{-8}$	$4.022x10^{-7}$	-7.297	-6.396	0.902
O_2	0.000	0.000	-55.627	-54.725	0.902
$MgSO_4$	$9.336x10^{-1}$	7.442	-0.030	0.872	0.902
SO_4^{2-}	$7.810x10^{-2}$	$3.164x10^{-3}$	-1.107	-2.500	-1.392
$NaSO_4^-$	$1.629x10^{-2}$	$1.612x10^{-1}$	-1.788	-0.793	0.995
$CaSO_4$	$1.698x10^{-3}$	$1.354x10^{-2}$	-2.770	-1.868	0.902
KSO_4^-	$4.203x10^{-4}$	$4.160x10^{-3}$	-3.376	-2.381	0.995
HSO_4^-	$3.914x10^{-9}$	$3.873x10^{-8}$	-8.407	-7.412	0.995
$CaHSO_4^+$	$1.009x10^{-9}$	$9.984x10^{-9}$	-8.996	-8.001	0.995

----------Saturation indexes----------

	Phase	*SI*	*log IAP*	*log KT*
Anhydrite	0.19	-4.17	-4.36	$CaSO_4$
Aragonite	-0.95	-9.29	-8.34	$CaCO_3$
Calcite	-0.81	-9.29	-8.48	$CaCO_3$
Dolomite	1.18	-15.91	-17.09	$CaMg(CO_3)_2$
Gypsum	0.17	-4.41	-4.58	$CaSO_4:2H_2O$
Halite	0.08	1.66	1.58	NaCl

BRINE - MARGI

Ionic strength = 9.986e+00
Total carbon (mol/kg) = 2.172x10-3
Electrical balance, percent error, 100*(Cat-|An|)/(Cat+|An|) = 0.14%

----------Distribution of species----------

Species	*Molality*	*Activity*	*Log Molality*	*Log Activity*	*Log Gamma*
H^+	$4.526x10^{-7}$	$3.162x10^{-7}$	-6.344	-6.500	-0.156
OH^-	$5.487x10^{-8}$	$2.465x10^{-8}$	-7.261	-7.608	-0.348
H_2O	$5.551x10^{1}$	$7.786x10^{-1}$	1.744	-0.109	0.000
$MgHCO_3^+$	$1.941x10^{-3}$	$2.673x10^{-2}$	-2.712	-1.573	1.139
HCO_3^-	$1.358x10^{-4}$	$7.747x10^{-5}$	-3.867	-4.111	-0.244
$CaHCO_3^+$	$3.825x10^{-5}$	$2.182x10^{-5}$	-4.417	-4.661	-0.244
$MgCO_3$	$3.243x10^{-5}$	$3.233x10^{-4}$	-4.489	-3.490	0.999
$NaHCO_3$	$1.687x10^{-5}$	$1.682x10^{-4}$	-4.773	-3.774	0.999
CO_2	$7.097x10^{-6}$	$7.074x10^{-5}$	-5.149	-4.150	0.999
CO_3^{2-}	$1.085x10^{-7}$	$1.149x10^{-8}$	-6.965	-7.940	-0.975
$NaCO_3^-$	$5.999x10^{-8}$	$8.259x10^{-7}$	-7.222	-6.083	1.139
$CaCO_3$	$4.275x10^{-8}$	$4.261x10^{-7}$	-7.369	-6.370	0.999
Ca^{2+}	$5.454x10^{-3}$	$2.208x10^{-2}$	-2.263	-1.656	0.607
$CaSO_4$	$8.584x10^{-4}$	$8.556x10^{-3}$	-3.066	-2.068	0.999
$CaHCO_3^+$	$3.825x10^{-5}$	$2.182x10^{-5}$	-4.417	-4.661	-0.244
$CaCO_3$	$4.275x10^{-8}$	$4.261x10^{-7}$	-7.369	-6.370	0.999
$CaHSO_4^+$	$1.151x10^{-9}$	$1.585x10^{-8}$	-8.939	-7.800	1.139
$CaOH^+$	$6.552e^{-10}$	$9.022x10^{-9}$	-9.184	-8.045	1.139
Cl^-	7.100	4.503	0.851	0.654	-0.198
H_2	$7.102x10^{-20}$	$7.079x10^{-19}$	-19.149	-18.150	0.999
K^+	$3.907x10^{-1}$	$2.478x10^{-1}$	-0.408	-0.606	-0.198
KSO_4^-	$2.456x10^{-4}$	$3.382x10^{-3}$	-3.610	-2.471	1.139
KOH	$2.123x^{-10}$	$2.116x10^{-9}$	-9.673	-8.675	0.999
Mg^{2+}	2.707	$2.949x0^{1}$	0.432	1.470	1.037
$MgSO_4$	1.347	$1.343x10^{1}$	0.129	1.128	0.999
$MgHCO_3^+$	$1.941x10^{-3}$	$2.673x10^{-2}$	-2.712	-1.573	1.139
$MgCO_3$	$3.243x10^{-5}$	$3.233x10^{-4}$	-4.489	-3.490	0.999

$MgOH^+$	$1.915x10^{-5}$	$2.636x10^{-4}$	-4.718	-3.579	1.139
Na+	1.413	3.861	0.150	0.587	0.436
$NaSO_4^-$	$2.729x10^{-3}$	$3.758x10^{-2}$	-2.564	-1.425	1.139
$NaHCO_3$	$1.687x10^{-5}$	$1.682x10^{-4}$	-4.773	-3.774	0.999
$NaCO_3^-$	$5.999x10^{-8}$	$8.259x10^{-7}$	-7.222	-6.083	1.139
NaOH	$6.301x10^{-9}$	$6.280x10^{-8}$	-8.201	-7.202	0.999
O_2	0.000	0.000	-57.296	-56.297	0.999
$MgSO_4$	1.347	$1.343e+0^1$	0.129	1.128	0.999
SO_4^{2-}	$5.348x10^{-2}$	$1.942x10^{-3}$	-1.272	-2.712	-1.440
$NaSO_4^-$	$2.729x10^{-3}$	$3.758x10^{-2}$	-2.564	-1.425	1.139
$CaSO_4$	$8.584x10^{-4}$	$8.556x10^{-3}$	-3.066	-2.068	0.999
KSO4-	$2.456x10^{-4}$	$3.382x10^{-3}$	-3.610	-2.471	1.139
HSO_4^-	$4.337x10^{-9}$	$5.971x10^{-8}$	-8.363	-7.224	1.139
$CaHSO_4^+$	$1.151x10^{-9}$	$1.585x10^{-8}$	-8.939	-7.800	1.139

----------Saturation indexes----------

Phase	*SI*	*log IAP*	*log KT*	
Anhydrite	-0.01	-4.37	-4.36	$CaSO_4$
Aragonite	-1.26	-9.60	-8.34	$CaCO_3$
Calcite	-1.12	-9.60	-8.48	$CaCO_3$
Dolomite	1.02	-16.07	-17.09	$CaMg(CO_3)_2$
Gypsum	0.00	-4.59	-4.58	$CaSO_4$:$2H_2O$
Halite	-0.34	1.24	1.58	NaCl

Chapter 6

Power Generation by an Industrial-Scale Reverse Electrodialysis (RE) Unit: Experimental Investigation and Performance Evaluation

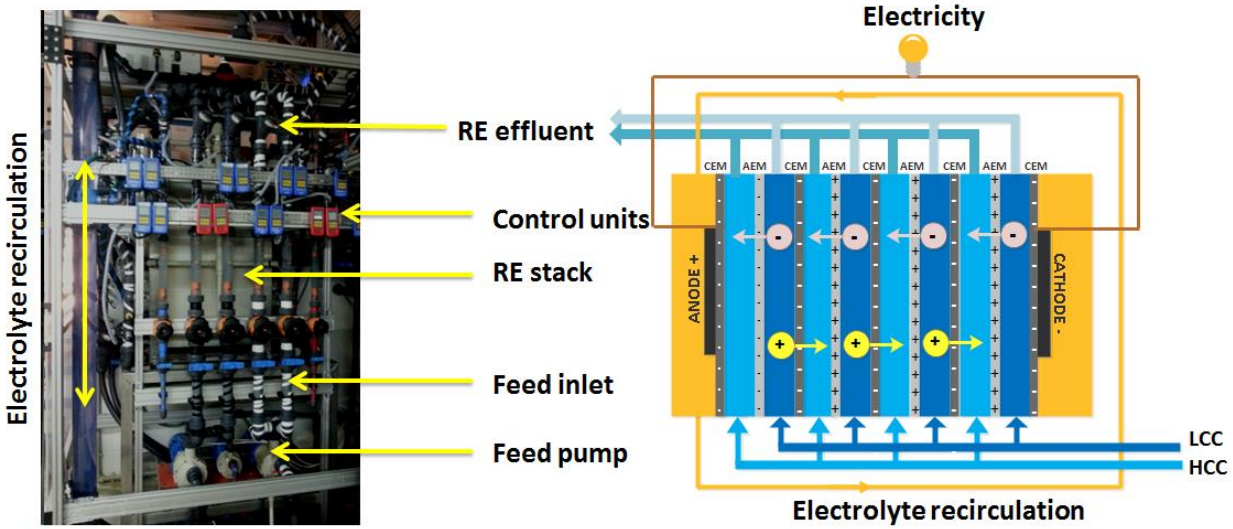

Abstract

In the present study, an industrial scale Reverse Electrodialysis unit, equipped with 200 pairs of heterogeneous Relax membranes with an effective area of 0.315x0.635 m^2 was tested experimentally; on average, cell size and active membrane area are projected 20 times compared to previously demonstrate small scale operations. The influence of main operating parameters (temperature 15-35 ^oC, flow velocity 0.48-5.3 cm/s and concentration 0.01-3.8 M) on key performance indicators of Salinity Gradient Power Reverse Electrodialysis (SGP-RE) is evaluated systematically. Investigations were done on monovalent (NaCl) and divalent (Na_2SO_4) ionic feed compositions. Results indicate that operational switching from monovalent to divalent ionic feed compositions is accompanied by a drastic loss in performance (above 50% difference in power density). The effect of flow velocity on power density is similar to small scale operations with a positive impact. The trend in energy efficiency and power density over the temperature range of 15-35 °C is opposite; on average power density increases at a maximal rate of 9 mW/°C (quite lower than small scale applications) whereas energy efficiency decreases at a maximal rate of 1.8%/°C. In general, test profiles within experimental boundaries indicate significant internal losses proportional to flow path length compared to small scale operations.

This Chapter submitted to the Journal of *Industrial and Chemical Engineering Research.*

6.1 Introduction

Alternative clean energy resources are urgently required as a result of increasing exploitation of the limited and unsustainable fossil based energy resources. Reverse electrodialysis (RE) is among the emerging membrane based salinity gradient power (SGP) technologies for clean energy generation from mixing solutions of different concentrations like river water/seawater [1-4], brackish water/seawater/brine [5-7].

In RE, cation and anion conductive membrane are placed in an alternating way in order to create a low concentration compartment (LCC) and high concentration compartments (HCC). If the HCC is filled with a high concentration solution and the LCC with the low concentration solution, the concentration gradient between the compartments originates a Nernst potential across the cell pair which causes an electrical current to flow through an external load connected to the electrodes. In this way, direct conversion of salinity gradients energy into electrical power is possible. Theoretically, a single cell pair stack operated with seawater and river water generates an open circuit voltage of about 0.16 V and a three cell pair stack generates about 0.48 V [4, 8].

In general, OCV is proportional to the number of cell pair that exist. So, the OCV increases proportionally to the level of scale up [3, 8]. The generated OCV is mainly governed by the perm selectivity of the membranes, and governs the output power from the stack.

Research progress so far on a lab-scale RE indicated a promising outcomes. Investigations have been performed on different cell designs; for example from 3 cells to 50 cells and active membrane area from 4 cm^2 to 1875 cm^2. At early stages, quite limited power density (0.4 W/m^2) was reported when working on a 5 cell RE system with low effective membrane area (4 cm^2)[9]. Improvements in optimal stack design specially using lower resistances membranes and thin spacers (200 μm) resulted in satisfactory power density improvements (above 1.2 W/m^2, 50 cells) [4]. Later, Vermaas *et al*. (2011) demonstrated that this power density can be doubled to 2.2 W/m^2 (5 cell stack) by reduction of inter-membrane distance to 60 μm as well as the use of specially designed low resistance membranes.

It's still possible to increase the power density further by working at different operating conditions, for example by working at higher gradients and temperatures; Daniilidis *et al.* (2014) reported a power density of 7.6 W/m^2_{MP} and 12.4 W/m^2_{MP} with 0.01 M and 5 M NaCl solutions when working at 25 ^oC and 60 ^oC, respectively [6]. Very recently, Tedesco *et al.* (2015) tested a

large scale RE unit (100 cell pairs) equipped with membranes of 20x20 cm^2 active area and 120 μm thickness. They found that experimental testes using brine (5 M) and brackish water (0.1 M) feeds resulted in a maximum power density of 4.5 W/m^2_{MP} and 8 W/m^2_{MP} at 20 ^oC and 40 ^oC, respectively. The power density drastically increased to 12 W/m^2_{MP} when thinner (60 μm) membranes where used at 40 ^oC experimental conditions. In general, the reduction in power density of such large stack compared to smaller stack was correlated to the performance losses due to the reduction in deriving force particularly at lower flow velocities, changes in flow hydrodynamics and manifestation of ionic shortcut currents within the SGP channel in the process of scale-up.

For a scaled-up application of RE, clear understanding of influence of main operational parameters in operations involving projected cell sizes and active membrane area is crucial. For small scale operations, the general trend is that energy efficiency reaches its maximum at relatively low flow velocities or high residence time and low flow path length, while power density increases when working at higher feed temperature and flow velocities over a large membrane area at an optimal current density. Although high flow rates and temperatures are mostly beneficial in terms of performance enhancement, it may not be always attractive due to high energy input which is unfavourable from economical point of view. Previous investigations have demonstrated a substantial effect of temperature and flow velocity on the overall stack performance [4, 8, 10, 11].

In RE, efficiencies are usually limited below 50 %, but this value can be passed by re-circulating the feed or use of multiple electrodes [1, 2]. On the other hand, the gross power density drops slowly when recirculating the feed as a result of the steady state ion transport from concentrated solution to dilute solution [5]. Our recent ion transport analysis from concentrated solution to dilute solution at a steady state operation indicates that sodium and chlorine ions are transported at a flux of 2.84 $meqm^{-2}s^1$ and 4.32 $meqm^{-2}s^1$ across cation exchange membranes (CEM) and anion exchange membranes (AEM), respectively, under real solution composition. The generalization based on the above observation is that optimization of the stack for higher power generation requires highly permeable low resistance ion exchange membranes which are economically unaffordable.

There are attempts in implementation of RE for large scale applications currently. RE power plant foreseen in Afsluitdijk (the Netherlands) is deemed to generate blue energy from mixing salt water and fresh water [12]. This pilot plant is installed by REDstack B.V. (The

Netherlands) with the membrane from the Fujifilm Manufacturing Europe B.V. (The Netherlands). Feed water is pumped at a flow rate of 200,000 L/h from Wadden Sea and mixed with about 757,082 L of fresh water from the IJsselmeer. This pilot plant is not yet optimized for efficient power supply; however, positive outcome is expected in the coming years with a potential power supply in the range of 1 to 2 MW which would be sufficient to supply power for up to 2,500-5,000 households. Recently, Tedesco *et al*. (2015) compared a small scale laboratory stack (10x10 cm^2, 50 cell pairs), and a large scale RE unit (20x20 cm^2, 100 cell pairs) with an 8-folds increase in the stack membrane area [13]. It was noted that the power density of the larger stack was slightly lower (6.7 W/m^2MP at 40 ^oC) than the small scale stack (8 W/m^2MP at 40 ^oC), both stacks equipped with ion exchange membranes from Fujifilm membranes. The reduction in power density was correlated to increase in cell pair resistance.

In the present study, the performance of a large scale reverse electrodialysis unit, equipped with 200 pairs (maximum number of cell tested so far) of heterogonous Relax membranes with an effective membrane area of 0.315x0.635 cm^2 was tested experimentally. This stack cell size and active membrane area are approximately projected by about 20-fold and the channel thickness by 3 times compared to smaller stacks (cell size of 10 and below). The variations of internal stack resistance, power density and energy efficiency with changes in the main operational parameters of RE unit is investigated. Moreover, the SGP-RE unit was also operated with sulphate solution simulating industrial effluent for testing the applicability of RE using feed solutions bearing SO_4^{2-} ion. The output will be useful in tracing the variations of response parameters with respect to changes in stack flow hydrodynamics and varying operating conditions compared to small scale stacks in the process of scale-up.

6.2 Materials and Methods

6.2.1 RE stack

Figure 6.1 show the picture of the industrial scale RE unit used in the present study. A commercial industrial-scale ED unit (EDR-III/500/0.8, MEGA a.s., Czeck Republic) was operated in a reverse co-flow mode, i.e. feeding the stack with two solutions of different salinity as to the principle of RE. The stack had 200 cell pairs constituted from a pile of ion exchange membranes separated by non-woven net like spacers made of polyethylene having porosity of 0.88 and thickness 0.8 mm. Non-woven design of spacer generally provides a lower pressure drop (up to 43

%) than those based on woven fabrics [14]. These spacers have openings in their frame resulting in a horizontal feed and drain channels in the membrane stack, allowing the supply and distribution of feeds into and out of the membrane compartment. The electrodes used were made of platinised titanium (Ti/Pt) having the same effective area as the membrane. A solution of Na_2SO_4 (0.5 M) was used as an electrode rinse sustaining the redox reaction for continuous flow of electricity through the external load. Although the overpotential of electrode reaction is expected to be a bit higher compared to the mostly used hexacyanoferrate/ferrite solutions, the use of Na_2SO_4 as an electrode rinse is environmentally safe when used for large scale operations.

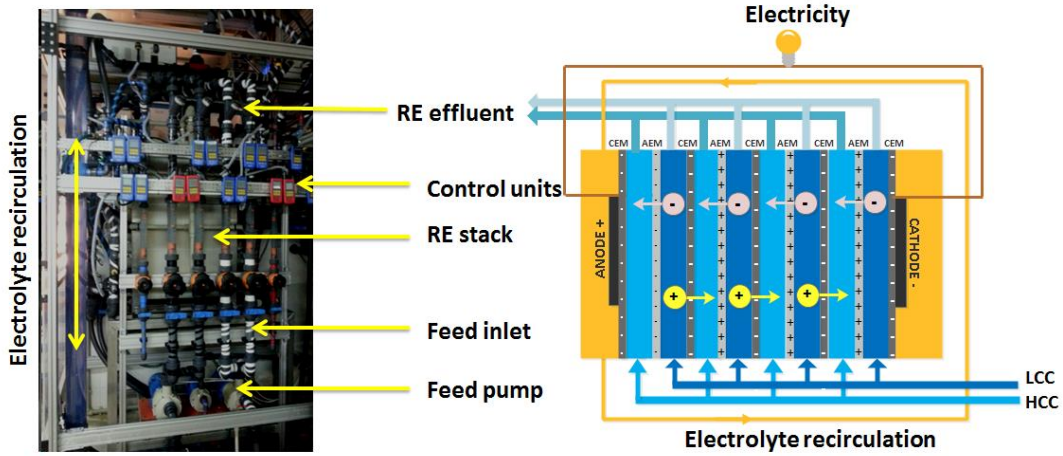

Figure 6.1. Industrial scale RE unit investigated in the present study; the stack was in a vertical orientation and feed flow was allowed in two controlled inlet units. Feed heating was performed by running the stack in electrodialytic mode.

6.2.2 Membranes

Ralex ion exchange membranes (MEGA a.s., Czech Republic) having a thickness of 0.57 mm, effective area 0.2 m^2 (0.635 m x 0.315 m) and total membrane area of 80 m^2 were used in industrial RE unit. These membranes have good permeability with a higher ion exchange capacity compared to other commercial membranes [15]. Electrochemical properties of Ralex ion exchange membranes are shown in Table 6.1.

Table 6.1. Properties of the ion exchange membrane used in the RE unit[16].

Membrane	Areal resistance (Ωcm^2)	Permselectivity (%)	Ion exchange capacity (meq./g)	Charge density (meq./g H_2O)
Ralex AMH-PES	7.66	94.7	2.34	7.6
Ralex CMH-PES	11.3	89.3	1.97	3.5

6.2.3 Feed solutions

Aqueous solutions of N_2SO_4 (0.01 M - 0.32 M) and NaCl (0.01 - 3.8 M) were used in each experimental runs, so experiments were performed at low concentration gradients (0.01 M - 0.3 M) and high concentration gradients (3.8 M - 0.5 M). The use of N_2SO_4 is envisaged as helpful in testing the potential applicability of RE to sulphate-rich aqueous wastes from industries (anticipated to have the selected concentration range, private communication). Initial experiments were run with low concentration solutions followed by final experiments with concentrated brines, to avoid the risk of membrane scaling which could a have effects on RE performance. Solution concentrations were monitored by calibrations prepared from the measurement of conductivity of solutions (GREISINGER GMH 3430, Czech Republic). Experiments were performed in batch-mode through recirculation of feed solutions at a flow rates in the range of 1-11 kL/h (flow meter GEORG FISHER+GF+, USA) corresponding to a linear flow velocity of 0.6-7.1 cm/s. Heating of the feed solutions (15 – 35 ^oC) was performed by a reversible process operating the unit in electrodialysis and reverse electrodialysis mode.

6.2.4 Performance analysis

Since experiments are performed in larger operational scale, some minor changes in the variation of the electrical measurements and operating conditions were not considered much influential on the system performance. The parameters considered were open circuit voltage (OCV), internal resistance (R_i) and power density (P_d) and energy efficiency (η) as the main performance indicators. These parameters are interdependent.

The industrial-scale RE unit was loaded by an external precision load resistance (Fuel Cell test load, TL4A, Astris Energy ING), connected in series with the stack [5]. Direct current (I) and voltage (V) were measured by a Fluke 87-V Digital Multimeter. Each time a feed solution is run, an equilibration time of about 30 minutes was maintained in order to get a stable response, for studying the changes under the varying stack operating condition.

6.2.4.1 OCV measurement

The OCV is measured at zero current condition. OCV apparently indicates transport rate in the system, and hence the level of achievable power. Theoretical OCV estimations can be obtained by using Nernst equations;

$$OCV = \frac{2NRT}{F}\left[\frac{\alpha_{AEM}}{z_a}\ln\left(\frac{\gamma_{a,HCC}\,C_{a,HCC}}{\gamma_{a,LCC}\,C_{a,LCC}}\right)+\frac{\alpha_{CEM}}{z_c}\ln\left(\frac{\gamma_{c,HCC}\,C_{c,HCC}}{\gamma_{c,LCC}\,C_{c,LCC}}\right)\right] \quad (6.1)$$

where N is number of cell pairs, R is gas constant (8.314 $Jmol^{-1}K^{-1}$), α is the membrane permselectivity, γ is activity coefficient and C is concentration (mol/L) of the ions; subscripts a, c, HCC and LCC refer to anion, cation, High Concentration Compartment and Low Concentration Compartment, respectively. The value of OCV approaching the theoretical limit implies high permselectivity of the membranes. In addition, the deviation of the OCV from the theoretical value can be used to estimate the losses due to ionic shortcuts if losses due to co-ion transport and osmotic flux across the membranes are known.

6.2.4.2 Stack Resistance

Internal stack resistance (R_i) is the key parameter in RE, mainly accounted by the membrane and feed solutions, and determine the overall performance. R_i is generally calculated as [8];

$$R_i = N(R_{AEM} + R_{CEM} + \frac{\delta_{LC}}{A\sigma_{LC}} + \frac{\delta_{HC}}{A\sigma_{HC}}) + R_{el} \quad (6.2)$$

where N is the number of cell pairs, A is the effective membrane area (cm^2), R_{AEM} and R_{CEM} is the resistance (Ω) of AEM and CEM, respectively; δ_{LC} is thickness of LCC, δ_{HC} is thickness of high concentration compartment, σ_{HC} is the conductivity of the HCC solution and σ_{LC} is the conductivity of LCC solution, and R_{el} the electrode resistance (Ω). It's appropriate to neglect R_{el} for the large scale RE unit.

Internal resistance has two main contributions;

$$R_i = R_{Ohmic} + R_{non\text{-}Ohmic} \quad (6.3)$$

where the Ohmic part (R_{ohm}) is the resistance resulting from the intrinsic feed characteristics and membrane material affecting the ion transport within the SGP channel and the non-Ohmic part ($R_{non\text{-}Ohmic}$) results from the concentration polarization phenomenon occurring in the boundary layer (diffusion boundary layer resistance, R_{dbl}) and concentration changes in the bulk solution

leading to the drop down of the local electromotive force (electrical double layer resistance, R_{edl}) [1];

$$R_{non\text{-}Ohmic} = R_{edl} + R_{dbl} \tag{6.4}$$

It's possible to calculate R_{edl} from the and OCV and local electromotive force (E), by assuming a uniform distribution across the membranes between the potential at the inlet concentration (i.e. OCV) and potential at outlet concentrations (E_{out}) [1]. By defining 'electrical double layer potential, E_{edl}' as the potential loss due to the concentrations changes in the bulk solution, it can be estimated as an average of the potential between the inlet and outlet [1];

$$E_{edl} = \frac{1}{2}(OCV + E_{out}) \tag{6.5}$$

Thus, R_{edl} can be determined from;

$$R_{edl} = \frac{E_{edl}}{IA} \tag{6.6}$$

where I is the current. Combining Eq. (6.5) and Eq. (6.6);

$$R_{edl} = \frac{OCV + E_{out}}{2IA} \tag{6.7}$$

E_{out} can be estimated using Nernst equation;

$$E_{out} = \frac{N\alpha RT}{z} \ln \frac{\gamma_{HCC} C_{HCC}}{\gamma_{LCC} C_{LCC}} \tag{6.9}$$

In order to compare the sensitivity of power density to IAR and membrane permselectivity, a model was developed based on a central composite design [17] using experimentally predicted electrochemical membrane properties within the stack.

6.2.4.3 Power density and energy efficiency

The electric power density P_d as a function of the current density i (A/m^2) can be fitted by a second order equation:

$$P_d = -a \cdot i^2 + b \cdot i \tag{6.10}$$

where a and b are two fitting parameters of the experimental data.

It's possible to determine the maximum power density $P_{d,max}$ and the corresponding current density (i_{max}) from the peak values of the parabolic curve as follows;

$$\left(P_{d,\max} = \frac{b^2}{4a}, i_{\max} = \frac{b}{2a} \right) \tag{6.11}$$

Based on the Ohm's law, the voltage drop over the varying external load will be directly proportion to the current produced by the RE stack. Thus, R_i can be easily obtained from the slope of polarization curves (*V-I* curves) of the RE stack system.

$$\eta = \frac{P}{P_t} x100 \tag{6.12}$$

Energy efficiency (η) is one of the key parameters in RE representing the fraction of practically obtainable amount of energy from the theoretically achievable energy by mixing two salts of different salinity. In the present work, energy efficiency (η) was calculated as the ratio of experimentally obtainable power (P) to the theoretical power (P_t) that can be obtained from the system [18]. The theoretical power can be calculated based on the Gibbs free energy that can be harnessed from mixing the salutations;

$$P_t = 2RT\left(\phi_{HCC} C_{HCC} \ln \frac{C_{HCC}}{C_m} + \phi_{LCC} C_{LCC} \ln \frac{C_{LCC}}{C_m} \right) \tag{6.13}$$

where ϕ is flow rate of feed solutions in m^3/s and C_m is equilibrium concentrations expressed as;

$$C_m = \frac{C_{HCC} + C_{LCC}}{2} \tag{6.14}$$

and all concentrations in mol/m^3.

6.3 Results and discussion

6.3.1 Stack voltage

Figure 6.1 presents the effect of flow velocity and temperature parameters on the OCV and hence membrane permselectivity are indicated. In the investigated experimental boundaries, OCV increases slightly with temperature and flow velocities for NaCl solution (Figure 6.1a). This could be related to the increase in ion transport across the membranes between compartments. However, the case seems a bit different for Na_2SO_4 feed solution. As shown in Figure 6.1b, OCV starts to increase at moderate values and decline slightly at higher values of flow rate and temperature (30 ^oC and 3.9 cm/s). This could be attributed to ionic shortcuts occurring at higher ion transport regime and higher feed conductivities. The higher OCV of stack operated with

Na_2SO_4 test solution (12.7 V) compared to NaCl (10.2 V) is due to the difference in the feed concentrations. However, the theoretical OCV obtained with NaCl is about 57% higher than that of Na_2SO_4 for experiments under the similar operating conditions.

The permselectivity of the membranes in the stack can be obtained as the ratio of measured OCV to the theoretical OCV. At moderate temperature operations (15 - 30 ^oC), only a slight rise in permselectivity with temperature is observed for both salts solutions, however, a slight decrease is observed at higher temperature e.g. at 35 ^oC for Na_2SO_4 (see Figure 6.1b). The observed trend is quite different from smaller stacks; experiments on a 5 cell stack equipped with Neosepta membranes showed a decrease in permselctivity for temperature above 25 ^oC which becomes significant above 60 ^oC [6]. The decrease in permselecitivty due to the increase in temperature is explained by rise in solutions conductivity and hence higher ionic shortcuts. This has to do with the stack design and intrinsic membrane properties. The low permselectivity of the membranes in Na_2SO_4 solutions compared to NaCl can be explained by the lower ionic fluxes and bulk transport numbers of SO_4^{2-} ion ($J_{SO_4^{2-}} = 5.58x10^{-8} mol/cm^2 s$ and $t_{SO_4^{2-}} = 0.449$) across AMX compared to that of Cl^- ($J_{Cl^-} = 6.56x10^{-8} mol/cm^2 s$ and $t_{Cl^-} = 0.519$) [19]. In addition, the higher valence of SO_4^{2-} as a co-ion can have a limiting effect on permselectivity of CEMs according to the principle of the Donnan exclusion. Steric hindrance of the bulky and highly hydrated SO_4^{2-} ion could also account for the low permselecitvity. As the Ralex membranes used here are normally designed for a moderate temperature operations, experiments were not performed at higher temperature. It would be worthy to make a further investigations for other types of the membranes at much higher temperature for better clarity. This is also important in energy-exergy analysis of RE and economic evaluations for upscale potential.

Although Ralex membranes have high IEC, the low permselectivity is also attributed to the low charge density as well as higher swelling degree [16]. Moreover, the permselectivity lowering here is quite higher compared to small stacks operations indicating the magnification of internal losses on large scale operations. The performance is also reduced at this stage, and this is very important in feasibility analysis and techno-economical evaluations for

practical implementation of RE in large scale applications.

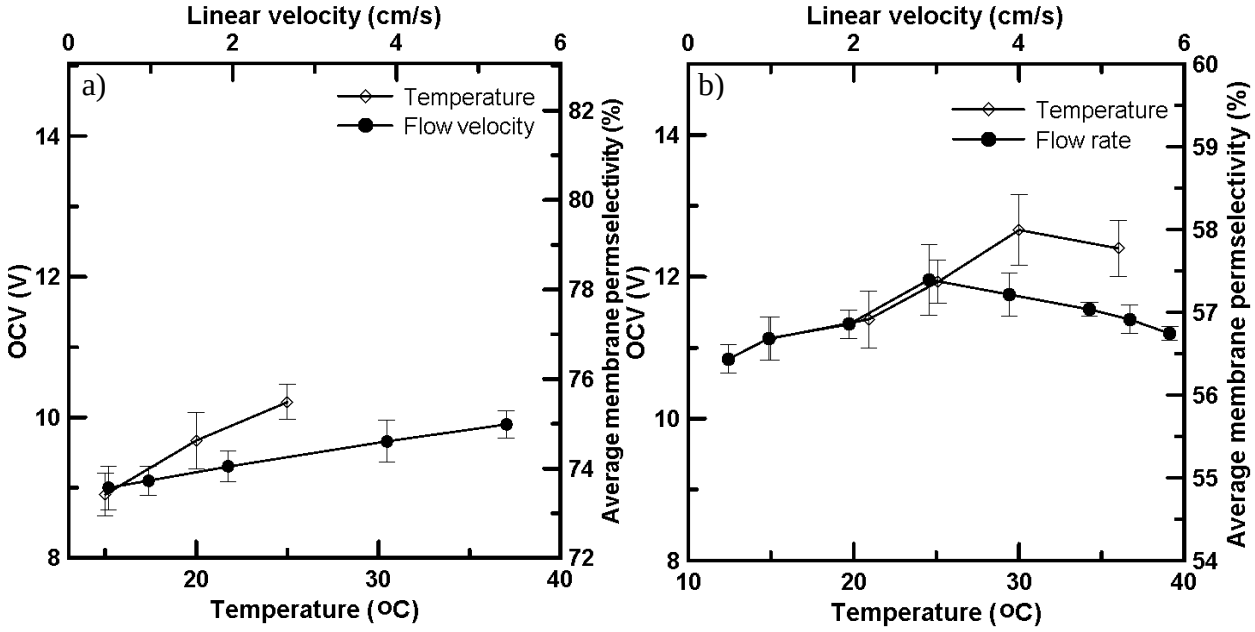

Figure 6.1. OCV and membrane permselectivity variations for an industrial scale RE unit at a varying temperature and linear velocity for a) NaCl stream (3.7 M: 0.5 M) and b) Na_2SO_4 stream (0.3 M, 0.01 M); full lines represent temperature measurements, dashed lines represent flow velocity measurements.

So far, a well optimized RE stack equipped with homogenous Fumatech ion exchange membranes resulted in an OCV in the range of 93-98 % of the theoretical value when operated at a moderately high linear velocity (above 0.11 cm/s) [1]. This indicates quite good permeability of the employed membranes [16, 20]. Neosepta membranes also exhibit a good permselectivity in RE stack, as demonstrated by Długołecki *et al*.(2008); for a single cell at 0.152 V of OCV, permselectivity reached 94.4%. The promising permselectivity of these membranes can be correlated to their sufficient ion exchange capacity (IEC) as well as moderate swelling degree. However, this is not always the case, as for example for the Ralex membranes used in our investigation.

6.3.2 Power density

Figure 6.2 illustrates the power curves for the stack operated with Na_2SO_4 and NaCl feed streams. At salinity ratio (SR) of 30 (0.3 M: 0.01 M), the maximum power density observed reached 0.26 W/m^{2}MP at current density of 3.8 A/m^2 for NaCl and 0.14 W/m^{2}MP at 3.9 A/m^2 for Na_2SO_4 solution. This value is much less than half of the power density obtained by smaller stacks equipped with Ralex membranes which reached up to 1.2 W/m^{2}MP [16, 21]. When the SR is

reduced by 3-fold (0.3 M: 0.03), the loss in power density followed a similar trend (about 33 % reduction) for both salts. This is also linked to the drop down in OCV as shown in Figure 6.2a; on average OCV drops by 25 % for 3-fold decrease in SR (from 10 to 30).

The poor performance of RE operated with Na_2SO_4 can be explained by several reasons. At concentration of 0.3 M, the specific conductivity of Na_2SO_4 (5.2 mS/cm) is very low compared to NaCl (24.7 mS/cm). This results in greater Ohmic losses in the case of Na_2SO_4. In additions, the permselectivity of the membrane is drastically reduced (below 60 %) when using Na_2SO_4 compared to NaCl.

The presence of SO_4^{2-} when NaCl is used for SGP generation have been observed to have a lowering effect on power density. For example, a 5 cell stack equipped with the Ralex membrane (10x10 cm^2 membrane area) generated a power density below 0.05 W/m^2 when operated with pure $MgSO_4$ as feed solutions (0.017 M of HC 0.5 M of HC) [22]. Under similar condition, NaCl feed solution which is 10 % in $MgSO_4$ (both feeds) resulted in a significant reduction of power density, up to 50% compared to the pure NaCl solution. In addition, when using brine (0.5 M, 53% in Mg^{2+}) and brackish water (0.1 M, 20% in Mg^{2+}), the reduction in power density reached 63% [5]. RE equipped with Neosepta membranes (10 cells) resulted in a power density up to 0.5 W/m^2 when using Na_2SO_4 solution at SR of 29 (0.035 M: 1M) and flow rate 1 cm/s[23]. Model simulation predicts a 20 % reduction in power density when a mixture of NaCl and Na_2SO_4 (LC = 0.012 M, 1.6 % in Na_2SO_4, HC=0.5 M, 9 % in Na_2SO_4) is used compared to pure NaCl [24]. The overall implication is the enhanced performance losses in the presence of SO_4^{2-} ions in RE feed solutions, and thus lower expectation in the performance when using Na_2SO_4 as a feed solution.

Eventually, the industrial scale unit stack is designed for better flow in the channel as the sheet-like open spacer designs have an effect in reducing the hydrodynamic friction. In addition, the co-flow operational mode has some advantage in terms of performance as demonstrated in previous study; for larger stack of up to 50 cells and 25x75 cm^2 active area, operations in a co-flow mode resulted in higher power density compared to operations is a cross flow, and generally allow lower pressure difference between compartments [3]. However, power output in a co-flow mode will be lower compared to the cross flow mode as the Ohmic losses increase in co-flow mode operations [25].

Generally, the power output increase linearly with the number of cells in the process of scale-up, but the overall power density is somehow limited, especially with the increasing path

length of the dilute channel. Up to 22 W was possible to generate with the present RE unit of 200 cells at an optimal operation conditions. Veerman *et al*. (2010) demonstrated an almost 5-fold increase in power output (0.2 W to 0.93 W) when the number of cell pairs within the stack increase from 10 to 50 [3]. One advantages of scaled up RE operations is that the Ohmic losses due to electrode overpotential is minimized [4], but this doesn't have a significant contribution to the overall performance.

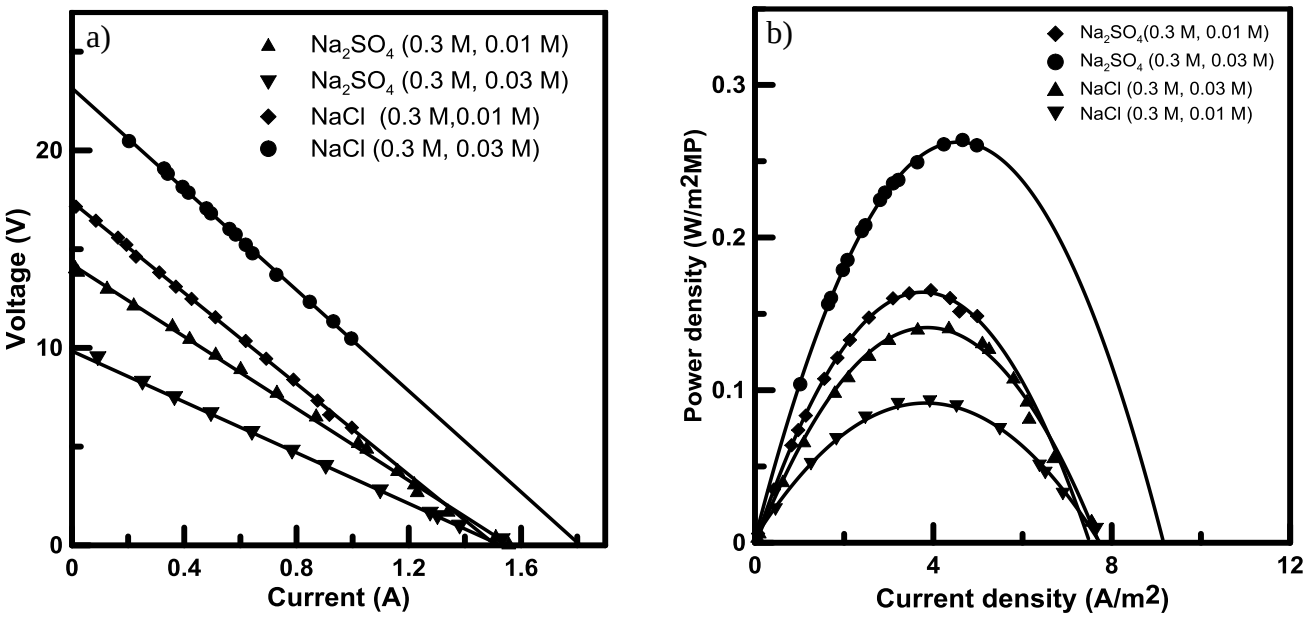

Figure 6.2. a) *I-V* curves and b) power curves for NaCl and Na_2SO_4 at different SR (10-30) for an industrial scale RE system; measurements were performed at feed temperature of 20 ^{o}C and linear velocity of 5.3 cm/s.

6.3.3 Effect of temperature and flow velocity

Figure 6.3 show the variation of the power density with temperature and flow velocity. For NaCl solutions, we measured temperature variations in the range of 15-25 ^{O}C. Experiments were not performed at higher temperature (above 25 ^{o}C) with brine solution (3.8 NaCl) recommended by the stack supplier (MEGA a.s., Czeck Republic) due to the anticipated adverse effect of this condition on the membranes designed for electrodialysis. At the flow velocity of 5.3 cm/s, the power density increased by 47% (from 0.19 W/m^{2}MP to 2.8 W/m^{2}MP) when the NaCl feed temperature is raised from 15 ^{o}C to 25 ^{o}C (see Figure 6.3a). Increasing the flow rate of NaCl feed solutions from 0.48 cm/s to 5.3 cm/s enhances the power density by 80% on average (varying in the range of 0.1 - 0.28 W/m^{2}MP) over the experimental temperatures range of 15 - 25 ^{o}C. The effect of flow rate was higher compared to our previous instigation on a small scale RE stack which

showed only up to 47 % increase in power density, however, at lower flow velocity range (0.7 - 1.1 cm/s) [26].

When the flow velocity of Na_2SO_4 solution increases from 0.48 to 5.3 cm/s, the power density increases by 57 % (i.e. from 0.08 to 0.13 W/m^2) and 90 % (0.12 to 0.22 W/m^2) at temperature of 20 ^oC and 35 ^oC, respectively (see Figure 6.3b). The lower benefit in power for Na_2SO_4 compared to NaCl solution is mainly accounted by the difference in the conductivity of the solution and hence internal stack resistance.

The trend in power density variations is similar for both salts; performance improves with increasing flow velocity and temperature. At higher flow velocities, increase in hydrodynamic resistances results in a higher pressure drop. Apart from the enhanced mixing and boundary layer resistance reduction, flow rate could also have a limiting effect on co-ion transport and water transport through the membranes, thereby magnifying performance. Low power densities at lower flow rates can be explained by the increase in electrical resistance due to the low conductivity of the solution as a result of low residence times i.e increase in boundary layer resistance. Apart from flow velocity, flow distribution within the salinity gradient channel has an influence on the power density, especially at lower flow velocities. Computational fluid dynamic analysis on a RE operated with concentrated brine indicates a negative of impact of bad flow distribution on SGP [14].

Increasing temperature increases conductivity of solutions and on ions mobility through the membranes, thereby reducing the overall resistance of the stack resulting in higher performance. In our experiment, temperature effect is observed to be higher at higher flow velocity. However, when working below 25 ^oC, the temperature influence remains similar for both salts at lower and higher flow rates; for examples a power density increment rate of 0.05 W/m^2 per 5 ^oC is obtained.

In general, magnification of internal losses is observed when working on scaled-up RE system which a challenging aspect in optimizing the operational parameters. It's worthy to evaluate individual and interaction effect of process variables during optimizations for a RE for scaled-up applications.

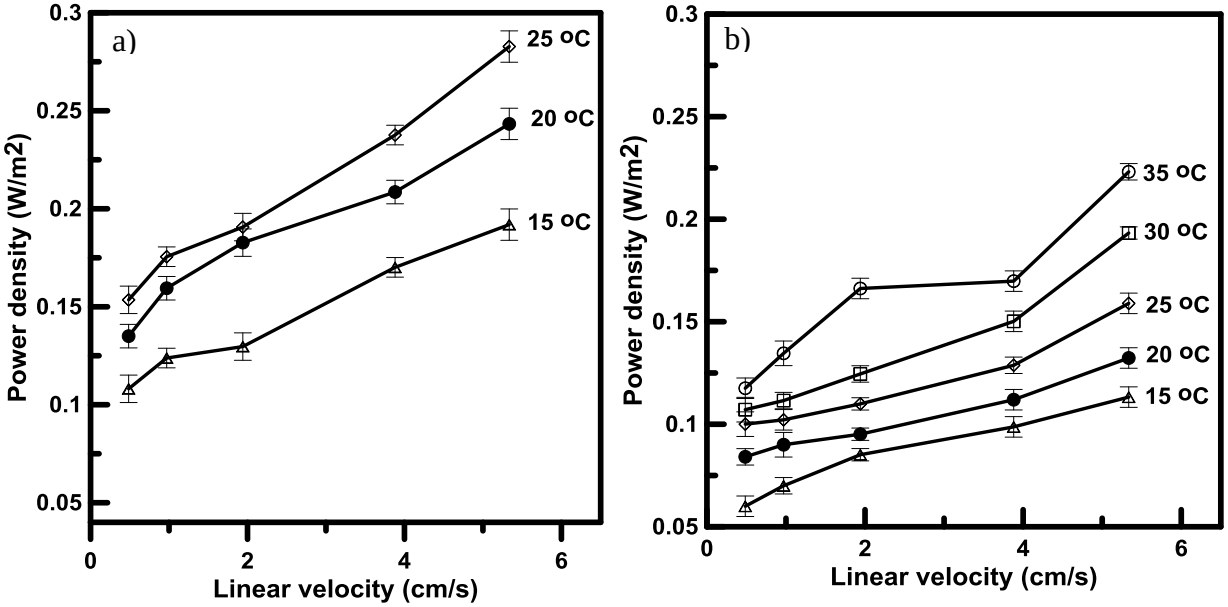

Figure 6.3. Variation of the power density with temperature and flow velocity for an industrial scale RE unit operated with a) NaCl solution (3.8 M : 0.5 M) b) Na_2SO_4 solution (0.30 M : 0.02 M).

Process simulation developed by Tedesco *et al.*(2014) predicts a power density of 4 W/m^2 for a 500 cell stack with an active membrane area of 44 × 88 cm^2 [27], when a RE is operated with brine and brackish water (inflow velocity 1-2 cm/s, temperature 30 ^{o}C). Operations over larger projections (increasing aspect ratio from 1 to 5) results in a reduction of power density by 7-20 %.

6.3.4 Internal stack resistance

In large scale applications when using a large number of membranes and thick spacers, Ohmic losses are expected to be quite high. The internal losses and hence increased resistance is visible when working over a varying flow velocity, temperature and concentrations ranges. Potential losses from the electrode compartments can be neglected since the induced electromotive force is very high compared to the voltage lost in sustaining the redox reactions.

Figure 6.4 shows the variation of internal stack resistance with flow velocity and temperature. For NaCl solution, there was no significant effect of flow velocity on the internal stack resistance for NaCl. Increase in flow velocity from 0.4 cm/s to 5.3 cm/s retains internal area resistance (IAR) per cell in the range of 35 - 38 Ωcm^2/cell.

Previous works on small stack designs show that higher flow rates reduce the internal stack resistance by maintaining high concentration difference across the compartments and reducing the concentration polarization phenomenon. Investigation on a 3 cells stack with standard Neosepta

membranes demonstrated that an increase in a flow velocity (above 0.3 cm/s) have a significant reduction effect on stack resistance when using a thinner spacers of 2 mm thickness compared to the ones with 0.485 mm thickness [8]; the contribution from the spacer shadow effect will dominate the concentration polarization phenomenon when thicker spacers are used (above 0.5 mm). This implies that the resistance is more of the Ohmic one than the non-Ohmic ones from the boundary layer resistance and electrical double layer resistance. As discussed earlier, Ralex membranes have quite higher resistance and the employed spacer is non-conductive and thick with quite high resistances. Similarly, the change in internal resistance was not significant at even higher flow rates for NaCl solutions. Długołecki *et al.* (2010) observed that the membrane resistance remained unaffected by higher flow rates (above 0.5 L/min) when working at high concentration solutions (above 0.1 M in NaCl)[28].

The trend in IAR per cell with flow velocity in the case of Na_2SO_4 is different from that of NaCl as shown in Figure 6.4. When increasing flow velocity of Na_2SO_4 from 0.4 cm/s to 5.3 cm/s, the IAR per cell of the stack decreases by 19 % (from 95.6 to 66 Ωcm^2/cell). IAR is in general very high in the case of Na_2SO_4 solution compared to NaCl. Thus, we expect that non-Ohmic contributions will be higher in the case of Na_2SO_4 solution which can be optimized by the flow hydrodynamics. Comparison of previously investigated small RE stack (25 cells, Fujifilm membranes, flow velocity 0.5 -1.2 cm/s)[5] with the large scale stack in the present study indicates about 45 % (from 15 Ωcm^2/cell to 36 Ωcm^2/cell) increase of IAR per cell for the larger stack. As we are using brine (3.7 M NaCl) solution, the IAR per cell is expected to be lower than the case of river water and sea water operated RE systems. Vermaas *et al.* reported the IAR per cell above 50 Ωcm^2/cell for a 5 cells stack equipped with Fumatech membranes, and IAR per cell up to 40 Ωcm^2/cell for a RE stack equipped with Ralex membranes and normal spacers [1, 21]. The low conductivity of river water has observed to have a significant contribution to Ohmic losses.

In general, there are no literature reporting the resistance of small stacks operated with Ralex membranes and concentrated brines for direct comparison in the case of NaCl solution. However, it can be seen that the resistance of the stack increases when the stack is scale-up.

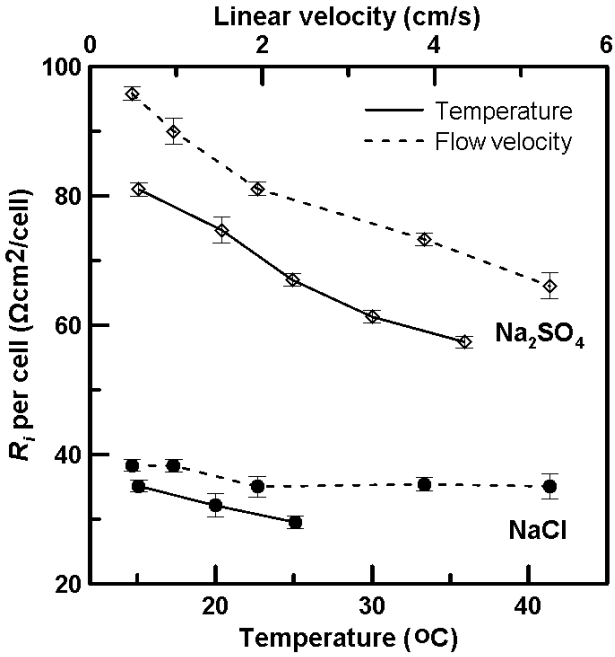

Figure 6.4. Variation of R_i with temperature and flow velocity; experiments performed at low salinity gradient (0.3 M : 0.01 M) for Na_2SO_4 and high salinity gradient (3.7 M : 0.5 M) for NaCl. Temperature curves represent data at linear velocity of 1 cm/s.

6.3.5 Ohmic and Non-Ohmic resistances

Table 6.2 presents the membrane resistance, solution resistance and interfacial resistances in the RE stack at a varying solution velocity. Interfacial resistance values are comparable for both salts expect at high flow velocity regime. Results show no significant variation of the interface resistances with flow velocity for NaCl feed. However, a general remark in the slight reduction of interface resistances with flow velocity can be set for Na_2SO_4, particularly the R_{edl}. In general, electrical double layer and diffusion layer with the large scale RE stack is over a projected area, indicating their persistence even at higher flow velocities. Further investigation on quantitative measurements of the resistance to the charge transport within the bulk and interfacial regions along the membranes and the SGR-RE channels is important to investigate by a more powerful tools like impedance spectroscopy [2-3].

Table 6.3 presents Variations of $R_{non\text{-}Ohmic}$ and R_{Ohm} with temperature. At higher temperature, R_{Ohm} (mainly from membranes in the case of NaCl and both from feed and feed solutions in the case of Na_2SO_4) show a slight reduction. The observed reduction trend which is about 0.14 $\Omega cm^2/°C$ for NaCl and 0.56 $\Omega cm^2/°C$ is comparable to that of small stack determinations; ~ 0.1 $\Omega cm^2/°C$ for NaCl (brine) and ~ 0.3 $\Omega cm^2/°C$ for Na_2SO_4 [1, 4], with a little

higher increment rate is observed for Na_2SO_4 compared to NaCl solution. Besides, interfacial resistances show a slight reduction with temperature implying the charge transfer resistance can be reduced by increasing feed conductivity and ionic nobilities. A similar trend has been observed by Fontananova *el al.* for membranes tested in NaCl concentrated brine solutions [29].

Table 6.2. Variations of Ohmic and non-Ohmic resistances at a varying feed velocity; measurements are in a recirculation mode at 20 °C, Recirculation volume is about 400 L.

			Feed* concentrations (M)		R_{Ohm} per cell (Ωcm^2)**			$R_{non\text{-}Ohm}$ per cell (Ωcm^2)		
Solution	Recirculation time (minutes)	Flow velocity (cm/s)	HCC	LCC	Membranes***	HCC	LCC	R_{edl}	R_{dbl}	IAR per cell (Ωcm^2)
NaCl	0	97.0	3.76	0.515	~18.96	0.52	2.75	3.90	12.17	38.27
	10	194.0	3.76	0.535		0.52	2.66	0.90	11.94	35.02
	20	388.0	3.74	0.556		0.52	2.56	2.20	11.17	35.40
	30	533.5	3.73	0.579		0.52	2.46	1.10	11.98	35.07
Na_2SO_4	0	48.5	0.325	0.009	~37.92	2.185	51.65	2.94	1.13	95.82
	10	97.0	0.321	0.011		2.250	44.56	1.49	3.76	90.00
	20	194.0	0.320	0.014		2.261	35.37	1.02	4.54	81.10
	30	388.0	0.313	0.018		2.256	27.3	0.82	4.99	73.29
	40	533.5	0.311	0.021		2.261	23.13	0.86	1.93	66.08

*Feed concentrations are monitored based on the conductivities at the inlet and outlet.

** Rohm doesn't take into account the non-conductive spacers.

***Calculated as the sum of all CEM and AEM resistances. The assumption is flow rate doesn't significantly influence the membrane areal resistances.

Table 6.3. Variations of Ohmic and non-Ohmic resistances at a varying temperature; Feed concentrations: 0.3M//0.01M for Na_2SO_4 and 3.7M//0.5M for NaCl; flow velocity at 1 cm/s, Recirculation volume is about 400 L.

Feed solution	Temperature (°C)	R_{Ohm} per cell (Ωcm^2)					$R_{non\text{-}Ohmic}$ per cell (Ωcm^2)		*IAR* per cell (Ωcm^2)
		CEM*	AEM*	HC	LC	Total	R_{edl}	R_{dbl}	
NaCl	15	12.3	8.3	2.8	0.51	23.9	1.6	9.5	35.1
	20	11.9	8.1	2.7	0.51	23.1	1.8	7.2	32.1
	25	11.5	7.8	2.6	0.49	22.4	2.0	5.1	29.5
Na_2SO_4	15	24.6	16.7	2.7	28.0	72.0	3.5	5.5	81.0
	20	23.4	15.9	2.3	24.6	66.2	2.9	5.7	74.7
	25	22.2	15.2	2.0	21.1	60.6	2.1	4.2	67.0
	30	21.1	14.5	1.9	19.3	56.9	1.9	2.5	61.3
	35	20.1	13.9	1.7	17.8	53.4	1.2	2.8	57.4

* The decrease of area resistance of membrane with temperature is modelled based on experimental results performed on membrane using Na_2SO_4 test solution (results not shown here) and literature results on membranes for NaCl test solution [29].

6.3.6 Efficiency

Figure 6.5 shows the energy efficiency of the RE stack operated with NaCl and Na_2SO_4 solutions at different temperature and flow velocity. At 20 °C, energy efficiency reached up to 41.5 % and 28.9 % for Na_2SO_4 and NaCl, respectively. These results are calculated at the maximum power density conditions where the theoretical energy efficiency is 50 %, and are comparable to the values reported for small scale operations (without electrode segmentation and feed recirculation). There is no significant loss in efficiency at projected RE system which may be attributed to some factors; i) reduced osmotic flux and co-ion loss over the large membrane area with negligible hydrodynamic permeability ii) the longer flow path length for higher apparent residence time of feed solutions iii) Although the co-ion flow mode is deemed to increase the Ohmic losses [25], the possibility to reduce the local pressure difference between the HCC and LCC compartments is enhanced for large stacks thereby reducing hydrodynamic losses, and increasing efficiency [3].

The higher energy efficiency recorded for Na_2SO_4 compared to NaCl is attributed to the employed salinity gradient level and operational current density. In the current density range of 4-7 A/m^2 at maximum power density condition, internal losses due to water transport and co-ion transport is expected to be higher salinity gradient condition for the case of NaCl compared to the lower salinity gradient of Na_2SO_4 with higher salinity gradient. Internal losses associated with flow dynamics of the viscous NaCl brine can also be taken into account.

Previous investigations on energy efficiency of RE operated with NaCl solutions over a wide concentration range (0.01 - 5 M) showed higher efficiency when operations are carried out at lower current densities for lower gradients and at higher current densities for higher gradients [4].

As shown in Figure 6.5a, flow velocity has a negative impact on energy efficiency [3]. Energy efficiency up to 28.9 % and 41.5 % (at flow velocity of 5.3 cm/s, and temperature 20 ^{o}C) was obtained for NaCl and Na_2SO_4 solutions, respectively. A drastic reduction in energy efficiency (85 % on average for both feed solutions) was observed when the flow velocity increased from 0.49 cm/s to 5.3 cm/s. Lower flow velocity or higher residence time leads to higher energy efficiency as a result of reduced internal losses due to sufficient feed mixing time allowing better power extraction [3]. Inadequate hydrodynamic mixing and high local pressure drops lead to poor efficiency at higher flow velocity. In larger stacks, this effect is deemed to be much pronounced (low efficiency below 10 % at higher flow velocities above 1 cm/s) as demonstrated by the present study.

Although the influence of temperature on energy efficiency is not so significant in the investigated experimental boundaries (15 - 35 ^{o}C), a slight decrease with the rise of feed temperature was observed (see Figure 6.5). Energy efficiency decreases at a rate of 1.8 %/^{o}C and 1 %/^{o}C for NaCl and Na_2SO_4 feed solutions, respectively. For investigations on a small scale stack (5 cell) with NaCl solution over a temperature range of 25-60 ^{o}C, a similar trend of variation of energy efficiency with temperature was reported, with a comparable decrement rate of about 1.4 %/^{o}C (an average over the experimental boundaries) [6].

In general, the loss in efficiency at elevated temperature is mainly attributed to the increased ionic shortcuts overcoming the power gain at high operating temperatures. As shown in Figure 6.5b, ionic shortcuts increase at a rate of 0.03 A/^{o}C for Na_2SO_4 and 0.09/^{o}C for NaCl feed solution. Large current leakage in the case of NaCl solution compared to Na_2SO_4 is due to the higher conductivity in the feed drain channel. Besides, quite larger shortcut current are reported here compared to small scale operations (increment rate of 0.02 A /^{o}C).

In general, energy efficiency can be increase by operating at low current density, however, at the expense of power density indicating the existence of trade of between this two parameters [4]. Also increasing the flow velocity or temperature has a positive influence on the power density while energy efficiency decreases a little bit due to lower residence time and the effects of ionic

shortcut currents. The influence of temperature on energy efficiency depends on the employed stack design and component properties but in general, a negative effect has been demonstrated for a RE system [6], although the power density was observed to improve [13, 30].

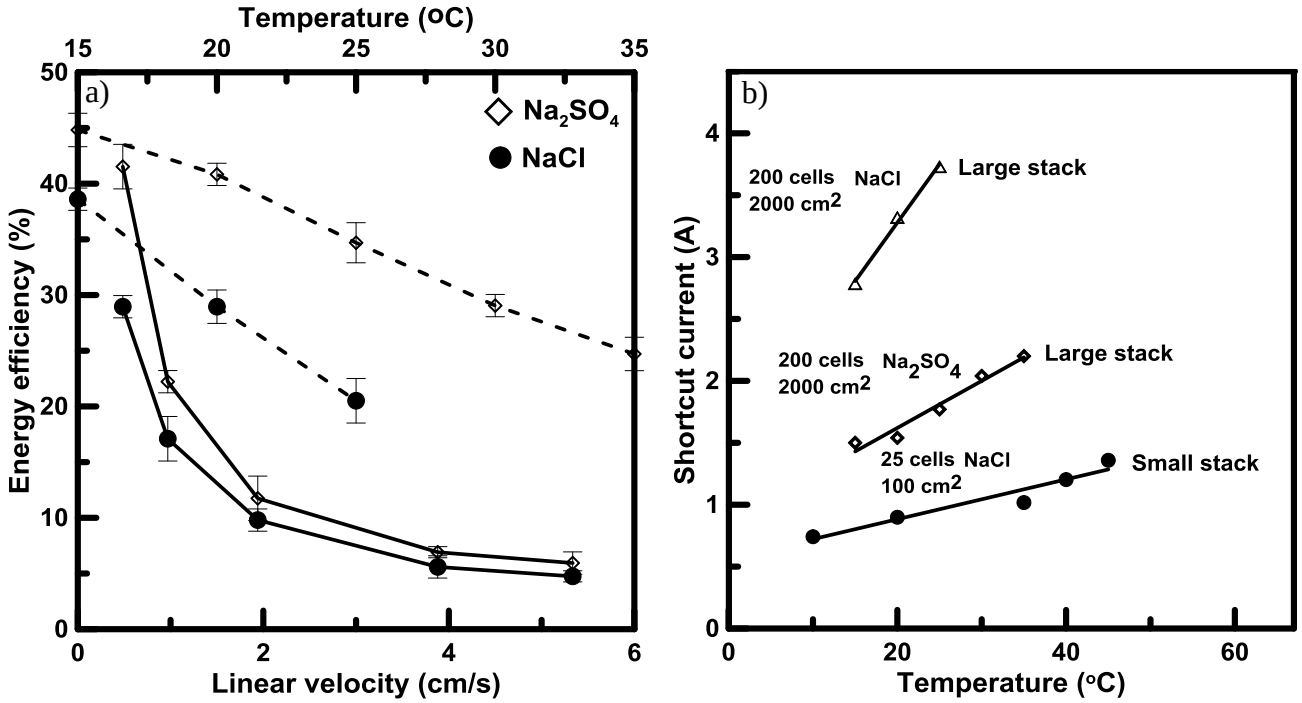

Figure 6.5. a) Efficiency at different temperature and flow rates for the tested industrial scale RE unit and b) short current at different temperature and stack sizes; feed concentrations: 0.3 M/0.01 M for Na_2SO_4 tests, 3.7 M/0.5 M for industrial scale stack, 5 M/0.5M NaCl for smaller (25 cell) stack [10]; efficiency determinations at varying temperature was performed at linear velocity of 4.4 cm/s.

6.3.7 Optimal Condition

Permselectivity and resistance properties based on standard tests are different than the properties within the stack. The response surface model developed shown in Figure 6.6 indicates a influence of permselectivity of membranes in the stack and IAR. Power density values are more sensitive to resistance than permselectivity which is confirmed by much higher power density in the lower extreme region of IAR than the lower extreme region of perm-selectivity. This is useful in strategic design of optimal IEM for RE for a scaled-up application.

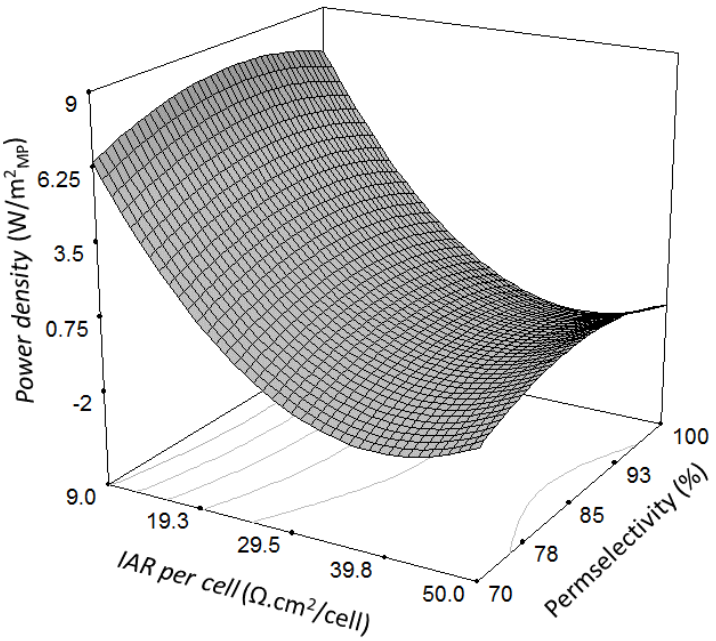

Figure 6.6. Response surface Model for prediction of changes in P_d with respect to IAR per cell and permselectivity (flow velocity 5.3 cm/s, temperature 20 ^{o}C, feed concentration 3.7 M//0.5 M).

Stack resistance and membrane permselectivity are conflicting when designing optimal membranes for RE. For examples, thin membranes for low resistance are designed by reducing membrane cross-linking degree while higher permselectivity is achieved at increased cross-linking degree [16]. Although the Ralex membranes employed in the present study have a good permselectivity, the areal resistance is quite low (see Table 6.1) being the major limiting factor.

6.4 Conclusions and Outlook

An industrial scale RE unit with scaled-up of about 20-fold compared to small scale RE stacks is successfully tested with different salt solutions and operating conditions. In general, the stack with 200 cells shows a loss in performance in proportion to scale-up level. Increase in stack resistance with an increase in flow path and channel thickness showed a higher level of lowering impact on power density in comparison to small scale applications (almost a double effect with 20-fold scale up). This was evident from the fact that the benefit in power density obtained for the industrial scale RE unit when increasing the operating parameters like flow velocity and temperature were above 50 % lower than the small scale operations. This shows that the optimal conditions for maximal power output could be different when working with small scale and large

scale RE systems.

The trend in OCV for the industrial scale RE was similar to small scale operations evident from the permselectivity with in the stack 72-83% which is comparable to small scale applications 76-78% [30]. Operation of the stack with Na_2SO_4 solution resulted in low membrane permselectivity (54-61%) mainly attributed to transport limitation of the bulky, highly hydrated and doubly charged SO_4^{2-} ion.

Efficiency of the industrial scale RE unit was observed to be much sensitive to flow rate than temperature within the experimental boundaries. However, further investigations is crucial for clear evaluation of the changes in these parameters over wider experimental boundaries. Experiments in feed recirculation mode using segmented electrodes would be highly beneficial in order to determine the maximum possible power production and energy efficiency for clear insight in system design and scale-up procedures.

Further experiments are required at much higher projected active areas and number cell pairs with different RE designs. The development of low cost, highly permeable and low resistance. Focus on the optimal stack design, reduced hydraulic friction losses as well as adaptability to pre-treatment requirements should be emphasized clearly. Clear conceptualization of influence of stack operational parameters through systematic experimentation and significant advance in development of suitable membrane are the key issues for the success of large scale RE energy generation [31]. These have benefit on techno-economic evaluations of RE for up-scaling and establish real economic figures for commercialization.

Reference

[1] D.A. Vermaas, M. Saakes, K. Nijmeijer, Doubled Power Density from Salinity Gradients at Reduced Intermembrane Distance, Environmental Science & Technology, 45 (2011) 7089-7095.
[2] J.W. Post, H.V.M. Hamelers, C.J.N. Buisman, Energy recovery from controlled mixing salt and fresh water with a reverse electrodialysis system, Environmental Science and Technology, 42 (2008) 5785-5790.
[3] J. Veerman, M. Saakes, S.J. Metz, G.J. Harmsen, Electrical power from sea and river water by reverse electrodialysis: A first step from the laboratory to a real power plant, Environmental Science and Technology, 44 (2010) 9207-9212.
[4] J. Veerman, M. Saakes, S.J. Metz, G.J. Harmsen, Reverse electrodialysis: Performance of a stack with 50 cells on the mixing of sea and river water, Journal of Membrane Science, 327 (2009) 136-144.
[5] R.A. Tufa, E. Curcio, W. van Baak, J. Veerman, S. Grasman, E. Fontananova, G. Di Profio, Potential of brackish water and brine for energy generation by salinity gradient power-reverse electrodialysis (SGP-RE), RSC Advances, 4 (2014) 42617-42623.
[6] A. Daniilidis, D.A. Vermaas, R. Herber, K. Nijmeijer, Experimentally obtainable energy from mixing river water, seawater or brines with reverse electrodialysis, Renewable Energy, 64 (2014) 123-131.
[7] M. Tedesco, A. Cipollina, A. Tamburini, G. Micale, J. Helsen, M. Papapetrou, REAPower: use of desalination brine for power production through reverse electrodialysis, Desalination and Water Treatment, (2014) 1-9.

[8] P. Długołęcki, A. Gambier, K. Nijmeijer, M. Wessling, Practical potential of reverse electrodialysis as process for sustainable energy generation, Environmental Science and Technology, 43 (2009) 6888-6894.
[9] M. Turek, B. Bandura, Renewable energy by reverse electrodialysis, Desalination, 205 (2007) 67-74.
[10] E.C. Ramato Ashu Tufa, Enrico Drioli, Membrane Distillation – Reverse Electrodialysis for Zero Energy and Liquid Discharge (ZELD) in seawater desalination (2015).
[11] J. Veerman, M. Saakes, S.J. Metz, G.J. Harmsen, Electrical Power from Sea and River Water by Reverse Electrodialysis: A First Step from the Laboratory to a Real Power Plant, Environmental Science & Technology, 44 (2010) 9207-9212.
[12] REDstack, http://www.redstack.nl/, in, accessed on 2015.
[13] M. Tedesco, E. Brauns, A. Cipollina, G. Micale, P. Modica, G. Russo, J. Helsen, Reverse Electrodialysis with saline waters and concentrated brines: a laboratory investigation towards technology scale-up, Journal of Membrane Science, (2015).
[14] L. Gurreri, A. Tamburini, A. Cipollina, G. Micale, CFD analysis of the fluid flow behavior in a reverse electrodialysis stack, Desalination and Water Treatment, 48 (2012) 390-403.
[15] E. Güler, R. Elizen, D.A. Vermaas, M. Saakes, K. Nijmeijer, Performance-determining membrane properties in reverse electrodialysis, Journal of Membrane Science, 446 (2013) 266-276.
[16] E. Güler, R. Elizen, D.A. Vermaas, M. Saakes, K. Nijmeijer, Performance-determining membrane properties in reverse electrodialysis, Journal of Membrane Science, 446 (2013) 266-276.
[17] M.A. Bezerra, R.E. Santelli, E.P. Oliveira, L.S. Villar, L.A. Escaleira, Response surface methodology (RSM) as a tool for optimization in analytical chemistry, Talanta, 76 (2008) 965-977.
[18] J. Veerman, R.M. de Jong, M. Saakes, S.J. Metz, G.J. Harmsen, Reverse electrodialysis: Comparison of six commercial membrane pairs on the thermodynamic efficiency and power density, Journal of Membrane Science, 343 (2009) 7-15.
[19] E. Güler, W. van Baak, M. Saakes, K. Nijmeijer, Monovalent-ion-selective membranes for reverse electrodialysis, Journal of Membrane Science, 455 (2014) 254-270.
[20] P. Długołęcki, K. Nymeijer, S. Metz, M. Wessling, Current status of ion exchange membranes for power generation from salinity gradients, Journal of Membrane Science, 319 (2008) 214-222.
[21] D.A. Vermaas, M. Saakes, K. Nijmeijer, Enhanced mixing in the diffusive boundary layer for energy generation in reverse electrodialysis, Journal of Membrane Science, 453 (2014) 312-319.
[22] D.A. Vermaas, J. Veerman, M. Saakes, K. Nijmeijer, Influence of multivalent ions on renewable energy generation in reverse electrodialysis, Energy & Environmental Science, (2014).
[23] E.C. Ramato Ashu , Timon Rijnaarts, Kitty Neijmeir, Renewable energy from aqueous sulfate streams by reverse electrodialysis for sustainable waste management, (2015).
[24] J.G. Hong, W. Zhang, J. Luo, Y. Chen, Modeling of power generation from the mixing of simulated saline and freshwater with a reverse electrodialysis system: The effect of monovalent and multivalent ions, Applied Energy, 110 (2013) 244-251.
[25] D.A. Vermaas, J. Veerman, N.Y. Yip, M. Elimelech, M. Saakes, K. Nijmeijer, High Efficiency in Energy Generation from Salinity Gradients with Reverse Electrodialysis, ACS Sustainable Chemistry & Engineering, 1 (2013) 1295-1302.
[26] Ramato A. Tufa, E. Curcio, E. Brauns, W. van Baak, E. Fontananova, G. Di Profio, Membrane Distillation and Reverse Electrodialysis for Near-Zero Liquid Discharge and low energy seawater desalination, Journal of Membrane Science, 496 (2015) 325-333.
[27] M. Tedesco, P. Mazzola, A. Tamburini, G. Micale, I.D.L. Bogle, M. Papapetrou, A. Cipollina, Analysis and simulation of scale-up potentials in reverse electrodialysis, Desalination and Water Treatment, (2014) 1-13.
[28] P. Długołęcki, P. Ogonowski, S.J. Metz, M. Saakes, K. Nijmeijer, M. Wessling, On the resistances of membrane, diffusion boundary layer and double layer in ion exchange membrane transport, Journal of Membrane Science, 349 (2010) 369-379.
[29] E. Fontananova, W. Zhang, I. Nicotera, C. Simari, W. van Baak, G. Di Profio, E. Curcio, E. Drioli, Probing membrane and interface properties in concentrated electrolyte solutions, Journal of Membrane Science, 459 (2014) 177-189.
[30] A. Daniilidis, D.A. Vermaas, R. Herber, K. Nijmeijer, Experimentally obtainable energy from mixing river water, seawater or brines with reverse electrodialysis, Renewable Energy, 64 (2014) 123-131.
[31] L.F. Weinstein JN, Electric power from differences in salinity: the dialytic battery, 191 (1976) 557-559.

Chapter 7

Salinity Gradient Power-Reverse Electrodialysis (SGP-RE) and Alkaline Polymer Electrolyte (APE) Water Electrolysis for Hydrogen Production

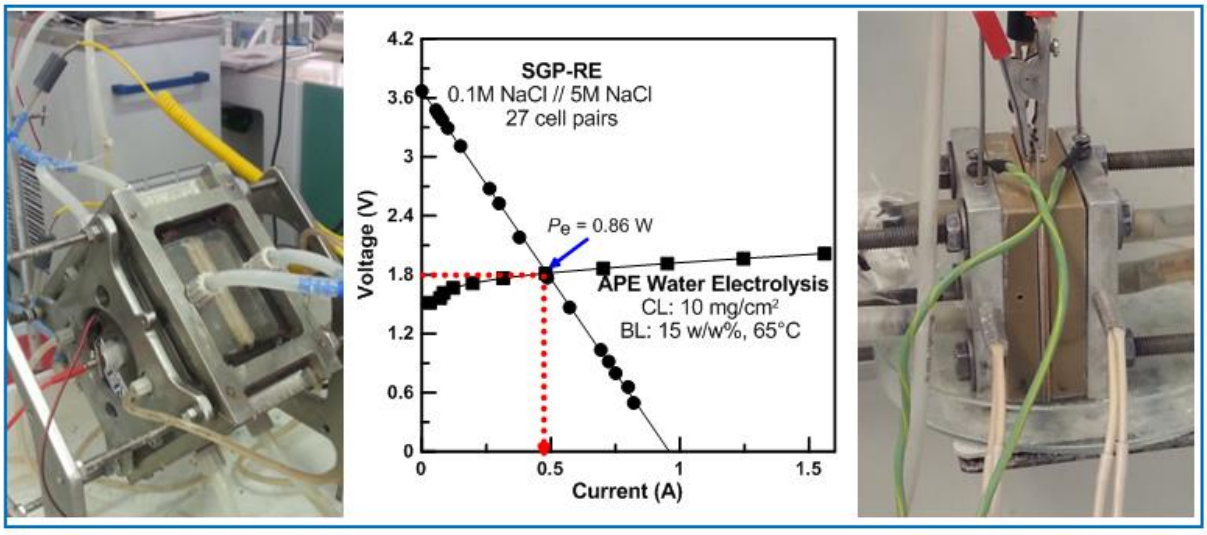

Abstract

In this work, innovative use of Salinity Gradient Power (SGP) as renewable energy source for indirect production of hydrogen is addressed. A lab-scale Reverse Electrodialysis (RE) unit, fed with different NaCl solutions mimicking highly concentrated brine (5M), Reverse Osmosis retentate (1M), seawater (0.5M) and brackish water (0.1M), was coupled to an Alkaline Polymer Electrolyte (APE) water electrolysis cell. SGP-RE unit, equipped with 27 cell-pairs, reached an Open Circuit Voltage (OCV) of 3.7 V and gross maximum power density of 3.2 W/m^2_{MP} (membrane pair) when feeding the Low Concentration Compartment (LCC) with 0.1 M NaCl and the High Concentration Compartment (HCC) with 5 M NaCl. The single-cell APE water electrolysis unit, operated at 1.8 V, attained a current density of 120 mA/cm2 (falling in the usual range of industrial practice) in the following configuration: 10%wt KOH electrolyte, highly conductive anion selective membrane composed of inert low-density polyethylene, finelly milled anion selective particles and water-soluble poly (ethylene glycol-ran-propylene glycol), non-Platinum catalysts ($NiCo_2O_4$ and $NiFe_2O_4$) loading of 10 mg/cm^2 and 15%wt polymer binder at both cathode and anode, and operational temperature of 65°C. The integrated system resulted in a maximum hydrogen production rate of 55 cm^3/h per cm^2 of electrode surface area.

This chapter has been submitted to the journal *of Energy and Environmental Science*

7.1 Introduction

With more than 50 million metric tons produced annually worldwide [1], hydrogen plays a strategic role in petroleum refining (i.e. hydrocracking, hydrodesulphurisation, hydroisomerization, dearomatisation), in ammonia production and in a range of applications of the electronics industry [2]; moreover, it is also recognized as a clean, efficient and versatile energy vector [3]. Large-scale H_2 generation has been so far dominated by fossil fuels: nearly 50% via steam reforming of natural gas, and about 46% from oil/naphtha reformingand coal gasification [4]. Water electrolysis, typically limited to small scale and so far representing only 4% of the world hydrogen production, is now receiving increased attention due to the possibility to use renewable power supply in the logic of a sustainable growth. Renewable energy resources such as photovoltaic and wind have been explored for electrolytic production of hydrogen from water [5]. However, use of solar and wind energy is limited by stability issues caused by intrinsic seasonal and weather-dependent character. Dutton *et al*. (2000) investigated the effects of power fluctuations on alkaline electrolyzers powered by wind turbines: although short-term variations do not have significant effects, intermittent operations protracted over several days resulted in pressure fluctuations with adverse effects on gas purity level [6]. In general, intermittent electrolysis operations may lead to damage and degradation of the separators due to local overload, deactivation of the electrode catalysts, corrosion caused by shortcut currents, gas crossover and pressure equalization between cathode and anode [7]. The capacity factor of intermittent renewable sources usually falls below 40% [8].

Salinity Gradient Power (SGP), the renewable energy extracted from mixing two solutions at different salinity, is recently attracting growing interest among the scientific community. Unexploited estuarial SGP, released when river and seawater mix together, has an estimated global potential of 2000 TWh/yr, which is more than 10% of the current world energy demand [9]. In principle, considering that energy requirement of electrolyzes falls in the range of 53-70 kWh/kg [10], an efficient utilization of the available SGP would produce up to 38 Mt/yr of hydrogen.

One of the primary technologies capable to exploit SGP is Reverse Electrodialysis (RE) [11-19]. In RE, anion exchange membranes (AEM) and cation exchange membranes (CEM) are alternatively stacked between spacers to create adjacent low concentration and high concentration compartments (thereafter indicated as LCC and HCC, respectively). Ions migrate selectively across the permselective membranes driven by the salinity gradient across the compartments, while

electricity is continuously generated by a redox occurring at the electrodes placed at both sides of the membrane piles. The open circuit voltage (OCV) of the unit is given by the sum of Nernst potential drops over the cell pairs. A typical scheme of RE unit is illustrated in Figure 7.1.

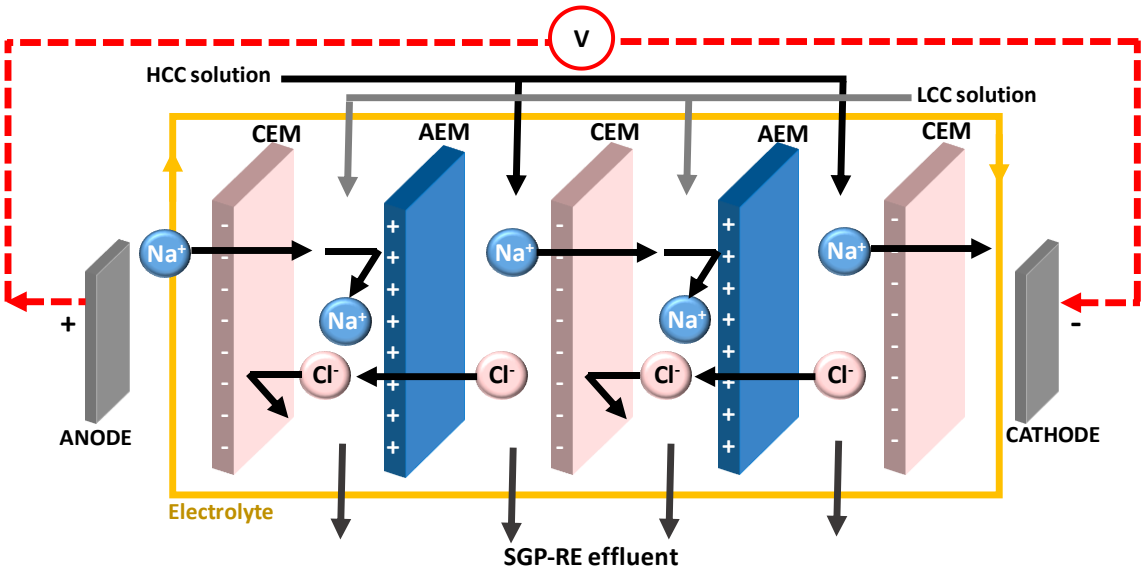

Figure 7.1. The principle of energy production by SGP-RE stack. A voltage is continuously generated so long as the Low Concentration Compartment (LCC) and the High Concentration Compartment (HCC) are fed with NaCl solutions at different salinity.

The potential generated by RE depends on the properties of the membranes, spacer material, geometry, number of cell pairs, operating conditions including salinity gradient level, temperature, flow velocity etc. For ideally permselective ion exchange membranes, the theoretical potential generated by a single cell pair is about0.076 V for seawater/brackish water, 0.13V brine/seawater, 0.21 V brine/brackish water.

The thermodynamic threshold for water electrolysis is 1.23 V at 25°C [20].

Among the currently available water splitting technologies, alkaline polymer electrolyte (APE) electrolysis works in alkaline environment using non-precious metal catalysts [21, 22]. A scheme of a typical APE water electrolysis unit for hydrogen production consisting of a single cell equipped with a anion selective membrane (ASM) is reported in Figure 7.2. When a direct current is applied to the electrodes, electrons flow from the anode to the cathode where hydrogen ions (protons) are reduced to gaseous hydrogen. Driven by the electrical field between the two

electrodes, hydroxide ions are transferred through the AEM to the anode, and here are oxidized to O_2 returning electrons to the positive terminal.

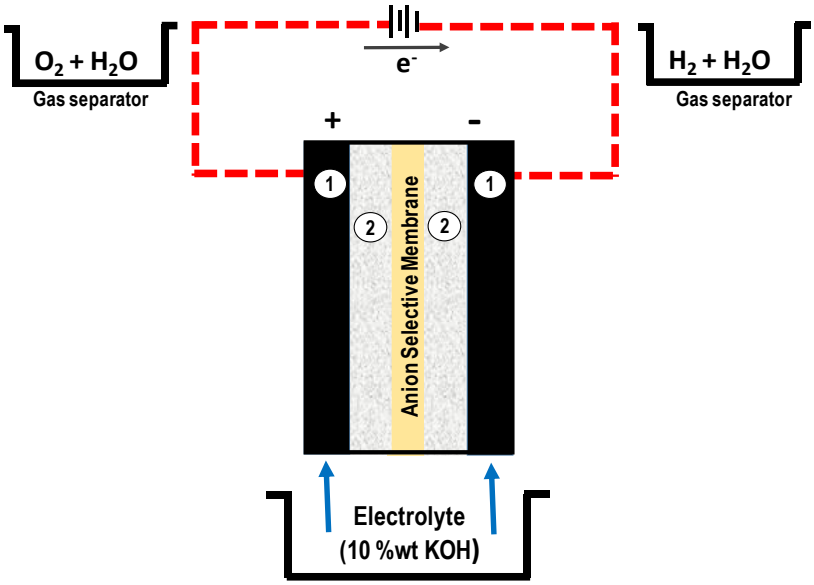

Figure 7.2. Schematic illustration of alkaline electrolysis unit equipped with a solid polymer electrolyte (Anion Selective Membrane): 1) gas diffusion layer; 2) catalyst layer.

The half reactions occurring at the electrode surfaces of APEME are:

$$2H_2O + 2e^- \rightarrow 2OH^- + H_2 \qquad [R1]$$

$$2OH^- \rightarrow H_2O + \frac{1}{2}O_2 + 2e^- \qquad [R2]$$

resulting in the following overall reaction:

$$H_2O \rightarrow \frac{1}{2}O_2 + H_2 \qquad [R3]$$

Few previous attempts in using RE for hydrogen production are reported in literature. In 2006, Seale patented a RE system for simultaneous generation of electricity and electrolytic production of hydrogen [23], followed by a patent of Logan et al. in 2014 [24]. Integration of reverse electrodialysis with microbial electrolysis cell (MEC) in a system called "microbial reverse-electrodialysis electrolysis cell (MREC)" was proposed by Logan et al. (2011) with the aim to produce hydrogen from renewable biomass [25-27]. Hatzell et al. (2014) investigated the use of thermolitic ammonium bicarbonate solutions for energy capture in a closed-loop RE system

using either oxygen reduction or hydrogen evolution [28]. The promotion of H_2 evolution directly at the cathode of the RE unit, so far is considered unpractical due to requirement of both electrodes with low overpotentials and limited number of cells (as remarked by Weinstein and Leitz: "*Electrode reactions could be chosen to yield useful products, but the first law of thermodynamics dictates that any energy so used would represent an inefficiency in power generation*"[29]). On the other hand, the integration of SGP-RE and APE water electrolysis might offer the advantage of maximizing both energy generation and hydrogen production via optimization of operative conditions and materials for both units.

In this work, the potential of an innovative SGP-RE-APE system for hydrogen production driven by SGP as non-fluctuating renewable energy source is implemented and tested. The performance of the RE stack, fed with NaCl solutions at molar concentration of 0.1, 0.5, 1 and 5 M (mimicking brackish water, seawater, RO retentate and brine, respectively), acting as power supplier to alkaline water electrolysis unit, is investigated in terms of generated power density and voltage. The APE system is optimized for catalyst and polymer binder loadings and temperature with the aim to get the highest power density at 1.8V.

7.2 Theoretical background

7.2.1 Reverse electrodialysis

For NaCl solutions, the open circuit voltage of a RE unit generated across CEM and AEM is:

$$OCV = \frac{2NRT}{F}\left[\alpha_{CEM}\ln\frac{c_{HCC}\gamma_{HCC}^{Na^+}}{c_{LCC}\gamma_{LCC}^{Na^+}} + \alpha_{AEM}\ln\frac{c_{HCC}\gamma_{HCC}^{Cl^-}}{c_{LCC}\gamma_{LCC}^{Cl^-}}\right] \quad [7.1]$$

where N is the number of cell pairs, R the gas constant (8.314 J/mol K), T the temperature (K), F the Faraday constant (96485 C/mol), α the membrane permselectivity, c the molar concentration (mol/l), and γ the activity coefficient. Subscripts 'HCC' and 'LCC' stand for high concentration compartment and low concentration compartment, respectively.

The overall performance of RE stack, evaluated in terms of voltage (V), current (I) and gross power density (P_d), is limited by the total internal resistance (R_{stack}) which includes Ohmic and non-ohmic losses. According to Ohm' law, the voltage drop is linearly related to the current as:

$$V = OCV - R_{stack} \cdot I \quad [7.2]$$

The electric power density P_d, plotted versus the current density i (W/m^2), exhibits a typical parabolic trend described by a second order equation:

$$P_d = -a \cdot i^2 + b \cdot i \quad [7.3]$$

where *a* and *b* are two fitting parameters. According to Eq. 7.3, P_d reaches its maximum value $P_{d,max} = b^2/4a$ for a maximum current density $i_{max} = b/2$.

7.2.2 Alkaline water electrolysis

From a thermodynamic point of view, the variation in Gibbs free energy (ΔG) for the electrochemical reaction is expressed by:

$$\Delta G = -n F \Delta E° \quad [7.4]$$

where ΔE° is the equilibrium cell voltage and *n* is the number of electrons involved in the redox. At standard ambient conditions (25 ºC and 1 atm), a ΔG = 237.2 kJ/mol is theoretically required to initiate the water electrolysis reaction, corresponding to a reversible cell potential of 1.23 V.

Due to inherently slow electrode kinetics, an overpotential above the equilibrium cell voltage is required to overcome the activation barrier of the electrochemical reactions. In addition, transport-related resistances due to the ionic transfer in the electrolyte and membrane, and to gas bubbles covering the electrode surfaces, call for an extra-energy input that causes a potential drop through the cell. As a consequence, in industrial practice, the cell potential ΔE_{cell} is always 1.8–2.0 V at the current density of 1–3 kA/m^2 [30].

The power consumed by the electrolyser (P_e) is given by:

$$P_e = \Delta E_{cell} I_e \quad [7.5]$$

where I_e is the current flows through the system.

According to the Faraday's laws, the hydrogen production rate (HPR) (mol/h) is theoretically estimated by:

$$HPR = \frac{3600 \cdot I_e}{zF} \quad [7.6]$$

where z represents the equivalent electrons per mole of hydrogen, and 3600 is a conversion constant (seconds per hour).

7.3 Materials and Methods

7.3.1 Reverse Electrodialysis

The electrolyte solution, consisting of 0.3 M $K_4Fe(CN)_6$, 0.3 M $K_3Fe(CN)_6$ and 2.5 M NaCl (Sigma-Aldrich S.r.l., Italy), was prepared by dissolving reagents in deionized water (PURELAB, Elga LabWater®, 0.055 μS/cm), and re-circulated at a flow rate of 20 L/h between the anodic and cathodic compartments to sustain the redox reaction. Feed solutions were prepared by using analytical reagent grade NaCl (Carlo Erba, Italy) dissolved in water, and recirculated at flow velocity of 0.7 cm/s using Masteflex L/S digital peristaltic pumps (Cole-Palmer, US).

A 25-cell pairs cross flow RE stack (REDstack B.V., The Netherlands), equipped with AEM-80045 and CEM-80050 ion exchange membranes (Fujifilm Manufacturing Europe B.V, The Netherlands) having active area of 10x10 cm^2, was operated in cross-flow configuration (Figure 7.3a). Main properties of ion exchange membranes are reported in Table 7.1 Spacers made in PET (Deukum GMBH, Germany) with thickness of 270 μm, were placed between membranes to create compartments. The electrode compartments are composed of 10x10 cm^2 inert Ti-Ru/Ir mesh (MAGNETO Special Anodes B.V., The Netherlands). Flow temperatures were stabilized at 25°C by using a Digital Plus RTE201 thermostatic bath (Neslab, US); SPER SCIENTIFIC 800012 Pt multi-channel thermocouples with sensitivity ± 0.1 ◦C and pressure gauges RF-D201 (DUNGS®, Germany) were used to monitor temperatures and pressures.

A resistance box (high dissipation five decade) in the range of 0.1-1000 Ω (CROPICO, Bracken Hill, US) was used to load the SGP-RE unit. The resulting DC voltage drop across the resistors and current were measured by Agilent 34422A 6½ Digit Multimeter.

Table 7.1. Relevant properties of the ion exchange membranes used in RE unit [31].

Membrane code	**Thickness† (μm)**	**Ion exchange capacity† (mmol/g membrane)**	**Density of fixed charges (mol/L) †**	**Membrane areal resistance‡ (Ω cm^2)**
Fuji-AEM-80045	129±2	1.4±0.1	3.8±0.2	1.551±0.001
Fuji-CEM-80050	114±2	1.1±0.1	2.4±0.2	2.974±0.001

†Measurement conditions: NaCl 0.5 M, 20°C
‡ Measurement conditions: NaCl 0.5 M, 20°C, 2.8 cm/s.

7.3.2 Alkaline water electrolysis

A single cell APE water electrolysis unit (Figure 7.3b) was used in electrolytic tests for hydrogen production driven by RE stack. The two side blocks of the cell were made of steel terminal plates and polyether-ether-ketone (PEEK) inner plates sealed by expanded Teflon (GORE GR 05, W. L. Gore & Associates Inc.). Sheets of anodic and cathodic materials based on 1.7 mm thick porous Ni foam (INCO Advanced Technology Materials Co, Ltd.) with active area of 2x2 cm^2 and pore diameter of 0.58 mm were used as a electrode. Gold plated nickel was used as current feeder/electrolyte (10 %w/w potassium hydroxide, KOH) distributor. The electrolyte was fed to the APE water electrolysis unit at flow velocity of 1.6 cm/s. Experiments were performed in the temperature range of 25-65 ^oC.

Highly active spinel family metal oxides based on Ni served as catalysts. $NiCo_2O_4$ and $NiFe_2O_4$ (prepared by co-precipitation method as detailed in [32]) were used for coating anode and cathode, respectively. Catalyst-binder ink was prepared by mixing different amounts of catalyst material and polymer binder solutions (consisting of a 60% w/w suspension of polytetrafluoroethylene, PTFE) in equal portions with deionised water and isopropyl alcohol. After sufficient homogenization of catalyst-binder ink in an ultrasonic bath, catalyst coated electrodes (CC-GDL) were prepared by spraying the catalyst-binder ink on the nickel foam placed on the hot plate at 120°C to ensure quick evaporation of the solvents and forming catalytic layer. In all experiments, the $NiCo_2O_4$ load in the anode was the same as that of the $NiFe_2O_4$ load in the catode; loads were varied in the range of 5-15 mg/cm^2.The CC-GDL was then heated at 325 °C for 15 min to bind the catalyst to the Ni foam. Compostion of the prepared catalytic layers varied from 75% w/w of the catalyst + 25% w/w of the PTFE to 95% w/w of the catalyst + 5% w/w of the PTFE.

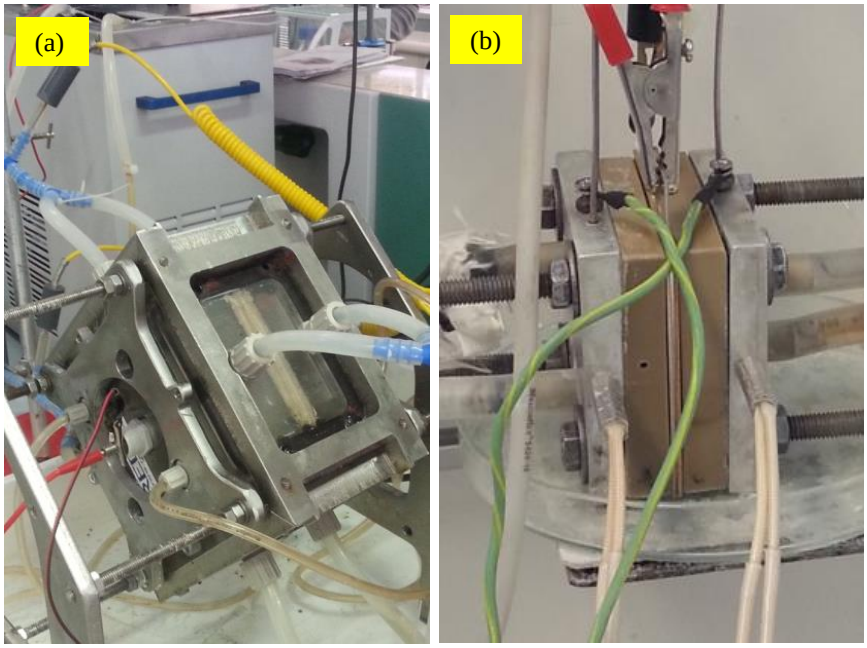

Figure 7.3. Lab-scale setup of a) SGP-RE stack; b) APE water electrolysis unit.

The AEM, specifically tailored for high ionic-conductivity, was composed of low-density polyethylene (ExxonMobil TM, LD 605BA) and a water-soluble component of poly (ethylene glycol-ran-propylene glycol) (PEG–PPG) (Sigma-Aldrich) blended with anion selective resins made of styrene-divinyl benzene copolymer matrix with quaternary ammonium functional groups (MEGA Co., Czech Republic). The detailed preparation and activation protocol of the membrane is described elsewhere [33]. Relevant properties of the AEM are presented Table 7.2.

Table 7.2. Properties of the heterogeneous AEM used in APEME unit [33]

Membrane Properties	**Temperature**	**Values determined**
Tensile strength (MPA)	20 ºC	0.82
Ion exchange capacity (mmol/g dry)	30-50 ºC	2
Conductivity (S/m)	30 ºC	3.6
	50 ºC	5.7
	70 ºC	7.2

A voltage of 1.5-2 V was applied to the electrolysis unit by DC power source Statron 3251.1 (Statron Gerätetechnik GmbH, Germany) in order to evaluate the dependence of the current

on input voltage (load curve). In order to determine resistances of the membrane and solution (R_{m+s}), anode (R_a) and cathode (R_c), Solartron SI 1287 Electrochemical Interface was used to input perturbation signal in the frequency range of 65 kHz-10 Hz and amplitude of 20 mV at 1.8 V, and Solartron SI 1250 Frequency Response Analyzer to investigate the changes in the input signal after passing through the system. Experiments were carried out at the corresponding conditions of the alkaline water electrolysis. Figure 7.4 presents equivalent circuit used for fitting the data from electrochemical impedance spectroscopy.

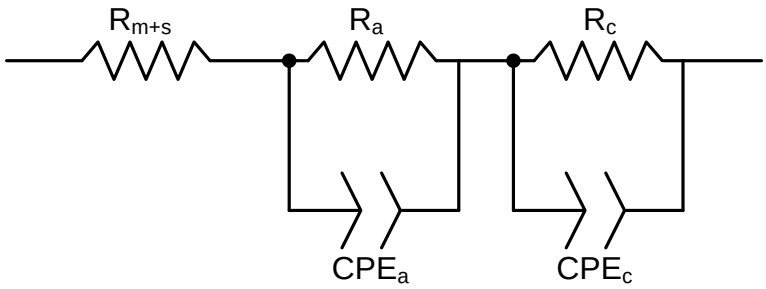

Figure 7.4. Equivalent circuit used to fit data from Electrochemical Impedance Spectroscopy, composed by three resistances (R_{m+s}, R_a and R_c) and two capacitive phase elements (CPE_a and CPE_c).

7.4 Results and Discussion

7.4.1 Reverse electrodialysis

Figure 7.5 shows the polarization curves of the SGP-RE unit at different LCC and HCC concentration. The diagram confirms the linear relationship between current and voltage according to Eq. 7.2. When feeding the SGP-RE stack with 0.1 M NaCl//5 M NaCl solutions at flow velocity of 0.7 cm/s and room temperature, the highest OCV (3.4 V) was measured; at zero voltage, a shortcut current ($I_{shortcut}$) of 0.89A was determined. Under these conditions, the internal areal resistance (IAR), evaluated from the slope of the V vs I straight-line, was 15.3 Ωcm^2/cell. When reducing the HCC concentration to 1M NaCl, the OCV decreased by 38% down to 2.1V, while $I_{shortcut}$ remarkably reduced by 60%, due to the lowering of diffusive flux of ions across the membranes driven by the salinity gradient. The observed enhancement of IAR to 23.5 Ωcm^2/cell, as a result of the decrease of the NaCl solution conductivity, is in coherent with previous investigations [16].

Increasing LCC concentration has a negative impact of the RE performance [17]. The combination 0.5M NaCl//5M NaCl resulted in a 45% decrease of OCV (1.9 V) with respect to the

case 0.1M NaCl//5M NaCl What about shortcut current? What about the slopes? It seems to be better in this case. In the first case (OCV 3.4 V, $I_{shortcut}$ 0.89) slope is 3.82 V/A besides in this case OCV (1.9 V) and $I_{shortcut}$ (0.6 V) gives 3.17 V/A, which is better.

The lowest OCV (1.0V) and $I_{shortcut}$ (0.04A) were measured in correspondence of the lowest feed salinity ratio (0.5M NaCl//1M NaCl).

Although the above results indicate the possibility to increase the SGP-RE performance by working at high HCC and low LCC concentration, some operative limitations exist: NaCl concentration above 5M negatively affects the membrane permselectivity [34], while LCC concentration below 0.1 M enhances the Ohmic losses [35].

Gross power density (per membrane pair, MP) curves resulting from RE unit operated at different LCC and HCC concentrations are illustrated in Figure 7.6. The highest $P_{d,max}$ (3.0 W/m^2_{MP}) was obtained when working with 0.1M NaCl//5M NaCl solutions; the maximum of the parabolic curve was attained for a current density i_{max} of 45 A/m^2. However, a significant reduction (-63%) was observed for a 5-fold increase of the LCC concentration (0.5 M NaCl), resulting in a $P_{d,max}$ of 1.1 W/m^2_{MP}; under the same condition, i_{max} decreased by 33%. Experimental tests carried out with 0.1M NaCl//1M NaCl resulted in a $P_{d,max}$ of 0.77 W/m^2_{MP} and in a i_{max} of 17.9 A/m^2. Mixing 0.5M NaCl (mimicking seawater salinity) and 1M NaCl (mimicking brine from Reverse Osmosis operated at 50% recovery factor) led to impractically low values of $P_{d,max}$ around 0.1 $W/m^2_{MP.}$

Early investigations by Audinos *et al*. (1983) attained power density values up 0.8 W/m^2_{MP} from mixing river water and brine [36]. More recently, Veerman *et al.* (2008) reported a maximum power density of 2.86 W/m^2_{MP} for a RE operated with seawater and river water [37]. The maximum power density reported so far for mixing seawater and river water is about 4.4 W/m^2_{MP} [35]: this work benefits from specially designed ion exchange membranes. When using concentrated brine, power densities up to 2.7 W/m^2_{MP} have been reported from experiments on a pilot-scale RE plant located in Sicily [38].

Keeping constant the salinity ratio to 10, the better performance detected when working with more concentrated solutions (0.5 M NaCl//5 M NaCl instead of 0.1 M NaCl//1 M NaCl) is due to the reduction of Ohmic losses as a consequence of the increased conductivity of the solutions. Changes in LCC and HCC concentration had a moderate impact on the fitting parameter *a* (Eq. 3), which is related to stack resistance, showing values from 0.0013 (0.5M NaCl//5M NaCl)

to 0.0024 (0.1M NaCl//1M NaCl). Parameter *b*, which is related to the electromotive force over the membranes is sensitive to the salinity gradient and varied from 0.029 (0.5M NaCl//1M NaCl) to 0.13 (0.1M NaCl//5M NaCl) [15].

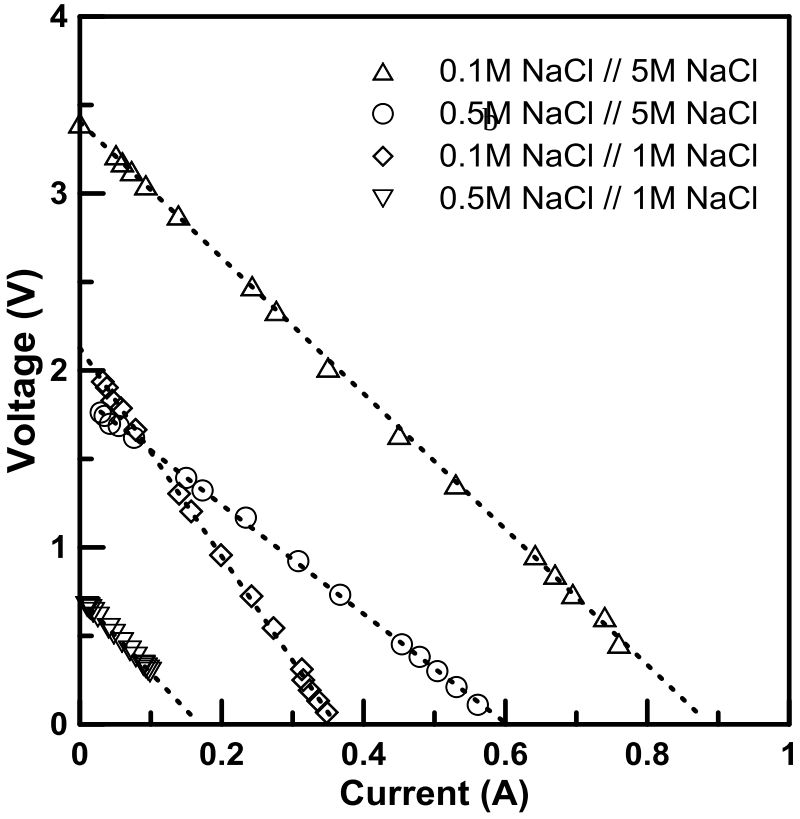

Figure 7.5. Voltage vs current measured in the SGP-RE stack at different HCC and LCC concentrations (25 cell pairs, flow velocity: 0.7 cm/s, 25°C).

Fluid recirculation across the stack requires a given amount of pumping energy that increases with flow velocity; therefore, the net amount of power density is sensitive to the energy loss in the SGP-RE system due to pressure drop [15, 39]. Referring to the operative conditions resulting in the generation of the highest gross power density (0.1M NaCl//5M NaCl and flowrate of 0.7 cm/s), pressure drops detected in low (Δp_{LCC}) and high concentration compartments (Δp_{HCC}) were 0.06 and 0.14 bar, respectively. As a result, the value of net power density represent about the 80% of the gross power density.

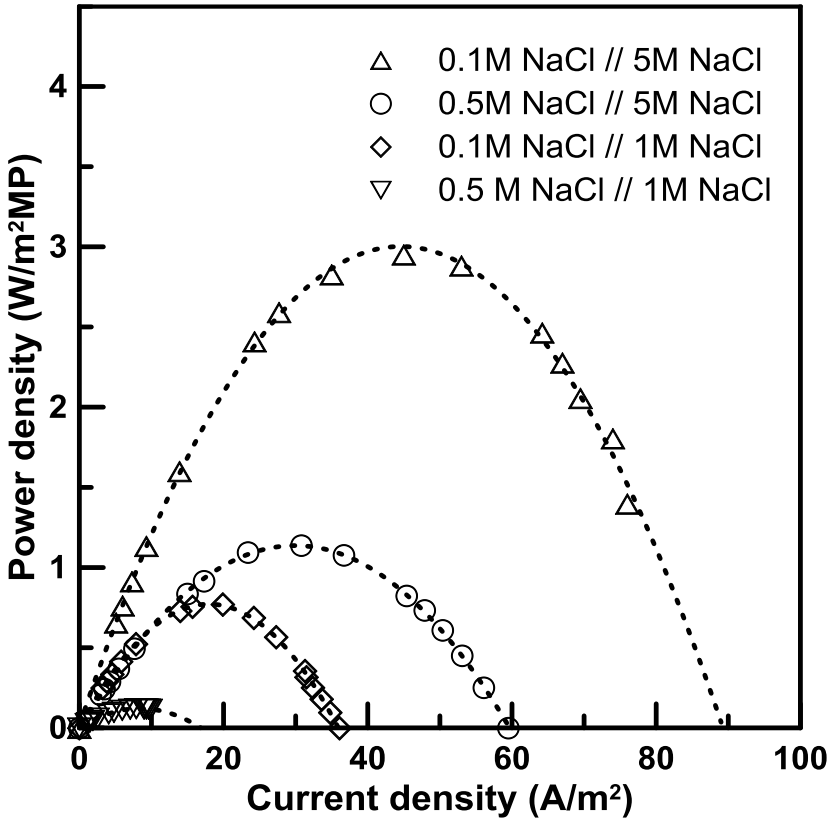

Figure 7.6. Gross power density vs current density measured in the SGP-RE stack at different HCC and LCC concentrations (25 cell pairs, flow velocity: 0.7 cm/s, 25°C)

7.4.2 APE water electrolysis tests

7.4.2.1 Effect of catalyst loading

The electrode activity depends on many parameters. One of these represents the loading level of the catalytic material used in catalytic layer. In the present study, investigations were experimentally carried out in the range of 5 - 15 mg/cm^2 (keeping constant the binder loading at 15% w/w) and at working temperature of 65°C; the corresponding electrolysis load curves are shown in Figure 7.7. Current density enhanced by 12% (from 107 mA/cm^2 to 120 mA/cm^2) at 1.8V when the catalyst loading was increased from 5 mg/cm^2 to 10 mg/cm^2. The better performance is due to the increase of contact area available to electrochemical reaction, leading to a higher hydrogen evolution reaction (HER) rate. The enhancement in process efficiency was more noticeable at higher voltage: current density increased by 44 % at 2V. However, further increase of the catalyst load from 10 to 15 mg/cm^2 at 1.8V resulted in a performance loss, and current

density reduced by 26% (from 120 mA/cm^2 to 89 mA/cm^2). This is probably due to the decrease of the electron contact for the catalyst particle. It represents one of the three essential demands on the composition of the catalytic layer in order to achieve optimal three phase contact in the catalytic layer, i.e. catalytical particle has to be in contact with reagent, electrons and ions.

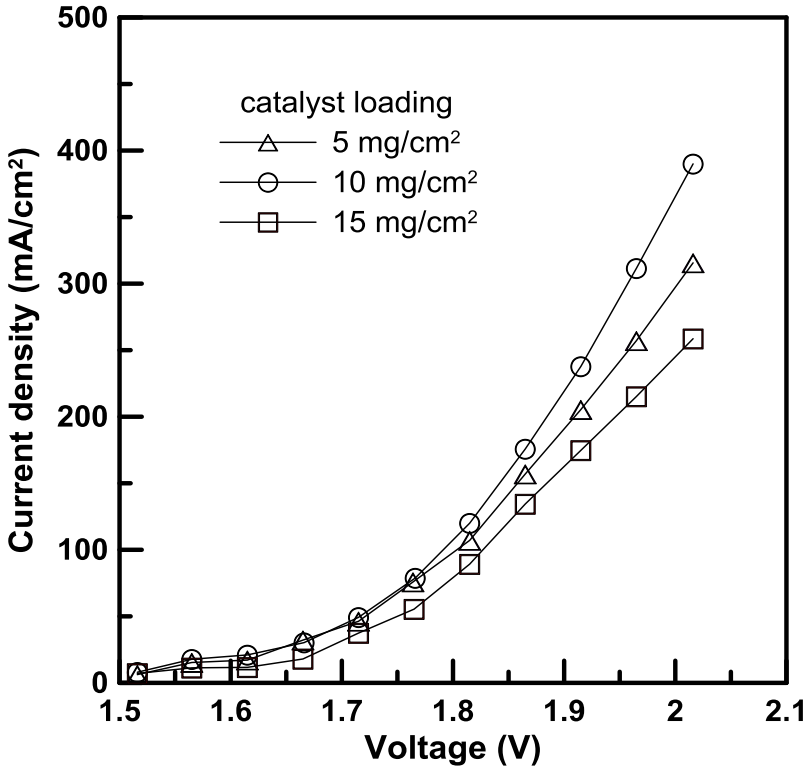

Figure 7.7. Load curves of the alkaline water electrolysis. Separator: heterogeneous anion selective polymer membrane; Anode: $NiCo_2O_4$ (load of the catalyst indicated in the Figure) + PTFE binder (85% w/w catalyst + 15% w/w PTFE); Cathode: $NiFe_2O_4$ (load of the catalyst indicated in the Figure) + PTFE binder (85% w/w catalyst + 15% w/w PTFE); temperature: 65 ^oC; geometric electrode area: 4 cm^2, Electrolyte flow 5 ml/min.

Evidence for an optimal catalyst loading is reported in literature. Ma *et al.* (2009) tested different MEA based on supported Iridium/titanium carbide electrocatalysts prepared at different Ir catalyst loading for polymer electrolyte membrane (PEM) water electrolysis [40]. A remarkable improvement of the cell performance (about 30% increase of power density) was detected when Ir loading in the anode varied from 1.0 mg/cm^2 to 2.5 mg/cm^2 due to the enlarged electrochemically active area. On the other hand, for higher catalyst loading, the performance gain was almost

completely lost as a consequence of the increase in ohmic resistance attributed to a thicker catalyst layer.

7.4.2.2 Effect of binder loading

In MEA, a polymer binder is required in order to attach a catalytic layer to a gas-diffusion layer, so creating a gas diffusion electrode (GDE) [41-44]. GDE improves the stability of the catalyst by counteracting its rapid loss. Additionally, in case of massive gas bubbling at the electrode, the appropriate choice of binder loading improves the adhesion of the catalyst layer. In the present work, PTFE was used as a polymeric binder ensuring adequate mechanical stability to the GDE.

Table 7.4 summarizes the experimental results obtained from tests on the alkaline electrolyser operated at 10 mg/cm^2 catalyst loading. Data indicate that the best performance was achieved for a binder loading of 15%w/w, and a current density of 120 mA/cm^2 at 1.8 V was measured at temperature of 65 ^{o}C and electrolyte flow rate of 5 ml/min. It was also observed that the current density declined by 55% when the binder loading was reduced to 5% w/w: a low content of polymeric binder in the catalyst layer reduces the utilization surface at the gas/electrolyte/electrode interface, thus resulting in a lower current density at the same potential. On the other hand, when the binder loading was increased to 25 w/w%, the current density decreased by 52%: an excessive binder content results in catalyst area coverage that avoids an efficient electron exchange and leads to an increase of electrode resistance. Moreover, high loading levels of polymeric binders reduce gas permeability of GDE.

Song *et al.* (2006) investigated the effect of Nafion® content in the Pt black catalyst of a PEM fuel cell electrode; a binder loading greater than 35wt% in the cathode led to a significant loss of performance even with a little further increase in Nafion® content due to blockage of the catalyst sites and a reduction of gas permeability in the catalytic layer, while an opposite trend was detected when increasing the binder content from 15 to 35wt% [44].

Table 7.4. Effect of binder loading on APE water electrolysis performance (1.8V, catalyst loading: 10 mg/cm^2, flow velocity: 1.6 cm/s).

	Current density (mA/cm^2)		
Temperature (°C)	**BL**: 5 %wt	**BL**: 15%wt	**BL**: 25%wt
25 ± 2	-	25 ± 3	-
45 ± 3	-	57 ± 4	-
65 ± 5	54.5 ± 3	120 ± 6	57.2 ± 4

BL: binder loading

Temperature enhances the electrochemical reaction rate and reduces the electrode overpotential, thereby improving the cell performance. As reported in Table 7.4, for a 15%wt binder loading, the current density increased by +128 % when the temperature shifted from 25 ^{o}C to 45 ^{o}C; further increase of the temperature from 45 ^{o}C to 65 ^{o}C resulted in a 110% increase of current density; at the average, the increase of current density was 2.3 mA/cm^2/°C.

Santarelli *et al.* (2009) investigated the influence of temperature on a high-pressure PEM electrolyser for hydrogen production; they observed an improvement of current density by about 20% when increasing the temperature from 42 to 58 °C at cell voltage higher than 1.8V and pressure of 7 bar [45].

For HER on pure nickel electrodes operated at 2.5 atm, a decrease of 115 mV for a current density of 100 mA/cm^2 was observed when the temperature increased from 70 to 150^{o}C [46].

7.4.2.3 Cell resistance

Table 7.5 shows the results from electrochemical impedance spectroscopy (EIS) measurements for the resistance of single components in the electrolytic cell, on the bases of the equivalent electrical circuit shown in Figure 7.8. The *in situ* measurements displayed a slightly decreasing Ohmic resistance of the heterogeneous AEM and electrolyte solution (R_{m+s}) within the range of 0.22-0.19 Ω for a temperature interval of 25-65°C, due to a progressive increase of ion mobility. A similar decreasing trend of AEM resistance with temperature was reported by Fontananova *et al.* (2014) [31].

In the investigated range of temperature, while there was no significant variation of the polarization resistance of the cathode (R_c), the anode resistance (R_a) fell down by 50% when heating the system from 25 ^{o}C to 65 ^{o}C. In general, the higher polarization resistance of the anode

with respect to the cathode is due to the fact that oxygen evolution reaction is significantly slower and more energy-demand than HER [21].

Table 7.5. Resistance measurements by Electrochemical Impedance Spectroscopy for AEM in electrolyte solution (R_{m+s}), anode (R_a) and cathode (R_c).

T(°C)	R_{m+s}(Ω)*	R_a(Ω)	R_c(Ω)
25	0.22	0.58	0.06
45	0.20	0.40	0.07
65	0.19	0.29	0.07

7.4.3 Hydrogen prodution rate

Figure 7.8 shows the effect of the main operating parameters on the performance of the water electrolysis unit. The hydrogen production rate (HPR), evaluated by Eq. 7.6 and expressed as number of moles of H_2 produced per electrode surface area per hour, was sensitive to changes in the temperature: HPR increased by 1.1cm^3/cm^2h per °C, reaching its maximum value of 55 cm^3/cm^2 h, corresponding to $2.3 \cdot 10^{-3}$ mol H_2/cm^2h considering a 4 cm^2 electrode geometrical area. The positive impact of increasing temperature is explained in terms of reduction of the electrode overpotential and enhancement of solution conductivity [21, 46].

The highest HPR was achieved for an optimal binder loading of 15%wt, decreasing by 50-60% when the binder loading was either reduced to 5%wt or increased to 25%wt. The impact of catalyst loading was less relevant: the HPR variation margin was below 20% when changing catalyst loading by ±50% with respect to its optimal level (10 mg/cm^2).

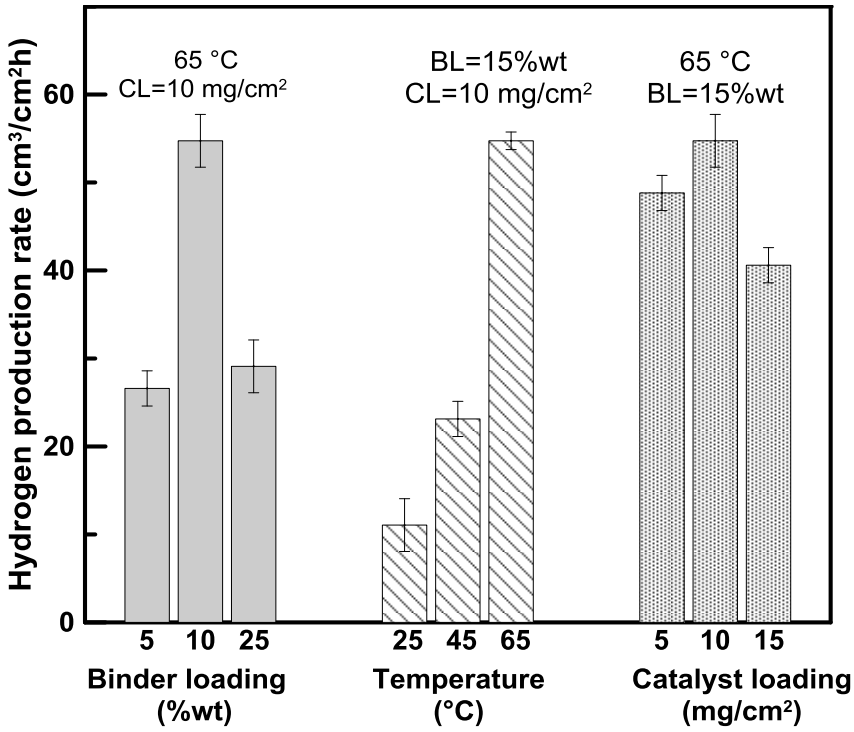

Figure 7.8. Hydrogen production rate (HPR) at different polymer binder loading (BL), temperature and catalyst loading (CL).

Luo *et al.* (2013) tested a microbial reverse-electrodialysis electrolysis cells (MRECs) using ammonium bicarbonate as thermolytic solution [47]. The 7-cell pairs membrane stack configuration (cathode projected area: 7cm^2, effective area of each membrane: 8 cm^2, electrode chamber volume: 30 mL each allowed a maximum volumetric hydrogen production rate of ~ 1.5 m^{3}H$_2$/m^{3}anolyte/d, corresponding to $1.1 \cdot 10^{-5}$ molH$_2$/cm^2 h.

Hatzell *et al.* (2014) investigated the production of hydrogen and generation of electrical power in a closed-loop ammonium bicarbonate reverse electrodialysis systems with 20 cell pairs and total active membrane area of 0.87 m^2, projected electrode area of 207 cm^2, Ti Pt/Ir anode, two different cathodes for hydrogen evolution reaction or oxygen reduction reaction, operated at low concentrate solution flowrate of 400 mL/min. In the case of direct hydrogen and electricity generation, the maximum energy extracted as hydrogen gas at the limiting current point was ~10.6 Wh/m^3 (95% of the total generated energy, including electrode overpotentials) corresponding to $1.6 \cdot 10^{-5}$ molH$_2$/cm^{2}h, that is significantly lower than HPR observed in the present APE water electrolysis unit. If a HER based RE was operated at the peak power position, 4.75 Wh/m^3 were

obtained from hydrogen (~50% of the total generated energy, including electrode overpotentials) corresponding to $7.1 \cdot 10^{-6}$ molH_2/cm^{2}h.

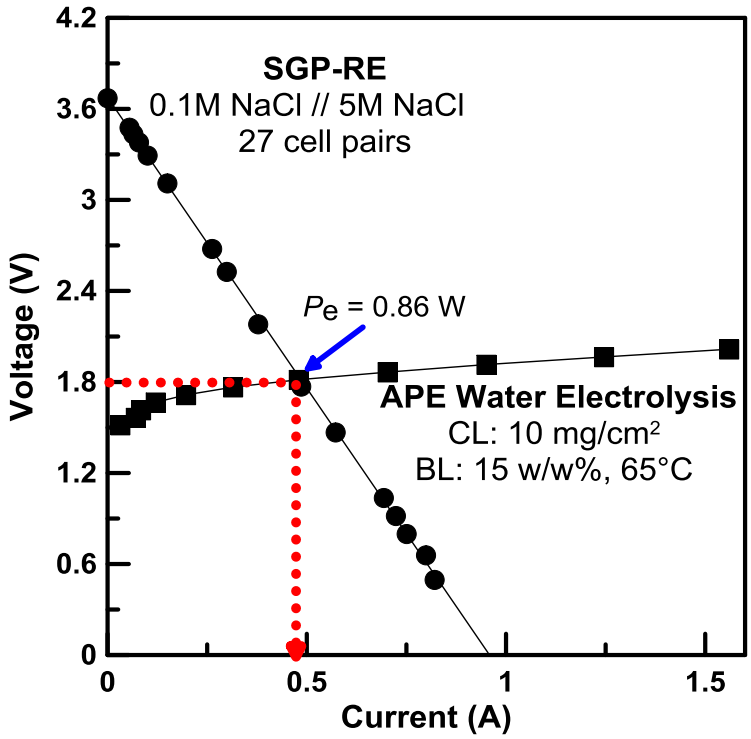

Figure 7.9. Polarization curves of SGP-RE and APE water electrolysis intersect at 1.8V and 0.48A, leading to a H_2 production rate of 55 cm^3/cm^2 h.

The experimental activity allowed at identifying the best operational conditions for APE water electrolysis cell at catalyst loading of 10 mg/cm^2, polymer binder of 15%wt and temperature of 65°C. Driving the system at 1.8V, the polarization curve in Figure 7.7 indicates a current density of 120 mA/cm^2, corresponding to a current of 0.48 A considering geometrical electrode surface area of 4 cm^2. The intersection point (0.48 A, 1.8 V) of polarization curves for the SGP-RE unit and the APE water electrolysis cell, corresponds to a power of 0.86 W, is illustrated in Figure 7.9. In order to achieve this target, the number of cell pairs in the SGP-RE stack was slightly increased to 27, giving a OCV of 3.7 V that is generated when working with 0.1M NaCl // 5 M NaCl at room temperature and 0.7 cm/s.

7.5 Conclusions

This work proves the viability of Salinity Gradient Power as renewable and non-intermittent energy source for indirect production of hydrogen. The integration, at lab-scale, of a reverse electrodialysis (SGP-RE) unit - fed with different NaCl solutions mimicking highly concentrated brine (5M), RO concentrate (1M), seawater (0.5M) and brackish water (0.1M) - with an alkaline polymer electrolyte (APE) water electrolysis cell, resulted in a maximum hydrogen production rate of 55 cm^3/h per cm^2 of electrode surface area (optimal conditions: LCC 0.1M NaCl//HCC 5M NaCl, 15%wt polymer binder loading, 10 mg/cm^2 catalyst loading, 65°C).

At salinity ratio of 50, the maximum gross power density achieved by the SGP-RE unit equipped with 25 cell-pairs was about 3 W/m^2_{MP}.

The use of brine (from solar ponds or membrane distillation [15]) has the interesting potential to mitigate the impact of desalination industry on the environment; in addition, hydrogen is today recognized as an intrinsically eco-friendly energy vector assuring zero-CO_2 emission. A successful scale-up of SGP-RE to industrial level strongly depends on the availability of ion exchange membranes exhibiting low electrical resistance, high permselectivity and stability under real conditions. Specifically, the influence of multivalent ions (mostly Mg^{2+} and SO_4^{2-}) present in natural water sources, as well as the impact of fouling on long-term performance, need to be deeply investigated.

Concerning APE water electrolysis, further research efforts need to be addressed on the development of better performing electrodes, use of more stable and active electrocatalysts, synthesis and fabrication of highly conductive polymer electrolyte membranes exhibiting good chemical and mechanical stability in corrosive OH^- environment [22, 30, 48, 49].

References

[1] Report of the Hydrogen Production Expert Panel to HTAC. United States Department of Energy Washington; 2013.

[2] Mueller-Langer F, Tzimas E, Kaltschmitt M, Peteves S. Techno-economic assessment of hydrogen production processes for the hydrogen economy for the short and medium term. International Journal of Hydrogen Energy. 2007;32:3797-810.

[3] Granovskii M, Dincer I, Rosen MA. Environmental and economic aspects of hydrogen production and utilization in fuel cell vehicles. Journal of Power Sources. 2006;157:411-21.

[4] Muradov N, Veziroğlu T. From hydrocarbon to hydrogen–carbon to hydrogen economy. International Journal of Hydrogen Energy. 2005;30:225-37.

[5] Santarelli M, Call M, Macagno S. Design and analysis of stand-alone hydrogen energy systems with different renewable sources. International Journal of Hydrogen Energy. 2004;29:1571-86.

[6] Dutton AG, Bleijs JAM, Dienhart H, Falchetta M, Hug W, Prischich D, et al. Experience in the design, sizing, economics, and implementation of autonomous wind-powered hydrogen production systems. International Journal of Hydrogen Energy. 2000;25:705-22.
[7] Chadwick SS. Ullmann's Encyclopedia of Industrial Chemistry. Reference Services Review. 1988;16:31-4.
[8] Gandía LM, Oroz R, Ursúa A, Sanchis P, Diéguez PM. Renewable hydrogen production: performance of an alkaline water electrolyzer working under emulated wind conditions. Energy & fuels. 2007;21:1699-706.
[9] Klaysom C, Cath TY, Depuydt T, Vankelecom IFJ. Forward and pressure retarded osmosis: potential solutions for global challenges in energy and water supply. Chemical Society Reviews. 2013;42:6959-89.
[10] Levene JI, Mann MK, Margolis RM, Milbrandt A. An analysis of hydrogen production from renewable electricity sources. Solar Energy. 2007;81:773-80.
[11] Logan BE, Elimelech M. Membrane-based processes for sustainable power generation using water. Nature. 2012;488:313-9.
[12] Ramon GZ, Feinberg BJ, Hoek EMV. Membrane-based production of salinity-gradient power. Energy & Environmental Science. 2011;4:4423-34.
[13] Vermaas DA, Veerman J, Saakes M, Nijmeijer K. Influence of multivalent ions on renewable energy generation in reverse electrodialysis. Energy & Environmental Science. 2014;7:1434-45.
[14] Długołęcki P, Gambier A, Nijmeijer K, Wessling M. Practical potential of reverse electrodialysis as process for sustainable energy generation. Environmental Science and Technology. 2009;43:6888-94.
[15] Tufa RA, Curcio E, Brauns E, van Baak W, Fontananova E, Di Profio G. Membrane distillation and reverse electrodialysis for near-zero liquid discharge and low energy seawater desalination. Journal of Membrane Science. 2015.
[16] Tufa RA, Curcio E, van Baak W, Veerman J, Grasman S, Fontananova E, et al. Potential of brackish water and brine for energy generation by salinity gradient power-reverse electrodialysis (SGP-RE). RSC Advances. 2014;4:42617-23.
[17] Tedesco M, Brauns E, Cipollina A, Micale G, Modica P, Russo G, et al. Reverse Electrodialysis with saline waters and concentrated brines: a laboratory investigation towards technology scale-up. Journal of Membrane Science. 2015.
[18] Brauns E. Towards a worldwide sustainable and simultaneous large-scale production of renewable energy and potable water through salinity gradient power by combining reversed electrodialysis and solar power? Desalination. 2008;219:312-23.
[19] Pawlowski S, Crespo JPG, Velizarov S. Sustainable Energy Generation by Reverse Electrodialysis. Procedia Engineering. 2012;44:1013-6.
[20] Kim S, Koratkar N, Karabacak T, Lu T-M. Water electrolysis activated by Ru nanorod array electrodes. Applied physics letters. 2006;88:263106.
[21] Hnát J, Paidar M, Schauer J, Bouzek K. Polymer anion-selective membrane for electrolytic water splitting: The impact of a liquid electrolyte composition on the process parameters and long-term stability. International Journal of Hydrogen Energy. 2014;39:4779-87.
[22] Xiao L, Zhang S, Pan J, Yang C, He M, Zhuang L, et al. First implementation of alkaline polymer electrolyte water electrolysis working only with pure water. Energy & Environmental Science. 2012;5:7869-71.
[23] Seale J. Reverse electrodialysis for generation of hydrogen. Google Patents; 2006.
[24] Waterman LC. Method and apparatus for separating mixtures of gas,water and oil. Google Patents; 1970.
[25] Kim Y, Logan BE. Hydrogen production from inexhaustible supplies of fresh and salt water using microbial reverse-electrodialysis electrolysis cells. Proceedings of the National Academy of Sciences of the United States of America. 2011;108:16176-81.
[26] Nam JY, Cusick RD, Kim Y, Logan BE. Hydrogen generation in microbial reverse-electrodialysis electrolysis cells using a heat-regenerated salt solution. Environmental Science and Technology. 2012;46:5240-6.
[27] Watson VJ, Hatzell M, Logan BE. Hydrogen production from continuous flow, microbial reverse–electrodialysis electrolysis cells treating fermentation wastewater. Bioresource Technology. 2015.
[28] Hatzell MC, Ivanov I, D. Cusick R, Zhu X, Logan BE. Comparison of hydrogen production and electrical power generation for energy capture in closed-loop ammonium bicarbonate reverse electrodialysis systems. Physical Chemistry Chemical Physics. 2014;16:1632-8.
[29] WEINSTEIN JN, LEITZ FB. Electric Power from Differences in Salinity: The Dialytic Battery. Science. 1976;191:557-9.
[30] Zeng K, Zhang D. Recent progress in alkaline water electrolysis for hydrogen production and applications. Progress in Energy and Combustion Science. 2010;36:307-26.

[31] Fontananova E, Zhang W, Nicotera I, Simari C, van Baak W, Di Profio G, et al. Probing membrane and interface properties in concentrated electrolyte solutions. Journal of Membrane Science. 2014;459:177-89.
[32] Scott K. 10 - Microbial fuel cells: transformation of wastes into clean energy. In: Gugliuzza A, Basile A, editors. Membranes for Clean and Renewable Power Applications: Woodhead Publishing; 2014. p. 266-300.
[33] Hnát J, Paidar M, Schauer J, Žitka J, Bouzek K. Polymer anion-selective membranes for electrolytic splitting of water. Part II: Enhancement of ionic conductivity and performance under conditions of alkaline water electrolysis. Journal of Applied Electrochemistry. 2012;42:545-54.
[34] Daniilidis A, Vermaas DA, Herber R, Nijmeijer K. Experimentally obtainable energy from mixing river water, seawater or brines with reverse electrodialysis. Renewable Energy. 2014;64:123-31.
[35] Vermaas DA, Saakes M, Nijmeijer K. Doubled Power Density from Salinity Gradients at Reduced Intermembrane Distance. Environmental Science & Technology. 2011;45:7089-95.
[36] Audinos R. Electrodialyse inverse. Etude de l'energie electrique obtenue a partir de deux solutions de salinites differentes. Journal of Power Sources. 1983;10:203-17.
[37] Veerman J, Saakes M, Metz SJ, Harmsen GJ. Reverse electrodialysis: Performance of a stack with 50 cells on the mixing of sea and river water. Journal of Membrane Science. 2009;327:136-44.
[38] Tedesco M, Scalici C, Vaccari D, Cipollina A, Tamburini A, Micale G. Performance of the first Reverse Electrodialysis pilot plant for power production from saline waters and concentrated brines. Journal of Membrane Science. 2015.
[39] Pawlowski S, Crespo JG, Velizarov S. Pressure drop in reverse electrodialysis: Experimental and modeling studies for stacks with variable number of cell pairs. Journal of Membrane Science. 2014;462:96-111.
[40] Ma L, Sui S, Zhai Y. Investigations on high performance proton exchange membrane water electrolyzer. International Journal of Hydrogen Energy. 2009;34:678-84.
[41] Ahn SH, Choi I, Park H-Y, Hwang SJ, Yoo SJ, Cho E, et al. Effect of morphology of electrodeposited Ni catalysts on the behavior of bubbles generated during the oxygen evolution reaction in alkaline water electrolysis. Chemical Communications. 2013;49:9323-5.
[42] Cheng S, Liu H, Logan BE. Power Densities Using Different Cathode Catalysts (Pt and CoTMPP) and Polymer Binders (Nafion and PTFE) in Single Chamber Microbial Fuel Cells. Environmental Science & Technology. 2006;40:364-9.
[43] Sasikumar G, Ihm JW, Ryu H. Dependence of optimum Nafion content in catalyst layer on platinum loading. Journal of Power Sources. 2004;132:11-7.
[44] Song Y, Xu H, Wei Y, Kunz HR, Bonville LJ, Fenton JM. Dependence of high-temperature PEM fuel cell performance on Nafion® content. Journal of Power Sources. 2006;154:138-44.
[45] Santarelli M, Medina P, Cali M. Fitting regression model and experimental validation for a high-pressure PEM electrolyzer. International Journal of Hydrogen Energy. 2009;34:2519-30.
[46] Ferreira AC, Gonzalez ER, Ticianelli EA, Avaca LA, Matvienko B. The effect of temperature on the water electrolysis reactions on nickel and nickel-based codeposits. Journal of Applied Electrochemistry. 1988;18:894-8.
[47] Luo X, Nam J-Y, Zhang F, Zhang X, Liang P, Huang X, et al. Optimization of membrane stack configuration for efficient hydrogen production in microbial reverse-electrodialysis electrolysis cells coupled with thermolytic solutions. Bioresource Technology. 2013;140:399-405.
[48] Safizadeh F, Ghali E, Houlachi G. Electrocatalysis developments for hydrogen evolution reaction in alkaline solutions – A Review. International Journal of Hydrogen Energy. 2015;40:256-74.
[49] Albert A, Barnett AO, Thomassen MS, Schmidt TJ, Gubler L. Radiation-Grafted Polymer Electrolyte Membranes for Water Electrolysis Cells: Evaluation of Key Membrane Properties. ACS Applied Materials & Interfaces. 2015;7:22203-12.

Energetic-Exergetic Analysis of Integrated Reverse Electrodialysis-Membrane Desalination Systems

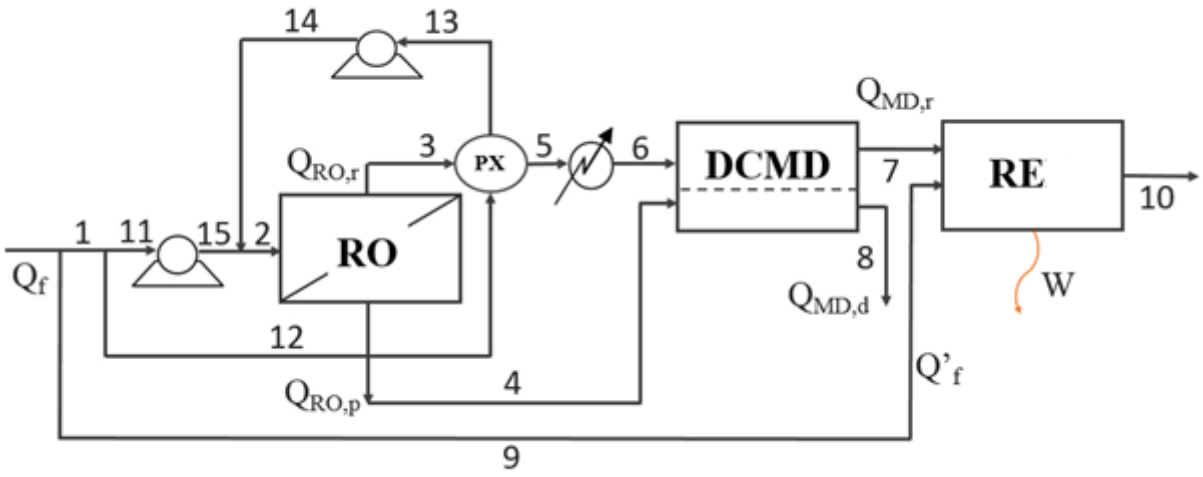

Abstract

Seawater reverse osmosis (SWRO) is the most widespread technology for fresh water supply in many coastal regions of the world. Many technological advances have been demonstrated in process design and development with special focus on the reduction of energy consumption, in particular the use of renewable energy resources. In this aspect, Reverse Electrodialysis (RE) can be integrated with desalination technologies in order to recover the electrochemical potential of highly concentrated brine discharge from desalination practice. In the present work, energetic and exegetic analysis of integrated application RE for energy recovery from RO brine and/or Direct Contact Membrane Distillation Brine (DCMD) is assessed for the feasibility of low energy seawater desalination. A RE was feed with different feed solutions: 0.1 M NaCl, 0.5 M NaCl, 1 M NaCl solutions mimicking brackish water, seawater, RO brine and DCMD brine, respectively. Experiments were performed in the temperature range of 20 - 60 ^{o}C envisaging the variation of DCMD brine depending on the inlet feed temperature. Results from energetic-exergetic analysis revealed that the optimum condition is the use of greater concentration of HCC solution (5 M NaCl) at high temperatures (60 ^{o}C) in the presence of both PX and RE module, although the benefit from a standalone RE application is not remarkable at this stage, requiring further optimization.

This chapter is submitted to the *Journal of Membrane Science*.

8.1 Introduction

The capacity of desalination plants is increasing globally as a result of population growth and increase in living standards. In the current practice of desalination, the energy requirement is met by the use of fossil fuel which is accompanied by the emission of greenhouse gases. This practice is not sustainable since the exploitation of limited fossil resources is accompanied by thermal and environmental pollutions which could lead to adverse ecological impact as well as energy insecurity in the future. Thus, the use of renewable energy resources like solar, wind and geothermal can be a solutions to the associated energy and environmental sustainability issues.

As can be seen from Figure 8.1, Reverse Osmosis (RO) is the membrane based desalination process which is the dominant technology holding 53% of the global installations [1]; this trend is expected to grow in time. Thermal processes like Multistage Flash (MSF) distillation and multi-effect distillation (MED) account for 25% and 8%, respectively. Most of the current desalination plants process use seawater (60%) as a feed.

Currently, the total global desalination capacity is about 66.4 m^3/day and is expected to increase by 15-fold (100 million m^3/day) by 2015 [1]. The main source of desalination processes is seawater (58.9 %) followed by brackish water (21.2 %).

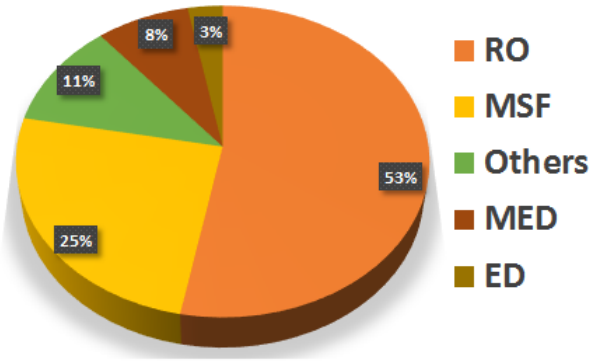

Figure 8.1. The global capacity of different desalination processes [2]; ED: Electrodialysis.

RE can be integrated with membrane processes of potential interest for industrial desalination in order to increase the overall performance of the process through the exploitation of the electrochemical potential of the highly concentrated discharge (brine).

This work presents energetic and exegetic analysis of integrated application of three membrane based processes; two of which (reverse osmosis and membrane distillation) target pure water production, and the third (RE) target energy recovery from concentrated brine obtained as an output from desalination plants. Conceptual illustration of the processes is presented in Figure 8.2. Partial energy recovery by the use of one or more RE units is considered in the present study to approach a

sustainable desalination process. In this way, environmental problems related to excessive brine discharge into natural water bodies is also prevented.

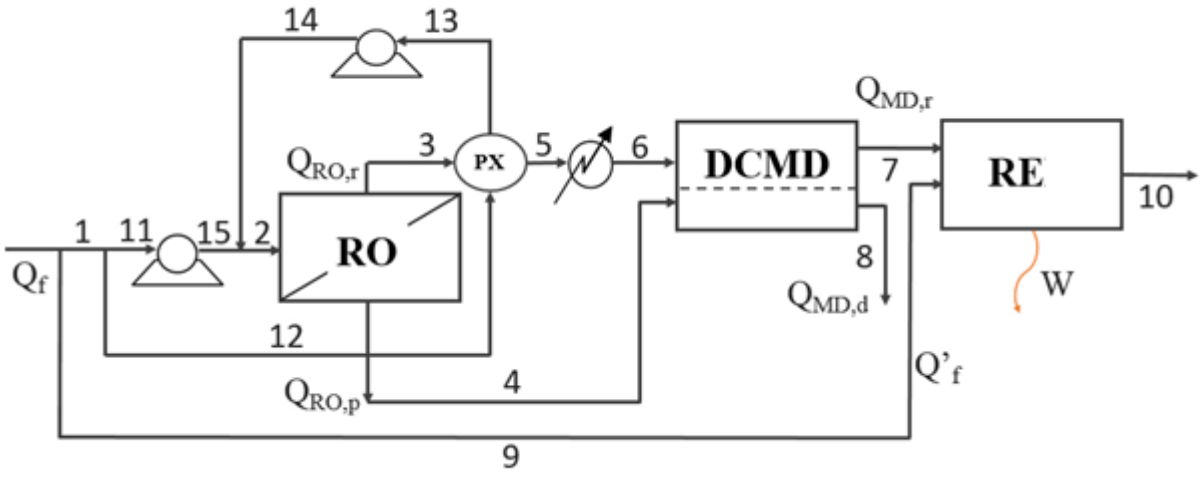

Figure 8.2. Scheme of an integrated membrane desalination processes with recovery of energy from concentrated brine using reverse electrodialysis.

8.1.1 System Description

Nowadays, the most interesting developments for industrial membrane technologies involve the possibility of integrating various membrane operations in the logic of process intensification. In this way, there is a possibility to implement hybrid application of the desalination processes to harness all the benefits[3]. The scheme presented in Figure 8.2 is a typical hybrid application of membrane based processes beyond water production, thereby introducing a processes for energy extraction like RE.

The principle of RO is illustrated in Figure 8.3. A salt solution containing low molecular weight component is separated from a solvent by a semi-permeable membrane. The application of a hydrostatic pressure difference across the membrane results in a flux of solvent. A fairly high pressure (55 to 68 bar for seawater desalination) is applied to overcome the osmotic pressure on the feed side [4]. The process doesn't require heating or water phase change. RO is relatively simple process and modules can be readily replaced. The advantage involves compactness due to the use of feed in liquid phase and hydrostatic pressure as an energy source [5]. The main success in RO is the development of customized pretreatment for increased membrane lifetime [6]. The development of new membrane material, module and process design are among the research trends [7].

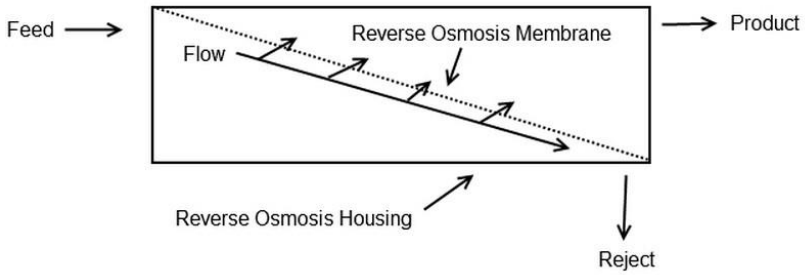

Figure 8.3. Illustration of the principle of RO process.

The reliability of RO has greatly increased as it can be combined with other processes like microfiltration (MF), ultrafiltration (UF) and nanofiltration (NF) as a pre-treatment steps. In this way, it's possible to remove suspended solids, bacteria, dissolved macromolecules, and reduce the SDI (Silt Density Index). This minimizes the fouling potential and allows the units to work with higher recovery factors thereby reducing the frequencies of cleaning and replacement of membranes.

Direct Contact Membrane Distillation (DCMD) is a simple and low cost emerging technology which is the mostly used for desalination of seawater and brackish waters [8-12]. The principle of DCMD is show in Figure 8.4. In this process, a water molecule evaporates from the hot feed solution to the cold distillate water stream separated by microporous hydrophobic membranes. Condensation of volatile molecules takes places inside the membrane module resulting in a highly concentrated hot brine as a retentate and pure water as permeate. The driving force for the mass transfer is the vapor pressure difference across the membrane. Theoretically, non-volatile substances are 100% rejected. High quality distillate, simple pre-treatment step and low temperature requirement makes DCMD an attractive desalination process, especially where low-grade thermal energy or solar heat sources are available.

DCMD can potentially be integrated with RO in the logic of process intensification. RO brine can be concentrated by DCMD to produce a hypersaline distillate (up to 5.4 M), which can be further be used as a feed in RE for power generation.

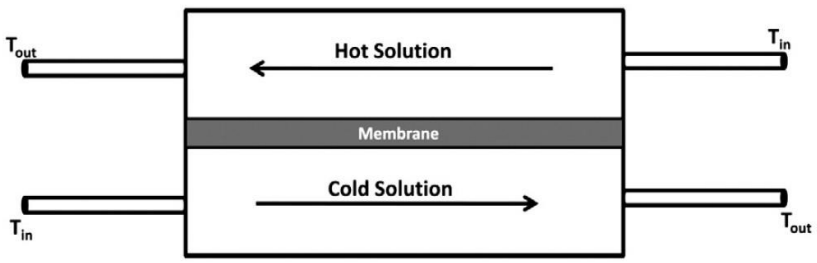

Figure 8.4. Illustration of DCMD.

8.1.2 Energy and Exergy: theory

From thermodynamic point of view, the total energy is conserved. Thus, the input and output energy should be balanced. The total energy of a system is considered as the sum of two contributions: i) the exergy which gives the maximum work that can be distracted from the system when it is brought to a thermodynamic equilibrium state from a reference state, and ii) the anergy which is degraded completely in the form of heat into the environment [3, 13].

Underlying the concept of exergy is the fact that, when two systems with different physical states are placed in connection, work is done to achieve a state of equilibrium. The exergy is the work of a theoretical maximum obtainable from the interaction between the two systems.

Exergy is the work that could be obtained when the system is brought reversibly to a state of equilibrium (mechanical, thermal, chemical) with the environment. The concept of work is considered to form a qualitatively superior form of energy (compared to heat) and optimal thermodynamic efficiency tends to match the process.

The reference is essentially represented by a system that remains in a state of thermodynamic equilibrium. A simple example of system at a standard state is given by atmospheric air having a temperature and pressure which is practically constant. A system which is not at a standard state has a varying extensive parameters (U, S, V), but not an intensive parameters (T, P). If the state of a defined thermodynamic system is different from that of the system which is not at a standard state, interaction of the two systems results in a work done until it reaches an equilibrium. At this state, the temperature and pressure remains constant, so the there is no exergy from the system.
The exergy for a fluid stream is defined mathematically by the following equation [3]:

$$E_x = G\left[c_p(T - T_o) - c_p T_o ln\left(\frac{T}{T_o}\right) + \frac{(P-P_o)}{\rho} - N_s R T_o ln\gamma x_i\right] = E_x^T - E_x^P - E_x^c \quad (8.1)$$

where E_x is the exergy which can be positive or negative, G is the mass flow rate, c_p is the specific heat of solution, and the subscript $_o$ indicates the reference state for the system considered which is a pure water at T_o and P_o. The number of moles of solvent per mass unit of solution (N_s) is given by;

$$N_s = \frac{1000 - \sum\frac{c_i}{\rho}}{MW_s} \quad (8.2)$$

and the mole fraction of the solvent x_1

$$x_1 = \frac{N_s}{\left[N_s - \sum\left(\frac{\beta_i c_i}{\rho MW_i}\right)\right]} \quad (8.3)$$

where β_i is the number of particles generated by dissociation of a species i, ρ is density of liquid solution, c_i is mass concentration of the i-th chemical component per liter of solution; MW_s, MW_i is

the molecular weight of the solvent and the *i*-th chemical component, respectively.

Based on the second law of thermodynamics, the exergentic balance can be described as:

$$\Delta E_{x,i} = -T_o R_s + W_U + W_U' \tag{8.4}$$

where R_s is the speed of entropy production, and $T_o R_s$ represents the total exergy lost in the form of entropy. The exergy variation between the inlet and outlet streams is given as;

$$\Delta E_x = \sum_i E_{x,i} - \sum_k E_{x,k} \tag{8.5}$$

Electrical exergy (E_{el}) is given by the following equation;

$$E_{el} = E \cdot 3600 \tag{8.6}$$

The thermal energy supplied to the system $W_{U,t}$ is given by;

$$W_{U,t} = G_V \left[(h_V - h_c) - T_o (s_v - s_c \right] \tag{8.7}$$

Where G_V is the required stream mass flow rate which can described as;

$$G_V = \frac{Q}{\lambda_V} \tag{8.8}$$

where Q is the heat required to warm-up the fluid G from temperature T_1 to temperature T_2, calculated as;

$$Q = G \cdot c_p \cdot (T_2 - T_1) \tag{8.9}$$

The energy supplied by a fuel combustion to produce thermal energy (*PE*) is termed as the primary energy E_p, and is calculated as;

$$E_p = G_V \cdot 0.8 \tag{8.10}$$

The use of exergetic analysis is beneficial in improving the performance of desalination processes through identification of the units in which more exegetic lost. Previous studies indicate that most of the exergy destruction occur on pump/motor, throttling valves where the pressure of liquid is reduced and the separation units; in RO over the membrane module where the separation of water as a permeate from salt solution remaining as a brine retentate [3, 13]. Although these exergy loss cannot be avoided, there is a possibility to reduce the input power by using energy recovery systems like pressure exchangers (PX). In this way it is possible to recover the pressure over the brine at the outlet of the module leading to the reduction in energy consumption of the plant.

8.2 Experimental

8.2.1 Energy recovery by reverse electrodialysis

The RE stack used is described elsewhere [14, 15]. The stack operating in cross-flow configuration was provided by REDstack B.V (The Netherlands), consisted of membranes with an effective area of 0.01m^2 (10 cm x 10 cm) and 25 cell pairs and PET spacers (Deukum GMBH, Germany) of thickness 270 µm . Electrodes used were made of inert Ti-Ru/Ir mesh with dimension of 10cm×10cm (MAGNETO Special Anodes B.V., The Netherlands). All experiments were carried out at 20°C.

Ion Exchange Membranes (IEM) used were supplied by Fujifilm Manufacturing Europe B.V (The Netherlands). Membrane characteristics are described elsewhere [16].

The electrolyte solution used was composed of a solution of 0.3 M $K_4Fe(CN)_6$, 0.3 M $K_3Fe(CN)_6$ and 2.5 M NaCl (chemicals from Sigma-Aldrich S.r.l., Italy) in de-ionized water (PURELAB, Elga LabWater®, 0.055 uS/cm). The solution was recirculated in the electrolytic compartments at 30 L/h by Masterflex L/S digital peristaltic pumps (Cole-Palmer, US).

The SGP potential of different combination of salt solutions (obtained as discharge of desalination systems and/or from natural resources) was determined at different at two different scenarios: I) LCC//HCC mimicking RO brine//seawater, brackish water, II) LCC//HCC mimicking MD brine//RO brine, seawater, brackish water. Table 8.1 shows the different scenarios followed for experimental test of SGP-RE system. Each feed solution was recirculated in a volume of 10 L. The temperature of the HCC was varied anticipating the thermal variations of the hot brine from MD.

Table 8.1. Experimental tests performed with different feed solutions

<table>
<tr><th rowspan="2">Scenario</th><th colspan="3">NaCl concentrations (M)</th><th rowspan="2">Temperatures</th></tr>
<tr><th colspan="2">HCC</th><th>LCC</th></tr>
<tr><td rowspan="2">I</td><td rowspan="2">RO brine</td><td rowspan="2">1</td><td>0.1*</td><td rowspan="5">20 - 60 ºC</td></tr>
<tr><td>0.5</td></tr>
<tr><td rowspan="3">II</td><td rowspan="3">MD brine</td><td>2</td><td rowspan="3">0.5</td></tr>
<tr><td>3</td></tr>
<tr><td>4</td></tr>
<tr><td></td><td></td><td>5</td><td></td><td></td></tr>
</table>

*Experiments performed only at 20 ºC feed concentrations

Performance evaluation was done by loading the SGP-RE system with a high dissipation five decade resistance box in the range of 0.1-1000 Ω (CROPICO, Bracken Hill, US), and measuring the DC voltage drop across the load resistors by a 3½ digital multimeter with accuracy of ±0.5% in the range of range 200 mV-200 V (Valleman, DVM760). Besides, the current flowing across the load resistors was measured by Agilent 34422A 6½ Digit Multimeter. The performance of SGP-RE unit was evaluated by the parameters voltage (V), current (I) and power density (P_d). The experimental points V vs I were fitted by a straight line having equation:

$$V(I) = OCV - R_{stack} \cdot I \tag{8.11}$$

where OCV is Open Circuit Voltage is the voltage measured at zero current and R_{stack} is the stack resistance (the slope of I-V curve). The shortcut current $I_{shortcut}$ is given by the intercept of $V(I)$ with the current axis (V=0) represents. The calculated electric power density P_d plotted against the current density i shows a typical parabolic trend.

8.3 Result and discussion

8.3.1 SGP-RE performance

8.3.1.1 Effect of Concentration

Figure 8.5 presents the variation of the voltage with respect to current for the two experimental scenarios. When 1 M//0.5 M NaCl solutions is used to feed the SGP-RE, an OCV of 0.7 V was recorded (the least among the experimental scenarios). As shown in Figure 6a, Reduction of the LCC by 5-fold (0.1 M NaCl) results 68 % and 53 % enhancement of OCV (from 0.7 V to 2.2 V) and $I_{shortcut}$ (from 0.17 A to 0.36 A). A maximum OCV (3.08 V) was obtained when working with 0.5 M NaCl//5 M NaCl. Under similar condition, OCV and $I_{shortcut}$ increases by 18.5 % and 26.7 % (on average), respectively, per 1 M increase of HCC concentration (see Figure 8.6b).

The variation in OCV has a direct influence on the power obtained from RE and hence the overall stack performance. Figure 8.6 shows the parabolic power curves obtained for the SGP-RE tested under different experimental scenarios. About 0.12 W/m$^2_{MP}$ (MP: membrane pair) of $P_{d,max}$ was obtained when working with 1 M//0.5 M NaCl solutions which increases by about 6-fold (0.78 W/m$^2_{MP)}$ when reducing the LCC concentration down to 0.1 M NaCl (see Figure 8.6a). Under the considered experimental scenarios, the highest $P_{d,max}$ (2.26 W/m$^2_{MP}$ corresponding to i_{max} of 37.4 A/m^2) was obtained when feeding the SGP-RE stack with 5 M // 0.1 M NaCl solutions (see Figure 8.6b). In this case, when the LCC concentration was increased by 5-fold (0.5 M NaCl), the $P_{d,max}$ dropped significantly (almost by -50% down to 1.12 W/m$^2_{MP}$) whereas i_{max} reduced by 22% (down

to 22.2 A/m^2). On average, $P_{d,max}$ almost doubles for 1 M increase in HCC concentration in the range of 2-5 M NaCl (LCC: 0.5 M NaCl).

The observed trend in OCV and $P_{d,max}$ is almost similar to our previous investigations using different LCC and HCC feed solutions [14, 15]. Both parameters are enhanced by working with hypersaline solution like MD brine which allows the reduction of Ohmic losses. In this sense, pre-concentration of RO brines by MD before use for energy recovery by RE is advantageous in order to achieve low energy desalination. Although the performance of SGP-RE performance can be enhanced by using highly concentrated solutions, the adverse effect of brine on membrane permselectivity and long term stability need to be optimized [17].

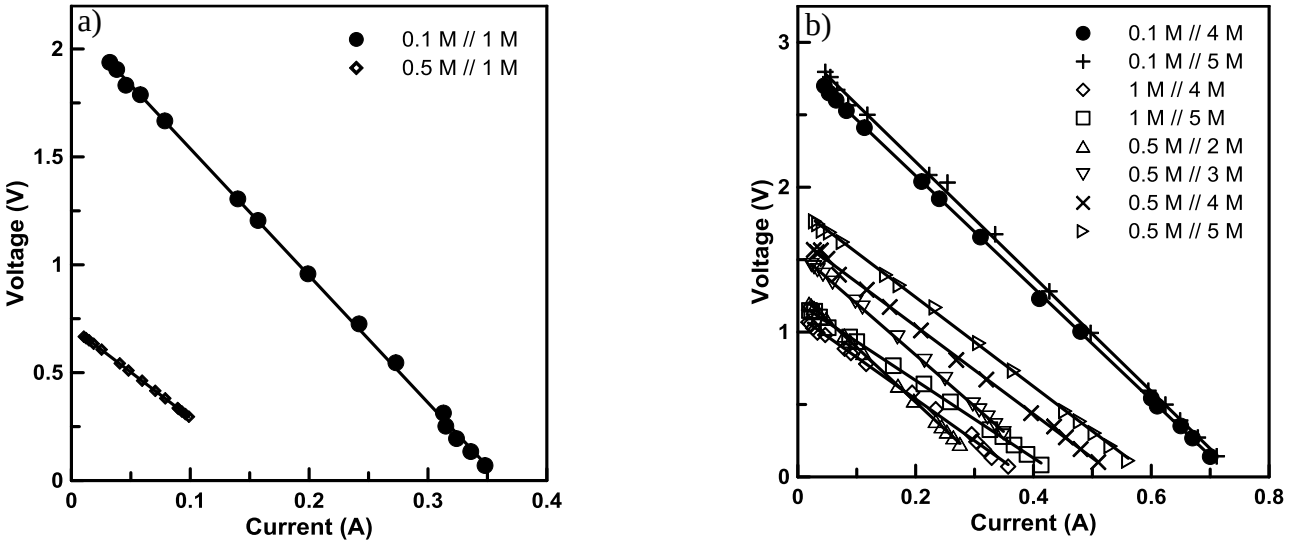

Figure 8.5. Voltage current curves for for different LCC//HCC concentrations mimicking a) seawater and brackish water with RO brine, b) RO brine, brackish water and seawater with MD brine (20 ^{o}C).

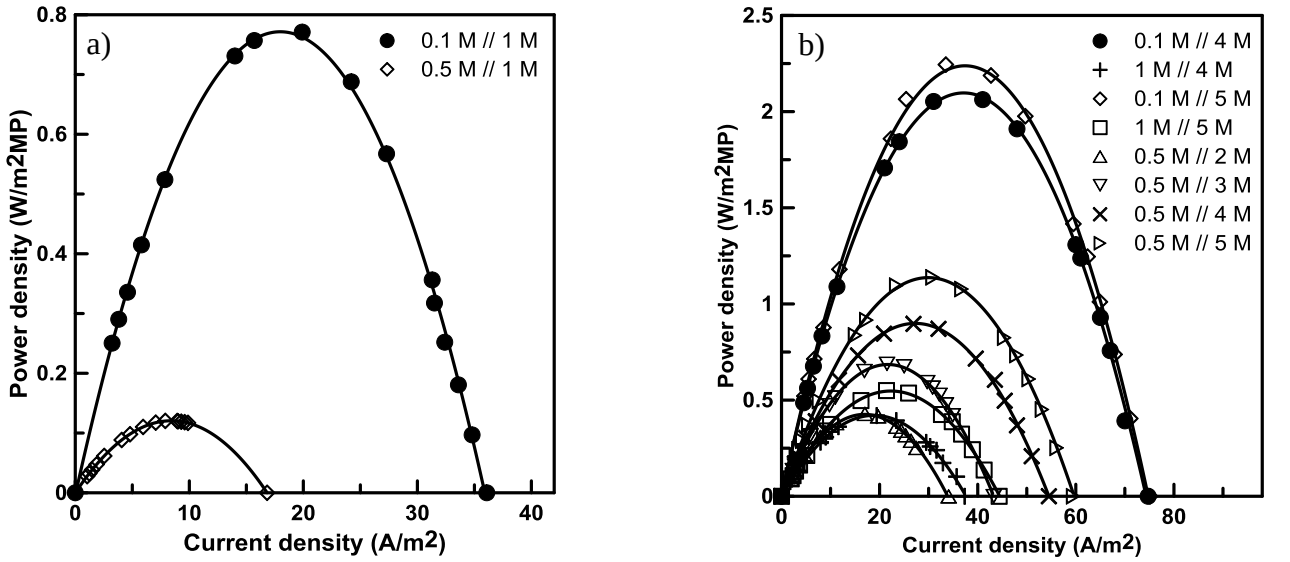

Figure 8.6. Power curves for for different LCC//HCC concentrations mimicking a) seawater and brackish water with RO brine, b) RO brine, brackish water and seawater with MD brine; experiments at 20 ^{o}C.

8.3.1.2 Effect of temperature

The temperature of the brine for MD to be used as an HCC for RE depends on the temperature of the inlet feed. The performance of the RE also varies depending on temperature which has a huge impact on ionic mobility and membrane resistivity. Figure 8.7 shows the I-V curves for RE at different HCC temperatures (40-60 ^{o}C). Results indicate that the effect of HCC temperature on OCV is not remarkable: The variation in OCV falls in the range of 2-15 % for the tested feed combinations when over the temperature range of 20 - 50 ^{o}C. The maximum OCV obtained was 1.95 V (corresponding to $I_{shortcut}$ = 1.17 A) at 60 ^{o}C when working with 0.5 M//5 M NaCl solutions. However, a significant increment of $I_{shortcut}$ was observed (+95-117 %) when the feed HCC temperature changes from 20 ^{o}C to 60 ^{o}C. Similarly, a notable enhancement of $P_{d,max}$ was observed unlike OCV: For 0.5 M//5 M NaCl solutions, increasing the feed HCC temperature from 20 ^{o}C to 60 ^{o}C resulted in 151 % enhancement of $P_{d,max}$ (2.19 W/m$^2_{MP}$), with current density increasing proportionally from 29 A/cm^2 to 56 A/cm^2 (see Figure 8.8). Under this condition, $P_{d,max}$ varies increases at a rate of 0.028 W/m$^2_{MP}$/^{o}C rise of HCC temperature. A linear trend between $I_{shortcut}$ and HCC temperature was observed with a slope of 0.027 A/^{o}C, quite higher than our result (0.017 A/^{o}C) from study on RE operated with MD brine and seawater [14].

The remarkable change in $P_{d,max}$ with the rise of HCC temperature irrespective of the stability in OCV is attributed to the reduction Ohmic losses. Higher HCC temperature facilitates ionic mobility while lowering the membrane resistivity with an overall enhancement $P_{d,max}$. However, too high temperature have a negative impact on the process efficiency due to the rise in $I_{shortcut}$ [17]. In addition, the cost of energy input need to be optimized when working at extreme temperature.

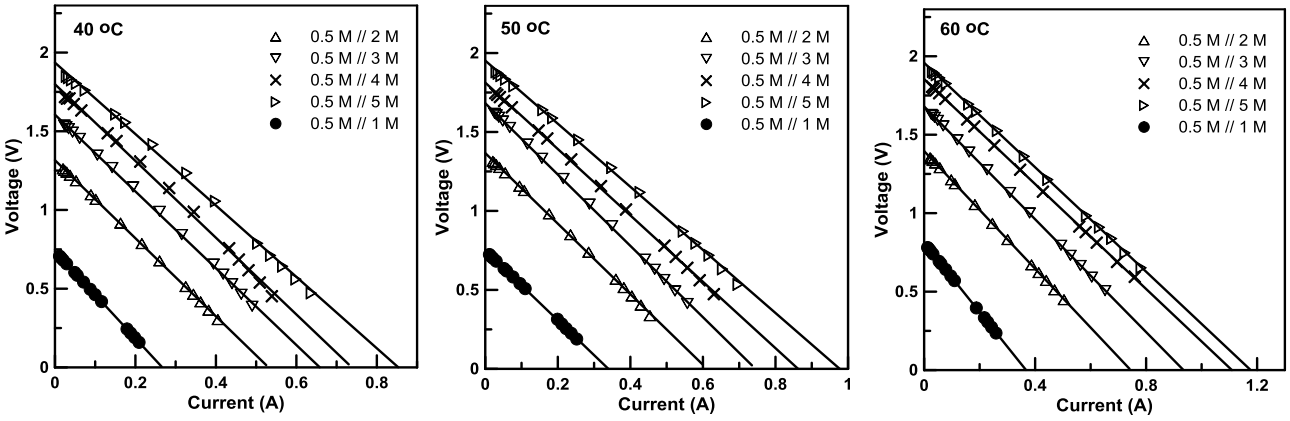

Figure 8.7. Power curves for RE operated with different LCC//HCC concentrations mimicking seawater and MD brine at different temperature (40 ^{o}C, 50 ^{o}C, 60 ^{o}C).

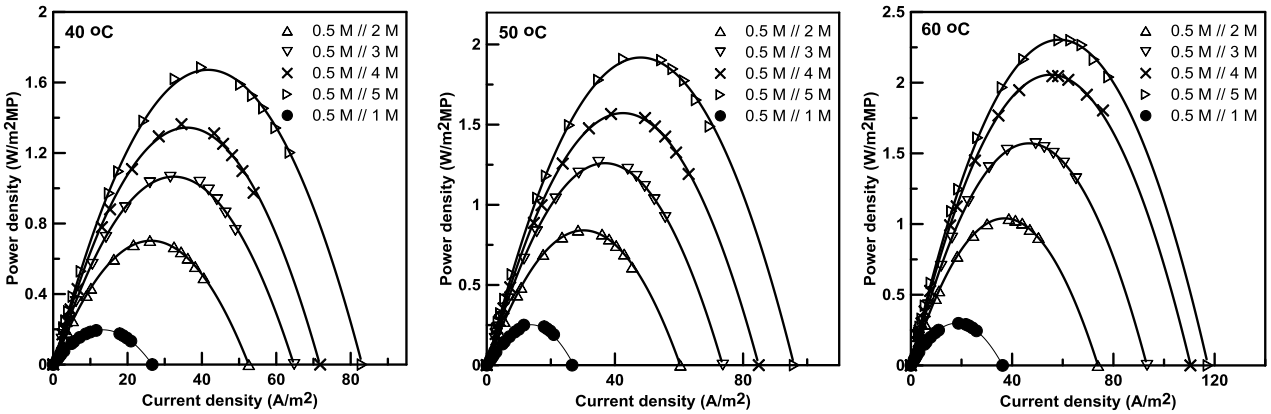

Figure 8.8. Power curves for RE operated with different LCC//HCC concentrations mimicking seawater and MD brine at different temperature (40 ºC, 50 ºC, 60 ºC).

8.3.1.3 Effect of flow velocity

Flow velocity has a direct impact on the OCV and the power density as it affect the mass transfer over the feeds along the SGP channel. At high feed velocity, efficient mixing of feed solutions in the SGP channel is maintained which enhances the local electromotive force over the membrane and increases the output power. Moreover, improvement in the hydrodynamic distribution is deemed to reduce the effect of concentration polarization at the boundary layer along the membrane-solution interface. The reduction of diffusion boundary layer resistance by increasing flow velocity due to enhanced mixing have been demonstrated in literatures [16, 18]. This has a direct impact on the output power and OCV of RE. Our recent investigation shows that the gross power density and OCV can be increased by 47% and 35%, respectively, when increasing the flow velocity from 0.7 to 1.1 cm/s [19]. However, an increase in flow velocity is accompanied by higher pumping energy required to recirculate feed solutions with a lowering effect on the net power density. At flow velocity 0.7 cm/s, the hydrodynamic losses accounted for about 23 % of the power density which was raised to 39 % when the flow velocity was increased to 1.1 cm/s [19]. Therefore, optimization is required to identify the optimal condition to balance the benefit obtained from high flow velocity and cost of input energy.

8.3.2 Stack resistance

The variation in concentration of the brine retentate (HCC) coming from MD and LCC concentrations strongly influences the Internal Area Resistance (IAR) per cell of the SGP-RE stack. Figure 8.9 presents the contour plot of IAR for a varying concentration of both HCC and LCC concentrations. In general, the use of hypersaline solution has an advantage in terms of reduction of Ohmic losses [15, 20]. When using LCC of 0.5 M NaCl, up to 27.5 % reduction (from 16.8 Ωcm^2 to 12.2 Ωcm^2) in terms of IAR per cell was observed when increasing the HCC concentration by 5-fold (from 1 M NaCl to 5 M NaCl). On average, the IAR per cell declines at a rate of 9.8 Ωcm^2 per 1 M increase of HCC concentration in the range of 1- 5 M. This is comparable to our previous investigation

which demonstrating a 10% reduction of OAR per cell for an increase of HCC concentration from 4 to 5.4 M [19]. The IAR decrement can be correlated with the rise in feed and membrane conductivity for higher feed concentrations.

Table 8.3 shows the variation of IAR with HCC temperature. For experiments with 0.5 M // 1 M NaCl solutions, IAR per cell reduced by 47 % (from 16.8 Ωcm^2 to 8.84 Ωcm^2) when increasing the HCC temperature from 20 ^oC to 50 ^oC corresponding to decrement rate of 0.2 $\Omega cm^2/°C$. Low decrement rate (0.13 $\Omega cm^2/°C$) was observed at high HCC concentration (5 M NaCl) with an overall reduction of internal resistance by 45 % (from 12.1 to 6.6 $\Omega cm^2/°C$) when the HCC temperature is raised from 20 ^oC to 50 ^oC.

The general trend is a reduction of Ohmic losses with the rise of HCC temperature. It has been observed that an increase in feed temperature reduces the ion transport resistance through the membrane and the interface by facilitation of ionic transport [16]. In addition, membrane resistance lowers when working with feeds at high temperatures. The overall effect is benefit gained items of output power from SGP-RE system at high HCC temperature. However, this is achieved at the cost of high energy input which requires thermo-economic optimization.

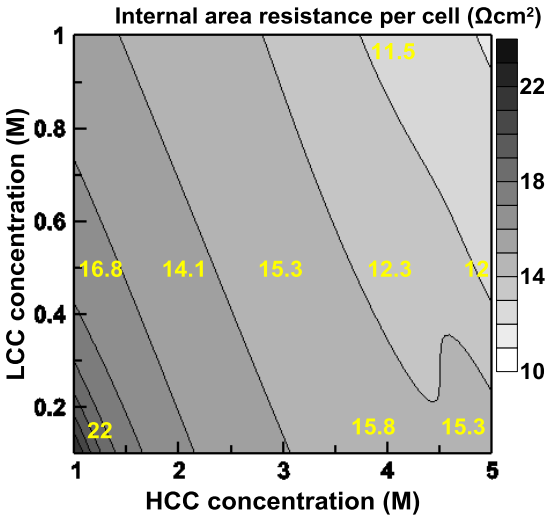

Figure 8.5. Contour plot of internal area resistance for feed concentrations in the considered experimental range; HCC: 1-5 M and LCC: 0.1-1 M.

Table 8.3. Variations of internal area resistance with temperatures (20 - 60 ºC)

Scenario	NaCl concentrations (M)			IAR per cell (Ωcm^2) at different temperatures			
	HCC		LCC	20 ºC	40 ºC	50 ºC	60 ºC
I	RO brine	1	0.5	16.8	11.08	8.84	8.84
II	MD brine	2	0.5	15.12	9.92	8.92	7.48
		3		14.16	9.68	8.64	7.20
		4		12.32	9.76	8.4	6.68
		5		12.12	9.08	8.00	6.64

8.3.3 Energy and exergy analysis

A representative diagram for the energetic analysis of the integrated approach is already presented in Figure 8.1. The main elements that make up the system are RO unit, DCMD unit and RE unit for energy recovery. In RO process, the concentrated brine in the exit from the system can pass through the PX where pressure is transferred directly to a portion of input power at an efficiency of up to 91 %. The input energy can be further be reduced by recovering the electrochemical potential of MD and/or RO brine using RE.

Table 8.1 presents the operational conditions and mass balance at different feed flow rates. Mass balance for the system under investigation was carried out at a maximum flow rate of 1000 m^3/h. Similar operation is carried out for the RE at three different temperature considered for the different pairs of feed solution (see Appendix 8.1 Table A.8.1.1-A.8.1.1).

Table 8.1. Operational conditions and material balance for the employed process at T = 60 ºC, concentrations 0.5 M - 5 M for running RE.

No	T (K)	*P*	*G (kg/h)*	*G'*(m^3//h)	M_{NaCl} (mol/L)	c_i
1	298	1	$1.03x10^6$	1000	0.5	0.0294
2	303	60	$1.03x10^6$	1000	0.5	0.0294
3	303	60	$5.30x10^5$	500	1	0.0588
4	303	1	$5.00x10^5$	500	0	0.000
5	303	1	$5.30x10^5$	500	1	0.0588
6	335	1	$5.30x10^5$	500	1	0.0588
7	333	1	$1.30x10^5$	100	5	0.2940
8	305	1	$9.00x10^5$	900	0	0.000
9	298	1	$1.03x10^5$	100	0.5	0.0294
10	315.5	1	$2.34x10^5$	200	2.75	0.1617
11	298	1	$6.70x10^5$	650	0.5	0.0294
12	298	1	$3.61x10^5$	350	0.5	0.0294
13	300	55.2	$3.61x10^5$	350	0.5	0.0294
14	303	60	$3.61x10^5$	350	0.5	0.0294
15	303	60	$6.70x10^5$	650	0.5	0.0294

Table 8.2 presents the results obtained from exergetic analysis of an integrated application of RE used for energy recovery from brine solutions at different HCC concentrations. Electrical power per m^3 of desalted water was determined for three cases; i) in the presence of pressure exchanger, ii) absence of pressure exchanger and iii) the combination of the pressure exchanger and RE module.

Table 8.2. Results from exergetic analysis for different concentrations of brine used for energy recovery by means of RE unit operating at a temperature of 60 ^oC.

	0.5 M-2 M NaCl	0.5 M-3 M NaCl	0. 5M-4 M NaCl	0.5 M-5 M NaCl
ΔE_x (kJ/h)	$-2.20x10^6$	$-1.49 x10^6$	$-1.12x10^6$	$8.71x10^5$
E_{el} (kWh/h)[a]	1390	1390	1390	1390
E_{el} (kWh/h)[b]	2049	2049	2049	2049
E_{el} (kWh/h)[c]	1313	1290	1277	1270
$_{WU}$ (kJ/h)[a]	$5.00x10^6$	$5.00 x10^6$	$5.00x10^6$	$5.00x10^6$
$_{WU}$ (kJ/h)[b]	$7.38x10^6$	$7.38 x10^6$	$7.38x10^6$	$7.38x10^6$
$_{WU}$ (kJ/h)[c]	$4.73x10^6$	$4.65 x10^6$	$4.60x10^6$	$4.58x10^6$
Q (kJ/h)	$6.79x10^6$	$6.79x10^7$	$6.79x10^7$	$6.79x10^7$
G_v (kWh/h)	30138	30138	30138	30138
$W_{U,t}$ (kWh/h)	$1.37x10^6$	$1.37 x10^6$	$1.37 x10^6$	$1.37x10^6$
T_oR_s (kJ/h)[a]	$2.09x10^7$	$2.02x10^7$	$1.98x10^7$	$1.96x10^7$
T_oR_s (kJ/h)[b]	$2.33x10^7$	$2.26x10^7$	$2.22x10^7$	$1.83x10^7$
T_oR_s (kJ/h)[c]	$1.84x10^7$	$1.83x10^7$	$1.83x10^7$	$1.83x10^7$

[a]With PX, [b]without PX and [c]PX and RE.

In general there is a reduction of the term representing exergy destruction. All the results from the exergy analysis at other temperatures can be referred to Appendix (Table A.8.12 and Table A.8.13).

It is important to note that in the process of thermodynamic optimization, analysis should be related to the conservation of exergy, not the anergy, which (by the first law of thermodynamics) is not lost, but transformed. From a technical point of view, it's valuable if the greater part is potentially convertible to the mechanical work. In particular, a process is optimal from the thermodynamic point of view if it does not involve the destruction of exergy. Of course, since all real processes always involve consumption of exergy, the best processes will be the one characterized by lower consumption of exergy.

Figure 8.5 presents the recovery factor for DCMD for different concentration of distillate (brine). The highest concentration DCMD brine (5M) is obtained at a recovery factor of 90 %, whereas only 2 M DCMD brine is obtained at the recovery factor of 75 %.

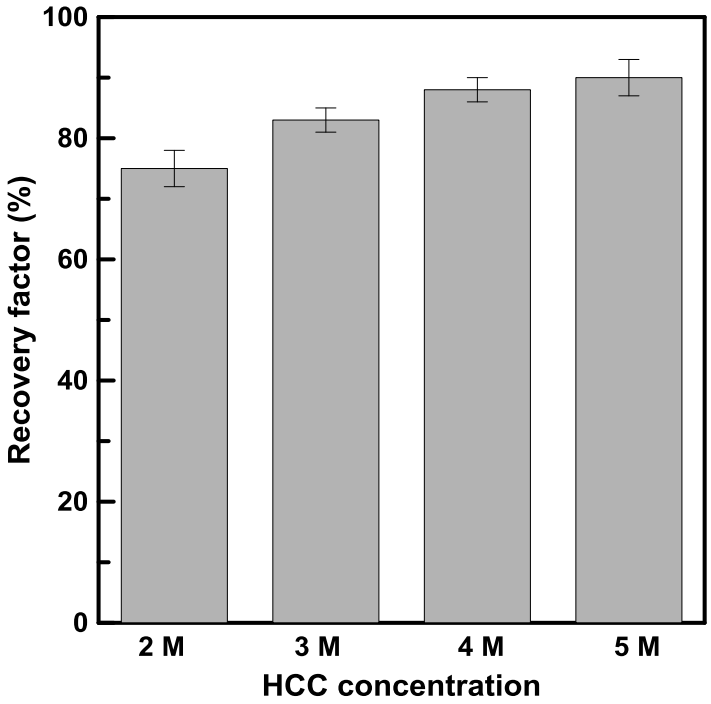

Figure 8.5. Trends in the variation of the recovery factor of desalted water for different concentration of the DCMD retentate (brine).

The variation of the electrical power required per cubic meter (E_e) of desalinated water is presented in Figure 8.6. In general, the required electrical power decreases with the increase of the HCC concentration. The introduction of PX reduces the values further, which even decreases more when RE is used in the system. In the presence of PX, E_e was obtained as 1.85 kWh/m^3 for 2 M HCC concentration which drops by 17.5 % when the HCC concentration is increased to 5 M NaCl solution. In general, exergy determination without PX shows high E_e; the values determined fall in the range of 2.28-2.73 kWh/m^3 for all HCC concentration of 2-5 M NaCl. In the presence of both PX and RE, E_e reaches 1.75 kWh/m^3 at 2 M NaCl of HCC which reduces by 18.8 % when the HCC concentration increases to 5 M. The E_e obtained at different concentrations for the case with both PX and RE were up to 5-8 % lower that the case with only PX. This indicate that the optimum condition is the use of greater concentration of HCC in the presence of PX than the RE module, although the benefit from RE is not remarkable at this stage. Further optimization RE is required for a better energy recovery.

The temperature of DCMD brine supply depends on the temperature of inlet feed. So the temperature of HCC increases proportionally with DCMD inlet temperature. Besides, the output power from RE can be enhanced by increasing the HCC temperature as described earlier. However, working with higher temperatures require greater amount of thermal energy for warming up feed solutions. In fact, the required thermal energy to warm up feed solutions increases with rising

temperature (see Figure 8.7). On average, the required thermal energy increases at a rate of 2.1 GJ/ºC with the rise in HCC temperature. This should be compromised with the output power from obtained by RE at a specific HCC temperature.

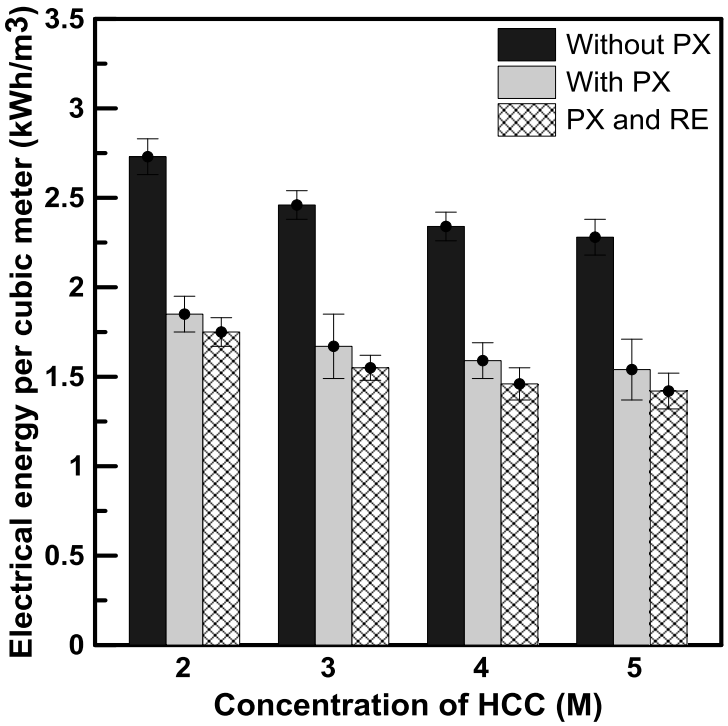

Figure 8.6. Electric energy per cubic meter of desalted water for different concentration of HCC Solution (2-5 M NaCl); LCC: 0.5 M NaCl.

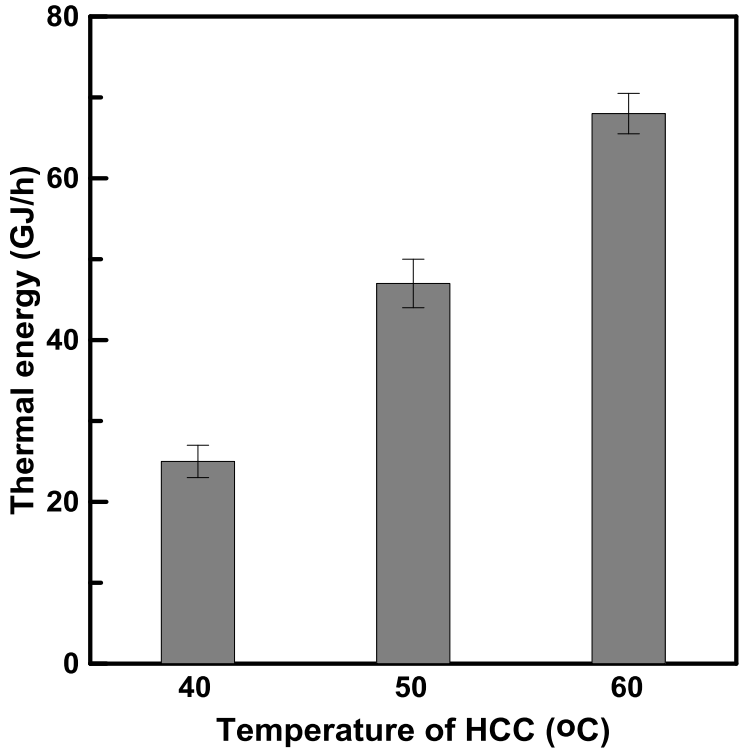

Figure 8.7. Thermal energy required to heat the HCC solutions for different temperatures LCC: 0.5 M NaCl.

8.4 Conclusion

Integrate application of Reverse Electrodialysis in SWRO practice is a promising approach towards a low energy desalination. As demonstrated in the present study, the use of SGP-RE can potentially generate up to 2.3 W/m^2_{MP} at 20 ^oC using 0.1 M // 5 M NaCl solutions mimicking brackish water and DCMD brine. Results from exegetic analysis indicate the advantage of using of SGP-RE leads to reduction in energy consumption of desalination plants. Besides, the use of PX is an alternative approach to recover the pressure over the brine solution at the outlet of the module.

Comparative assessment in the use of standalone and combined application of RE and PX show that the optimal condition is the combined application of both energy recovery systems at high HCC concentration and temperature. It was possible to reduce the electrical exergy by 39% (from 2.3 to 1.4 kWh/m^3) when using PX and SGP-RE fed with 0.5 M // 5 M NaCl at HCC temperature of 60 ^oC.

At this stage, the energy from a standalone RE is not sufficient requiring further optimization of the technology. Highly performance membranes (good permeability and low resistance) at an affordable cost is needed. In addition, the development of fouling resistant and stable ion exchange membrane in hot brine is essential for integrated application of RE with desalination technologies.

Alternative approaches to achieve the low energy desalination target involve the use of other renewable energy sources like solar thermal energy or waste heat at the DCMD stage. This can be combined with the SGP-RE unit to recover the energy from concentrated brine to reduce the overall energy demand of the integrated process. Eventually, cascading RE to recover energy from brine at each outlet is also possible.

For large scale implementation of RE in desalination technologies, optimal conditions need to be identified through extensive economic analysis and cost optimization. The benefits obtained at conditions for enhancing the process performance and high cost of input energy need further optimization to set a threshold values for technology commercialization.

References

[1] E. Curcio, G.D. Profio, E. Fontananova, E. Drioli, 13 - Membrane technologies for seawater desalination and brackish water treatment, in: A. Basile, A.C.K. Rastogi (Eds.) Advances in Membrane Technologies for Water Treatment, Woodhead Publishing, Oxford, 2015, pp. 411-441.
[2] T. Mezher, H. Fath, Z. Abbas, A. Khaled, Techno-economic assessment and environmental impacts of desalination technologies, Desalination, 266 (2011) 263-273.
[3] F. Macedonio, E. Curcio, E. Drioli, Integrated membrane systems for seawater desalination: energetic and exergetic analysis, economic evaluation, experimental study, Desalination, 203 (2007) 260-276.
[4] C. Fritzmann, J. Löwenberg, T. Wintgens, T. Melin, State-of-the-art of reverse osmosis desalination, Desalination, 216 (2007) 1-76.
[5] E. Drioli, L. Giorno, Comprehensive membrane science and engineering, Newnes, 2010.
[6] S. Jamaly, N. Darwish, I. Ahmed, S. Hasan, A short review on reverse osmosis pretreatment technologies, Desalination, 354 (2014) 30-38.
[7] R.A. Tufa, Perspectives on environmental ethics in sustainability of membrane based technologies for water and energy production, Environmental Technology & Innovation, 4 (2015) 182-193.

[8] D. Hou, G. Dai, J. Wang, H. Fan, Z. Luan, C. Fu, Boron removal and desalination from seawater by PVDF flat-sheet membrane through direct contact membrane distillation, Desalination, 326 (2013) 115-124.
[9] S.T. Hsu, K.T. Cheng, J.S. Chiou, Seawater desalination by direct contact membrane distillation, Desalination, 143 (2002) 279-287.
[10] E. Drioli, Y. Wu, V. Calabro, Membrane distillataion in the treatment of aqueous solutions, Journal of Membrane Science, 33 (1987) 277-284.
[11] B. Li, K.K. Sirkar, Novel Membrane and Device for Direct Contact Membrane Distillation-Based Desalination Process, Industrial & Engineering Chemistry Research, 43 (2004) 5300-5309.
[12] S. Al-Obaidani, E. Curcio, F. Macedonio, G. Di Profio, H. Al-Hinai, E. Drioli, Potential of membrane distillation in seawater desalination: Thermal efficiency, sensitivity study and cost estimation, Journal of Membrane Science, 323 (2008) 85-98.
[13] N. Kahraman, Y.A. Cengel, B. Wood, Y. Cerci, Exergy analysis of a combined RO, NF, andEDR desalination plant, Desalination, 171 (2005) 217-232.
[14] Ramato A. Tufa, E. Curcio, E. Brauns, W. van Baak, E. Fontananova, G. Di Profio, Membrane Distillation and Reverse Electrodialysis for Near-Zero Liquid Discharge and low energy seawater desalination, Journal of Membrane Science, 496 (2015) 325-333.
[15] R.A. Tufa, E. Curcio, W. van Baak, J. Veerman, S. Grasman, E. Fontananova, G. Di Profio, Potential of brackish water and brine for energy generation by salinity gradient power-reverse electrodialysis (SGP-RE), RSC Advances, 4 (2014) 42617-42623.
[16] E. Fontananova, W. Zhang, I. Nicotera, C. Simari, W. van Baak, G. Di Profio, E. Curcio, E. Drioli, Probing membrane and interface properties in concentrated electrolyte solutions, Journal of Membrane Science, 459 (2014) 177-189.
[17] A. Daniilidis, D.A. Vermaas, R. Herber, K. Nijmeijer, Experimentally obtainable energy from mixing river water, seawater or brines with reverse electrodialysis, Renewable Energy, 64 (2014) 123-131.
[18] P. Długołęcki, P. Ogonowski, S.J. Metz, M. Saakes, K. Nijmeijer, M. Wessling, On the resistances of membrane, diffusion boundary layer and double layer in ion exchange membrane transport, Journal of Membrane Science, 349 (2010) 369-379.
[19] R.A. Tufa, E. Curcio, E. Brauns, W. van Baak, E. Fontananova, G. Di Profio, Membrane distillation and reverse electrodialysis for near-zero liquid discharge and low energy seawater desalination, Journal of Membrane Science, (2015).
[20] E. Brauns, Salinity gradient power by reverse electrodialysis: effect of model parameters on electrical power output, Desalination, 237 (2009) 378-391.

Appendix 8.1

Table A.8.1.1 Operational Conditions and material budgets for the employed process at T = 40 °C, concentrations 0.5 M - 2 M an input to RE.

No	T (K)	P (bar)	G (kg/h)	G' (m^3/h)	M_{NaCl} (mol/L)	c_i (kg/L)
1	298	1	$1.03x10^6$	1000	0.5	0.029
2	303	60	$1.03x10^6$	1000	0.5	0.029
3	303	60	$5.30x10^5$	500	1	0.058
4	303	1	$5.00x10^5$	500	0	0.000
5	303	1	$5.30x10^5$	500	1	0.058
6	315	1	$5.30x10^5$	500	1	0.058
7	313	1	$2.80x10^5$	250	2	0.117
8	305	1	$7.50x10^5$	750	0	0.000
9	298	1	$2.58x10^5$	250	0.5	0.029
10	305.5	1	$5.38x10^5$	500	1.25	0.073
11	298	1	$6.70x10^5$	650	0.5	0.029
12	298	1	$3.61x10^5$	350	0.5	0.029
13	300	55.2	$3.61x10^5$	350	0.5	0.029
14	303	60	$3.61x10^5$	350	0.5	0.029
15	303	60	$6.70x10^5$	650	0.5	0.029

Table A.8.1.2 Operational Conditions and material budgets for the employed process at T = 40 °C, concentrations 0.5 M - 3 M an input to RE.

No	T (K)	P (bar)	G (kg/h)	G' (m3/h)	MNaCl (mol/L)	ci (kg/L)
1	298	1	1.03x106	1000	0.5	0.0294
2	303	60	1.03x106	1000	0.5	0.0294
3	303	60	5.30x105	500	1	0.0588
4	303	1	5.00x105	500	0	0.0000
5	303	1	5.30x105	500	1	0.0588
6	315	1	5.30x105	500	1	0.0588
7	313	1	2.80x105	250	3	0.1176
8	305	1	7.50x105	750	0	0.0000
9	298	1	2.58x105	250	0.5	0.0294
10	305.5	1	5.38x105	500	1.75	0.1029
11	298	1	6.70x105	650	0.5	0.0294
12	298	1	3.61x105	350	0.5	0.0294
13	300	55.2	3.61x105	350	0.5	0.0294
14	303	60	3.61x105	350	0.5	0.0294
15	303	60	6.70x105	650	0.5	0.0294

Table A.8.1.3 Operational Conditions and material budgets for the employed process at T = 40 ºC, concentrations 0.5 M - 4 M an input to RE.

No	T (K)	P (bar)	G (kg/h)	G' (m^3/h)	M_{NaCl} (mol/L)	c_i (kg/L)
1	298	1	$1.03x10^6$	1000	0.5	0.0294
2	303	60	$1.03x10^6$	1000	0.5	0.0294
3	303	60	$5.30x10^5$	500	1	0.0588
4	303	1	$5.00x10^5$	500	0	0.0000
5	303	1	$5.30x10^5$	500	1	0.0588
6	315	1	$5.30x10^5$	500	1	0.0588
7	313	1	$8.75x10^5$	150	3	0.2352
8	305	1	$7.50x10^5$	850	0	0.0000
9	298	1	$1.29x10^5$	150	0.5	0.0294
10	305.5	1	$2.84x10^5$	500	2.0	0.1029
11	298	1	$6.70x10^5$	650	0.5	0.0294
12	298	1	$3.61x10^5$	350	0.5	0.0294
13	300	55.2	$3.61x10^5$	350	0.5	0.0294
14	303	60	$3.61x10^5$	350	0.5	0.0294
15	303	60	$6.70x10^5$	650	0.5	0.0294

Table A.8.4 Operational Conditions and material budgets for the employed process at T = 40 ºC, concentrations 0.5 M - 5 M an input to RE.

No	T (K)	P (bar)	G (kg/h)	G' (m^3/h)	M_{NaCl} (mol/L)	c_i (kg/L)
1	298	1	$1.03x10^6$	1000	0.5	0.0294
2	303	60	$1.03x10^6$	1000	0.5	0.0294
3	303	60	$5.30x10^5$	500	1	0.0588
4	303	1	$5.00x10^5$	500	0	0.000
5	303	1	$5.30x10^5$	500	1	0.0588
6	315	1	$5.30x10^5$	500	1	0.0588
7	313	1	$1.30x10^5$	100	5	0.2940
8	305	1	$9.00x10^5$	900	0	0.000
9	298	1	$1.03x10^5$	100	0.5	0.0294
10	305.5	1	$2.34x10^5$	200	2.75	0.1617
11	298	1	$6.70x10^5$	650	0.5	0.0294
12	298	1	$3.61x10^5$	350	0.5	0.0294
13	300	55.2	$3.61x10^5$	350	0.5	0.0294
14	303	60	$3.61x10^5$	350	0.5	0.0294
15	303	60	$6.70x10^5$	650	0.5	0.0294

Table A.8.1.5 Operational Conditions and material budgets for the employed process at T = 50 ºC, concentrations 0.5 M - 2 M an input to RE.

No	T (K)	P (bar)	G (kg/h)	G' (m^3/h)	M_{NaCl} (mol/L)	c_i (kg/L)
1	298	1	$1.03x10^6$	1000	0.5	0.0294
2	303	60	$1.03x10^6$	1000	0.5	0.0294
3	303	60	$5.30x10^5$	500	1	0.0588
4	303	1	$5.00x10^5$	500	0	0.000
5	303	1	$5.30x10^5$	500	1	0.0588
6	325	1	$5.30x10^5$	500	1	0.0588
7	323	1	$2.80x10^5$	250	2	0.1176
8	305	1	$7.50x10^5$	750	0	0.000
9	298	1	$2.58x10^5$	250	0.5	0.0294
10	310.5	1	$5.38x10^5$	500	1.75	0.0735
11	298	1	$6.70x10^5$	650	0.5	0.0294
12	298	1	$3.61x10^5$	350	0.5	0.0294
13	300	55.2	$3.61x10^5$	350	0.5	0.0294
14	303	60	$3.61x10^5$	350	0.5	0.0294
15	303	60	$6.70x10^5$	650	0.5	0.0294

Table A.8.1.6 Operational Conditions and material budgets for the employed process at T = 50 ºC, concentrations 0.5 M - 3 M an input to RE.

No	T (K)	P (bar)	G (kg/h)	G' (m^3/h)	M_{NaCl} (mol/L)	c_i (kg/L)
1	298	1	$1.03x10^6$	1000	0.5	0.0294
2	303	60	$1.03x10^6$	1000	0.5	0.0294
3	303	60	$5.30x10^5$	500	1	0.0588
4	303	1	$5.00x10^5$	500	0	0.000
5	303	1	$5.30x10^5$	500	1	0.0588
6	325	1	$5.30x10^5$	500	1	0.0588
7	323	1	$1.97x10^5$	116.7	3	0.1764
8	305	1	$8.33x10^5$	833.3	0	0.0000
9	298	1	$1.72x10^5$	166.7	0.5	0.0294
10	310.5	1	$3.69x10^5$	333.3	1.75	0.1029
11	298	1	$6.70x10^5$	650	0.5	0.0294
12	298	1	$3.61x10^5$	350	0.5	0.0294
13	300	55.2	$3.61x10^5$	350	0.5	0.0294
14	303	60	$3.61x10^5$	350	0.5	0.0294
15	303	60	$6.70x10^5$	650	0.5	0.0294

Table A.8.1.7 Operational Conditions and material budgets for the employed process at T = 50 ºC, concentrations 0.5 M - 4 M an input to RE.

No	T (K)	P (bar)	G (kg/h)	G' (m^3/h)	M_{NaCl} (mol/L)	c_i (kg/L)
1	298	1	$1.03x10^6$	1000	0.5	0.0294
2	303	60	$1.03x10^6$	1000	0.5	0.0294
3	303	60	$5.30x10^5$	500	1	0.0588
4	303	1	$5.00x10^5$	500	0	0.000
5	303	1	$5.30x10^5$	500	1	0.0588
6	325	1	$5.30x10^5$	500	1	0.0588
7	323	1	$1.55x10^5$	125	4	0.2352
8	305	1	$8.75x10^5$	875	0	0.000
9	298	1	$1.29x10^5$	125	0.5	0.0294
10	310.5	1	$2.84x10^5$	250	2.25	0.1313
11	298	1	$6.70x10^5$	650	0.5	0.0294
12	298	1	$3.61x10^5$	350	0.5	0.0294
13	300	55.2	$3.61x10^5$	350	0.5	0.0294
14	303	60	$3.61x10^5$	350	0.5	0.0294
15	303	60	$6.70x10^5$	650	0.5	0.0294

Table A.8.1.8 Operational Conditions and material budgets for the employed process at T = 50 ºC, concentrations 0.5 M - 5 M an input to RE.

No	T (K)	P (bar)	G (kg/h)	G' (m^3/h)	M_{NaCl} (mol/L)	c_i (kg/L)
1	298	1	$1.03x10^6$	1000	0.5	0.0294
2	303	60	$1.03x10^6$	1000	0.5	0.0294
3	303	60	$5.30x10^5$	500	1	0.0588
4	303	1	$5.00x10^5$	500	0	0.0000
5	303	1	$5.30x10^5$	500	1	0.0588
6	325	1	$5.30x10^5$	500	1	0.0588
7	323	1	$1.55x10^5$	125	5	0.2940
8	305	1	$8.75x10^5$	875	0	0.0000
9	298	1	$1.29x10^5$	125	0.5	0.0294
10	310.5	1	$2.84x10^5$	250	2.75	0.1617
11	298	1	$6.70x10^5$	650	0.5	0.0294
12	298	1	$3.61x10^5$	350	0.5	0.0294
13	300	55.2	$3.61x10^5$	350	0.5	0.0294
14	303	60	$3.61x10^5$	350	0.5	0.0294
15	303	60	$6.70x10^5$	650	0.5	0.0294

Table A.8.9 Operational Conditions and material budgets for the employed process at T = 60 ºC, concentrations 0.5 M - 2 M an input to RE.

No	T (K)	P (bar)	G (kg/h)	G' (m^3/h)	M_{NaCl} (mol/L)	c_i (kg/L)
1	298	1	$1.03x10^6$	1000	0.5	0.0294
2	303	60	$1.03x10^6$	1000	0.5	0.0294
3	303	60	$5.30x10^5$	500	1	0.0588
4	303	1	$5.00x10^5$	500	0	0.000
5	303	1	$5.30x10^5$	500	1	0.0588
6	335	1	$5.30x10^5$	500	1	0.0588
7	333	1	$2.80x10^5$	250	2	0.2940
8	305	1	$7.50x10^5$	750	0	0.000
9	298	1	$2.58x10^5$	250	0.5	0.0294
10	315.5	1	$5.38x10^5$	500	1.25	0.1617
11	298	1	$6.70x10^5$	650	0.5	0.0294
12	298	1	$3.61x10^5$	350	0.5	0.0294
13	300	55.2	$3.61x10^5$	350	0.5	0.0294
14	303	60	$3.61x10^5$	350	0.5	0.0294
15	303	60	$6.70x10^5$	650	0.5	0.0294

Table A.8.1.10 Operational Conditions and material budgets for the employed process at T = 60 ºC, concentrations 0.5 M - 3 M an input to RE.

No	T (K)	P (bar)	G (kg/h)	G' (m^3/h)	M_{NaCl} (mol/L)	c_i (kg/L)
1	298	1	$1.03x10^6$	1000	0.5	0.0294
2	303	60	$1.03x10^6$	1000	0.5	0.0294
3	303	60	$5.30x10^5$	500	1	0.0588
4	303	1	$5.00x10^5$	500	0	0.0000
5	303	1	$5.30x10^5$	500	1	0.0588
6	335	1	$5.30x10^5$	500	1	0.0588
7	333	1	$1.97x10^5$	166.7	3	0.1764
8	305	1	$8.33x10^5$	833.3	0	0.0000
9	298	1	$1.72x10^5$	166.7	0.5	0.0294
10	315.5	1	$3.69x10^5$	333.3	1.75	0.1029
11	298	1	$6.70x10^5$	650	0.5	0.0294
12	298	1	$3.61x10^5$	350	0.5	0.0294
13	300	55.2	$3.61x10^5$	350	0.5	0.0294
14	303	60	$3.61x10^5$	350	0.5	0.0294
15	303	60	$6.70x10^5$	650	0.5	0.0294

Table A.8.1.11 Operational Conditions and material budgets for the employed process at T = 60 °C, concentrations 0.5 M - 4 M an input to RE.

No	T (K)	P (bar)	G (kg/h)	G' (m^3/h)	M_{NaCl} (mol/L)	c_i (kg/L)
1	298	1	$1.03x10^6$	1000	0.5	0.0294
2	303	60	$1.03x10^6$	1000	0.5	0.0294
3	303	60	$5.30x10^5$	500	1	0.0588
4	303	1	$5.00x10^5$	500	0	0.0000
5	303	1	$5.30x10^5$	500	1	0.0588
6	335	1	$5.30x10^5$	500	1	0.0588
7	333	1	$1.55x10^5$	250	4	0.2352
8	305	1	$8.75x10^5$	750	0	0.0000
9	298	1	$1.29x10^5$	250	0.5	0.0294
10	315.5	1	$2.84x10^5$	500	2.25	0.1323
11	298	1	$6.70x10^5$	650	0.5	0.0294
12	298	1	$3.61x10^5$	350	0.5	0.0294
13	300	55.2	$3.61x10^5$	350	0.5	0.0294
14	303	60	$3.61x10^5$	350	0.5	0.0294
15	303	60	$6.70x10^5$	650	0.5	0.0294

Table A.8.1.12 Results from exergetic analysis for different concentrations of brine used for energy recovery by means of RE unit operating at a temperature of 40 °C.

	0.5M-2M NaCl	0.5M-3M NaCl	0.5M-4M NaCl	0.5M-5M NaCl
ΔE_x (kJ/h)	$-1.34x10^6$	-9.20 x105	-6.84x105	$-5.23x10^5$
E_{el} (kWh/h)[a]	1390	1390	1390	1390
E_{el} (kWh/h)[b]	2049	2049	2049	2049
E_{el} (kWh/h)[c]	1316	1293	1280	1274
W_U (kJ/h)[a]	$5.00x10^6$	$5.00x10^6$	$5.00x10^6$	5.00x106
W_U (kJ/h)[b]	$7.38x10^6$	7.38 $x10^6$	$7.38x10^6$	7.38x106
W_U (kJ/h)[c]	$4.73x10^6$	4.65 $x10^6$	$4.60x10^6$	4.58x106
Q (kJ/h)	$2.55x10^6$	$2.55x10^7$	$2.55x10^7$	2.55x107
G_v (kWh/h)	11302	11302	11302	11302
$W_{U,t}$ (kWh/h)	5.14 $x10^6$	$5.14x10^6$	$5.14x10^6$	5.14 $x10^6$
T_oR_s (kJ/h)[a]	$1.15x10^7$	$1.11x10^7$	$1.08x10^7$	$1.07x10^7$
T_oR_s (kJ/h)[b]	$1.39x10^7$	$1.34x10^7$	$1.32x10^7$	$1.30x10^7$
T_oR_s (kJ/h)[c]	$9.88x10^6$	$9.79x10^6$	$9.75x10^6$	$9.73x10^6$

[a]With PX, [b]without PXC and [c]PX and RE.

Table A.8.1.13 Results from exergetic analysis for different concentrations of brine used for energy recovery by means of RE unit operating at a temperature of 50 ºC.

	0.5M-2M NaCl	0.5M-3M NaCl	0.5M-4M NaCl	0.5M-5M NaCl
ΔE_x (kJ/h)	-1.69x10^6	-1.15 x10^5	-8.58x10^5	-6.64x10^5
E_{el} (kWh/h)^a	1390	1390	1390	1390
E_{el} (kWh/h)^b	2049	2049	2049	2049
E_{el} (kWh/h)^c	1315	1291	1279	1272
W_U (kJ/h)^a	5.00x10^6	5.00x10^6	5.00x10^6	5.00x10^6
W_U (kJ/h)^b	7.38x10^6	7.38 x10^6	7.38x10^6	7.38x10^6
W_U (kJ/h)^c	4.73x10^6	4.65 x10^6	4.60x10^6	4.58x10^6
Q (kJ/h)	4.67x10^6	4.67x10^6	4.67x10^6	4.67x10^6
G_v (kWh/h)	20810	20810	20710	20710
$W_{U,t}$ (kWh/h)	9.46x10^6	9.42x10^6	9.42x10^6	9.42x10^6
T_oR_s (kJ/h)^a	1.61x10^7	1.56x10^7	1.53x10^7	1.51x10^7
T_oR_s (kJ/h)^b	1.85x10^7	1.80x10^7	1.77x10^7	1.75x10^7
T_oR_s (kJ/h)^c	1.42x10^7	1.41x10^7	1.40x10^7	1.40x10^7

[a]With PX, [b]without PXC and [c]PX and RE.

Chapter 9

Perspectives on Environmental Ethics in Sustainability of Membrane Based Technologies for Water and Energy Production

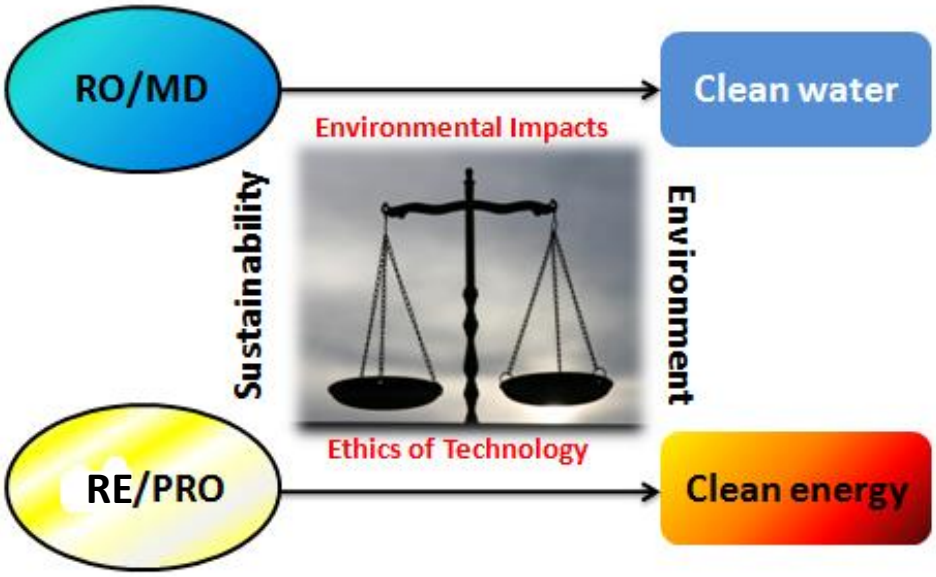

Abstract

Securing a sustainable supply of water and energy is nowadays a key global issue. In the current practice of water and energy supply, there is still some gap in meeting the value criteria for sustainable development mainly related to environmental pollution as well as ecosystem disturbances. In this work, the sustainability of integrated membrane based processes for water and energy production is assessed with a special focus on environmental and ecosystem impacts. Feasibility of bridging the available gaps through process performance improvements is presented. Major environmental impacts from hybrid membrane based technologies for water and energy production are identified and considered for upstream balance of social benefits and burdens to the present and future generations. Ethical considerations were pointed mainly in the aspect of intergenerational justice (IRG-J) and ecological justice (EC-J) while setting value criteria for sustainability. The ethical significance of the identified impacts was predicted based on the associated difficulties to meet these criteria. The overall outcome will be beneficial in designing strategies for development and implementation of sustainable hybrid processes for clean water and energy production.

This chapter has been published as;

R. A. Tufa, Perspectives on environmental ethics in sustainability of membrane based technologies for water and energy production, *Environmental Technology & Innovation*, 4 (**2015**) 182-93.

9.1 Introduction

The need to meet basic human needs in a sustainable manner is a major challenge nowadays for developing and developed countries. Key issues involve depletion of fossil fuels, global warming, water scarcity, rise in energy demand, loss of biodiversity and the human health impact which are exaggerated with the global expansion. The global demand for the two essential resources (water and energy) is drastically increasing due to economic expansion, population growth and increasing living standard in emerging countries. In 30 years, it is expected that energy demand will be projected by 50 % while water withdrawal could go beyond 50 % in developing countries and 18 % in developed countries over the same period [1]. Thus, technological innovations for sustainable water and energy production are highly demanding for societal and ecological benefits in terms of economic advantages, environmental safety, public welfare and national security.

This study presents a methodology for an integrated analysis in planning and technological implementations for sustainability of membrane processes for water and energy production. Emphasis is mainly given to reverse osmosis (RO) for clean water production and reverse electrodialysis (RE) for clean energy generation. Trends in research progress and recent technological development are highlighted. Identification of potential environmental threats and ecological impacts is done for justification of related ethical issues. Integrated analysis of the various factors that should be considered in technological advance of desalination processes; possibly in reduction of energy demand, use of clean energy sources, advanced materials, innovative system designs and social acceptance, were performed and evaluated according to a value criteria set for sustainability. From ethical point of view concerning justice, the listed factors were evaluated in terms of intergenerational equity in sustaining the processes without any damage to humans, non-humans and the whole ecosystem. This will be helpful in paving a way for the technological advancement through upstream balance of social burdens and benefits.

9.1.1 Current state-of-the-art technologies

9.1.1.1 Reverse Osmosis: Water

Production of pure water is mainly done by desalination of seawater. The major Desalination Technologies (DT) currently in practice is based on RO and thermal distillation

(multistage flash and effect distillation). Thermal desalination is energy intensive compared to the membrane based processes like RO seawater desalination which is expanding rapidly due to its lower cost and simplicity. Currently, RO is the most widely used technology and accounts for over 50% of the installed capacity. However, at the current state-of-art, desalination of 1 m^2 seawater by RO (50% recovery) results in about 0.5 m^3 of pure water and 0.5 m^3 of retentate (brine), which is usually discharged into sea. Figure 9.1 presents major steps involved in a typical seawater RO process.

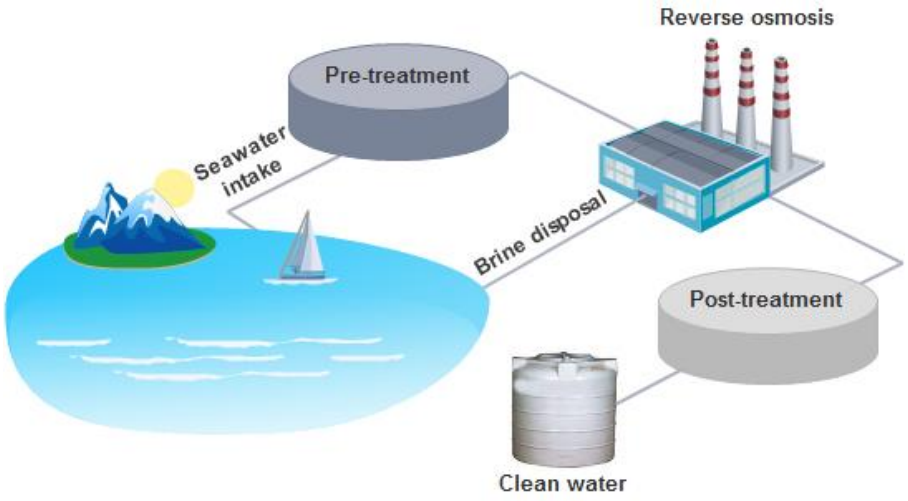

Figure 9.1. Illustration of typical seawater reverses osmosis process. Technological advance is noticed mainly observed in the improvements of pretreatment step allowing prevention of membrane fouling as well as in the RO process with high performance membrane materials, modules and process design.

Recent advances in RO development involves new membrane materials, modules and process design [2]. The search for optimal polymeric membrane materials started early in 1950s, and the RO industry is nowadays dominated by these type materials. Promising progress is observed in membrane research mainly in performance optimization through improvements in physico-chemical properties [3, 4]. Significant improvement in mechanical, biological and chemical strength of RO membranes have been observed in the last decades. Modification of the structure and morphology of membranes for functionality improvement is observed to enhance the permeability and selectivity properties. This together with energy optimization has reduced the membrane and operational cost per unit volume of water produced, thus reducing the overall energy consumption down to 1.06 $kWhm^{-3}$ (at about 50 % recovery) which is much lower than thermal systems.

Different types of RO membranes have come into applications from early stages up to now. New developments in polymeric membranes based on cellulose acetate asymmetric morphology formed with a dense 200 nm thin layer over a thick micro-porous body resulted in higher water flux than the early symmetric membrane [5]. However, formation of asymmetric membranes is based on a single step casting limited to a few soluble membranes and the level of permeability and salt rejection is not commercially attractive. This led to development of new membrane termed as composite membranes based on a two step-casting involving a separate optimization procedure for the barrier layer and support layer [6]. Currently, thin film composite (TFC) polyamide membranes having high salt rejection, good chemical stability and mechanical strength dominate the RO market. Later, the development of novel membranes based on rigid star amphiphiles, ceramic membranes, and mixed matrix membranes come in to applications in RO desalinations [7]. In very recent developments, nano-technology has emerged as an attractive alternative to polymeric materials. Nano-structured membranes like zeolite membranes, thin film nano-composite

Various module designs can be used in RO for efficient recovery of pure water from seawater. This involves configurations like pleated flat sheet, spiral wound flat sheet, ceramic monolith element membrane and tubular membrane. Spiral wound membrane module which is cheaply produced from flat sheet TFC membrane configuration, is the most extensively used design in RO desalination due to its high specific membrane surface area, easy scale up operation and low cost. The dominant modules in the market are the ones based on polyimide membranes i.e. polyamide spiral wound membranes and asymmetric cellulose acetate hollow fiber membranes [7].

Although the emerging novel materials are envisaged to improve RO performance, challenges still remain with respect to their practical applications. There are still challenges in membrane permselectivity and mitigation strategies of membrane fouling. In this regard, other cost effective thermally-driven DTs like Membrane Distillation (MD) are emerging for production of high quality distillate (recovery above 90 %) using low grade waste[8]. Other problem with the RO practice is the degradation of commercial membranes by chlorine. Thus, pre-treatment analysis, prevention of fouling and concentration polarization is urgently required in order to minimize these

problems. Moreover, reduction of energy consumption has a huge advantage in terms of economy and environment.

9.1.1.2 Reverse Electrodialysis: Energy

There are two promising membrane based technologies for clean energy production in the form of salinity gradient power (SGP) from mixing two solutions of different salinity; reverse electrodialysis (RO) and pressure retarded osmosis (PRO). In RE, salinity gradient power is generated by ionic migration across alternatively aligned ion exchange membranes driven by the difference in the chemical potential of the mixing solutions. In PRO, power is generated by depressurizing a portion of diluted solution through a hydro-turbine when two solutions of different salinity are contacted by semi-permeable hydrophilic membranes.

Progresses in RE research have shown promising milestones in the past decades. The increasing demand in the alternative clean energy resources as well as the new era in the development of membranes increased attention to rise of a research on this technology although the technological concept was introduced in long ago in 1950s [9]. Interesting outcomes have been demonstrated through a research focusing on membrane development [10-14], stack design and testing [15-17], process modeling and optimization[18, 19], performance analysis and testing [15, 20], investigation on fouling[21, 22], and scale-up potential [23].

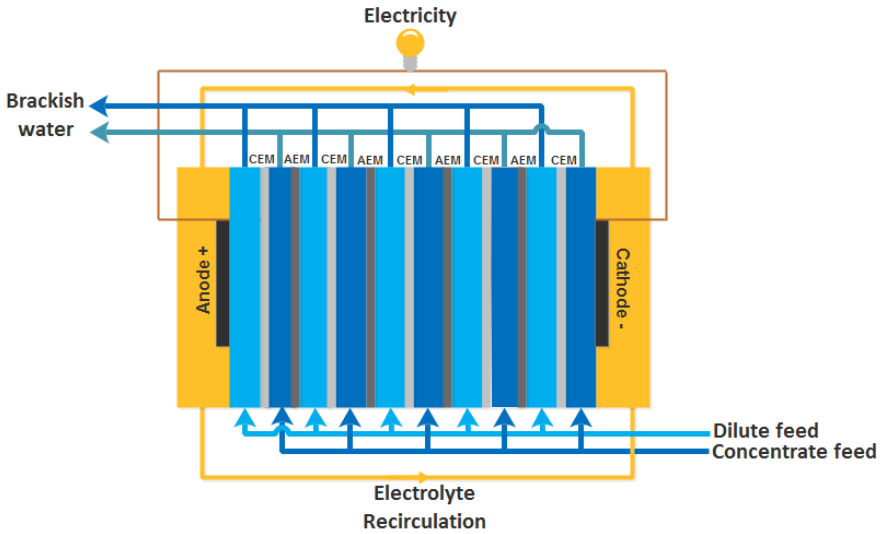

Figure 9.2. Conversion of Salinity gradient energy into electrical power by reverse electrodialysis. The outlet from RED is indicated as brackish water since the technology is mostly applied for seawater and river water. In the application for energy recovery from brine, the outlet concentration outlet can be of much higher than brackish water concentration.

IEMs can be regarded as the heart of RE system. The commercial success of this technology is unthinkable unless the properties of IEMs especially resistance and permselectivity is not well optimized at an affordable cost for scaled-up application. Recently, lots of efforts have been done in preparation, characterization and modification of IEMs for enhancement of the overall RE performance. Commercial homogeneous and heterogeneous membranes as well as tailor made membranes have been tested in RE process involving lower feed concentration like seawater and river water [24, 25] and higher feed concentrations like brine [26, 27]. Some of the important millstones involve the membrane development is the application of profiled membranes in RE process. Vermaas *el al.* demonstrated that the use of profiled membranes significantly reduces the internal stack resistance (up to 30 %) and hydrodynamic loss (4-fold lower) compared to classical stacks using non-conductive ion spacers [11]. The overall consequence is advantage gained in terms of enhanced power density and open circuit voltage, however with possibility to improve the performance further with different profile geometries. Güler *et al.* prepared profiled membranes in different geometries like ridges, waves and pillars profiles, and tested for the RE applications [12]. They observed 21 % reduction in internal stack resistance resulting in up to 38% increase in power density compared to the stacks with flat membranes. Recently, Hong and Chen designed organic–inorganic nanocomposite CEM and analyzed their electrochemical properties for RE applications [13, 28]. A maximum power density of 1.3 W/m^2 was achieved through control of the electrochemical membrane properties by optimization of the loading of sulfate functionalized iron (III) oxide within the sulfonated polymer matrix of the CEM [28]. The maximum power density so far is about 2.2 W/m^2 using commercial Fumatech membranes (FAS and FKS) combined with the use of thin spacers within the RE stack. These membranes have are very thin in structure and have low area resistance (below $1.5\Omega.cm^2$) compared to other commercial membranes. Although promising progress is achieved with respect of improvements in membrane performance so far, further optimization through appropriate design and IEM development is required for scale-up at an affordable cost and commercial success. The high cost of commercially available ion exchange membranes in the current market is the main limitation in this regard.

Research in RE is broadening from time to time. Other innovative applications are being introduced based on the power generation in hybrid applications with other technologies like desalination and bio-electrochemical systems. This has a huge advantage in terms of energy and

environmental issues. For example, there is a huge possibility of concentration of the brine from RO desalination plant to be used in the LC compartment of the RE system [29, 30]. Promising power density (up to 1.5 W/m^2) can be obtained when mixing brine with brackish water [26]. This is a good opportunity in reducing back the energy for desalination and environmental problems related to brine discharge. Other interesting applications involve the integration of RE with microbial fuel cells [31] and hydrogen energy systems [32]. They combined two systems into a single process which was able to produce about 6-fold power density (4.3 W/m^2) compared to the stand-alone microbial fuel cell when operating at feed flow rate of 1.55 mL/min. In hydrogen production systems, RE can be a perpetual power source for sustainability as well as storage of SGP in the form of hydrogen [32].

9.2 Key Environmental Impacts

DTs play an important role in potable water supply with a worldwide production capacity of 24.5 million m^3/day. However, the process is also accompanied by adverse environmental effects. Figure 9.3 illustrates potential environmental impacts from DTs. The major impacts can be categorized in two aspects; '*direct*' and '*indirect*' impacts. One of the direct impact is the significant loss of aquatic organisms specially those at the early stage and planktonic ones due to impingement and entrainment resulting from seawater intake[33]. For example, the use of open intake may result in losses of aquatic organisms when drawn into the plant with water or collision with intake screens.

Huge amount of brine is rejected from DTs with high load of TDS. For example, Ashkelon desalination plant which is one of the largest in the world and the largest in the Levant Basin, has an annual seawater intake of about 315 MCM (million m^3) and produces brine with a salt concentration of 7.35% TDS (1.86 times that of seawater) that is discharged at a rate of 160 MCM per year [34].

Brine reject may contain residues of pretreatment and cleaning chemicals required for prevention of biofouling, scaling, suspended solids, foaming and corrosion. It may also contain chemicals due to side reactions of pretreatment and cleaning chemicals involving halogenated organics and heavy metals due to corrosion (usually at low concentrations). Rejects containing these chemicals is basically discharged continuously into the sea. Thus, the release of toxic anti-

foulants and anti-scalants is also another issue of environmental concern of DTs. For example, about 10-25% of the dosing concentration of Cl_2 (anti-foulant) in the process of desalination is released as a residue which can be hazardous threat to aquatic environment. Cleaning chemicals and their additives like dodecylbenzene sulfonate and sodium perborate can have a negative impact on the aquatic life if discharged into the sea without treatment.

Environmental threats may depend on the properties of the reject brine as well as the hydrographical feature of the accepting environment. Salinity and temperature are among the reject properties potentially affecting the distribution of aquatic organisms. Continues exposure of marine organisms to extreme condition of this properties might be intolerable[33].

Other issues related to land use is also considered as a negative impact, however with a low emphasis.

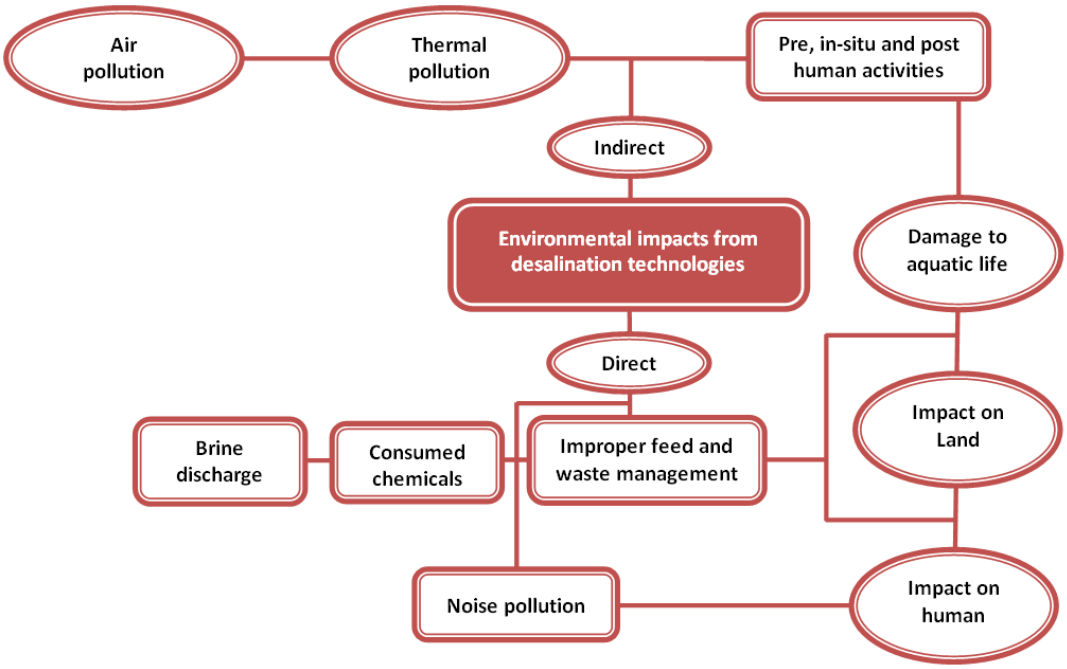

Figure 9.3. Direct and indirect environmental impacts expected from membrane based DTs. In integrated application to energy technologies, membrane processes like RE for conversion of hypersaline brine in to energy could also have a similar environmental threat especially to the marine life if the concentrated discharge at outlets is not properly managed.

Despite the fact that the level of overall effect of these elements differs from plant to plant and species to specie, there is no enough experimental data for clear understanding of the tolerance limit of marine organisms.

High energy demand of seawater desalination plants requires use of large amount of thermoelectric energy which is accompanied by emission of air pollutants and greenhouse gases that further exacerbate global warming. Modern seawater RO plants have energy consumption rate in the range of 3-4 kWh/m^3 with net CO_2 emission rate of 0.4-1.8 kg/m^3 [35]. Unless alternative energy resources like renewable are developed for desalination, expansion of the plant's capacity with the projection of water demand is expected to raise the level of greenhouse gas emissions. Thermal stress associated with the release of heat associated with plant operation or effluents may also be considered as an indirect impact. Other concerns may involve the impact on groundwater due to leakage from seawater pipes and noise (~90 dB) due to high pressure pumps.

In general, many of the published literatures do not present enough data to support the ideas regarding the adverse environmental effects of desalination systems especially long term effects on marine organisms.

Environmental impact from the emerging SGP technologies like RE could be mainly viewed in terms of the effect of seawater intake and outlet discharge. If seawater and river water is used, outlet discharge from the SGP system is mainly composed of brackish water which is about 50 times less concentrated than brine, and it could not have a potential harm on the marine organisms. For example, in a RE pilot plant installed at Afsluitdijk (The Netherlands), salt water from Wadden sea is pumped at a flow rate of 200,000 L/h to be mixed with 740,000 L/h of fresh water from IJsselmeer to produce SGP, and the effluent (brackish water) is discharged back to the sea.

However, if brine and brackish water are used as RE feed, the outlet concentration will be about 3.5 M which is quite higher than the RO brine concentration, and this will have even more pronounced environmental effect. Though sufficient experimental data is not yet available to support the pre-treatment requirement of RE technology as well fouling potential of the membranes, discharges composed of chemicals that could possibly be used in pre-treatment and membrane cleaning may also be considered as a potential threat to marine ecosystem.

In addition, hexacyanoferrate/ferrite solution which is mostly used as an electrode rinse in SGP-RE system [36] can have a hazardous effect in case of high current leakage within the stack leading to the release of toxic HCN during plant operations. In addition, decomposition from the discharge of these chemicals into sea can result in a release of HCN which could have an acute or chronic toxicity to the marine ecosystem.

9.3 Sustainability assessment and ethical issues

From philosophical point of view, ethics represents systematizing, defending, and recommending concepts of right and wrong behavior [37]. Environmental ethics deals with the conceptual foundations of environmental values as well as issues related to actions and policies of the society to protect and sustain biodiversity and ecological systems. The view involves concern to humans (anthropocentric view) and extends to non-humans (non-anthropocentric view)[38]. In the process of sustainability assessment of DTs, identification of the benefits used to evaluate distributive outcomes with time in relation to environmental ethics is crucial.

Environmental threats as a result of high emissions from non-renewable energy based intensive desalination practice can be viewed in many dimensions of ethical concerns; for example '*Intergenerational Justice*' (IRG-J) [39] questioning the welfare of the present and future generations, and '*Ecological Justice*' (EC-J) in relation to consequential damage to marine organisms, land, aquifers as well as any useful non-living matter which can be adversely affected by the process. Although not of significant importance, '*Intragenerational Justice*' (IRAG-J) considering the potential risk of desalination practice for the people leaving nearby and employees in desalination plant is also another consideration.

Despite technological progress, human beings are still dependent on environment as well as on natural resources. In addition, the scale and the nature of these issues in a world striving for sustainable development have evolved over time. The focus of sustainability is mainly the changing of various practices in an effort to carry on certain patterns of human and ecological existence in a safe and secure way. Theories adhering sustainability to intergenerational equity as a main topic are emerging substantially in the world of sciences. IRG-J is basically interpreted as a concern for the welfare of future generations along a range of ecological and social dimensions. Thus, equitable sharing of benefits (values of sustainability) and the burdens (environmental

threat) between generations is important. This complies with the Brundtland definition which addresses sustainable development without a compromising the ability of future generations to meet their own needs, with the aim to fulfil intergenerational equity [40].

The rate at which human activities adversely affect the environment and ecosystem as a whole is rising with global population growth and socio-economic production model. In the case of DTs and energy technologies considered here by which human actions are leading towards extinction of non-humans, the argument starts weather doing this is just or unjust. This could be viewed in different ways depending on the scope of different social aspects like culture, tradition or religion. However, any of the beliefs conceiving of the morality of human relationships with non-human organisms is similar to behavior influencing considerations obtained from the purely prudential concern to maintain a healthy non-human environment for the benefit of present or future generations. In short, apart from reasoning that peoples believe in verge of justice for non-humans, at least the moral responsibilities account for the way in which human beings conduct themselves towards non-humans in order to assure EC-J[41].

There are lots of evidences regarding the negative impact of GHG emissions on the integrity of biosphere and wellbeing of future generations and the whole ecosystem. From ethical point of view and supporting evidences that climate change will have an adverse impacts on health, cultural life and economic growth of future generations, Intergovernmental Panel on Climate Change (IPCC) concludes that global climate change issues raise questions of equity among generations [42].

9.4 Mitigation strategies

It would be worthy to note that the future peoples have the right to have all the opportunities, if not exactly to the same, at least with present people being aware of their responsibility and obligations when practicing socio-economic and techno-economic developments. Thus, when it comes to DTs, it would be promising to find ways to mitigate the adverse environmental and ecological effects, now and in the future. Without this, it will be very difficult to lead a sustainable practice in fulfilling the need for ever-growing demand of water and energy with membrane based processes and other potential technologies for production of these essential resources. In this regard, approaches based on the concept of process intensification strategy as well as new material

and technological developments could have a direct impact in minimizing the expected environmental threat.

9.5 New technological developments

Research advances show the possibility of reducing the energy demand of DTs by improving process performance through development of advanced materials and technological innovations thereby ensuring sustainability along with the ever growing global water demand [43, 44]. In the process of sketching the principles of distributive justice with respect to DTs, it's important to identify clearly the cause and adverse effects of factors involved and try to predict the extent to which emphasis should be given based on the different theories of justice; IRG-J, IRAG-J and EJ. Table 9.1 illustrates the sources for the environmental and ecological effects of DTs, as well as mitigation requirements, related ethical concerns and ethical significance of the adverse effects. Priorities can be made based on the related ethical concerns in order to lead a sustainable practice keeping the security of natural resources and non-human habitants in relation to the whole ecosystem. Level of ethical significance of each adverse effect is proposed based on an ethical scale developed through a value criteria consideration. Greenhouse gas emissions (GHG) and ecological damage are marked as a significant consequence and hence open to the questions related theories of justice from ethical (environmental) point of view.

In comparing the problems on ethical scale, the benefit that can be obtained through control of the problem can be directly linked to the level of ethical significance. Prior inspection of solutions for the high energy demand of DTs is important and attention should be given to solve this problem which indirectly leads to the reduction of GHG emissions. The overall result is saving environment, avoiding climate change, and securing welfare for the present and future generations. Problems related to brine discharge and ecological damage are also important issues requiring more attention. The development of special discharge salinity devices for brine[43] and utilization of brine in other processes like SGP[29] can solve this problems. Problem related to the seawater intake can be of moderate concern which could be solved mainly by designing appropriate seawater intake technologies that have a minimal effect on the aquatic life. Effects from pre and post-treatment chemicals, the pipe leakages and noise pollutions are not of significant ethical concern and can be solved in the long run after the major issues are settled.

9.6 Process intensification: an integrated approach

As noted before, significant increase in water and energy demand with potential consequence of global warming is a critical issue requiring sustainable development all over the world urgently. Lots of research and developments are ongoing in search of green technologies for clean water and energy production. However, the route to meet sustainability requirement in the process of global development is complex and time taking. In this regards, process intensification (PI) is a promising approach to achieve sustainability through design and development of a fast, efficient, simple, cheap and safe processes.

Table 9.1. Identification of sources for the environmental/ecological effects, mitigation requirements based on technological advances and innovations, and related ethical concern in membrane processes for water and energy production.

Source*	Agents**	Acceptor	Environmental/ Ecological effects	Ethical issue	Mitigation requirements/ Goal to ethical justification	Significance of ethical concern
Requirement of high energy	Greenhouse gases-CO_2, NO_X, SO_X, NMVOC	Ecosphere	Air pollution; *Global warming*	IRG-J	<u>For operational factors</u> Ultrahigh-permeability Membranes [45, 46] Nanotube or aquaporin based membranes [46-48] Fouling-resistant membranes [49, 50] Chlorine-resistant membranes [51, 52] High energy recovery devices and use of efficient pumps [53, 54] Use of alternative energy resources (renewable energy) [29] <u>For socially induced factors</u> Reducing water network losses [55] reducing the water demand and consumption [56]	++++
Sea water intake	-	Aquatic organisms	Impingement and entrainment of aquatic animals; *damage on aquatic life*	EC-J	Design of equipment with optimal plant's life cycle as well as minimal effect on aquatic life [57]	+++
Corrosion products	Heavy metals; Fe, Cu, Ni, Zn	Sea/sediments/ aquatic organisms	Ecosystem disturbance; Sediment loading, Molecular/cellular/organismic effects, accumulation in organisms***	IRG-J, IRAG-J	Thermally stable and corrosion resistant materials[58]	++
Pre- and post-treatment chemicals	Anti-scaling additives (polycarbonic acids, polyphosphates)***, antifouling additives (chlorine and hypochlorite), anticorrosion additives	Sea/sediments/ Aquatic organisms	Ecosystem disturbance; eutrophication, anthropogenic effect	EC-J	Membranes less susceptible to fouling[59, 60] Non-chemical pre-treatment strategies; efficient membrane pre-treatment [61]	++
	Halogenated organic compounds, antifoaming additives, Oxygen scavengers (Na_2SO_4)	Seawater/ drinking water	Seawater pollution	IRAG-J, EC-J	Efficient technology (high recovery) [62] Highly permeable membranes [45, 46] Fouling resistant membranes [49, 50]	
Retentate/ accidental spills, feed drills	Hot concentrate (Brine)	Seawater	Seawater pollution, thermal pollution	EC-J	Appropriate site selection (hydro-geological, hydrodynamic conditions, local ecological value, etc.) [63, 64] Discharge devices that would ultimately reduce salinity [64] Use of brine for renewable energy production by SGP-RE or PRO [29, 65]	++++
	Contaminates from Pre-treatment chemicals, brine	Aquifer	Disturbance in the water table and aquifer damage	EC-J	Proper discharge planning [66] Strong, stable and durable materials [58]	++
Noise	-	Humans	Noise pollution	IRAG-J	Appropriate site selection for construction of desalination plant[63] Acoustic technology: building canopies over the pumps [67]	+

*Sources are directly linked to elements in the process of DTs. **Agents describe specific things (materials, chemicals, objects or solutions) resulting from the mentioned source pertaining to the cause for the effect bound to environmental or the whole ecosystem. ***Metals and hydrophobic by products from chemical pretreatment could have potential accumulation in edible sweater organisms and have adverse effect on humans depending on the threshold value. ++++ Of high concern and appropriate technological developments required urgently, +++of moderate concern and adverse effect which can be minimized with proper technology utilization, ++of considerable concern and effect, +Less important but considerable effect

The concept of PI can be implemented in disciples involving the application of membrane engineering; like desalination, membrane processes based on reactive separation and/or hybrid separations [68]. Figure 9.4 shows a scheme of integrated approaches for sustainable water and energy production by membrane processes.

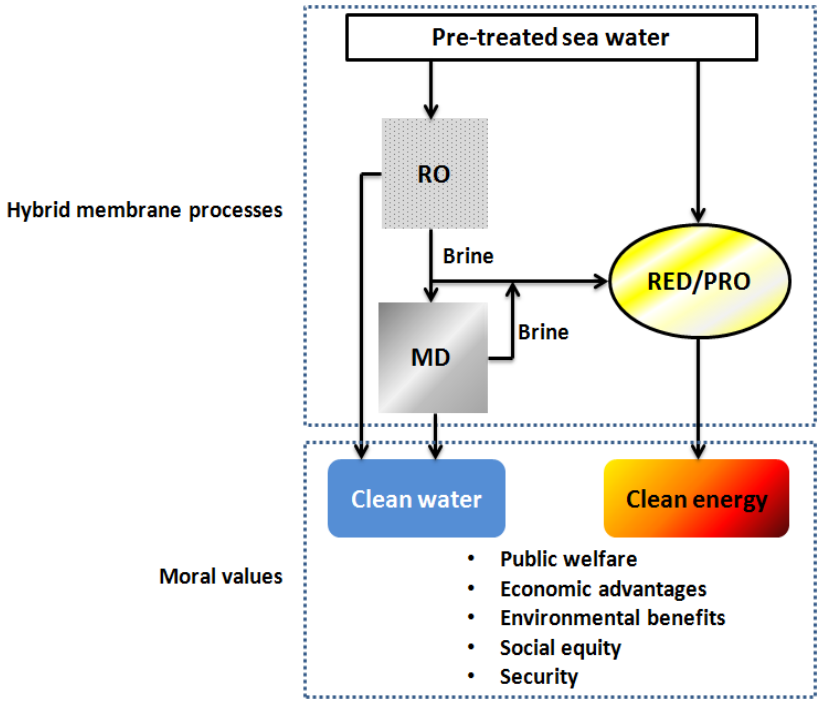

Figure 9.4. Hybrid membrane processes for clean water and energy production. Moral values represent the driving forces for achieving sustainable development. In energy recovery unit, outlet from RE can also be recycled back to MD for further concentration and reuse.

There is a huge possibility of integrating membrane process for sustainable applications in the concept of process intensification for water and energy production. Brauns elaborated the potential integration of the membrane based DTs and/or solar power DTs with SGP technologies for efficient production of clean energy as well as desalted water; this enables adequate production of large amounts of pure water[65]. For instance, RO produces large amount of hypersaline brine that can be recovered as a source of clean energy generation by RE [29, 65]. Further integration of MD with these processes can increase the water yield, brine volume reduction (concentration) and energy recovery by RE.

In addition, there is a possibility to use the energy recovered from the brine for the desalination itself. This will not only reduce the operating costs, but also keeps a sustainable desalination practice by avoiding the emissions from the traditional power plants.

9.7 Burden-Benefit Balance

Assessment of methodologies to fairly distribute benefits and burdens (benefit-burden balance) among the present and future generations is important in the sense of IRG-J. Figure 9.5 shows the achievement of IRG-J through distributive justice in a world striving for sustainable development. Obviously, the burdens considered mainly involve environmental damage, adverse effects on ecosystem and limited resources exploitation. The benefits gained include the moral values (motivating factors) from sustainability as described earlier. This is asserted as value criteria for sustainable development to assure environmental and ecological welfare, public welfare, social equity, security and resource durability.

In general, the notion of collective interests to bridge the gap between different understanding to the question of IRG-J among some philosophers asserts the difficulty of achieving IRG-J [69] and scientists predicting future harm of global climate change. For example, in the process of distributive justice, some believe that it's positive to give people of developing nations higher emission rights than the people of industrialized countries, for the implementation of benefit-burden balance [70]. This is based on the technological gap between the two categories of countries and a rapid development achievable at higher production and manufacturing rate in exhaustive operation of current technologies for the developing nations. In this sense, international agreements for sustainable advance and global environmental laws may compromise these types of constraints in the process of burden-benefit balance.

In general, a balance of benefits and burdens assures IRG-J through achievement of fundamental equality in the aspect of equal rights, responsibilities, vital interests and mutual advantages as described by Barry [39]. For this, intragenerational agreement among governments, global corporations, business sectors supported by all nations for actions to be taken for achievement of sustainable developments is highly important.

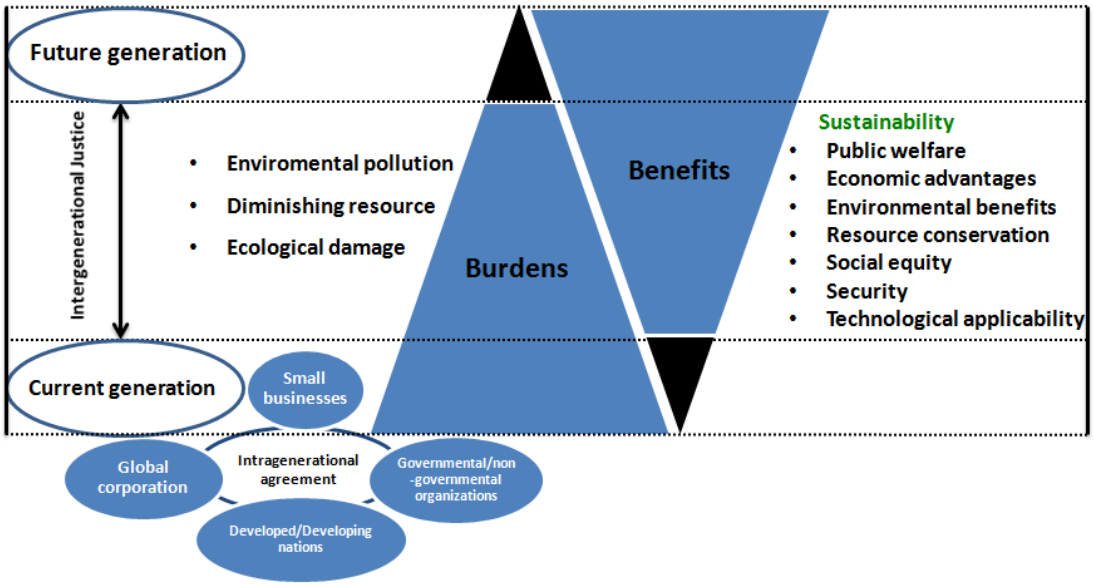

Figure 9.5. Equity through distributive justice in a sustainable development. The burdens and benefits are identified for membrane based processes applied for water and energy production. Intragenerational agreement is considered as a base line for the burden-balance to present and future generation in the process of sustainable development.

9.8 Conclusions and outlook

In the ever growing world where sustainable development is among the key issues, technological advancements are highly important to meet the needs of basic resources like water and energy. However, with the demands of these resources expected to be projected at a high rate from time to time, current DTs are posed to have an environmental issue.

When environmental ethics comes into play, DTs have a limitation as a technological application mainly in the aspect of environmental pollution and damage to marine ecosystem. This study shows that continued usage of currently available DT will automatically triggers ethical questions related to IRG-J and EC-J, which are in turn questions of environmental and ecological welfare as well as present and future generations, and hence its sustainability. Thus, the search journey to find answers to these ethical questions is feasible through strategic planning and implementation of appropriate mitigation methodologies. From scientific point of view, innovations of new technologies which are less energy intensive, design and development of novel materials for improved performance, and the possibility of use of alternative clean energy resources for desalination are recommended as the main mitigation strategies. For the challenges expected to occur in the era of distributive justice for equity, it's appropriate to consider

anthropocentric view in prioritizing the welfare of present generations which evolve to future generations.

Although some technologies are in question if they sustainable or fit to the theory of environmental justice eg. nuclear fusion, the search era is proceeding of course with a promising outcomes at some part. If we consider the sun, it can deliver about 6000 times (89,000 TW) the world's energy demand (15 TW), implying huge potential of solar energy. Nowadays, renewable energy resources account for only 19.5 % of global energy generation, which is expected to increase significantly in all long-term scenarios. In addition, the global potential of SGP is estimated to be about 1.7 TW with a huge potential for clean energy supply. Moreover, International Energy Agency (IEA) sets the growth of renewables threefold from 2009 to 2035 based on broad policy commitments and plans set by different countries [71]. This creates a good opportunity in implementation of renewable based desalination technologies for safe and efficient water supply. Thus, successes in innovative solutions that fulfill the value criteria directly avoid environmental problems related to technological advances in membrane processes for water and energy production.

Generally, the emerging salinity gradient power technologies like pressure retarded osmosis and reverse electrodialysis that are proposed as one solution for the brine managements have less environmental concern than DTs. Success in real application of these technologies will automatically imply the reality of hybrid desalination technologies for water and energy production and a relief from the huge environmental concern related to current DTs. Thus, the ongoing research and development progress with respect to salinity gradient power for clean energy generation is highly promising for those standing to be responsible to the welfare of the present and future generations (intergenerational justice/intergenerational justice) and ecological safety (Ecological justice).

References

[1] EIA, International Energy Outlook 2013, in, Washington, DC 20585, 2013, pp. 9-19.
[2] S.S. Shenvi, A.M. Isloor, A.F. Ismail, A review on RO membrane technology: Developments and challenges, Desalination, (2015).
[3] D.H.N. Perera, S.K. Nataraj, N.M. Thomson, A. Sepe, S. Hüttner, U. Steiner, H. Qiblawey, E. Sivaniah, Room-temperature development of thin film composite reverse osmosis membranes from cellulose acetate with antibacterial properties, Journal of Membrane Science, 453 (2014) 212-220.

[4] P. Gorgojo, M.F. Jimenez-Solomon, A.G. Livingston, Polyamide thin film composite membranes on cross-linked polyimide supports: IMPROVEMENT of RO performance via activating solvent, Desalination, 344 (2014) 181-188.
[5] L. Sidney, The Loeb-Sourirajan Membrane: How It Came About, in: Synthetic Membranes:, AMERICAN CHEMICAL SOCIETY, 1981, pp. 1-9.
[6] P.S. Francis, Fabrication and evaluation of new ultrathin reverse osmosis membranes, Available from the National Technical Information Service, Springfield VA 22161 as PB-177 083, Price codes: A 04 in paper copy, A 01 in microfiche. OSW Research and Development Progress Report, (1966).
[7] K.P. Lee, T.C. Arnot, D. Mattia, A review of reverse osmosis membrane materials for desalination—Development to date and future potential, Journal of Membrane Science, 370 (2011) 1-22.
[8] E. Drioli, A. Ali, F. Macedonio, Membrane distillation: Recent developments and perspectives, Desalination, 356 (2015) 56-84.
[9] R.E. Pattle, Production of Electric Power by mixing Fresh and Salt Water in the Hydroelectric Pile, Nature, 174 (1954) 660-660.
[10] P. Długołęcki, K. Nymeijer, S. Metz, M. Wessling, Current status of ion exchange membranes for power generation from salinity gradients, Journal of Membrane Science, 319 (2008) 214-222.
[11] D.A. Vermaas, M. Saakes, K. Nijmeijer, Power generation using profiled membranes in reverse electrodialysis, Journal of Membrane Science, 385-386 (2011) 234-242.
[12] E. Güler, R. Elizen, M. Saakes, K. Nijmeijer, Micro-structured membranes for electricity generation by reverse electrodialysis, Journal of Membrane Science, 458 (2014) 136-148.
[13] J. Gi Hong, Y. Chen, Evaluation of electrochemical properties and reverse electrodialysis performance for porous cation exchange membranes with sulfate-functionalized iron oxide, Journal of Membrane Science, 473 (2015) 210-217.
[14] J.G. Hong, B. Zhang, S. Glabman, N. Uzal, X. Dou, H. Zhang, X. Wei, Y. Chen, Potential ion exchange Membranes and system performance in reverse electrodialysis for Power Generation: A Review, Journal of Membrane Science, (2015).
[15] J. Veerman, M. Saakes, S.J. Metz, G.J. Harmsen, Reverse electrodialysis: Performance of a stack with 50 cells on the mixing of sea and river water, Journal of Membrane Science, 327 (2009) 136-144.
[16] J. Veerman, M. Saakes, S.J. Metz, G.J. Harmsen, Electrical Power from Sea and River Water by Reverse Electrodialysis: A First Step from the Laboratory to a Real Power Plant, Environmental Science & Technology, 44 (2010) 9207-9212.
[17] D.A. Vermaas, M. Saakes, K. Nijmeijer, Doubled Power Density from Salinity Gradients at Reduced Intermembrane Distance, Environmental Science & Technology, 45 (2011) 7089-7095.
[18] J. Veerman, M. Saakes, S.J. Metz, G.J. Harmsen, Reverse electrodialysis: A validated process model for design and optimization, Chemical Engineering Journal, 166 (2011) 256-268.
[19] M. Tedesco, P. Mazzola, A. Tamburini, G. Micale, I.D.L. Bogle, M. Papapetrou, A. Cipollina, Analysis and simulation of scale-up potentials in reverse electrodialysis, Desalination and Water Treatment, (2014) 1-13.
[20] J. Veerman, R.M. de Jong, M. Saakes, S.J. Metz, G.J. Harmsen, Reverse electrodialysis: Comparison of six commercial membrane pairs on the thermodynamic efficiency and power density, Journal of Membrane Science, 343 (2009) 7-15.
[21] D.A. Vermaas, D. Kunteng, M. Saakes, K. Nijmeijer, Fouling in reverse electrodialysis under natural conditions, Water Research, 47 (2013) 1289-1298.
[22] J.W. Post, Blue Energy: electricity production from salinity gradients by reverse electrodialysis, in, Wageningen University, 2009, pp. 244.
[23] A. Daniilidis, R. Herber, D.A. Vermaas, Upscale potential and financial feasibility of a reverse electrodialysis power plant, Applied Energy, 119 (2014) 257-265.
[24] P. Długołęcki, A. Gambier, K. Nijmeijer, M. Wessling, Practical potential of reverse electrodialysis as process for sustainable energy generation, Environmental Science and Technology, 43 (2009) 6888-6894.
[25] J.W. Post, H.V.M. Hamelers, C.J.N. Buisman, Energy recovery from controlled mixing salt and fresh water with a reverse electrodialysis system, Environmental Science and Technology, 42 (2008) 5785-5790.
[26] R.A. Tufa, E. Curcio, W. van Baak, J. Veerman, S. Grasman, E. Fontananova, G. Di Profio, Potential of brackish water and brine for energy generation by salinity gradient power-reverse electrodialysis (SGP-RE), RSC Advances, 4 (2014) 42617-42623.
[27] K. Kwon, J. Han, B.H. Park, Y. Shin, D. Kim, Brine recovery using reverse electrodialysis in membrane-based desalination processes, Desalination, 362 (2015) 1-10.
[28] J.G. Hong, Y. Chen, Nanocomposite reverse electrodialysis (RED) ion-exchange membranes for salinity gradient power generation, Journal of Membrane Science, 460 (2014) 139-147.

[29] E. Brauns, An alternative hybrid concept combining seawater desalination, solar energy and reverse electrodialysis for a sustainable production of sweet water and electrical energy, Desalination and Water Treatment, 13 (2010) 53-62.
[30] E.C. Ramato Ashu Tufa, Enrico Drioli, Practical Applicability of Reverse Elecrodialysis in Integrated Membrane Desalination Technologies for Salinity Gradient Power Generation, in: ICOM 2014, Suzhou, China, 2014.
[31] Y. Kim, B.E. Logan, Microbial reverse electrodialysis cells for synergistically enhanced power production, Environmental Science & Technology, 45 (2011) 5834-5839.
[32] D.C. Ramato Ashu Tufa, Roman Kodým, Michal Němeček, Efrem Curcio, Karel Bouzek, Hybrid Reverse Electrodialysis-Hydrogen (RED-H2) energy system: performance analysis and optimization, in: Hydrogen days 2015, Prague, Czech Republic, 2015.
[33] S. Lattemann, T. Höpner, Environmental impact and impact assessment of seawater desalination, Desalination, 220 (2008) 1-15.
[34] R. Einav, F. Lokiec, Environmental aspects of a desalination plant in Ashkelon, Desalination, 156 (2003) 79-85.
[35] G.L. Meerganz von Medeazza, "Direct" and socially-induced environmental impacts of desalination, Desalination, 185 (2005) 57-70.
[36] O. Scialdone, C. Guarisco, S. Grispo, A.D. Angelo, A. Galia, Investigation of electrode material - Redox couple systems for reverse electrodialysis processes. Part I: Iron redox couples, Journal of Electroanalytical Chemistry, 681 (2012) 66-75.
[37] J. Fieser, B. Dowden, Internet encyclopedia of philosophy, (2011).
[38] E.N. Zalta, S. Abramsky, Stanford encyclopedia of philosophy, in, Stanford University. The Metaphysics Research Lab, 2003.
[39] B. Barry, Sustainability and Intergenerational Justice, Theoria, 45 (1997) 43-65.
[40] A.S. Brundtland GH, Al-Athel S, Chidzero B., Our Common Future, in, 1987.
[41] B. Baxter, A theory of ecological justice, Taylor & Francis Group, New York, 2005.
[42] K.J. Arrow, W. Cline, K. Maler, M. Munasinghe, R. Squitieri, J. Stiglitz, Intertemporal equity, discounting, and economic efficiency, Cambridge, UK, New York and Melbourne: Cambridge University Press, 1996.
[43] M. Elimelech, W.A. Phillip, The Future of Seawater Desalination: Energy, Technology, and the Environment, Science, 333 (2011) 712-717.
[44] S. Latteman, Development of an environmental impact assessment and decision support system for seawater desalination plants, CRC Press Inc., 2010.
[45] D. Cohen-Tanugi, J.C. Grossman, Water permeability of nanoporous graphene at realistic pressures for reverse osmosis desalination, The Journal of Chemical Physics, 141 (2014) 074704.
[46] M. Kumar, M. Grzelakowski, J. Zilles, M. Clark, W. Meier, Highly permeable polymeric membranes based on the incorporation of the functional water channel protein Aquaporin Z, Proceedings of the National Academy of Sciences, 104 (2007) 20719-20724.
[47] J.K. Holt, H.G. Park, Y. Wang, M. Stadermann, A.B. Artyukhin, C.P. Grigoropoulos, A. Noy, O. Bakajin, Fast mass transport through sub-2-nanometer carbon nanotubes, Science, 312 (2006) 1034-1037.
[48] M. Majumder, N. Chopra, R. Andrews, B.J. Hinds, Nanoscale hydrodynamics: enhanced flow in carbon nanotubes, Nature, 438 (2005) 44-44.
[49] S. Kang, A. Asatekin, A.M. Mayes, M. Elimelech, Protein antifouling mechanisms of PAN UF membranes incorporating PAN-g-PEO additive, Journal of Membrane Science, 296 (2007) 42-50.
[50] A. Reddy, J. Trivedi, C. Devmurari, D. Mohan, P. Singh, A. Rao, S. Joshi, P. Ghosh, Fouling resistant membranes in desalination and water recovery, Desalination, 183 (2005) 301-306.
[51] H.B. Park, B.D. Freeman, Z.B. Zhang, M. Sankir, J.E. McGrath, Highly Chlorine-Tolerant Polymers for Desalination, Angewandte Chemie, 120 (2008) 6108-6113.
[52] M. Zhou, P.R. Nemade, X. Lu, X. Zeng, E.S. Hatakeyama, R.D. Noble, D.L. Gin, New type of membrane material for water desalination based on a cross-linked bicontinuous cubic lyotropic liquid crystal assembly, Journal of the American Chemical Society, 129 (2007) 9574-9575.
[53] C. Fritzmann, J. Löwenberg, T. Wintgens, T. Melin, State-of-the-art of reverse osmosis desalination, Desalination, 216 (2007) 1-76.
[54] R.L. Stover, Seawater reverse osmosis with isobaric energy recovery devices, Desalination, 203 (2007) 168-175.
[55] M. Farley, S. Trow, Losses in water distribution networks: a practitioner's guide to assessment, monitoring and control, IWA Publishing, 2003.
[56] A. Bodini, C. Bondavalli, Towards a sustainable use of water resources: a whole-ecosystem approach using network analysis, International Journal of Environment and Pollution, 18 (2002) 463-485.

[57] T. Pankratz, An overview of seawater intake facilities for seawater desalination, The future of desalination in Texas, 2 (2004).
[58] M. Schorr, B. Valdez, J. Ocampo, A. So, A. Eliezer, Materials and Corrosion Control in Desalination Plants, Materials Performance, 51 (2012) 56-60.
[59] M. Elimelech, X. Zhu, A.E. Childress, S. Hong, Role of membrane surface morphology in colloidal fouling of cellulose acetate and composite aromatic polyamide reverse osmosis membranes, Journal of Membrane Science, 127 (1997) 101-109.
[60] E. Ostuni, R.G. Chapman, R.E. Holmlin, S. Takayama, G.M. Whitesides, A survey of structure-property relationships of surfaces that resist the adsorption of protein, Langmuir, 17 (2001) 5605-5620.
[61] N. Prihasto, Q.-F. Liu, S.-H. Kim, Pre-treatment strategies for seawater desalination by reverse osmosis system, Desalination, 249 (2009) 308-316.
[62] A.D. Khawaji, I.K. Kutubkhanah, J.-M. Wie, Advances in seawater desalination technologies, Desalination, 221 (2008) 47-69.
[63] N.X. Tsiourtis, Criteria and procedure for selecting a site for a desalination plant, Desalination, 221 (2008) 114-125.
[64] D.A. Roberts, E.L. Johnston, N.A. Knott, Impacts of desalination plant discharges on the marine environment: A critical review of published studies, Water Research, 44 (2010) 5117-5128.
[65] E. Brauns, Combination of desalination plant and salinity gradient power reverse electrodialysis plant and usethereof, in: United States Patent, Vlaamse Instelling Voor Technologisch Onderzoek (VITO), Mol (BE), United States, 2012.
[66] R.L. Campbell, A.T. Jones, Appropriate disposal of effluent from coastal desalination facilities, Desalination, 182 (2005) 365-372.
[67] R. Einav, K. Harussi, D. Perry, The footprint of the desalination processes on the environment, Desalination, 152 (2003) 141-154.
[68] E. Drioli, E. Curcio, Membrane engineering for process intensification: a perspective, Journal of Chemical Technology and Biotechnology, 82 (2007) 223-227.
[69] W. Beckerman, The impossibility of a theory of intergenerational justice, Handbook of intergenerational justice, (2006) 53-71.
[70] L. Meyer, D. Roser, Distributive justice and climate change: the allocation of emission rights, Analyse und Kritik-Zeitschrift fur Sozialwissenschaften, 28 (2006) 223.
[71] IEA, Renewable energy, in, 2014.

Chapter 10

General Discussion and Future Prospects

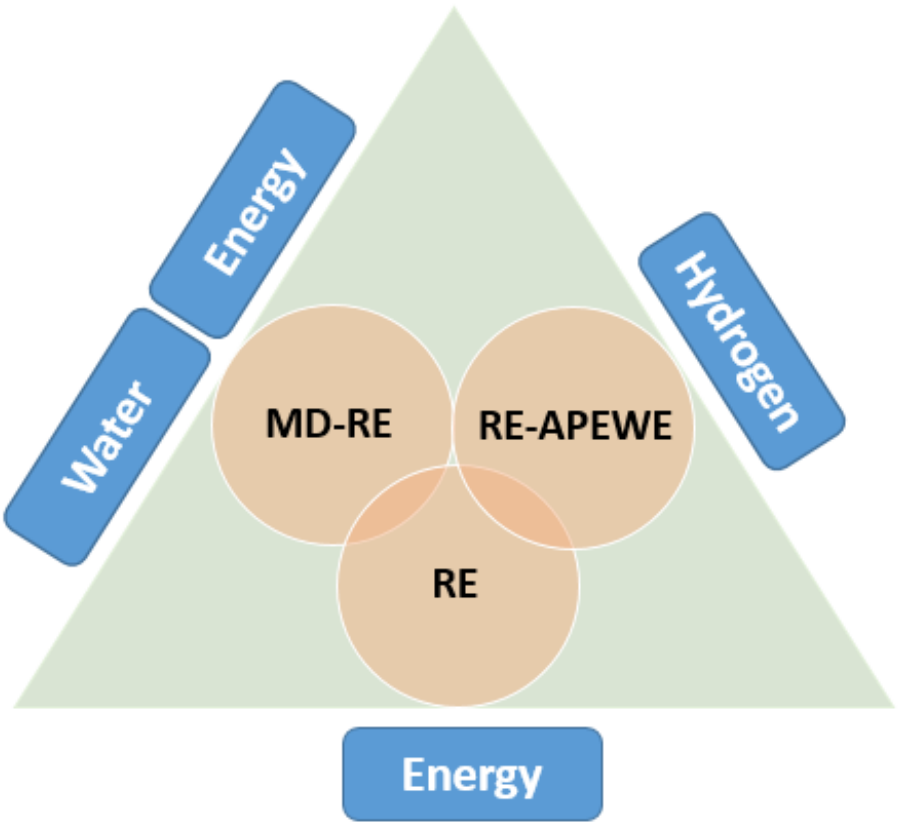

10.1 Introduction

This thesis demonstrates the application of RE for highly concentrated solutions like brine for energy generation in a standalone mode or an integrated approach. Implementation on real solutions and scaled up RE system requires well optimized materials and operating conditions. In this chapter, a general discussion on process optimization, material development for use of RE with concentrated brine solutions, multi-ion solutions and pre-treatment requirement is analyzed. Future directions for scale up and integrated applications is also highlighted.

10.2 Optimization of RE

The most important parameters for characterizing the performance of RE involve open circuit voltage (OCV), maximum power density (P_{max}) and internal area resistance (IAR) of the cell. Most of the literatures deal with optimizing the maximum power density [1-6], although the mentioned performance parameters are inter related. Therefore, consideration of each of this parameters is important from economical point of view.

The open circuit voltage of the RE stack is mainly dependent on the permselectivity and SR. Improvement in permselectivity of the membranes have a direct impact on the level of OCV. With the salinity gradient maintained between two compartments in RE, the selective transport of ion should be effective. The use of highly concentrated solutions like brine have a limitation on the permselectivity of ion exchange membranes. Based on the principle of Donnan exclusion, the membrane co-ion exclusion will be effective at low solution concentrations. Figure 10.1 shows experimentally tested permselectivity values of ion exchange membrane at different concentrations. Permselectivities values fall below 90 % for dilute solutions of concentration above 0.5 M and concentrated solutions levels above 2 M [7]. Permselectivities could go up to 65 % in solutions of 0.5 M and 4 M [8]. Reduction in permselectivity means reduction in both OCV and P_{max}. This is one of the limitations in using RE for concentrated brines. Thus, identification of optimal working concentrations and strategic design of highly selective membrane materials is important for high performance of RE.

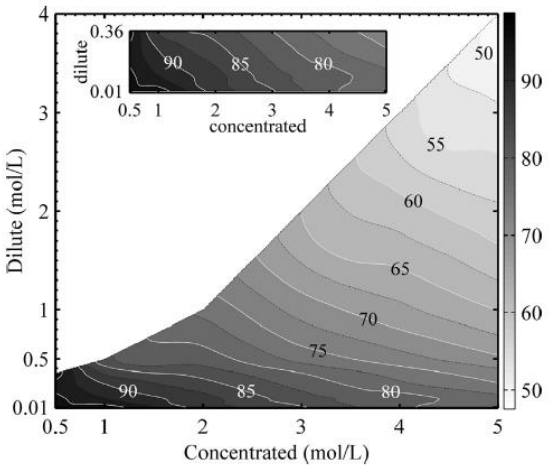

Figure 10.1. Variations of permselectivities with concentration of solutions [8].

Membrane development to overcome the permselectivity losses in highly concentrated solution would be challenging. Permselectivity improves when the cross linking of the membranes is improved, but this might increase in membrane resistance. So, consideration of the trade-off between permselectivity and resistance is required when the membrane properties have to be optimized for a certain application [9, 10], particularly in concentrated brines.

Trend in membrane resistances may also vary depending on solution concentration. For example, at low salt concentration (0.5 M NaCl), Fuji AEM and CEM showed a similar trend in area resistance. However, at higher test solution concentration (4 M NaCl), the trend was opposite: For Fuji CEM, area resistance increased and boundary layer diffusion resistance decreased whereas for Fuji AEM, area resistance decreased and boundary layer diffusion resistance increased [11].

Solution composition have an effect on the performance of the SGP-RE system. Recently, the presence of Mg^{2+} in feed water was observed to have a huge impact on the output power. Investigations also demonstrated that membrane resistance varies significantly in the presence of Mg^{2+} ion[6]. The presence of bulky and highly hydrated SO_4^{2-} also limits the transport phenomenon in the SGP-RE stack and have a negative impact on performance. Thus, further characterization of membranes in multi-ion solutions (under real solutions) and design of membranes suitable for such an environment is essential. Moreover, the development of multivalent permeable ion exchange membranes is a good strategy to solve problems associated with the transport of doubly charged ion across ion exchange membranes. This will also have a huge impact on the pre-treatment cost required for implementation of RE on large scale

applications.

Both temperature and flow velocity have a direct influence on the power density of the SGP-RE system [5, 12]. Temperature have a huge impact on the conductivity of solutions, particularly the LCC solution which have much contributes to the Ohmic losses. The membrane resistance may also be altered by changing the solutions temperature. Besides, flow hydrodynamics controls the mixing degree in RE stack and hence the performance. Although higher temperatures and flow velocity have a positive impact on output power, the energy cost must be compromised with the process economics. Also, much higher values may also have a limiting effect on the performance of the system. For example, high temperature reduces efficiency by increasing the ionic shortcuts[4] whereas high flow velocity reduces efficiency by reducing the residence time of ions in the stack[2]. However, the influence of flow velocity on membrane resistance is not so significant whereas the membrane and interfaces resistances reduce at higher temperatures [11] as shown in Figure 10.2. Thus, the choice of optimal operating conditions involves a compromise between the obtained benefit in terms of performance and the required inputs, for example energy.

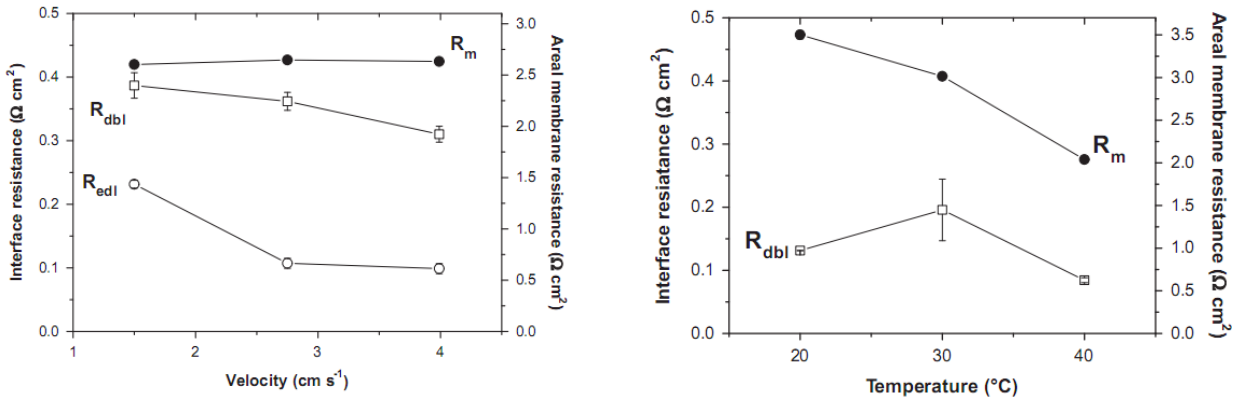

Figure 10.2. Variations of the membrane area resistance (R_m), diffusion boundary layer resistance (R_{dbl}) and electrical double layer resistance with temperature and flow velocity for Fuji CEM in 0.5 M NaCl solutions [11].

Novel RE designs like radial-axial feed flow have also been suggested to reduce the efficiency and economic challenges for the current RE designs [13].

10.3 Challenges in Integrated Applications

10.3.1 RE in Desalination Technologies

Desalination technologies are among the viable solutions to tackle the challenges associated with increasing water demand from time to time. However, desalination is an energy intensive process (3-4 KWh/m^3) with environmental footprints from the extensive use of fossil fuel. Thus, there is a huge potential in using the SGP-RE as a power source for running desalination industries.

The theoretical energy consumption for production of 1 m^3 of drinking water from seawater is presented in Figure 10.3. The results show that the desalination becomes more efficient when the recovery factor is low. This implies that the energy consumption reduces at relatively low concentration of retentate (brine) from desalination systems. Although law concentration of brine is advantageous in terms of environmental safety, it has low SGP when used in RE. For example, considering a moderate recovery value (30-50 %), the energy required for desalination falls in the range of 0.9-1 kWh/m^3 and the resulting in brine concentrations in the range of 0.8-1 M. At this brine concentration, the potential of RE for power output is quite low even when using brine and seawater as a LCC [6]. RO brine can be further concentrated by DCMD up to 6 M (supersaturation) to increase the efficiency of the process. The concentration of the RO brine by DCMD also reduces by volume reduction factor of up to 83.6 % [12]. Theoretically, the power output from RE is expected to increase by up to 13-fold when using brine from DCMD. Therefore, the energy consumption for desalination could be significantly reduced when using brine from DCMD. However, still development of highly efficient SGP energy generation technology is required to extract the available energy and cover the full energy required for desalination.

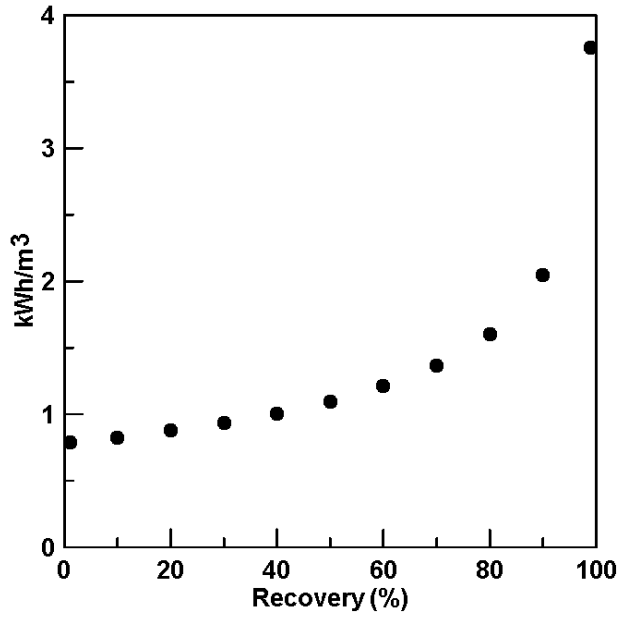

Figure 10.3. Theoretical amount of energy required to produce 1 m^3 of drinking water (0.3 g/L) from seawater (30 g/L).

One of the challenge for DCMD is operations under real conditions at high volume concentration factors. At this condition, there is a risk of scaling and fouling contamination which would potentially result in calcium carbonate precipitation by heterogeneous nucleation taking place at the membrane surface [14].

10.3.2 RE in hydrogen technologies

Another interesting application of RE is in hydrogen technologies. The possibility of continuous supply of SGP in fuelling electrolyzers have a benefit in minimizing problems related to dynamic electrolyser operations, thereby improving the capacity factor. The use of unpredictable solar or sun energy resources may be accompanied by start-up and shutdown of electrolyzers which may result in a potentially hazardous conditions. RE supplies a constant power as long as the feed solutions are supplied continuously.

Advantages from potential integration of RE with different electrolysis systems is presented in Figure 10.4. Coupling RE with alkaline water electrolysis implies establishment of a robust and economical hybrid process for hydrogen production compared to polymer electrolyte membrane electrolysis system. Integrated application of RE with a high temperature water electrolysis implies a system with high efficiency. Practical testes are required to assure the

potential applicability of such systems for indirect hydrogen production for concentrated brine.

Conversion of brine into hydrogen enables storage of SGP and allows the use for a wide range of applications. Hydrogen also have higher energy density (10^4 kJ/m^3) compared to SGP (for example, about 4500 kJ is generated when mixing 1 m^3 of 0.5 M and 5 M NaCl solution). Hydrogen can be transport in many forms to remote areas out of grid and be used for power generation. Other applications of hydrogen involve the use in households and chemical industries. This implies an indirect application of electrochemical potential of brine stored in the form of hydrogen.

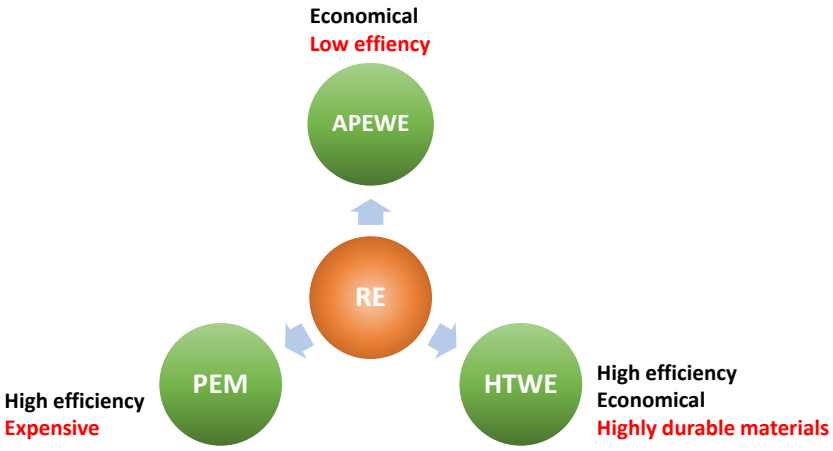

Figure 10.4. Potential advantages of coupling RE with various water electrolysis systems; APEWE: Alkaline Polymer Electrolyte Water Electrolysis, PEM is Polymer Electrolyte Membrane Electrolysis and HTWE is High Temperature Water Electrolysis.

The limitation in such a system lies in the efficiency or economical affordability of the processes. RE is not at its efficient power generation state currently. In addition, water electrolysis is a highly energy intensive process which is about 4-5 kWh/Nm^3 for industrial operations [15]. Therefore, intensification both processes is necessary for realization of the hybrid application.

Alkaline electrolyser is among the electrolysis system for potential integration to RE system, particularly because of its in suitability for a dynamic power input [16]. However, compared to the other electrolysis systems, its limited by low current density. The performance still needs to be improved in terms of material development and cell design. There are several ways to improve the performance, for example the use of anion selective membranes as a separator which reduces the Ohmic losses significantly [17]. Development of highly active electrocatalysts

for enhancing the oxygen evolution reaction is also crucial[18].

Low partial load range and operating pressures are also major issues in alkaline water electrolysis. At low partial load (above 40 %), there is a possibility of reduction in oxygen production rate and an increase in hydrogen production rate to dangerous levels (lower explosion limit above 4 mol % H_2). Improvement in the design of the cell is very crucial in order to tackle such a problem.

Moreover, identification of effective electrolyte additives to facilitate the electronic and ionic transfer as well as reduction of electrode surface tension, electrode modifications and minimization of the effects from the gas bubble are among strategies for enhanced performance of the alkaline water electrolysis.

In general, optimization of water electrolysis should focus mainly on improving the stability of cell components under mild operation condition for extended life time and flexibility of the cell. Besides, improvement in the hydrogen production rate and efficiency with simultaneous reduction of the installation costs essential.

10.4 Economic aspects

10.4.1 Standalone RE

The economic and financial feasibility of RE have been predicted for different scenarios of RE and compared with other renewable energy resources [13, 19]. Constant membrane price of 50 €/m^2 makes RE more expensive than other energy sources like solar and wind energy resources. For example, if a membrane price is reduced to 4.3 €/m^2 by cheap membrane development over ages, the cost of electricity can be reduced significantly to 0.18 €/kWh. This cost is lower than the solar energy whereas a bit higher than the wind energy. However, further reduction in cost (0.16 €/kWh) is possible by optimizing both the membrane and RE performance. However, the possibility of continuous power generation from SGP unlike the unpredictable nature of solar energy gives RE a high capacity factor to make it economically competitive [19].

Power generated from RE can be improved by the use of hot brine from desalination technologies like membrane distillation (MD). MD can take an advantage from waste heat so this cannot be an economic constraint for the supply of hot brine. Theoretically, the energy generated from mixing 1 m^3 of seawater (0.5 M) and 1 m^3 river water (0.017 M) is about 1.39 MJ, equivalent to 0.386 kWh. This amount can be increased by 3-fold (4.5 MJ) when working at higher salinity

gradient (using brine from MD, 5 M and seawater 0.5 M). Thus, the LCOE (0.18 €/kWh) estimated by assuming a power density of 5.4 W/m^{2}MP and 4 €/m^2 can be further reduced by working at higher salinity gradients. This could lead to the possibility of realization of cheap electricity by RE at a cost of 0.06 €/m^2.

For the investigation of economic feasibility of standalone RE, different cases are shown in Table 10.1 were considered. In this thesis, we consider the use of seawater/brackish water and highly concentrated brine (to supersaturation). This will increases the salinity gradient level and reduce the Ohmic losses compared to operations of RE with seawater and river water. However, the experimental results obtained in our previous investigations are lower that the case of seawater and river water as the membranes still need to be optimized. The change in membrane resistance with temperature is predicted based on the experimental results from Fontananova *et al.*(2014) [11]. The membrane price 50 €/m^2 is considered as the current price of ion exchange membranes [19] where as 4 €/m^2 is the price of the cheapest ion exchange membrane [20]. Power density for scenario 1 is based experimental results for the case of seawater and brine while the values for different temperatures in scenario 2 are projections based on the experimental data. The main assumption is scenario 2 is a high performance RE equipped with well optimized membranes available currently. Here the assumptions for the capital, operational and carbon emission costs are simulated to the data presented by post *et al.*(2014) [19]. The operational cost may be expected to be a little higher and membrane lifetime lower compared to the scenarios considered by Danilidis *et al.*(2014) since the concentration of the LCC solution used in the present study (seawater/brackish water) is higher compared to river water. Moreover, RE is a renewable energy technology, fuel and carbon costs are assumed to be zero. Cost estimations for scenario 1 (0.27 €/kWh) and 3 (0.20 €/kWh) are quite higher than the estimations of RE operated with brine and river water 0.16 €/kWh[19]. However, projections in the time range of 25-30 years for a well optimized membranes at an affordable cost with high performance RE results in 0.07-0.09 €/kWh cost of electricity, making it more competent. In the current state of art, it has been noted that RE for brine applications seem to be economically viable considering the use of well optimized membranes, however with limited upscale potential [19].

Table 10.1. Estimated cost of electricity for the different scenario is presented.

Feed water	Scenarios	Temperature (°C)	Membrane resistance	Membrane price (€/m^2)	Power Density (W/m^{2}MP)	Cost of electricity (€/kWh)
Brine and seawater	1	20	2.2	50	1.3	0.27
		35	1.3	50	1.6	0.22
		50	1	50	2.08	0.17
	2	50	1	4	12	0.09
Brine and brackish water	3	20	2.2	50	3	0.20
		35	1.3	50	3.9	0.16
		50	1	50	5.7	0.11
	4	50	1	4	18	0.07

Turek *et al.* (2007) estimated the cost of electricity generated by RE from mixing concentrated solutions (1.54 M) and dilute solution (0.02 M - 0.1 M) [21]. The assumption was based on an effective membrane area equal to 80 % of total membrane area, low membrane area resistance (1 Ωcm^2), 10 years of membrane life time, and a total investment cost of 83.3 €/kWh per 1 m^2 of installed membrane. The cost of electricity was estimated to be 5.35 €/kWh based on experimental outputs (maximum power density of 920 mW/m^{2}MP at a feed flow 0.54 cm/s). This results are based on a small scale RE designs (3 cm effective membrane length), and projections to industrial scale (effective membrane length in meters) may lead to less efficiency, and lower power output. They predict that the price of law resistance must be reduced hundred times to make RE available at an affordable cost. This outlines that the major challenge lies on the performance and cost of ion exchange membranes.

The power density obtained by Turek *et al.*(2007) [21] can be enhanced by better cell design and working at higher salinity gradients. For example, our recent result shows about +260 % increment of power density (2.4 W/m^{2}MP) when using MD brine and seawater as a feed solutions. This implies the possibility to reach cost price of 2 €/kWh for electricity generated by RE. Although, a significant reduction in cost is observed, this amount is quite high and uneconomical compared to other renewable energy resources.

Post *et al.*(2010) theoretically presented RE unit with 200 kW capacity for assessment of economic feasibility [22]. A modular design with frames containing six RE stacks having a total effective membrane 100,000 m^2 area was considered. For seawater and river water operations, the cost price was estimated to be 0.08 €/kWh at uncertainties below 20 % deviations.

10.4.2 ***RE in hybrid systems***

Economic evaluations for RE in hybrid applications will be a bit more complex as constraints for fixing the parameters get to increase. Synergetic advantage if any or challenges in an attempt to combine RE with other technologies need to be identified. The hybrid systems considered in this thesis (DCMD-RE and RE-APEME) are highlighted previously.

The major cost elements for desalination plants are capital cost and annual operating costs. In particular, DCMD is an energy intensive process compared to other desalination systems. However, there is a possibility to use low grade waste heat which have economic benefit [23]. Thus, DCMD or MD in general could be an ideal candidate for water purification where renewable energy (e.g. SGP) or low grade waste-heat sources are available.

For DCMD, there is a break-even point for membrane area below which a significant increases of water production with increasing membrane area leads to a significant decrease in the water production cost. Investigation by Zuo *et al.*(2011) shows a break-even area 4 m^2 corresponding to the minimum water production cost of \$1.1/m^3 [24]. Beyond this point, membrane area was observed to have a limited impact on water production and/or gain output ratio, and the membrane cost became the dominant factor for the water production costs. We have demonstrated in our previous investigation that increasing feed temperature and velocity have positive impacts on the water flux as well as water production, however, at the cost of input energy [25]. For this parameters, there is also an optimal level where the sensitivity of water production rate is no more affected by the variations. Therefore, operation of DCMD system at an optimal feed and permeate velocities is required for achieving low water production cost.

Hydrogen can be produced by RE indirectly by fuelling a separate electrolyser as we have demonstrated previously. However, electrolysis is an energy intensive process and this will have an overall impact on the affordability of the hybrid system. Industrial electrolysis plants usually operate at 70-90^oC and consume about 4-5 KWh/m^3 (ambient pressure and cell voltage of 1.85-2.05 V) of hydrogen.

The high energy consumption of hydrogen production via electrolysis has a direct impact on hydrogen costs which vary depending on the source of input electricity. For example, the cost of hydrogen generated by electricity from nuclear power plant (22 €/GJH_2) is less the one generated by photovoltaics (450 €/GJH_2) [26]. Traditional hydrogen production methodologies are much cheaper (70 times lower) compared to the costly renewable photovoltaic based hydrogen

production. In the current state-of-art, economic analysis indicate that electricity from RE is quite expensive compared to other renewable energy resources like wind and sun [19]. This makes the envisaged hybrid system economically unviable. However, positive insights on the future development of high performance and low cost membrane RE or other membrane based SGP technologies, subsequently leading to an acceptable cost of electricity is highly encouraging.

References

[1] Veerman J, de Jong RM, Saakes M, Metz SJ, Harmsen GJ. Reverse electrodialysis: Comparison of six commercial membrane pairs on the thermodynamic efficiency and power density. Journal of Membrane Science. 2009;343:7-15.
[2] Veerman J, Saakes M, Metz SJ, Harmsen GJ. Electrical power from sea and river water by reverse electrodialysis: A first step from the laboratory to a real power plant. Environmental Science and Technology. 2010;44:9207-12.
[3] Vermaas DA, Saakes M, Nijmeijer K. Doubled Power Density from Salinity Gradients at Reduced Intermembrane Distance. Environmental Science & Technology. 2011;45:7089-95.
[4] Daniilidis A, Vermaas DA, Herber R, Nijmeijer K. Experimentally obtainable energy from mixing river water, seawater or brines with reverse electrodialysis. Renewable Energy. 2014;64:123-31.
[5] Tedesco M, Brauns E, Cipollina A, Micale G, Modica P, Russo G, *et al.* Reverse Electrodialysis with saline waters and concentrated brines: a laboratory investigation towards technology scale-up. Journal of Membrane Science. 2015.
[6] Tufa RA, Curcio E, van Baak W, Veerman J, Grasman S, Fontananova E, *et al*. Potential of brackish water and brine for energy generation by salinity gradient power-reverse electrodialysis (SGP-RE). RSC Advances. 2014;4:42617-23.
[7] Daniilidis A, Vermaas DA, Herber R, Nijmeijer K. Experimentally obtainable energy from mixing river water, seawater or brines with reverse electrodialysis. Renewable Energy. 2014;64:123-31.
[8] Tedesco M, Cipollina A, Tamburini A, van Baak W, Micale G. Modelling the Reverse ElectroDialysis process with seawater and concentrated brines. Desalination and Water Treatment. 2012;49:404-24.
[9] Wilhelm FG, Pünt IGM, van der Vegt NFA, Strathmann H, Wessling M. Cation permeable membranes from blends of sulfonated poly(ether ether ketone) and poly(ether sulfone). Journal of Membrane Science. 2002;199:167-76.
[10] Guler E, Zhang Y, Saakes M, Nijmeijer K. Tailor-Made Anion-Exchange Membranes for Salinity Gradient Power Generation Using Reverse Electrodialysis. ChemSusChem. 2012;5:2262-70.
[11] Fontananova E, Zhang W, Nicotera I, Simari C, van Baak W, Di Profio G, *et al*. Probing membrane and interface properties in concentrated electrolyte solutions. Journal of Membrane Science. 2014;459:177-89.
[12] Ashu Tufa R, Curcio E, Brauns E, van Baak W, Fontananova E, Di Profio G. Membrane distillation and reverse electrodialysis for near-zero liquid discharge and low energy seawater desalination. Journal of Membrane Science.
[13] Vermaas DA. Energy Generation from Mixing Salt Water and Fresh Water: Smart Flow Strategies for Reverse Electrodialysis: University of Twente; 2014.
[14] Curcio E, Ji X, Di Profio G, Fontananova E, Drioli E. Membrane distillation operated at high seawater concentration factors: role of the membrane on CaCO 3 scaling in presence of humic acid. Journal of Membrane Science. 2010;346:263-9.
[15] Santos DMF, Sequeira CAC, Figueiredo JL. Hydrogen production by alkaline water electrolysis. Química Nova. 2013;36:1176-93.
[16] Carmo M, Fritz DL, Mergel J, Stolten D. A comprehensive review on PEM water electrolysis. International Journal of Hydrogen Energy. 2013;38:4901-34.
[17] Xiao L, Zhang S, Pan J, Yang C, He M, Zhuang L, *et al*. First implementation of alkaline polymer electrolyte water electrolysis working only with pure water. Energy & Environmental Science. 2012;5:7869-71.
[18] Chanda D, Hnát J, Paidar M, Bouzek K. Evolution of physicochemical and electrocatalytic properties of NiCo 2 O 4 (AB 2 O 4) spinel oxide with the effect of Fe substitution at the A site leading to efficient anodic O 2 evolution in an alkaline environment. International Journal of Hydrogen Energy. 2014;39:5713-22.
[19] Daniilidis A, Herber R, Vermaas DA. Upscale potential and financial feasibility of a reverse electrodialysis power plant. Applied Energy. 2014;119:257-65.

[20] Guler E, Zhang Y, Saakes M, Nijmeijer K. Tailor-made anion-exchange membranes for salinity gradient power generation using reverse electrodialysis. ChemSusChem. 2012;5:2262-70.
[21] Turek M, Bandura B. Renewable energy by reverse electrodialysis. Desalination. 2007;205:67-74.
[22] Post JW, Goeting CH, Valk J, Goinga S, Veerman J, Hamelers HVM, *et al*. Towards implementation of reverse electrodialysis for power generation from salinity gradients. Desalination and Water Treatment. 2010;16:182-93.
[23] Andrjesdóttir Ó, Ong CL, Nabavi M, Paredes S, Khalil ASG, Michel B, *et al*. An experimentally optimized model for heat and mass transfer in direct contact membrane distillation. International Journal of Heat and Mass Transfer. 2013;66:855-67.
[24] Zuo G, Wang R, Field R, Fane AG. Energy efficiency evaluation and economic analyses of direct contact membrane distillation system using Aspen Plus. Desalination. 2011;283:237-44.
[25] Tufa RA, Curcio E, Brauns E, van Baak W, Fontananova E, Di Profio G. Membrane distillation and reverse electrodialysis for near-zero liquid discharge and low energy seawater desalination. Journal of Membrane Science. 2015.
[26] Mueller-Langer F, Tzimas E, Kaltschmitt M, Peteves S. Techno-economic assessment of hydrogen production processes for the hydrogen economy for the short and medium term. International Journal of Hydrogen Energy. 2007;32:3797-810.

List of Publications

1. R. A. Tufa, Efrem Curcio, Willem van Baak, Joost Veerman, Simon Grasman, Enrica Fontananova, Gianluca Di Profio, Potential of brackish water and brine for energy generation by salinity gradient power-reverse electrodialysis (SGP-RE), ***RSC Adv.* 4 (2014) 42617-42623.**
2. R. A. Tufa, E. Curcio, E. Brauns, W. van Baak, E. Fontananova, G. Di Profio, Membrane Distillation and Reverse Electrodialysis for Near-Zero Liquid Discharge and low energy seawater desalination, ***Journal of Membrane Science*, 496 (2015) 325-333.**
3. R. A. Tufa, Perspectives on environmental ethics of membrane-based desalination technologies for water and energy production, ***Environmental Technology & Innovation*, 2015, 4, 182-193.**
4. R. A. Tufa, E. Rugiero, D. Chanda, J. Hnat, W. van Baak, J. Vermaan, E. Fontananova, G. Di Profio, E. Drioli, K. Bouzek, E. Curcio, Salinity Gradient Power-Reverse Electrodialysis (SGP-RE) and Alkaline Polymer Electrolyte (APE) water electrolysis for hydrogen production (*Submitted to the journal of Energy and Environmental Science*).
5. R. A. Tufa, R. Kodým, M. Němeček, E. Curcio, K. Bouzek, Power generation by an industrial-scale Reverse Electrodialysis (RE) Unit: Experimental Investigation and Performance Evaluation (submitted to the journal of *Industrial and Chemical Engineering Research*).
6. R. A. Tufa, T. Rijnaarts, E. Curcio, K. Nejmeijer, Renewable energy from aqueous sulphate wastes by reverse electrodialysis (*pending for submission*).
7. R. A. Tufa, E. Curcio, E. Fontananova, G. Di Profio, E. Drioli, Fouling tendency and stability of ion exchange membranes for reverse electrodialysis operated with concentrated brine (*submitted to the Journal of Membrane Science*).
8. R. A. Tufa, E. Curcio, E. Fontananova, G. Di Profio, E. Drioli, Energetic-Exergetic analysis of integrated Reverse Electrodialysis (RE)-Membrane Desalination Systems (*submitted to* the *Journal of Membrane Science*).
9. R. A. Tufa, E. Curcio, E. Drioli, Reverse Electrodialysis in Standalone and integrated applications: A review (*Pending for submission*).

Courses/Workshops

University of Calabria (UNICAL)

- Chemical Fundamentals of Membrane Operations (6 ECTS)
- Polymer chemistry (1 ECTS)
- Intellectual property and business entrepreneurship (2 ECTS)

University of Twente (UT)

- Ethics of Technology (5 ECTS)
- Introductory and Research Management Workshop (1 ECTS)

University of Chemistry and Technology Prague (UCTP)

- State exam on;
    - Membrane processes (pass)
    - Physical chemistry (pass)
    - Inorganic technology (pass)

Conference proceedings

- R. A. Tufa, D. Chanda, J. Hnat, E. Curcio, K. Bouzek, Coupling Reverses Electrodialysis (RE) with Alkaline Polymer Electrolyte Membrane Electrolysis (APEME) System for indirect hydrogen production from concentrated brines, October 1-3, **2015**, Rende, Italy **(Oral)**
- R. A. Tufa, D. Messana, E. Curcio, W. van Baak, E. Fontananova, G. di Profio, E. Drioli, Tracing the effect of multivalent ions on performance of reverse electrodialysis for power generation using concentrated brines, Euromembrane 2015, September 6-10, **2015**, Aachen, Germany. **(Oral)**
- R. A. Tufa, E. Curcio, E. Brauns, W. van Baak, J. Veerman, S. Grasman, E. Fontananova, G. Di Profio, E. Drioli Curcio, Membrane distillation-Reverse Electrodialysis for Zero Energy and Liquid Discharge (ZELD) in seawater desalination, 2nd International conference on desalination using membrane technology, July 26-29, **2015**, Singapore. **(Oral)**
- R. A. Tufa, D. Chanda, J. Hnat, E. Curcio, K. Bouzek, High performance, Reverse Electrodialysis-Alkaline Polymer Electrolyte Membrane (RED-APEM) electrolysis system for perpetual and sustainable hydrogen production, 25th North American Membrane Society Meeting (NAMS 2015), May 30 - June 3, **2015**, Boston, MA, USA. **(Oral)**
- R. A. Tufa, R. Kodým, M. Němeček, E. Curcio, K. Bouzek, Power Generation by an Industrial-Scale Reverse Electrodialysis (RED) Unit: Experimental investigation and performance evaluation, 25th North American Membrane Society Meeting (NAMS 2015), May 30 - June 3, **2015**, Boston, MA, USA. **(Oral)**

- R. A. Tufa, E. Curcio, D. Chanda, J. Hnát, R. Kodým, M. Němeček, K. Bouzek, Hybrid Reverse Electrodialysis-Hydrogen (RED-H_2) energy system: Performance analysis and optimization, Hydrogen Days 2015, May 18-20, 2015, Prague, Czech Republic. **(Poster)**
- R. A. Tufa, Timon Rijnaarts, Efrem Curcio, Enrico Drioli, Kitty Nejmeijer, Potential application of Reverse Electrodialysis (RED) for power generation from waste resources, xxxi EMS Summer School, September 28-October 3, **2014**, Cetraro, Italy. **(Poster)**
- R. A. Tufa, E. Curcio, W. van Baak, S. Grasman, E. Fontananova, G. Di Profio, Energy generation by salinity power gradient-Reverse Electrodialysis (SPG-RE), Atti del IX Convegno Nazionale dell'Associazione di Chimica per l'Ingegneria (AICIng **2014**), September 14-17, Lecce, Italy. **(Poster)**
- R. A. Tufa, E. Curcio, E. Drioli, Potential of salinity gradient power by reverse electrodialysis from various feed resources, EUDIME and EM3E Joint Workshop, September 2-5, **2014**, Montepellier, France. **(Oral)**
- R. A. Tufa, E. Curcio, E. Drioli, Practical applicability of reverse elecrodialysis in integrated membrane desalination technologies for salinity gradient power generation, The 10th International Congress on Membranes and Membrane Processes (ICOM2014), July 20-25, **2014**, Suzhou, China. **(Oral)**
- R. A. Tufa, E. Curcio, E. Drioli, Hybrid desalination technologies for salinity gradient power generation, ITM seminar in the framework of the 20th Anniversary of the Institute on Membrane Technology (ITM-CNR), October 30-31, **2013**, Rende, Italy. **(Oral)**
- R. A. Tufa, E. Curcio, E. Fontananova, G. Di Profio, E. Drioli, Integrated membrane desalination technology for water and energy production, September 29-October 3, **2013**: Advances in Science and Engineering for Brackish Water and Seawater Desalination II, Cetraro, Italy. **(Poster)**
- R. A. Tufa, E. C., E. Drioli, Integrated Membrane Desalination Systems for water and energy production, Indigo-BMG-EUDIME Workshop, September 17-20, **2013**, Leuven, Belgium. **(Oral)**
- R. A. Tufa, E. Curcio, E. Drioli, Scaling in membranes operated with concentrated brines, 29th Summer School on Membranes, July 22-26, **2013**, Essen, Germany **(Poster)**

Acknowledgements

First of all, glory is always to the almighty God with all my hearts for his endless help in every status of my life.

I would like to thank the EUDIME committee for their trust on me during the selection process. It was a great pleasure and opportunity to join the EUDIME programme which involves excellence and mobility in a multidisciplinary research implemented at an international level.

I am exceptionally grateful to Prof. Efrem Curcio for his constant support and follow up during my PhD career, without whom this work wouldn't have been complete. From the first day he picked me up from Lamezia Terme Airport, on my first arrival to Italy (November 2012), his kind assistance never (both in administrative issues and research activities) stopped. I benefitted a lot from his constructive comments and suggestions. Explorations and handling of research problems related the emerging technologies was not easy without him. In particular, knowhow and skills related to process intensification in an integrated approach for production of clean water and energy were achieved. I appreciate his capability of critical comments, fruitful suggestions and solving complex problems efficiently. Our collaboration was so intact to see him not only as my supervisor but also a close friend, which had a huge contribution for my success. God bless him.

I am deeply thankful to Prof. Enrico Drioli for the effective co-ordination of the EUDIME Programme. Besides, Prof. Enrico Drioli's general comments and suggestions on some of my research activities and mobility tracks was helpful for the success of my work. It's worth mentioning Prof. Raffaele Molinari who were so kind in his assistance for issues related to the department.

I have a special thanks to Dr. Enrica Fontananova for her assistance in impedance spectroscopic investigations and knowledge share through discussions. I am thankful to Dr. Gianluca de Profio for the support on investigations related to scaling of ion exchange membranes operated in concentrated brine, and of course a moral support. I should mention Ylenia Noviello for experiments related to energetic and exergetic analysis of integrated RE and membrane desalination systems.

REAPower project was a good opportunity to meet people active on blue energy research. I would like to thank Andrea Cipolina from University of Palermo for general

discussion on applicability of RE in concentrated brine. I am especially thankful for Joost Veerman from RED stack B.V. (The Netherlands) for the critical comments and suggestion which was helpful in the success of my first publication on RE. My gratitude also goes to Helsen Joost from VITO (Belgium) for his assistance during RE stack assembly with important technical information. The kindness of Willem van Baak from Fujifilm Manufacturing Europe B.V. (The Netherlands) in managing the supply of ion exchanger membranes is highly appreciated.

I would like to thank Prof. Dr. Ir. D.C (Kitty) Nijmeijer for welcoming me to membrane science and technology group (MST) at the University of Twente (UT) and for the guidance during my research for 6 months. I am grateful for her constant support and follow up during my research stay at the University of Twente. It was possible to investigate the applicability of 'blue energy' to a wider range, particularly for power generation from industrial effluents. My gratitude also goes to Prof. Henny J. M. Bouwmeester as coordinator of the EUDIME for supportive information during initial periods after my arrival at UT. I am thankful to Timon and Jordi for their good friendship and assistance during my lab works and critical discussions on the topic of Reverse Electrodialysis. My sincere gratitude also goes to all the MST group members at the UT for their nice friendship and motivating social activities: Batavierenrace was an incredible experience for cardio workout. Discussions with officemates Harmen and Joris covered broad topics from academic research to socio-cultural perspectives.

I would like to express my sincere gratitude to Prof. Dr. Ir. Karel Bouzek for accepting my request for mobility host at UCTP and his careful supervision. UCTP was a special place to practice the concepts of chemistry in an engineered approach specially integration of RED with water electrolysis for hydrogen production. I have benefitted a lot from his deep knowledge in the field of hydrogen technologies. I am grateful to Dr. Ing. Vlastimil Fíla for his informative supports during my first periods in Prague and highlts on tests related to hydrogen permeability of some ion exchange membranes. My appreciation also goes to some of the members in his research group, especially to Dabrabatan Chanda and Jaromir Hnat. We have shared a lot of ideas on theoretical and technical concepts. It's worth mentioning Michal Němeček for his assistance on experiments carried out on industrial scale RE, even during weekends in some cases. Roman Kodym's general suggestions related to my experimental activities in Prague were useful.

The moral support and encouragements of all Ethiopian friends in UNICAL was incredible. Weekly organized football matches were refreshing activities after laboratory works. My appreciation also goes to other international students who were motivating for involvement in many social activities for a mix of fun in PhD life.

Educational and cultural experiences with EUDIME colleagues during mobility periods and annual meetings were incredible.

The financial support of The Education, Audiovisual and Culture Executive Agency (EU-EACEA) within the EUDIME –"Erasmus Mundus Doctorate in Membrane Engineering" program (FPA 2011-0014, SGA 2012-1719, http://eudime.unical.it) is kindly acknowledged.

Last but not the least, I would like to express my since gratitude to all my family members, who never got tired in supporting me morally and spiritually from such a long distance, specially my mother Teyibe Aman Wosho and my father Ashu Tufa Washo. They created a feeling that they were with me all the time during my PhD career.

About the Author

Ramato Ashu Tufa was born on September 1, 1983 in Zeway, Ethiopia. After finishing his high school (Zeway Don Bosco Catholic Church School) in 2002, he started studying 'Applied Chemistry' at the Hawassa University, Ethiopia. This BSc study was completed on July 2015 with a theses; Multistep synthesis of sulfonamides. On September 2006, Ramato started MSc study to specialize in 'Analytical Chemistry', at Addis Abeba University, Ethiopia. This study was completed with a theses; Determination of essential and non-essential metals in commercially available Ethiopian roasted coffee powders and their infusions. He was later awarded with an Erasmus Mundus fellowship under 'European Master in Quality in Analytical Laboratories (EMQAL)' for another MSc study at Gdansk University of Technology and University of Barcelona. This study was completed on March 2011 with a theses on 'Assessment of the QuEChERS methodology for the determination of sulfonamides in animal feeds'. He continued a research work on similar research line at University of Barcelona. In September 2012, Ramato was awarded an Erasmus Mundus Joint doctorate fellowship under 'Erasmus Mundus Doctorate in Membrane Engineering (EUDIME)' for pursuing a PhD study at Department of Environmental and Chemical Engineering, University of Calabria as home university. This PhD involved nobilities to two different universities: University of Twente and University of Chemistry and Technology Prague. The research focused on the use of concentrated brine for salinity gradient power generation and hydrogen production by reverse electrodialysis, as presented in this theses.